22-st INTERNATIONAL CONFERENCE ON THE METHODS OF AEROPHYSICAL RESEARCH

July 1 – 5, 2024
Novosibirsk, Russia

Abstracts
Part II

Ministry of Science and Higher Education of the Russian Federation
Russian National Committee on Theoretical and Applied Mechanics
Siberian Branch of the Russian Academy of Sciences
Khristianovich Institute of Theoretical and Applied Mechanics
of the Russian Academy of Sciences
Central Aerodynamic Institute
Novosibirsk State University

International Conference on the Methods of Aerophysical Research

July 1–5, 2024
Novosibirsk, Russia

Abstracts
Part II

Edited by E.I. Kraus

Novosibirsk
Siberian Branch of the Russian Academy of Sciences
2024

INDEPENDENT ELECTRONIC PUBLICATION

UDK 533.6+532.5.013.4+551.5:371.3
BBK B253.33я431(0)

ICMAR-2024 is sponsored by:
Siberian Branch of the Russian Academy of Sciences
Novosibirsk State University

International Conference on the Methods of Aerophysical Research, Novosibirsk, Russia, July, 1 – 5, 2024: Abstracts. Pt. II / Ed. E.I. Kraus; Ministry of Science and Higher Education of the Russian Federation: on [et al.]. – Novosibirsk: SB RAS, 2024. – 215 p.

The 22th International Conference on the Methods of Aerophysical Research (ICMAR 2024) is to be held on July 1–5, 2024. The Conference is devoted to the 110th anniversary of academician V.V. Struminsky, who led ITAM SB RAS from 1966 to 1971.
This collection contains the abstracts of the conference. It includes the following main topics of ICMAR 2024:

- Physical modeling and mathematical simulation of aerogasdynamics of internal and external flows;
- Wind tunnels, gasdynamic facilities and methods of flow diagnostics;
- Hydrodynamic stability, turbulence and flow separation;
- Methods of aerophysical research in interdisciplinary problems.

A special section of ICMAR deals with artificial intelligence and mechanics in medicine.

The papers are printed by direct reproduction from the authors' originals. The authors are responsible for possible misprints and the quality of translations.

ISBN 978-5-6049901-4-8 (ч. 2)
ISBN 978-5-6049901-2-4

DOI 10.53954/9785604990148_3

CELLULAR STRUCTURES OF HYBRID DETONATION IN HYDROGEN-AIR MIXTURES WITH A HETEROGENEOUS DISTRIBUTION OF ALUMINUM PARTICLES

A.A. Afanasenkov, T.A. Khmel

Khristianovich Institute of Theoretical and Applied Mechanics SB RAS
630090, Novosibirsk, Russia

Introduction. The study of the combustion and detonation processes of hydrogen-air mixtures has recently attracted a great deal of attention. This interest is due to the search for ways to control detonation. One possible method is to add aluminum particles to the gas mixture.

This paper shows the results of numerical modelingcof detonation processes in a hydrogen-air environment and the effect of the addition of aluminum particlesчof different concentrations on detonation processes.

The physical and mathematical model is based on the Euler equations**.** The combustion of hydrogen is described by a modified model of the reduced kinetics by I. A. Bedarev [1]. The combustion of aluminum particles is described by the A.V. Fedorov model [2], extended to micron and submicron dimensions [3].

Numerical model. TVDThe Harten-Lax TVD scheme was used to calculate the gas phase, and the Gentry – Martin-Daly scheme was used for the particles. The program code is written in Fortran programming language, parallelization was performed on the basis of the OpenMP library.

Problem statement. A flat channel with thermally insulated walls 10 cm wide is considered. The channel is filled with a poor hydrogen-air mixture under normal conditions. Detonation is initiated due to the rupture of the film behind the high-pressure chamber (Fig. 1).

Results. The paper investigated the effect of adding aluminum particles with d = 1 μm and d = 3.5 μm diameters of various concentrations and distributions in the study.

Figure 2 shows a picture of the maximum detonation pressures of a poor oxygen-air mixture of $1.2H_2 + O_2 + 3.82N_2$ (equivalence ratio φ = 0.6).

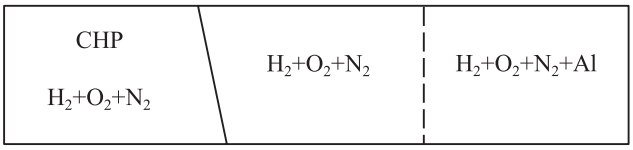

Fig. 1. Diagram of the problem under consideration

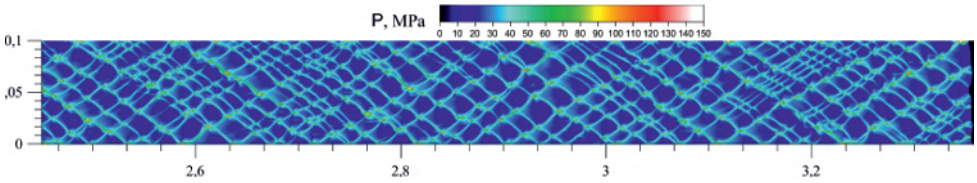

Fig. 2. Picture of maximum gas detonation pressures φ = 0.6

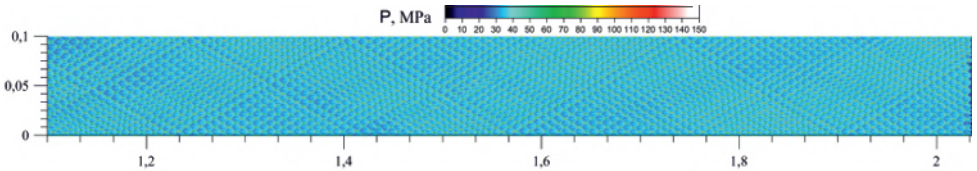

Fig. 3. Picture of the maximum hybrid detonation pressures φ = 0.6 with the addition of aluminum particles d = 1 μm ρ = 100 g/m^3

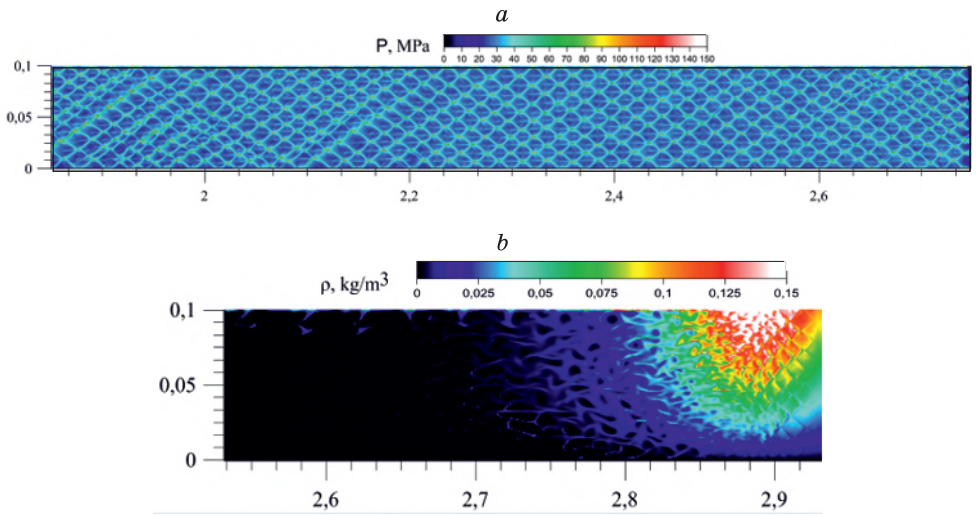

Fig. 4. a) picture of maximum pressures b) picture of the distribution of densities of aluminum particles in hybrid detonation φ = 0.6 with the addition of aluminum particles d = 3.5 μm with a gradient distribution of densities from ρ = 0 g/m^3 from below and up to ρ = 100 g/m^3 on top.

The cellular structure has an irregular character, the average cell size is 25 mm, and the detonation velocity is D = 1.68 km/sec. Figure 3 shows a picture of the hybrid detonation flow in the same mixture with φ = 0.6 with the addition of aluminum particles with a diameter of d = 1 μm and a density of ρ = 100 g/m^3.

When aluminum particles are added, the cellular structure is regularized, the average cell size decreases to 80 mm, and the detonation propagation velocity increases to D = 1.95 km/sec.

The results for hybrid detonation with a fuel excess coefficient of φ = 0.6 with the addition of aluminum particles with a diameter of d = 3.5 μm with an inhomogeneous particle distribution (with a density gradient from ρ = 0 g/m^3 on the lower wall to ρ = 100 g/m^3 on the upper wall) are shown in Fig. 4: a) a picture of the maximum pressure, b) the pattern of density distribution of aluminum particles. A regular cellular structure is formed here, the average size of the detonation cell is 16.7 mm, and the detonation velocity is D = 1.8 km/sec. In general, cellular structures are similar to those formed in a homogeneous cloud of particles, the detonation rate and cell size correspond to some average value of particle density. Spatial heterogeneity is manifested in the distribution of discrete phase parameters (Fig. 4b).

The research was carried out with the financial support of the Russian Science Foundation in the framework of scientific project No. 24-29-00336

REFERENCES

1. **Bedarev I.A., Rylova K.V., Fedorov A.V.** Application of detailed and reduced kinetic schemes for the description of detonation of diluted hydrogen–air mixtures // Combust. Explos. Shock Waves. 2015. Vol. 51, No. 5. P. 528–539.
2. **Khmel T.A. and Fedorov A.V.** Numerical modeling of the formation of cellular heterogeneous detonation of aluminum particles in oxygen, FGV 2005. Vol. 41, No. 4, P. 84–98.
3. **Khmel T.A. and Fedorov A.V.** Modeling of plane detonation waves in gases of large-sized aluminum particles, FGV 2018. Vol. 54, No. 2. P. 71–81.

DOI 10.53954/9785604990148_6

FEATURES OF GAS DYNAMIC PROCESSES IN THE FLOW TRACT DURING SIMULATION OF FLIGHT IN REDUCING ATMOSPHERES OF TITAN AND GIANT PLANETS

S.A. Akinin, A.V. Starov, I.S. Tsyrulnikov

Khristianovich Institute of Theoretical and Applied Mechanics SB RAS
630090, Novosibirsk, Russia

It is known that about 2.45 billion years ago an oxygen catastrophe occurred on Earth with a change in the general character of the atmosphere from reducing to oxidizing. All existing types of air-breathing engines are designed to fly in the Earth's oxidizing atmosphere, which is an exceptional case in the solar system. Such atmospheres are very rare in a large number of currently known exoplanets, since for long-term preservation of the oxidizer in the atmosphere, its constant source is necessary, such as, for example, in the Earth's biosphere. Currently, in addition to the extensive exploration of Mars by automata, there is interest in the giant planets and their satellites. In addition to flyby studies, probes were dropped into the atmosphere of Jupiter and landed on the surface of Saturn's moon Titan. The predominant gas in the atmospheres of the giant planets is hydrogen; in the atmosphere of Titan, the main gas is nitrogen; methane accounts for 1.6% of the atmosphere as a whole and 5% in the surface layer; in the upper layers it reaches 43% [1]. In the next decade, NASA, ESA, China and Russia have plans to explore giant planets as part of the Laplace-P project. Landing probes of such missions require both braking propulsion systems and systems that ensure prolonged flight in a reducing atmosphere. The advantage of an air-breathing engine is that such an engine can use one "free" component of the fuel pair from the atmosphere. In the reducing atmospheres of Titan and the giant planets, such a "free" component will be methane and hydrogen, respectively. Taking into account the required fuel-oxidizer mass ratios, issues of mixing and chemical kinetics (temperature of the fuel or oxidizer), the organization of the combustion process in the flow path during flight in a reducing atmosphere seems far from ambiguous and requires study.

As part of the work, preliminary computational and experimental studies of the features of gas-dynamic processes in the flow tract were carried out when modeling a nitrogen atmosphere with an admixture of methane or hydrogen at the channel entrance. The experiments were carried out on an attached pipeline using the discharge prechamber of the pulse wind tunnel of the ITAM SB RAS as a source of heated working fluid. 3D numerical modeling was carried out using the academic version of the commercial package ANSYS FLUENT. The channel had a back step at the entrance with a double vertical expansion of the cross section, a section of constant cross-section (Fig. 1) with a relative length of 12.8 (the height of the step). The experiments were carried out in the range of total temperatures from 1000 to 2000 K, total pressure from 0.8 to 1.6 MPa. A nozzle with Mach number M = 1.8 was used. Air was supplied in front of the step perpendicularly from the wall through 8 sound holes and a second supply zone through 8 sound holes on the channel walls behind the back step.

It should be noted that two distinct directions for future research need to be highlighted. The first is the issue of experimental modeling. The standard option is to heat the working fluid of the fasility before feeding it into the nozzle, which simulates a high-enthalpy

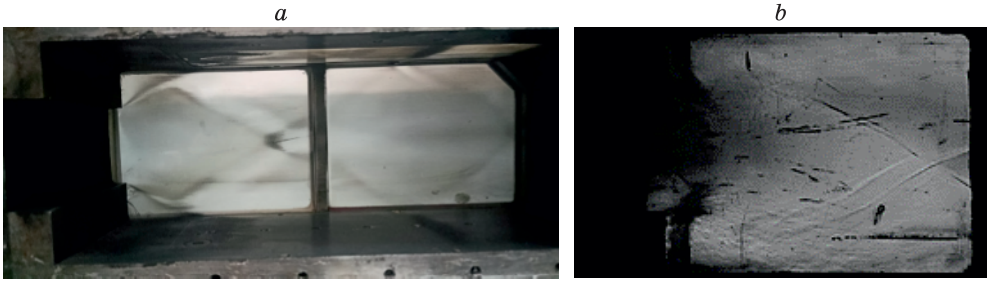

Fig. 1. Photo of the window after run with methane (*a*) and Schlieren visualization of the initial section of the channel with an air jets behind the back step (*b*).

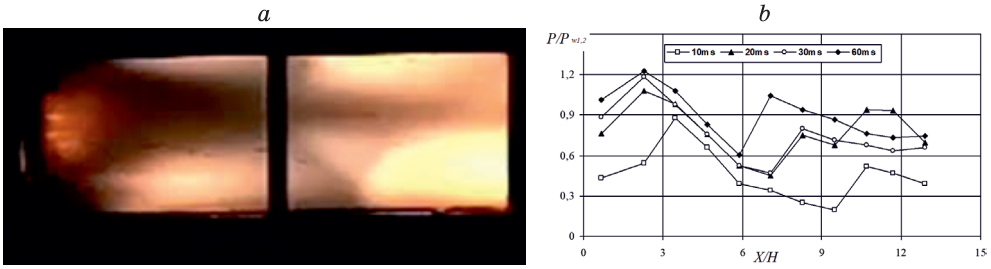

Fig. 2. Hydrogen flame photo (*a*) and longitudinal distribution of relative pressure in the channel when air is supplied at the step and behind the step (*б*).

high-speed flow. Methane, with sufficiently moderate heating, decomposes into hydrogen, acetylene and, ultimately, carbon, which is evident from soot formation in characteristic flow areas in the channel (see Fig. 1). A solution may be to mix methane into the nozzle after heating the nitrogen.

The second is the actual study of gas-dynamic processes in the flow path during "inversion," when the main hot flow is an inert gas with fuel, and an oxidizer (air or oxygen) is supplied from the walls. In Figure 1b, jets of air (dark areas due to high density) are visible behind the step, which penetrate into the core of the main flow.

For the first time, hydrogen combustion was obtained in a channel with an "inversion" supply when simulating a flight in a reducing atmosphere (Fig. 2). Combustion is observed in the separation zones behind the step and behind the repeated fall of the re-reflected shock waves. The fields of flow, pressure distribution and heat flows in the channel without air supply, with nitrogen supply (action of jets) and during combustion (air supply) were obtained. A comparison of the results of numerical modeling with experimental data showed their satisfactory agreement

The research was carried out within the state assignment of Ministry of Science and Higher Education of the Russian Federation. The study was conducted at the Equipment Sharing Center «Mechanics» of ITAM SB RAS.

REFERENCES

1. **Mingalev I.V., Rodin A.V., Orlov K.G.** Numerical modeling of the general circulation of Titan's atmosphere for equinox conditions// Astronomical Bulletin, 2019, T. 53, № 4, P. 291–308. [in Russian]

DOI 10.53954/9785604990148_8

MULTYPHYSICS SOFTWARE PLATFORM FLOWVISION

A.A. Aksenov

TESIS Ltd
127083, Moscow, Russia

The FlowVision software package [1] was originally created as a computational fluid dynamics code (CFD code), but now is evolving into an interdisciplinary platform for computer aided engineering. The "classical" physics of FlowVision is mathematical models of heat and mass transfer and fluid motion (Navier-Stokes and Darcy equations) implemented for three-dimensional, incompressible and compressible flows, Newtonian and non-Newtonian fluids. Now FlowVision software package has numerical solution of stationary Maxwell equations for simulating electric current and electromagnetic fields in a continuous medium, radiation transfer model for radiation heat exchange, model of dispersed phase motion (bubbles, drops, grains of sand), calculation of acoustic oscillations source and their transfer in computational domain. Tools for modeling complex flows are also being developed – among them are sliding surfaces, modeling of immiscible fluids with contact surfaces, motion of bodies relative to a fixed region, resolution of boundary layers using a prismatic grid to get y+<<1.

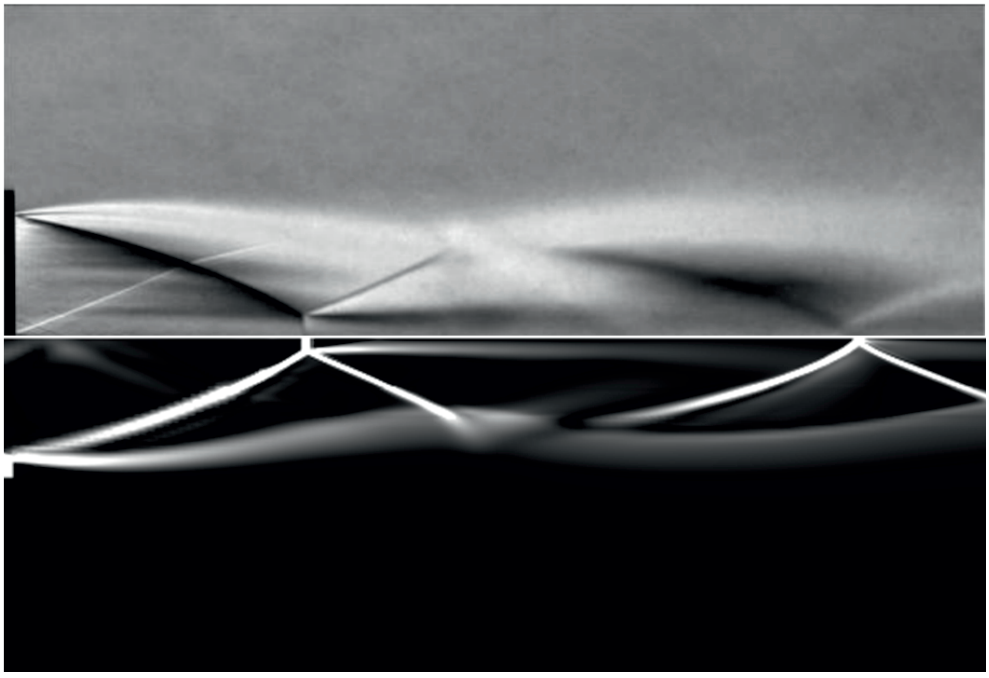

Fig. 1. Supersonic jet from a nozzle. Comparison with experiment: above – experiment, below – calculation.

FlowVision simulates turbulence by two different approaches – by using averaged Reynolds equations (RANS-approach) [2] and by vortex-resolving methods using implicit large eddy simulation (ILES) or using subgrid turbulence modeling (Smagorinsky model). The paper shows that the use of so-called skew schemes for the calculation of convective flows allows to increase an accuracy of vortex-resolving turbulence calculation techniques. A comparison with the experiment of different-temperature mixing of liquids in a T-junction is given.

To model fluids in which the Prandtl number is not equal to unity, the $k_\theta - \epsilon_\theta$ model is used, as well as its modification, which is "tuned" to simulate heat transfer in liquid sodium. This model is used to calculate heat transfer in new-generation nuclear reactors on fast neutrons with sodium coolant.

A modification of the well-known SST turbulence model, which takes into account the compressibility of the medium, allows to simulate the long-range wake of a supersonic nozzle with high accuracy. Comparison of simulation and experimental data obtained in [3] is given in Fig. 1.

To simulate the fluid-structure interaction problems FlowVision has information exchange with various Russian and foreign finite element codes (APM, Fidesis, Abaqus, Nastran), which allow to perform calculations of stress-strain state of structures. Simulation of flutter of an airplane wing and generation of acoustic vibrations of an automobile tire is given.

Also the application of FlowVision for solving medical problems – blood coagulation and determination of fractional blood flow reserve by non-invasive method is presented.

REFERENCES

1. **Aksenov A.A.** FlowVision: Industrial computational fluid dynamics // Computer Research and Modeling]. – Vol. 9, No. 1. – 2017. – P. 5–20 (in Russian).
2. **Zhluktov S.V., Aksenov A.A.** High-Reynolds number calculations of turbulent heat transfer in FlowVision software // Computer Research and Modeling. – Vol. 10, No. 4. – 2018. – P. 461–481 (in Russian).
3. **Zaprjagaev V.I., Kiselev N.P., Pivovarov A.A.** Gas-dynamic structure of axisymmetric supersonic underexpanded jet// Izvestija RAN. Mekhanika zhidkosti i gaza // Bulletin of the Russian Academy of Scienc-es: Fluid Mechanics]. – No. 1. – 2015. – P. 95–107 (in Russian).

DOI 10.53954/9785604990148_10

IMPACT OF A SMALL MOVING SPHERE ON BLASIUS BOUNDARY LAYER

F.V. Antakov, V.B. Zametaev

Moscow Institute of Physics and Technology, 140180, Zhukovsky, Russia

Central Aerohydrodynamic Institute, 140180, Zhukovsky, Russia

The laminar flow of a viscous incompressible fluid past a flat plate at high Reynolds numbers is considered. At a distance $\hat{L}$ from the leading edge of the plate and at a height $\hat{l}_d = \hat{L} \cdot l,\ l << 1$ from its surface there is a small sphere moving downstream with a given velocity $\hat{V}_d = \hat{V}_\infty u_w$, where $\hat{V}_\infty$ – is the velocity of the oncoming flow, and $u_w << 1$. It is convenient to model a sphere with a three-dimensional dipole with intensity $\hat{d} = \hat{V}_\infty \hat{L}^2 m$, because outside the boundary layer, the flow is inviscid and potential [1]. As a result, the sphere generates a pressure disturbance that acts on the Blasius boundary layer on the plate.

From the theory of interaction of the boundary layer with the external flow [2], it is known that the disturbed pressure acts primarily on the viscous thin sublayer (region I in the figure), located at the bottom of the boundary layer. The height of the dipole placement $l >> \mathrm{Re}^{-3/8}$ was chosen so as to exclude free interaction from consideration. The flow under study is unsteady, but when moving to a coordinate system related with a dipole, the problem becomes steady, but on a plate moving upstream. For viscous sublayer I, the boundary value problem has the form:

$$u\frac{\partial u}{\partial x} + v\frac{\partial u}{\partial y} + w\frac{\partial u}{\partial z} = -\frac{\partial p}{\partial x} + \frac{\partial^2 u}{\partial y^2}, \quad p = M\frac{2x^2 - 1 - z^2}{2\pi(x^2 + 1 + z^2)^{5/2}},$$

$$u\frac{\partial w}{\partial x} + v\frac{\partial w}{\partial y} + w\frac{\partial w}{\partial z} = -\frac{\partial p}{\partial z} + \frac{\partial^2 w}{\partial y^2}, \qquad \frac{\partial u}{\partial x} + \frac{\partial v}{\partial y} + \frac{\partial w}{\partial z} = 0,$$

$$y = 0: \quad u = -U_w, \quad v = w = 0; \quad y \to \infty: \quad u = y + A(x,z) + \ldots\ , \quad w \sim y^{-1} \to 0,$$

$$|x| \to \infty, \quad |z| \to \infty: \quad u = -U_w + y\ldots, \quad w = 0.$$

The problem contains two independent parameters: the pressure intensity M specified by the dipole and the wall velocity $-U_w$. From the boundary conditions it is clear that the directions of fluid motion at the lower ($y = 0$) and upper ($y \to \infty$) boundaries of the region are opposite. This means that the flow can be divided into two counter flows: the wall layer, moving from right to left, and the upper layer, moving from left to right, see [3]. It is obvious that there is an interface between layers $y = S(x,z)$, on which the longitudinal velocity is zero. The problem was solved in a linear approximation, with the parameter M tending to zero.

$$u(x,y,z) = -U_w + y + Mu_1 + \ldots, \quad v(x,y,z) = Mv_1 + \ldots, \quad w(x,y,z) = Mw_1 + \ldots,$$

$$S(x,z) = U_w + MS_1(x,z) + \ldots, \quad p = Mp_1, \quad M << 1.$$

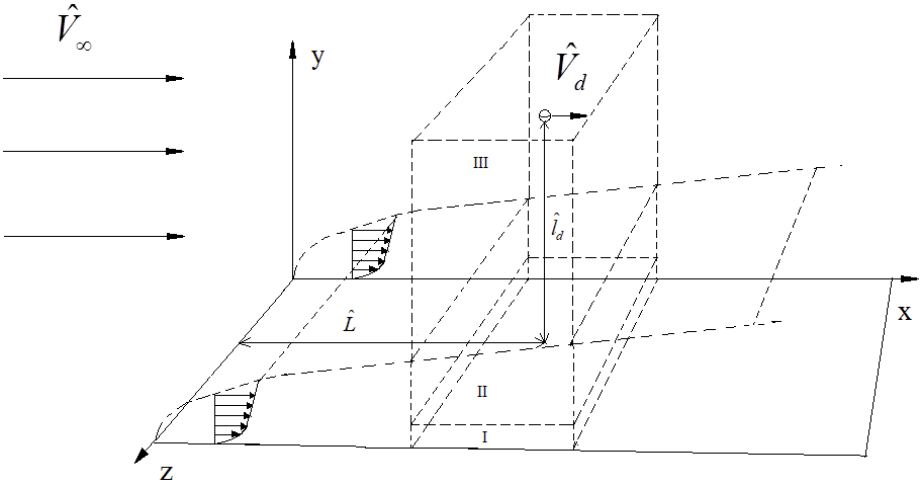

Regions: I – viscous sublayer, II – boundary layer, III – potential flow.

After applying the Fourier transform along the longitudinal coordinate x to the linear problem, the velocity components are expressed through special functions [4] in the form:

$$\hat{v}_1(k,y,z)=\int_{-\infty}^{\infty} v_1(x,y,z)e^{-ikx}dx=\frac{k_0^6\hat{p}_1-\dfrac{\partial^2\hat{p}_1}{\partial z^2}}{k_0Ai'\left(-k_0U_w\right)}\int_0^y\int_0^y Ai\left(k_0\left(-U_w+\xi\right)\right)d\xi,$$

$$\hat{w}_1(k,y,z)=\frac{\pi}{k_0^2}\frac{\partial\hat{p}_1}{\partial z}\left[\frac{Gi\left(-k_0U_w\right)}{Ai\left(-k_0U_w\right)}Ai\left(\left(-U_w+y\right)k_0\right)-Gi\left(\left(-U_w+y\right)k_0\right)\right],$$

$$\hat{u}_1(k,y,z)=-\frac{k_0^6\hat{p}_1-\dfrac{\partial^2\hat{p}_1}{\partial z^2}}{k_0^4Ai'\left(-k_0U_w\right)}\int_0^y Ai\left(k_0\left(-U_w+\xi\right)\right)d\xi-$$

$$-\frac{\pi}{k_0^5}\frac{\partial^2\hat{p}_1}{\partial z^2}\left[\frac{Gi\left(-k_0U_w\right)}{Ai\left(-k_0U_w\right)}Ai\left(\left(-U_w+y\right)k_0\right)-Gi\left(\left(-U_w+y\right)k_0\right)\right]$$

$$S_1(x,z)=-u_1\left(x,U_w,z\right),\ (ik)^{1/3}=k_0$$

Conclusions: An exact analytical solution to the linear problem in a viscous sublayer with counter flows has been found, containing a complex picture of spatial separation zones, even at small M.

The work was carried out with the financial support of the RSF (project No. 23-19-00041).

REFERENCES

1. **Antakov F.V., Zametaev V.B.** Distortion of the shape of a sphere modeled by a potential dipole in a uniform flow caused by a second dipole // Proceedings of MIPT. 2022. Vol. 14, No. 4, pp. 126–132.
2. **Sychev V.V., Ruban A.I., Sychev Vik.V., Korolev G.L. Sychev Ed.V.V.** Asymptotic theory of separated flows // M.: Nauka, 1987. 256 pp.
3. **Chzhun T.H., Bezrodnykh S.I., Zametaev V.B.** Incompressible boundary layer with countercurrents at a given pressure gradient // J. Comput. math. and math. physics 2022. V. 62. No. 6. P. 1007–1015.
4. **Abramowitz M., Stegun I.A.** Handbook of mathematical functions with formulas, graphs and mathematical tables // Translation from English edited by V.A. Ditkin and L.N. Karamzina. Moscow “Nauka”, 1979, 831 pp.

DOI 10.53954/9785604990148_12

METHOD FOR SIMULATION OF DISCHARGE OF COOLING AGENT DURING FIRE EXTINGUISHING

V.A. Arhipov, K.V. Kostyushin, V.I. Romandin, K.G. Perfil'eva, A.V. Yustus

National Research Tomsk State University
634050, Tomsk, Russian Federation

Discharge of the cooling agent into the fire center from an airplane or helicopter is one of the effective ways to extinguish large fires, especially in hard-to-reach areas. Thinly atomized water is used as a cooling agent. The volume-surface interaction mechanism is realized when exposed to atomized water affects the flame. Thinly sprayed water cools the combustion zone and at the same time blocks the vapor access of oxygen to the burning elements due to evaporation. Effective use of this method is based on the laws of liquid-drop cloud settling and its interaction with the medium near the fire center. These laws are the fundamental basis for the development of optimal modes of use of aviation means for fire extinguishing taking into account real conditions.

At simulation of the fire extinguishing processes it is necessary to consider three stages: the process of destruction of the macrovolume of liquid discharged from the discharge device with the formation of a primary cloud of polydispersed drops [1, 2]; the evolution of the aerosol cloud during settling under isothermal conditions; and the interaction of the liquid-drop cloud with the fire source [3–5].

At present, in the Russian Federation for large fires extinguishing in hard-to-reach areas, MI-8 helicopters with overflow device of VSU-5A type are used as means of delivery and discharge of the cooling agent. Conduction of the experiments and parametric studies for determining the surface irrigation density, motion dynamics, and settling dynamics of liquid-drop cloud using VSU-5A leads to large material costs. In connection, in the paper the method for modeling the discharge of cooling agent using an unmanned aerial vehicle and a model water-liquid device is proposed.

Experimental unmanned aircraft system to model the processes of discharge of the cooling agent and determine the irrigation density was developed. It includes an unmanned aircraft, cooling agent discharge system, external pilot station, control and monitoring lines, telemetry transmission system and scientific data recording system. The general scheme of the experimental complex is shown in Figure 1.

The cooling agent discharge system is shown in Figure 2 and consists of the following elements: overflow device housing, shut-off valves, water discharge actuator, housing hangers. The cooling agent discharge system is suspended from the hull of the unmanned aircraft using a set of side cables and one center cable. The unmanned aircraft is controlled and the command for cooling agent discharge is transmitted from the external pilot's station in both manual and automatic modes.

Nadir camera (planned vertical) located on the unmanned aircraft and system of high-speed cameras located in the area of cooling agent discharge are used for recording the experimental data. Machine vision algorithms are used to process the experimental data from the cameras.

Research was supported by the Russian Science Foundation № 22-19-00307, https://rscf.ru/project/22-19-00307/.

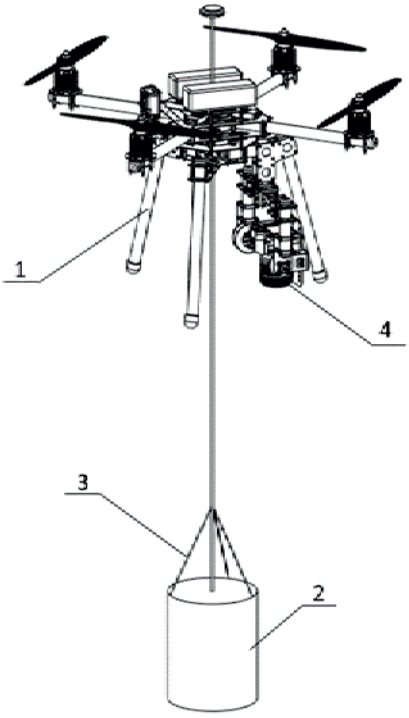

Fig. 1. Experimental unmanned aircraft system

1 – unmanned aircraft, 2 – spillway housing, 3 – supporting slings, 4 – nadir camera

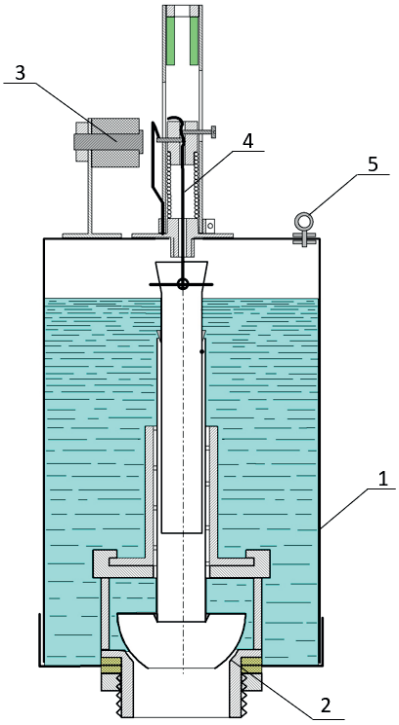

Fig. 2. Refrigerant discharge device

1 – case of overflow device, 2 – valve assembly, 3 – electromagnet, 4 – control cable, 5 – fastening elements of supporting slings

REFERENCES

1. **Kudrov M.A.** Dinamika ob”ema zhidkosti v gazovom potoke s uchetom deformatsii drobleniya i sryva kapel’ [Dynamics of the fluid volume in the gas flow considering deformation, fragmentation and blowoff of drops] // Nauchnyy vestnik MGTU GA – Civil Aviation High Technologies. 2010. Vol. 151. P. 163–168.
2. **Meshkov E.E., Oreshkov V.O., Yambaev G.M.** Obrazovanie oblakov kapel’ pri razrushenii vodyanogo yadra v protsesse svobodnogo padeniya [Droplet cloud formation upon disintegration of free-falling water ball] // Pis’ma v zhurnal tekhnicheskoy fiziki – Technical Physics Letters. 2011. Vol. 37, No 15. P. 79–85.
3. **Alekhanov Yu.V., Bliznetsov M.V., Vlasov Yu.A., Gerasimov S.I., Dudin V.I., Levushov A.E., Logvinov A.I., Lomtev S.A., MarmyshevV.V., Meshkov E.E., Semenov Yu.K., Tsykin S.V.** Metod issledovaniya vzaimodeystviya dispergirovannoy vody s plamenem [Method for studying the interaction of dispersed water with flame] // Fizika goreniya i vzryva – Combustion, Explosion, and Shock Waves. 2006. Vol. 42, No. 1. P. 57–64.
4. **Volkov R.S., Kuznetsov G.V., Strizhak P.A.** Analysis of the effect exerted by the Initial temperature of atomized water on the integral characteristics of its evaporation during motion through the zone of “hot” gases // Journal of Engineering Physics and Thermophysics. 2014. Vol. 87, No. 2. P. 450–458.
5. **Arhipov V.A, Basalaev S.A., Matvienko O.V., Perfil’eva K.G., Usanina A.S**. Generaciya i evolyuciya zhidko-kapel’nogo aerozol’nogo oblaka v pole sily tyazhesti [Generation and evolution of liquid-drop aerosol cloud in the gravity field], Tomsk, 2022. 264 p.

DOI 10.53954/9785604990148_14

METHOD FOR STUDYING THE LAWS OF THE DROPS EVAPORATION IN CONVECTIVE AIR FLOW

V.A. Arkhipov, S.A. Basalaev, O.V. Matvienko, K.G. Perfil'eva, V.I. Romandin

Tomsk State University,
634050, Tomsk, Russia

The study of the evaporation laws of liquid-drop aerosols is of practical importance at the design of energy devices, optimization of fire extinguishing technologies and in a number of other applied problems. The purpose of this work is to develop the method for experimental and theoretical studying of the evaporation laws of a single drop and cluster of monodispersed drops in order to assess the adequacy and specify the existing models of their evaporation.

Experimental studies of the evaporation rate of a single drop were carried out on a setup that included a hollow cylindrical heater, the liquid supply system, the drop size visualization system and the system for weighing a set of drops or a cluster of drops after passing through the heater. The heater consists of a ceramic tube with an internal diameter of 250 mm and a height of 1 m. The nichrome wire spirals are installed on the inner surface of the ceramic tube that are connected to the voltage source. The water supply system includes a Mariotte vessel with the studied liquid or the drop cluster supply device [1]. On the outlet of the tube the receiving tank is located on analytical balance. To determine the gas temperature in the heating zone of the tube the five thermocouples are located along its axis. The thermocouples are connected through an amplifier to an oscilloscope.

The results of the experimental study showed that the air temperature along the height of the heater changes due to the convective upward flow in the form of a dependence (Fig. 1).

Processing of the experimnetal data made it possible to obtain the approximation dependencies for the temperature distribution along the height of the heater for different values of its power (W = 1.35 kW и W = 5.20 kW).

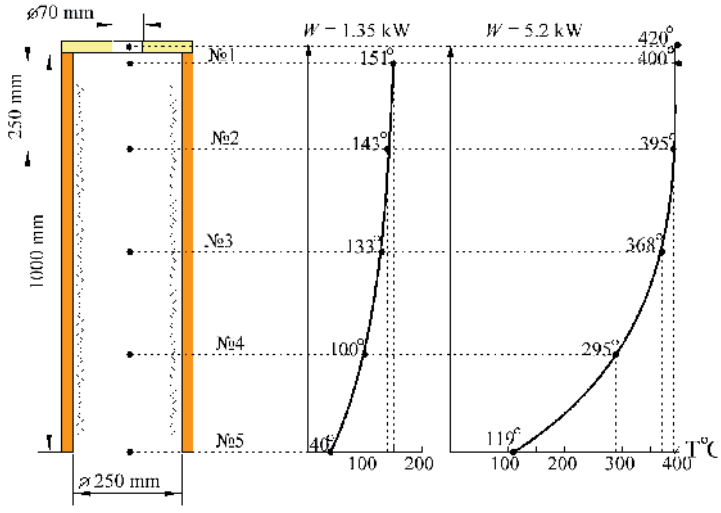

Fig. 1. Results of experimental measurements of the temperature distribution along the height of the tube for different power values of the heating device

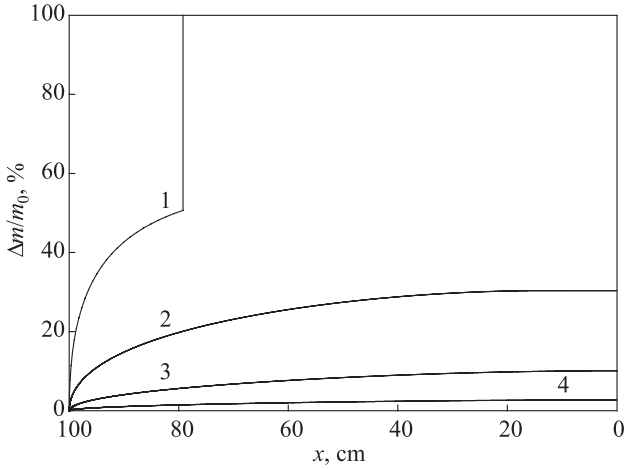

Fig. 2. Change in relative drop mass loss with height.

The drop dynamics equations can be written as [2]:

$$\rho_p \frac{dw_p}{dt} = \frac{3}{4} C_D \rho D^{-1} \left| w - w_p \right| \left(w - w_p \right) + \left(\rho - \rho_p \right) g , \quad (1)$$

where ρ_p, ρ is the drop density and air density; w_p, w is the projections of the velocity of the drop and air on the vertical axis OX directed vertically upward; t is the time; C_D is the drag coefficient; D is the drop diameter.

To calculate the drop temperature T_p the heat balance equation was used in the form [3]:

$$c \frac{dT_p}{dt} = 6 \frac{\lambda}{D^2 \rho_p} \mathrm{Nu} \left(T - T_p \right) + 3QD^{-2} \frac{dD}{dt} , \quad (2)$$

where c is the specific isobaric heat capacity of liquid; λ is the gas thermal conductivity coefficient; Nu is the Nusselt number; T is the air temperature; Q is the specific heat of evaporation.

The processes of the drop evaporation are illustrated in Fig. 2. The relative mass loss value $\Delta m/m_0$ increases as the drop size decreases. That is associated with the intensification of its heating. When the temperature of the drop reaches the boiling point, it completely evaporates: the value $\Delta m/m_0$ reaches 100%. An increase in the power of the supplied energy leads to intensified evaporation and greater mass loss. Small and medium-sized drops evaporate completely. Complete evaporation of small drops occurs at shorter distances from the top end. The temperature of small drops can reach boiling point that will cause almost instantaneous evaporation of these drops.

Research was supported by the Russian Science Foundation № 22-19-00307, https://rscf.ru/project/22-19-00307/.

REFERENCES

1. **Arkhipov V.A., Konovalenko A.I., Basalaev S.A., Zolotorev N.N., Perfil'eva K.G., Usanina A.S.** Method for determining the evaporation rate of a group of drops. Patent 2724140 RF, IPC G01N 25/12. Publ. 22.06.2020. Bull. № 18.
2. **Nigmatulin R.I.** Dynamics of Multiphase Media, Pt. 1. Moscow, 1987. 464 p.
3. **Terekhov V.I., Pakhomov M.A.** Heat and mass transfer and hydrodynamics in gas-droplet flows. Novosibirsk, 2009. 284 p.

DOI 10.53954/9785604990148_16

NUMERICAL SIMULATION OF ROTATING DETONATION OF HYDROGEN-AIR MIXTURE IN ANNULAR FLOWING CHAMBER

D.I. Babushenko, O.V. Gouskov, R.S. Sidorov

Central institute of aviation motors named after P.I. Baranov, 111116, Russia, Moscow, Aviamotornaya str., 2

For advanced power plants, one of the possible methods of organizing the operation in the combustion chamber is the combustion of a fuel-air mixture in detonation waves rotating in an annular flow path. Widely known experiments on the continuous rotating detonation of a hydrogen-air mixture were carried out at the Lavrentiev Institute of Hydrodynamics SB RAS [1]. Detonation in a flowing annular chamber of 306 mm diameter was investigated. One of the important and illustrative results is the dependence of the number and frequency of detonation waves on the mass flux density.

The results of numerical simulation of this experiment with a cylindrical annular chamber is performed in this paper. The parameters of the supplied components of the mixture were pre-calculated taking into account the behavior of their outflow from the receivers. The mass flow rate and the components ratio varied during the experiment. This variation led to the appearance of operating modes of the chamber with one, two and three detonation waves. The simulation of the flow in the chamber with taking into account the mixing of components in the three described modes was performed using an algorithm of solving of Favre-averaged Navier-Stokes equations for a reacting gas [2]. The figure shows the temperature and Mach number fields

It is shown that when combustion products flow into the atmosphere, supersonic outflow is not realized in the entire outlet section. The satisfactory correspondence of the calculated and experimental data on the number of detonation waves and the frequency of their passage is demonstrated.

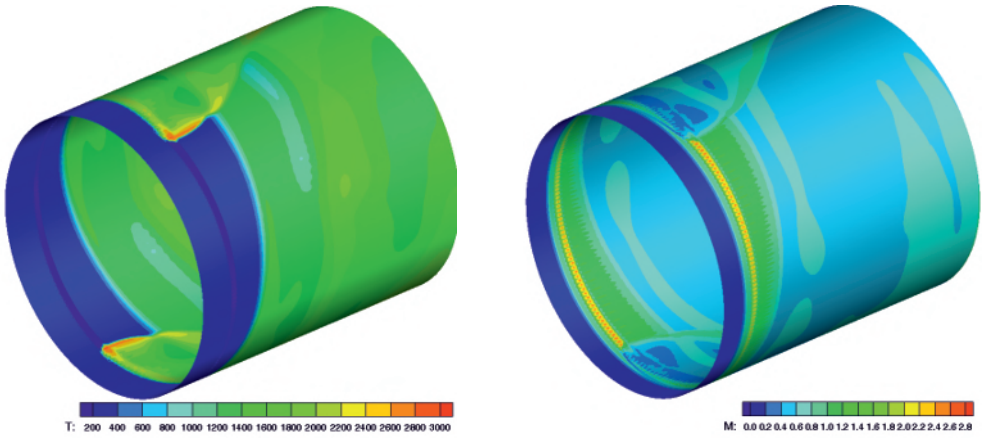

Fig. The temperature field (left) and the Mach number field (right) at the mode with two detonation waves

REFERENCES

1. **Bykovsky F.A., Zhdan S.A. and Vedernikov E.F.** Continuous spin detonation of fuel-air mixtures // Combustion, explosion and shock waves. 2006. Vol. 42, No. 4. P. 107–115.
2. **Gouskov O.V., Kopchenov V.I., Lomkov K.E., Mnatsakanyan Y.S., Prokhorov A.N., Shutov A.** Numerical and experimental investigation of supersonic mixing and combustion // AIAA Paper. 2001. No. 1821.

DOI 10.53954/9785604990148_18

PHYSICAL FOUNDATIONS OF IMPROVING PLASMA TECHNOLOGIES AT ITAM SB RAS*

D.Yu. Batomunkuev, S.P. Vashchenko, I.P. Gulyaev, O.B. Kovalev*, V.I. Kuzmin, D.V. Sergachev, A.S. Tambovtsev, P.A. Tyryshkin

Khristianovich Institute of Theoretical and Applied Mechanics SB RAS
630090, Novosibirsk, Russia

In connection with the fight against global warming, the decarbonization program of thermal technologies, aimed at eliminating or reducing the use of carbon-containing raw materials in them, is becoming of great importance. An important role in this regard is played by the development of various types of plasma technology, which makes it possible to heat almost any gas without using the heat of combustion of carbon. As part of the implementation of this task, the ITAM SB RAS is developing and researching both electric arc plasma torches [1] and thermal technologies associated with their use. Currently, two plasma research areas have emerged: the first covers the development of electric arc plasma torches of atmospheric and high pressure, as well as the creation on their basis of plasmathermal and plasmachemical technologies for heating (up to 1500–10000 K) inert gases, air, nitrogen, oxygen, methane, hydrogen, water vapor and other gases, processing of mineral raw materials, decontamination of toxic industrial and household waste, etc. The second direction combines research into the development of technologies for applying functional coatings using plasma spraying of powders, for restoration, strengthening and hardening shields for working surfaces of machine parts and mechanisms.

A series of technological plasma torches have been developed that operate with an external arc and in jet mode with an operating life of more than 1000 hours in neutral, oxidizing and chemically active gases. Figure 1, as an example, shows a jet-type electric-arc plasma torch with an intere-lectrode insert (IEI) and operating characteristics (gas flow, pressure and power) that make it possible to study the thermophysical properties of materials and coatings. The presence of a plastic housing significantly reduces the weight of the plasma torch, and also allows you to install in it collectors for supplying cooling water and plasma-forming gas, which allows you to significantly reduce the number of water and gas communications connected to the plasma torch.

Technologies have been developed for plasma spraying of protective coatings: wear-resistant (abrasion, erosion, fretting, cavitation), corrosion-resistant, heat-protective, electrical insulating, as well as with special properties: electrically conductive, anti-friction, sealing, etc.

Fig. 1. Jet plasma torch with IEI with power up to 5 MW and pressure up to 5 MPa: (a) – on a slipway; (b) – in start up mode.

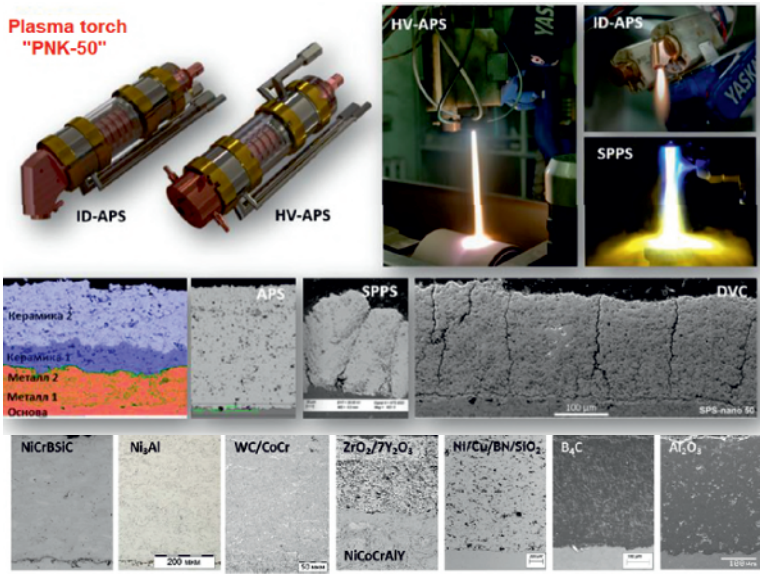

Fig. 2. Types of protective coatings obtained by atmospheric plasma spraying of powders using the "Thermo-Plasma 50-04" installation.

Materials used for spraying: metals and alloys (steels, (Ni,Co)CrAlY, Al, Co, Cu, Ni, Ti), oxides (Al_2O_3, ZrO_2, SiO_2, TiO_2, Cr_2O_3), carbides (WC, Cr_3C_2, B_4C) , metal-ceramics, composites, etc. A set of laboratory diagnostic equipment has been developed for recording two-phase flows created by nozzle attachments during plasma spraying [2]. An industrial version of plasma equipment for spraying dispersed materials (metal, ceramic, composite) has been created [3]. The "Thermo-Plasma 50-04" installation represents a modern domestic complex of atmospheric plasma spraying (APS), which uses original technical and software solutions. A digital control panel with an operator touch panel provides precise control and reproducibility of the operating mode, automation of spraying and compatibility with third-party equipment (robots, positioners, sensors, etc.). The basic installation is equipped with two electric arc plasma torches "PNK-50" with a power of up to 100 kW: high-velocity HV-APS ("supersonic") for applying dense coatings on a metal base (wear-resistant cermets WC/CoCr, Cr_3C_2/NiCr, heat-resistant alloys (Ni, Co)CrAlY, steel, bronze, etc.); high-enthalpy HE-APS ("ceramics") for applying refractory materials based on oxides (Al_2O_3, ZrO_2, Cr_2O_3, Y_2O_3, SiO_2, TiO_2). The installation can be equipped with a compact plasma torch APS-90, 185 mm long, with hoses exiting at an angle of 90 degrees, an ID-APS plasma torch for applying coatings to internal surfaces with a diameter of 115 mm, equipment for spraying suspensions and solutions of SPS/SPPS precursors, Fig. 2.

The PNK-50 plasma torch uses a circuit with IEI, which allows reducing the operating arc current to 100–200 A (at a voltage of 250–500 V) and eliminating voltage and power ripples, increasing the thermal efficiency of the plasma torch and the service life of the electrodes: cathode – up to 200–250 hours, anode – up to 400 hours. The use of air as a plasma-forming gas (instead of argon-hydrogen and argon-helium mixtures) allows reducing the cost of working gases up to 100 times, and the total operating costs up to 10 times. Plasma equipment and technologies developed on its basis are currently being successfully implemented at a number of enterprises in the Russian Federation.

REFERENCES

1. **Zhukov M.F., Zasypkin I.M., Timoshevsky A.N., Mikhailov B.I., Desyatkov G.A.** Electric arc generators of thermal plasma. Low temperature plasma. T. 17. ITAM SB RAS. Novosibirsk: Nauka, 1999.
2. **Gulyaev I.P., Dolmatov A.V., Gulyaev P.Yu., Boronenko M.P.** Method of spectral-brightness pyrometry of objects with non-uniform surface temperature. Patent RU RU2616937C2, 04/18/2017 Bulletin. No. 11.
3. **Kuzmin V.I., Kovalev O.B., Gulyaev I.P., Sergachev D.V., Vashchenko S.P., Zavarzin A.G., Shmykov S.N**. Installation of plasma spraying of coatings. Patent RU 2753844, 08.24.2021, Bull. No. 24.

DOI 10.53954/9785604990148_21

RESEARCH TO ENSURE THE CREATION OF PROMISING WIND TUNNELS OF HIGH SUBSONIC SPEEDS WITH AN OPEN TEST SECTION

N.I. Batura, G.G. Gadzhimagomedov, Yu.N. Galanskaya, A.Ya. Chudakov

Central Aerohydrodynamic Institute named after Prof. N.E. Zhukovsky, 140181, Zhukovsky, Russia

The paper presents the main results of computational and experimental studies carried out in recent years to ensure the creation of a promising wind tunnel (WT) of high subsonic speeds with high flow quality and low background noise in the open test section. The new multi–purpose industrial WT is being created to test large-scale models of aircraft for various purposes, including UAVs, high-speed rotary-wing aircraft with operating main, steering and tractor rotors at flight speeds of up to 450–550 km/h, as well as to provide research in almost all areas of aviation acoustics.

As experience in the operation of wind tunnels with an open test section shows, with certain features of their designs, significant low-frequency pressure fluctuations occur in the tunnel circuit, the amplitude and frequency of which increases with increasing speed of the flow, which leads to a deterioration in the quality of the flow, as well as to vibrations of WT structural elements and in some cases to emergency situations. According to the generally accepted concept, this problem is a consequence of the presence of a flow in the form of a free submerged jet in the open test section of the tunnel.

Turbulent jets were under close attention of researchers for quite a long time, which is determined by their wide practical application [1–4]. As is known, a mixing layer or jet turbulent layer is formed on the surface of the jet, in which large vortex structures appear, moving along the flow at speeds equal to almost half the speed of the flow. As a result, intense transfer of mass, momentum, and heat occurs in this region. In practice, there is often a need for targeted influence on the structure of the mixing layer and its characteristics. Sometimes this is due to the need for additional turbulization of the mixing layer compared to its natural level, in particular, to increase the efficiency of mixing media [2] or increase the intensity of heat transfer. In current research, it is necessary to solve the opposite problem, when it is necessary to obtain a flow in the open test section of a wind tunnel with high requirements for the uniformity and stability [3, 4].

A significant number of researches of free submerged jets was carried out in the 30–40s of the last century and was associated with the intensive development of the experimental base of subsonic aerodynamics. The relevance of this topic has not diminished in the future, in connection with the development of new wind tunnels, as well as the modernization of existing ones to obtain higher speeds of the flow compared to those implemented previously [3, 4].

The experimental part of the proposed work was carried out in a pilot TsAGI wind tunnel of a closed type with an open test section and rectangular nozzle 575 × 370 mm with beveled corners. Distance from nozzle to diffuser (jet length) L = 1300 mm. As part of the study, the speed of the flow varied in the range (10...45) m/s.

A comprehensive study of the flow structure for various variants of the design layout of the test section was carried out using modern flow diagnostic methods, in particular the PIV system for measuring velocity fields. As a result of measurements, instantaneous fields

of two velocity components in the XY plane were obtained both in the mixing layer of the jet and in flow core.

It is shown that the kinetic energy of the turbulent component of the flow in the mixing layer reaches 5% of the total kinetic energy of the flow at the nozzle exit.

In the course of the studies carried out in the operating speed range of the experimental wind tunnel, an option for the optimal configuration of the geometry of the exit edge of the nozzle and the diffuser inlet device was determined, which ensures improved characteristics in terms of uniformity and stability of the flow and significant reduction of pulsations in the mixing layer. The results of the obtained generalized experimental dependencies are presented.

The paper presents the results of computational studies of the flow features in the open test section of the wind tunnel based on numerical solutions of the Navier–Stokes equations using the ANSYS CFX software package, as well as a comparison of the calculation results with experimental data.

REFERENCES

1. **Abramovich G.N**. Theory of turbulent jets. M.: Fizmatgiz, 1960. 715 p.
2. **Zhdanov V.G.** The influence of the shape and size of vortex generators on the mixing of jet limited flows // MMF–2016: XV Minsk International Forum on Heat and Mass transfer (May 23–26, 2016): Tez. dokl. and communication. / Lykov Institute of Heat and Mass Transfer of the National Academy of Sciences of Belarus. Minsk, 2016. Vol. 1. pp. 88–93.
3. **Strelkov S.P., Bendrikov G.A., Smirnov N.A.** Pulsations in wind tunnels and methods of damping them // Proceedings of TsAGI. 1946. No. 593.
4. **Batura N.I., Vozhdaev V.V., Gadzhimagomedov G.G., Lipatov I.I.** Structure of the jet mixing layer in a wind tunnel with an open working part // Scientific notes of TsAGI. 2017. Vol. XLVIII, No. 8. Pp. 26–36.

DOI 10.53954/9785604990148_23

POSSIBLE DIRECTIONS OF TSAGI LOW-SPEED WIND TUNNEL COMPLEX EVOLUTION IN THE CONTEXT OF WORLD TRENDS

N.I. Batura, A.I. Ivanov, N.M. Lomova, A.V. Kharis

Federal Autonomous Enterprise "Central Aerohydrodynamic Institute n.a. prof. N.E. Zhukovsky" (FAE "TsAGI"), 140180, Zhukovsky, Moscow reg., Russia

Low-velocity wind tunnels (WT), which usually include facilities with air velocity less than M = 0.3, are the most numerous and diverse subclass of subsonic wind tunnels. Relative simplicity of construction and low power consumption allow to create aerodynamic laboratories on the basis of such facilities in various places: universities, colleges, industrial enterprises and even in residential premises. Naturally, the largest WTs of this class are built into the infrastructure of large aerodynamic centers, such as FAE "TsAGI". A wide variety of test types and relative ease of necessary modernizations make low-speed tunnels the most mobile group of facilities, promptly responding to the changing needs of society and industry. The main low-speed WTs have a long history of operation. Among the wind tunnels of this class there are two large facilities T-101 and T-104, which allow testing of real aircraft or their large-scale models. In ADT T-102 and T-103 a wide range of various studies are conducted, including aerodynamics at takeoff and landing conditions, as well as the study of stability and controllability characteristics of aircraft. The vertical WT T-105 simulates aircraft flat corkscrew mode and tests rotorcraft models. The T-124 low-turbulence facility allows studying laminar-turbulent transition and study laminarized aircraft layouts. The main parameters of low-speed facilities of FAE "TsAGI" are given in the table.

It should be noted that practically all large aerodynamic facilities of this speed range in all world aerospace centers have also significant age. New WTs of this class are usually created either for educational purposes or for solving certain narrowly specific tasks. The analysis of open press materials allows us to identify a number of worldwide trends characteristics of the current stage of modernization and technical re-equipment of low-speed units. The most typical are the following trends:

– focus on preferential testing of unmanned aircraft systems of different class and purpose;

– improving the productivity and energy efficiency of the experiment;

Main low-speed wind tunnels of FAE "TsAGI"

Identification	Cross-section, m	Velocity range, m/s	Origin
T-101	24 × 14 (elliptic)	5–55	1939
T-102	4 × 2,33 (elliptic)	10–55	1936
T-103	4 × 2,33 (elliptic)	10–80	1936
T-104	∅7	10–120	1939
T-105	∅4,5	2–35	1940
T-124	1 × 1	5–100	1970
T-129	∅1,2	10–80	1981
T-1-2	T-1 ∅3 T-2 ∅6	5–60	1926
T-5	∅2,2	5–55	1931

– improving the quality of the flow, reducing the level of random errors, increasing the accuracy and reliability of the results of balance tests;

– growth of informational saturation of tests, introduction of physical and panoramic-optical methods of research of flow over models. Technologies based on the use of luminescent pressure transducers (PSP) and thermal indicator coatings (TSP), methods of velocity measurement by particle images (PIV) have become widespread;

– improvement of suspension devices in the direction of expanding their capabilities, increasing the speed and accuracy of model positioning;

– capabilities of experimental facilities are supplemented by numerical modeling of flow, which increases the informativeness and productivity of the experiment;

– localization of noise sources and measurement of its parameters are performed both in specialized acoustic facilities and in conventional WTs with acoustic chambers;

– special interest in modeling the thrust reversal mode, in which the dangerous phenomenon of sucking objects from the runway into the engine intakes is studied;

– creation of special stands for modeling icing, inhomogeneous atmosphere, wind gusts, etc.

Necessity and efficiency of operation of low-speed aerodynamic installations of FAU «TsAGI» is directly related to their ability to provide the solution of urgent tasks arising before the country and society at each historical stage. The identified global trends in the development of this segment of the experimental base should be reflected in the plans for modernization and technical equipment of this class of facilities, implementation of new types of experiments and new experimental techniques.

REFERENCES

1. **Bushgens G.S., Bedrzhitskij E.L.** TsAGI is the center of aviation science. //Moscow. “Science”. 1993. – 272 p. (in Russian)
2. TsAGI – Main stages of the scientific activity, 1993–2003. Edited by G.S. Bushgens // Moscow, Fizmatlit, 2003, – 570 p. (in Russian)
3. Aerodynamics of Wind Tunnel Circuits and their Components //AGARD Conference Proceedings 585, Moscow, Russia, 1996.

DOI 10.53954/9785604990148_25

SIMULATION OF SOLID MATERIAL GASIFICATION WITH PHASE BOUNDARY DETECTION

I.A. Bedarev[1, 2], V.M. Temerbekov[1, 2]

[1]Khristianovich Institute of Theoretical and Applied Mechanics SB RAS, 630090, Novosibirsk, Russia

[2]Federal Research Center of Problems of Chemical Physics and Medicinal Chemistry RAS, 142432, Chernogolovka, Russia

The work presents the results of a numerical study of the solid material gasification when a high-temperature flow passing around it. The problem was solved in a direct formulation with the phase boundary identification [1–2]. On the left boundary of the simulated area (Fig. 1), the outflow of working gas with constant flow rate q = 0.1 kg/s, temperature T = 1500 K and pressure P = 2 MPa were set. On the right boundary, conditions of constant pressure and temperature were set. The upper boundary of the simulated area was specified as a solid wall with the no-slip condition and without heat flow. The lower boundary was the symmetry axis. The initial conditions in the simulated area were set to flow parameters identical to those at the inlet boundary. Nitrogen was used as a working gas, and a model substance with known parameters of heat capacity, density and thermal conductivity was used as a solid material. For the solid material, the conjugate problem of thermal conductivity was solved. The geometric parameters of the channel were selected in such a way that the channel throughput was approximately $\sigma = 0.33$.

Numerical modeling was carried out in a two-dimensional axisymmetric formulation based on the ANSYS Fluent software package. To simulate the phase transition from the solid to the gaseous state, a custom function was used that allows to rearrange the interface between the solid and the gaseous medium depending on the surface temperature of the body. Using built-in ANSYS Fluent tools (User Define Scalar), a source term was added at the interface to simulate the outflow of a gasified substance. Also, to additional correction of the boundary nodes movement, an implicit mesh update was used. This function updates the mesh a specified number of times during a time step. This approach allows more correctly calculation of the nodes movement and achieve a more stable solution. Test calculations showed that, within the framework of the problem under study, it is desirable to adjust the position of the nodes at least 20–25 times per time step.

As the result, the mathematical technology of direct modeling of the solid material gasification in the axisymmetric formulation with the detection of the phase transition

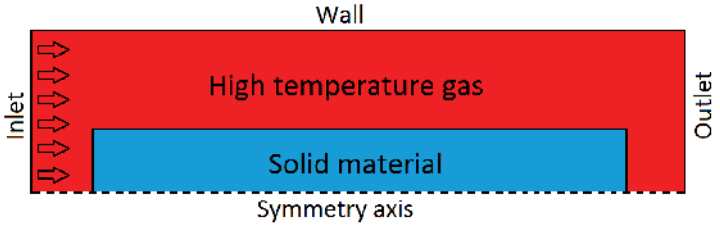

Fig. 1. Scheme of the simulated area.

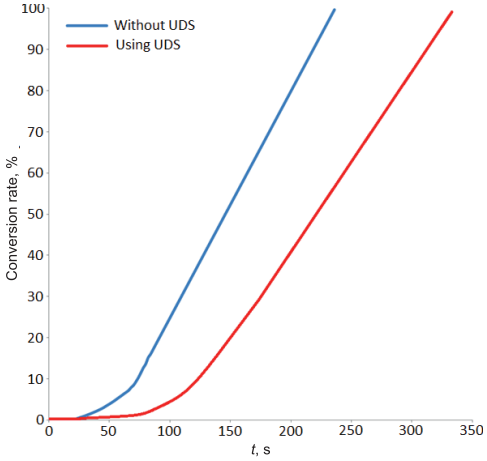

Fig. 2. Conversion rate with using UDS and without UDS.

boundary was improved. Parametric calculations of the solid material gasification taking into account the outflow of the gasified substance from the phase interface were performed.

It was shown that the addition of the gas source leads to a significant decrease in the downstream temperature from 1500 K to 900 K, which leads to a more uneven change in the position of the phase interface. The rear boundary warms up much longer than the front boundary and, as a result, gasifies less intensively. The presence of such temperature difference and uneven gasification leads to a more uneven change in the shape of the solid body and an increase in the time for complete conversion of the material (Fig. 2).

The influence of the phase transition temperature on the gasification process was studied without taking into account the outflow of gas from the phase interface. It is shown that at a sufficiently low transition temperature, the front and rear side of the object are gasified with the same intensity. An increase in temperature leads to more uneven evaporation of solid material, since the rear end of the object is slower to warm up to the desired temperature, which is consistent with experimental observations.

The influence of the speed of phase boundary nodes movement on the gasification process was studied. It was shown that parameters such as gasification temperature and the speed of boundary nodes have a significant impact on the degree of the material conversion and the uniformity of changes in the phase interface. An increase in the gasification temperature leads to a less intense conversion of the solid material. An increase in the speed of the phase boundary movement leads to intensification of the conversion. Thus, it was concluded that it is necessary to connect the step of moving the boundary with the gasification temperature and the intensity of heating of the solid material for a more correct modeling of the process under study.

The reported study was funded by the Russian Science Foundation grant No. 21-79-20008, https://rscf.ru/project/21-79-20008/.

REFERENCES

1. **Bedarev I.A., Temerbekov V.M.** Two approaches to simulation of solid fuel sublimation in a high-temperature gas flow // XXI International Conference on the Methods of Aerophysical Research (ICMAR – 2022) (Novosibirsk, 8-14 Aug. 2022): Abstr. Pt. II. – Novosibirsk: SB RAS, 2022. Vol. II. P. 16–17.
2. **Bedarev I.A., Temerbekov V.M.** Numerical modeling of the solid fuel sublimation in a high-temperature gas flow in the continuum approach and with boundary separation between two media // Chelyabinsk Physical and Mathematical Journal. 2022. Vol. 7. No. 3. P. 326–340.

DOI 10.53954/9785604990148_27

INVESTIGATION OF THE EFFECT OF MESH MODELS AND FLOW TURBULENCE ON THE FRICTION FORCE ON A FLAT SURFACE

D.B. Bekurin, V.O. Durnakov

"UEC-Aviadvigatel" JSC, 614010, Perm, Russia

The flat plate friction force obtained by a theoretical method [1] has been compared to the one obtained by mathematical simulation using computational grid of different density and at different turbulence intensities and Mach (M) number of the incoming flow. The work has been carried out to select the density of the computational grid near the surface, providing the closest to the theoretical calculated value of the friction force, as well as to assess the effect of the incoming flow turbulence intensity, set in the simulation, on the calculated friction force.

The friction force calculations were performed in two-dimensional formulation using a commercial software with k-omega SST turbulence model. The calculation model (Fig. 1) is a one-meter isolated flat plate with buffer sections, where a slipping wall is set as a boundary condition (friction force is zero). The length of the entire computational domain is 21 m, and the height is 10 m.

During the first stage, the effect of the number of mesh elements of the computational grid describing the plate (n_1) and the boundary layer (n_2) on the calculated value of the plate friction force was investigated, and then compared to the theoretical value that was calculated using the Equations (1):

$$\mathrm{Re}=\frac{\rho v L}{\mu},\quad C_W=\frac{0{,}073}{\mathrm{Re}^{0{,}2}},\quad F_X=C_W\left(\frac{\rho v^2}{2}bL\right), \tag{1}$$

where Re is the Reynold's number of the plate flow; ρ, ν, μ are the incoming flow density (kg/m^3), velocity (m/sec), and dynamic viscosity (kg/(m·sec)), respectively; C_W is the fric-

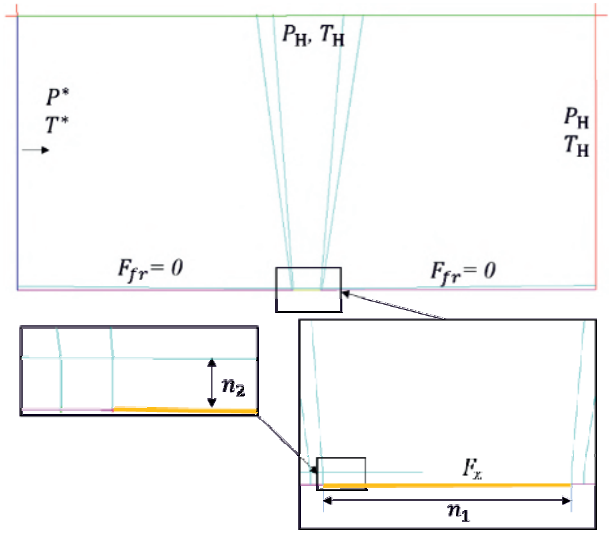

Fig. 1. Friction force simulation model

Effect of the computational grid density on the plate friction force

Total number of computational grid nodes / Number of nodes in the plate subdomain ($n_1 \times n_2$)	M	Calculated F_x, N	Theoretical F_x, N
367000 / (24 × 300)	0.8	27.29	33.09
460000 / (32 × 600)		27.82	
642000 / (40 × 1200)		27.26	

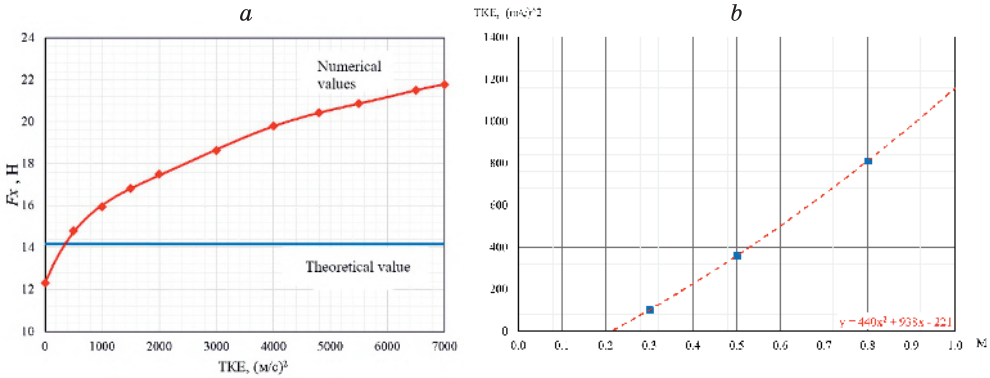

Fig. 2. TKE vs friction force at M = 0.5 (a). Combination of TKE and M to ensure that the theoretical and calculated friction force on the plate are equal (b).

tion coefficient; *b, L* are the plate width (assumed equal to 1 meter), and the plate length (m), respectively; F_x is the plate friction force (N).

Y^+ value on the plate on all computational grids does not exceed 1. According to table, there was no significant effect of the computational grid density on the friction force value: the maximum difference of the calculated friction force for different options of the computational grid was 3 %. The minimum deviation of the calculated friction force from the theoretical one was about 18 %.

During the final stage, the effect of the turbulence kinetic energy (TKE) of the incoming flow on the calculated friction force at different M was investigated. For example, Fig. 2a shows the F_x vs TKE for M = 0.5. Fig. 2b shows the TKE vs M plotted based on the results of calculations, wherein the calculated friction force agrees with the theoretical one. Given the TKE and M values calculated for the flow near any surface, we could assess the correctness of the calculated friction force on this surface.

REFERENCES

1. **Abramovich G.N.** Applied gas dynamics. Moscow, 1969, 824 pages.

DOI 10.53954/9785604990148_29

FLOW IN A PIPE WITH GAS INFLOW

A.V. Bernachuk, P.V. Chuvakhov, A.V. Fedorov

Moscow Institute of Physics and Technology
141701, Dolgoprudny, Russia

Suction of gas from the boundary layer (BL) is an effective method for reducing aircraft friction drag [1]. However, suction systems have not been used widely due to their complex design and difficulties in operation [2]. In this paper, we investigate the effectiveness of a new suction system which is glued to a wing and is a thin pipe with a gas permeable wall from above. The channel has height of H^* (hereafter, "*" denotes dimensional values) and length $\hat{L}$ its left side is sealed, and the right end is open. The external flow interconnects with the channel through permeable wall (with height l^*) from above, and through open end at the right (Fig. 1). Gas permeability of upper wall is implemented using thin cylindric pores with a diameter of d* and the distance between adjacent pores of s*.

It is assumed that such a suction system is glued to a straight wing with a sharp leading edge and to a thin parabolic airfoil of relative thickness τ. It is also assumed the wing is in the supersonic incoming flow, and its surface is uniformly heated to an adiabatic temperature T^*. In these conditions, suction is implemented in a passive way. Due to the pressure difference between the wing top and the pipe interior, gas leaks from the boundary layer into the pipe and diverts through it to the open end of the pipe, where the pressure is lowest. The gas is blown out of the pipe parallel to the surface of the wing. Here, we use numerical modeling to check the operability of the proposed suction system for a given external pressure distribution, assuming that the outlet section of the channel the pressure equals to the one above the wing in the same cross-section.

The task parameters are chosen as follows: $\tau = 0.05$ the Mach number of the incoming flow $\grave{I}_{\infty} = 2$ in each point of the channel gas temperature $T^* = 363.8\,K$; $\hat{L}^* = 4$, $H^* = 2$, $l^* = 0{,}2$, $d^* = 0.1 \cdot l^*$, Reynolds number $\mathrm{Re}_{\infty,L} = 4\nu 10^7$ heat capacity ratio $\gamma = 1.4$, Prandtl number $\mathrm{Pr} = 0.72$ A rectangular grid with uneven spacing has been created for numerical simulation. The grid cells density increases towards the top, left, and right edges of the grid. The isothermal wall condition is set on the left and lower boundaries, the subsonic extrapolation condition with a fixed pressure is set on the right, and the Darcy's law is set on the upper boundary. Viscosity is calculated according to the power law $\mu = T^{0.75}$. The problem is solved in a standard dimensionless form with characteristic scales $L^* = 4$ (length of chord), $V_{\infty}^* = 2 \cdot a_{\infty}^*$, $T_{\infty}^* = 216.7\,K$ and $\rho_{\infty}^* V_{\infty}^{*2}$ for pressure). External pressure distribution is

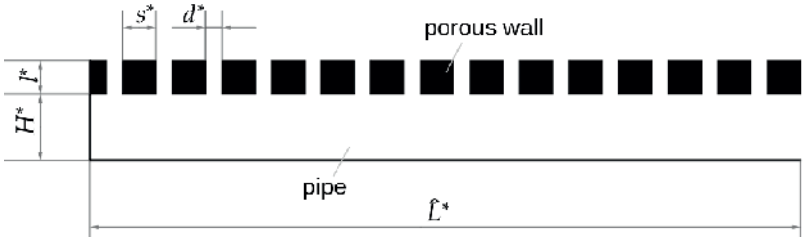

Fig. 1. The suction setup proposed by A.V. Fedorov.

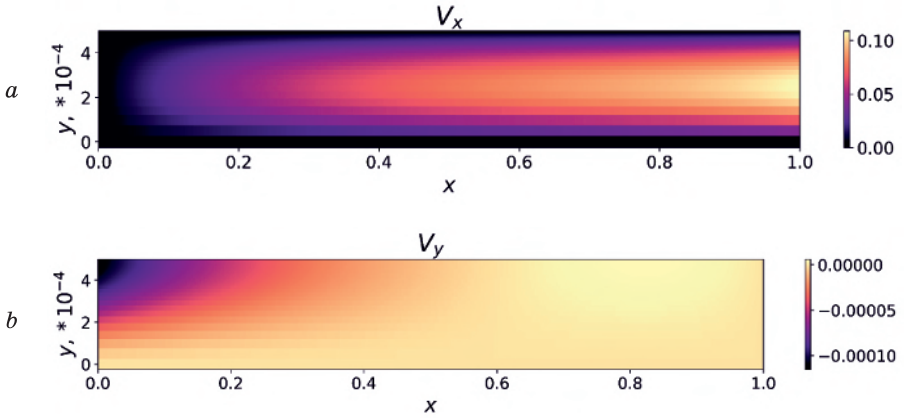

Fig. 2. Fields of gas parameters: *a* – the longitudinal velocity component, *b* – the vertical velocity component; *x* – the longitudinal coordinate, *y* – vertical coordinate of the pipe.

calculated according to the thin airfoil theory using the Ackeret's formula. The fields of gas dynamic quantities are set as initial conditions: the zero velocity field $\boldsymbol{V}_0 = (0,0)$, constant temperature field $T = 1.6788$, and pressure field in the pipe $p = 1$ Numerical modeling is carried out by establishing the solution of complete two-dimensional Navier-Stokes equations using the software package [3].

Figure 2 shows the obtained fields of longitudinal and transverse velocities. It was found that the flow accelerates towards the end of the pipe (Fig. 2a), the temperature of the gas in the pipe is not constant, but differs little from the temperature of the walls, the pressure drops towards the end of the pipe in a nonlinear manner. It was also found that for the selected configuration of the suction system, a situation emerges when gas is sucked from the BL into the pipe at the initial section of the channel, $x < x_0$ and downstream, $x > x_0$ gas is blown from the pipe into the BL (Fig. 2b), here x_0 s the section x n which the suction velocity changes sign.

In addition, we developed a simple theoretical model of the flow under consideration. A more detailed analysis of the results of numerical modeling, cross-verification of the theoretical model and numerical modeling, as well as the results of a parametric study of the problem will be presented in the report. Thus, we were able to confirm the operability of the proposed passive suction system.

REFERENCES

1. **Joslin R.D.** Aircraft laminar flow control // Annu. Rev. Fluid Mech. 1998. Vol. 30. P. 1–29.
2. **Ustinov M.V.** Laminar-turbulent transition in boundary layers (review). P. 2: Transition prediction and methods of boundary-layer laminarization// TsAGI Science Journal. 2014. Vol. 8.
3. **Novikov A.V.** Numerical simulation of stability and laminar-turbulent transition in the hypersonic boundary layer, dissertation for the degree of grand PhD in Physics and Mathematical Sciences, 2017, 229 p.

DOI 10.53954/9785604990148_31

RANS MODEL ENHANCEMENT BY MACHINE LEARNING METHODS

A. Bernard[1], S.N. Yakovenko[2]

[1]Novosibirsk State University, Novosibirsk 630090, Russia

[2]Khristianovich Institute of Theoretical and Applied Mechanics, Siberian Branch of RAS, Novosibirsk 630090, Russia

The prediction of turbulent flows is a challenging task as DNS or LES approaches require huge computing resources. Therefore, models of the Reynolds-averaged Navier-Stokes (RANS) equations are still of interest for their low computational costs. Machine learning (ML) algorithms can improve accuracy of these models [1]. To close the RANS equations, the Reynolds stress (RS) tensor τ_{ij} to be defined is often approximated using the linear eddy viscosity model, also known as the Boussinesq model (BM). It can lead to poor predictions in many cases, especially for flows with high Reynolds numbers. ML methods are used to improve RS approximations, taking high-fidelity data from experiments, DNS or LES to provide target values for RS.

The present study compares different ML methods to predict the RS anisotropy tensor, in particular: tensor basis neural network (TBNN) [2], tensor basis random forest (TBRF) [3, 4], multi-dimensional gene expression programming (MGEP) [5]. The selection of input features and tensors in the basis are discussed [3–5]. The RANS model computations are performed using OpenFOAM. Different ways to propagate the RS tensor into the RANS solver are explored.

The canonical turbulent flows considered are those in a channel with bump (BUMP) [6] and a square duct (SD) [7] with varied parameters: the bump height 20 mm $\leq H \leq$ 42 mm

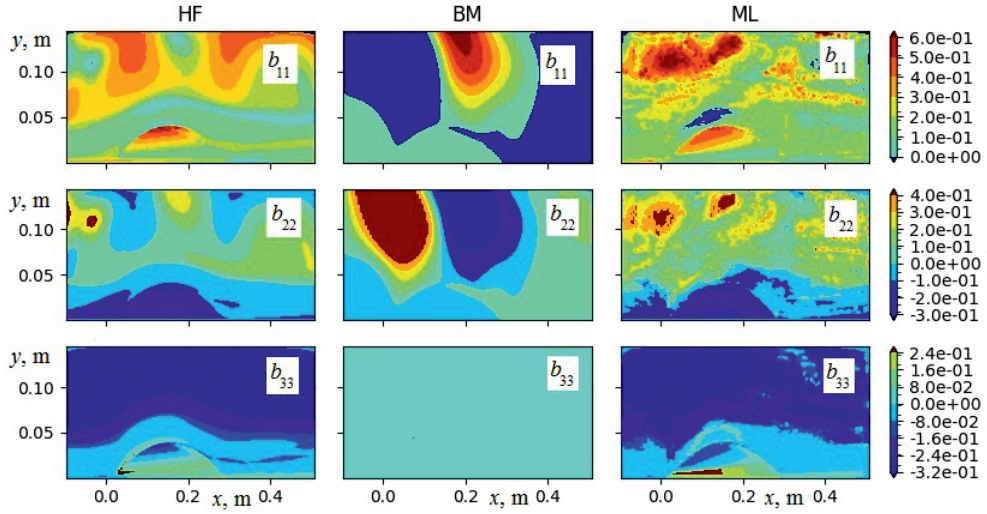

Fig. 1. Comparison between the high fidelity (HF) [6], Boussinesq model (BM), machine learning (ML) data for the Reynolds stress anisotropy tensor components normalized by the turbulent kinetic energy k.

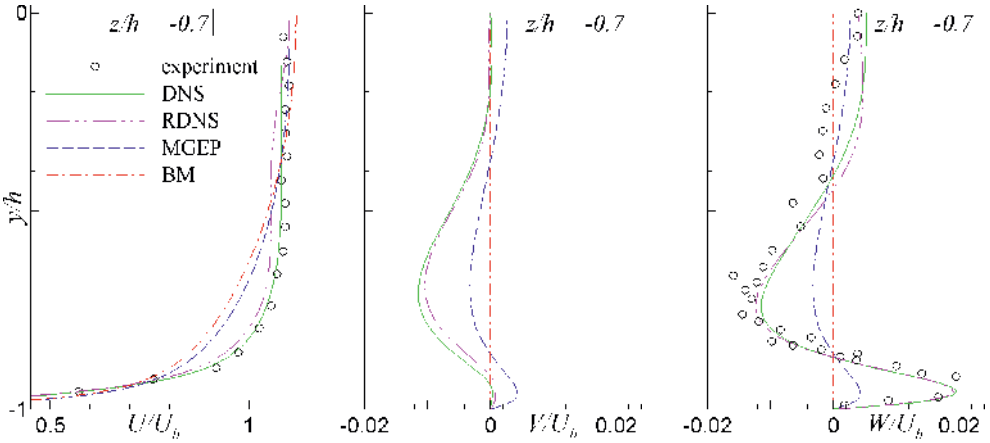

Fig. 2. The lateral distributions of the axial (U), spanwise (V) and vertical (W) mean velocity vector components from DNS [7], measurements [7], BM [5], MGEP [5], and RDNS (present study) at the section of $z = -0.7h$ for a SD flow at $\mathrm{Re} = U_b h/\nu = 3500$ where U_b is the bulk velocity, h is the duct half-height.

at the bump length 305 mm for BUMP cases, and Reynolds number $1100 \leq \mathrm{Re} \leq 3500$ for SD cases.

Figure 1 shows the obtained normal components of the normalized RS anisotropy tensor $a_{ij} = 2kb_{ij} = \tau_{ij} - (2/3)k\delta_{ij}$ for the BUMP case with $H = 38$ mm, illustrating how the TBRF algorithm can improve this quantity prediction. The a_{ij} values are to be propagated into the solver to compute other quantities of interest, e.g. the mean velocity vector components. Extra steps can be applied before propagation, such as enforcing the realizability constraints (by ensuring the values to propagate are physically realistic), and smoothing by applying a Gaussian filter.

The RS propagation from the conventional linear BM model yields the considerable deviation for the axial mean velocity component, and invalid (zero) reproduction for a secondary flow in the lateral cross-section of SD, whereas the data-driven quadratic MGEP approximation [5] improves the predictions (Fig. 2). On the other hand, the RANS-DNS runs (RDNS), where the 'frozen' a_{ij} values taken from the DNS data [7] are inserted into the RANS equations, reveal as in [8] the better performance versus that with BM or MGEP. It gives a room for further RS model enhancements by means of ML algorithms (like TBNN, TBRF or their extensions) where the high-fidelity DNS or LES data serve as target solutions, if the ML mimics are good enough.

The research was carried out within the state assignment of Ministry of Science and Higher Education of the Russian Federation.

REFERENCES

1. **Duraisamy K., Iaccarino G., Xiao H.** Turbulence modeling in the age of data // Annu. Rev. Fluid Mech. 2019. Vol. 51. P. 357–377.
2. **Ling J., Kurzawski A., Templeton J.** Reynolds averaged turbulence modelling using deep neural networks with embedded invariance // J. Fluid Mech. 2016. Vol. 807. P. 155–166.
3. **Kaandorp M., Dwight R.P.** Data-driven modelling of the Reynolds stress tensor using random forests with invariance // Comput. Fluids. 2020. Vol. 202. # 104497. P. 1–16.
4. **Bernard A., Yakovenko S.N.** Enhancement of RANS models by means of the tensor basis random forest for turbulent flows in two-dimensional channels with bumps // J. Appl. Mech. Tech. Phys. 2023. Vol. 64, No. 3. P. 437–441.

5. **Li H., Yakovenko S.N.** Application of machine learning methods to develop algebraic Reynolds-stress models for flows in channels // Turbulence, Heat and Mass Transfer 10: Proceedings of the Tenth International Symposium on Turbulence, Heat and Mass Transfer / Eds. K. Hanjalić et al. – Begell House Inc., 2023. P. 345–348.
6. **Matai R., Durbin P.** Large-eddy simulation of turbulent flow over a parametric set of bumps // J. Fluid Mech. 2019. Vol. 866. P. 503–525.
7. **Pinelli A., Uhlmann M., Sekimoto A., Kawahara G.** Reynolds number dependence of mean flow structure in square duct turbulence // J. Fluid Mech. 2010. Vol. 655. P. 107–122.
8. **Wu J.-L., Xiao H., Paterson P.** Physics-informed machine learning approach for augmenting turbulence models: A comprehensive framework // Phys. Rev. Fluids. 2018. Vol. 3. 074602. P. 1–28.

DOI 10.53954/9785604990148_34

SMALL ICING WIND TUNNEL OF ITAM: EXPERIMENTAL TECHNIQUES, INSTRUMENTATION, AND FLOW PARAMETERS

A.A. Bogdanov, Yu.M. Prikhodko, A.A. Sidorenko, A.M. Sorokin, A.M. Shevchenko, A.N. Shiplyuk, A.S. Shmakov

Khristianovich Institute of Theoretical and Applied Mechanics of the Russian Academy of Sciences, 630090, Novosubirsk, Russia

A brief overview of the work on the commissioning of the small icing wind tunnel (SIWT) of ITAM and the development of experimental techniques for studying the aircraft icing and industrial structures, and the development of methods and means of anti-icing protection is presented.

The small icing wind tunnel is a closed-type subsonic wind tunnel with a closed test section [1]. The test section size is 360×500×1000 mm. The air flow is generated by an onee-stage axial fan OV-8. The required power of the electric drive is 25 kW.

To date, the thermal insulation of the flow duct has been fully completed. Both flow cooling and flow watering system have been put into operation.

The system for measuring flow parameters in the working part of the MKAT includes equipment from the State Register of Measuring Instruments and allows you to measure:

– static pressure in the prechamber – using a Metran 150CGR pressure sensor;

– pressure difference between the prechamber and the test section – using a Metran 150CDR pressure sensor;

Fig. 1. SIWT of ITAM

– temperature and humidity in the flow duct – using the OWEN PVT100 temperature and humidity meter.

Data recording from pressure, temperature and humidity sensors is carried out by the LCard LTR measuring system with LCard Measurement Studio software. The injectors are controlled by the Simple Scada system.

The shape and size of the ice formed was determined using Thor3D Calibry and RangeVision PRO 3D scanners.

Determination of the dispersed composition of the cloud of droplets was carried out using a Malvern Spraytec spray analyzer and a software and hardware module for visualization and panoramic diagnostics of gas-droplet flows PolisSpray.

The water injection section is located in the prechamber at a distance of 3 m from the beginning of the test section. This distance is necessary to achieve thermal equilibrium of droplets with air. The section contains 6 rods that have an aerodynamic shape with low drag. Each boom contains 5 nozzles and 10 valves for remote shutdown of each nozzle. The injection system includes a system for purging the water supply lines with compressed dry air.

Pressure probe measurements in the test section showed the ability to maintain a stable velocity in the range from 10 to 65 m/s.

In experiments with the watering system to determine the dispersed composition of the droplet cloud, the average median droplet size was recorded from 12 to 80 μm and the liquid water content from 0.3 to 3 g/m^3.

Tests of a flow cooling system, consisting of a heat exchanger and a cooling module built into the flow path, showed the ability to maintain a given flow temperature in the range –30 C...+5 C with fluctuations not exceeding 1 C

Tests of a flow cooling system, consisting of a heat exchanger built into the flow duct, and a cooling module, showed the ability to maintain a flow temperature in the range –30 C...+5 C with fluctuations not exceeding 1 C.

The study was conducted at the Equipment Sharing Center «Mechanics» of ITAM SB RAS.

The research was carried out within the state assignment of Ministry of Science and Higher Education of the Russian Federation.

REFERENCES

1. **Prikhodko Yu.M., Sidorenko A.A., Shmakov A.S., Shevchenko A.M., Sorokin A.M., Bogdanov A.A., and Shiplyuk A.N.** Small icing wind tunnel based at the Khristianovich Institute of Theoretical and Applied Mechanics of the Siberian Branch of The Russian Academy of Sciences // Journal of Applied Mechanics and Technical Physics, 2023, Vol. 64, No. 6, pp. 1015–1024.

DOI 10.53954/9785604990148_36

SUBSONIC FLOW AT A TWO-DIMENSIONAL BACKWARD-FACING STEP UNDER CONDITIONS OF LOW-FREQUENCY IMPACT

A.V. Boiko, A.V. Dovgal, A.M. Sorokin

Khristianovich Institute of Theoretical and Applied Mechanics SB RAS
630090, Novosibirsk, Russia

The long-standing subject of research on subsonic shear flows is the assessment of different methods of boundary-layer separation control [1–3]. In particular, such methods include the use of control oscillations, which stimulate the amplification of boundary-layer instability waves at laminar flow separation, causing changes in its instantaneous and time-averaged characteristics. In the present work, a similar approach to control the separation of a laminar boundary layer by generating «slow» oscillations of the separation zone with frequency of an order of magnitude less than the characteristic frequency of disturbances of the separated layer with maximum increments is considered.

Experimental results were obtained in the low-turbulence subsonic wind tunnel T-324 of ITAM SB RAS, which is a facility with a closed test section with dimensions of $1\times1\times4$ m^3. The flow at a two-dimensional rectangular backward-facing step formed by a junction of two flat plates of 300 and 465 mm length and 995 mm width, located along the direction of the oncoming flow was studied. The height of the step was varied between 2.8 and 3.0 mm, and the free-stream flow velocity was varied between 8.7 and 10.0 m/s. Two flow configurations were considered. In the first one, the low-frequency oscillations of the separation zone

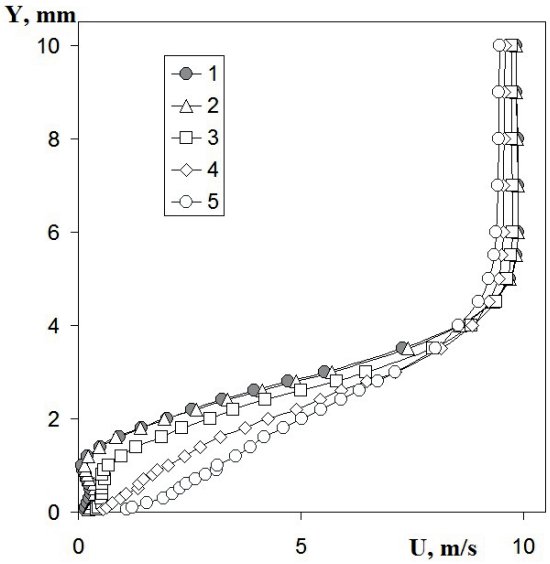

Fig. 1. Mean velocity profiles near the boundary-layer reattachment 45 mm downstream the step without low-frequency excitation (1) and as the amplitude of generation through the slit 1 mm downstream the step at frequency 10 Hz increases (2–5).

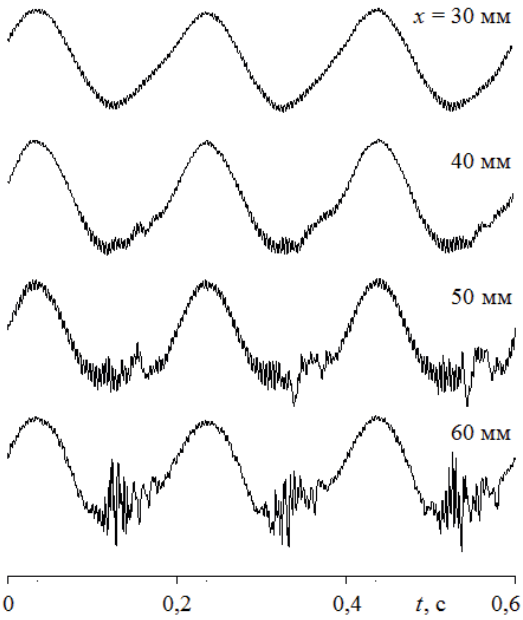

Fig. 2. Hot-wire anamometer signals with oscillations generated 55 mm downstream the step at a frequency of 5 Hz.

were excited by a dynamic loudspeaker, which was connected through a pipe to a 70 mm long and 0.4 mm wide spanwise slit in the back plate at a distance of 1 mm behind the step. In the second case, the slit was located near the flow reattachment 55 mm behind the step.

The initial data were obtained by a hot-wire anamometer with a single-wire, which was calibrated in free stream according to the readings of a Prandtl tube. The anamometer signal was processed with a personal computer. The measurements were performed in the central section of the experimental model.

The main result of the study is summarized in Fig. 1. It shows the mean-velocity profiles at the rear part of the separation zone in the absence of low-frequency excitation and with the increase of its intensity. As the amplitude of oscillations grows, the velocity distributions become more “filled”, which is an indication of a reduction of the extent of the separation region. A plausible explanation for the obtained result is that the low-frequency impact modulates in time the stability of the separated boundary layer, resulting in changes in the time-averaged flow characteristics. Figure 2 illustrates this idea: a synchronization of low-frequency oscillations with amplification of short-wave instability of the separated flow is evident, the maximum increments of convective disturbances being in the frequency range of 200–300 Hz.

The results of the experiments shows the applicability of generation of low-frequency oscillations to control the laminar boundary-layer separation at subsonic flow velocities. Excitation of low-frequency disturbances of the separation zone makes it possible to change its size and time-averaged velocity field.

The study was conducted at the Equipment Sharing Center «Mechanics» of ITAM SB RAS.

REFERENCES

1. **Chang P.K.** Control of flow separation. Washington: Hemisphere, 1976.
2. **Gad-el-Hak M.** Flow control: passive, active, and reactive flow management. Cambridge: Cambridge university press. 2000. 442 p.
3. **Greenblatt D., Wygnanski I.J.** The control of flow separation by periodic excitation // Prog. Aerosp Sci. 2000. Vol. 36. P. 487–545.

DOI 10.53954/9785604990148_39

ON INFLUENCE OF GASIFIER LENGTH ON GASIFICATION PROCESS OF SOLID POROUS FUEL IN A LOW TEMPERATURE GAS GENERATOR

K.G. Borovik, N.A. Lutsenko

Institute of Automation and Control Processes FEB RAS
690041, Vladivostok, Russia

Low-temperature gas generators (GG) produce gas flow at relatively low temperatures. They are used in various applications, including fire-extinguishing systems [1, 2], airbags [3], and the aviation industry [4–7]. The gas generator's charge consists of two separate parts [8]: the first part contains a solid propellant, which burns and transforms into hot gas, that enters the second part of the GG containing a cooler. In this paper, solid porous fuel is considered as the cooler. The part of the GG containing the solid porous fuel will be called a gasifier. The hot gas formed during the combustion of solid propellant in the GG enters the gasifier and is filtered through the solid porous fuel, which turns into gas when heated (gasified). As a result, the temperature of the incoming gas decreases and its mass increases due to the gasification products of the porous fuel [9, 10].

To describe the processes taking place in the gasifier, we use a mathematical model based on the interaction of interpenetrating continua [11], which is described in detail in [12]. It includes the energy equations for the solid medium and the gas, the equations of motion, continuity and the perfect gas state, and also takes into account the change in the molar mass of the gas mixture. In order to calculate the processes described by this model, a finite volume numerical method was developed and implemented as a solver for the OpenFOAM package [13]; the method is based on the SIMPLE algorithm [14]. The solver was tested on known experimental data and showed good agreement between the computational results and the experimental data.

The present work is devoted to the study of the influence of the gasifier length on the gasification process of the solid porous fuel, which is contained in the gasifier, and on the operating characteristics of the low temperature gas generator. For this purpose, numerical calculations of the process in gasifiers with lengths of 0.25, 0.5, 1 and 2 m have been carried out at different temperatures and flow rates of incoming gas. Polyethylene, polymethylmethacrylate and urotropine have been considered as solid porous fuels, and nitrogen has been considered as the incoming inert gas.

Numerical calculations have shown that the operating time of the gasifier depends on its length disproportionately: an increase in the length of the gasifier does not lead to a proportional increase in its operating time, but to a much smaller one. The reason for this non-proportional dependence is a delay in the gasification process at the initial time, which is not affected by the length of the gasifier: such a delay occurs for both long and short gasifiers. It has been shown that the gasification wave velocity depends on the temperature and flow rate of the gas entering the gasifier, but not on the length of the gasifier. An important regularity has been found: if the length of the gasifier and the flow rate of the gas entering the gasifier are changed in the same way (i.e., if the Strouhal number is the same), then the operating time of the gasifier does not change. This can be seen from Figure 1, which shows the gas temperature at the outlet of the gasifier containing polymethylmethacrylate: curves 1 and 4, 3 and 6, 5 and 8, corresponding to the same Strouhal number, coincide.

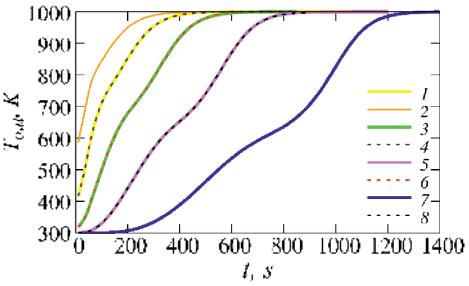

Fig. 1. The gas temperature at the outlet of the gasifier for different lengths of the gasifier H and the gas filtration rate at the inlet u_{in}:

1 – H = 0.25 m, u_{in} = 0.5 m/c; 2 – H = 0.25 m, u_{in} = 1 m/c; 3 – H = 0.5 m, u_{in} = 0.5 m/c; 4 – H = 0.5 m, u_{in} = 1 m/c; 5 – H = 1 m, u_{in} = 0.5 m/c; 6 – H = 1 m, u_{in} = 1 m/c; 7 – H = 2 m, u_{in} = 0.5 m/c; 8 – H = 2 m, u_{in} = 1 m/c.

REFERENCES

1. **Kim A., Liu Z., Crampton G.** Study of Explosion Protection in a Small Compartment // Fire Technol. 2007. Vol. 43, No. 2. P. 145–172. doi.org/10.1007/s10694-007-0008-6
2. **Karpov A.I., Leschev A.Y., Lipanov A.M., Leschev G.A.** Production of fire extinguishing mixture by solid propellant propulsion // J. Loss. Prev. Process. Ind. 2013. Vol. 26, Issue 2. P. 338–343. doi.org/10.1016/j.jlp.2011.10.007
3. **Seo Y.-D., Chung S.H., Yoh J.J.** Automotive Airbag Inflator Analysis Using the Measured Properties of Modern Propellants // Fuel. 2011. Vol. 90, No. 4. P. 1395–1401. doi.org/ 10.1016/j.fuel.2010.12.042
4. **Yang S., He G.Q., Liu Y., Li J.** Turbocharged Solid Propellant Ramjet for Tactical Missile // Appl. Mech. Mater. 2012. Vol. 152–154. P. 204–209. doi.org/ 10.4028/www.scientific.net/AMM.152-154.204
5. **Hong M.** Experimental Correction of Combustion Gas Properties of AN-based Composite Solid Propellant Used for Turbo-Pump Starter // Aerosp. Sci. Technol. 2012. Vol. 16. P. 56–60.
6. **Patel A., Frederick R.A.** Gas cooling generator technologies for aerospace applications // AIAA Propulsion and Energy Forum. 2019. doi.org/10.2514/6.2019-4068
7. **Zhao X., Xia Z., Ma L. Li Ch, Fang Ch.** Research progress on solid-fueled Scramjet // Chinese J. Aeronaut. 2022. Vol. 35, Issue 1. P. 398–415. doi.org/10.1016/j.cja.2021.06.002
8. **Salgansky E.A., Lutsenko N.A.** Effect of solid fuel characteristics on operating conditions of low-temperature gas generator for high-speed flying vehicle // Aerosp. Sci. Technol. 2021. Vol. 109. Article 106420. doi.org/10.1016/j.ast.2020.106420
9. **Li Ch., Xia Zh., Ma L., Zhao X., Chen B., Feng Y., Yang P.** Experimental investigation on the ignition delay of fuel-rich mixture in solid rocket scramjet // Acta Astronaut. 2022. Vol. 190. P. 112–117. doi.org/10.1016/j.actaastro.2021.10.001
10. **Amelin I.I., Salgansky E.A., Volkova N.N., Zholudev A.F., Alekseev A.P., Polianczyk E.V., Manelis G.B.** Parametric domain of the stationary filtration combustion wave in the charge with a low carbon content // Russ Chem. B+. 2011. Vol. 60, No. 6. P. 1150–1157. doi.org/10.1007/s11172-011-0180-1
11. **Nigmatulin R. I.** Dynamics of Multiphase Media, Hemisphere Publ. Corp., New York, 1990. 507 p.
12. **Borovik K.G., Lutsenko N.A., Fetsov S.S., Salgansky E.A.** Simulation of Gasification of a Two-Layer Porous Polymer in a Low-Temperature Gas Generator // Combustion, Explosion, and Shock Waves. 2023. Vol. 59, No. 4. P. 432–439. DOI: 10.1134/S0010508223040056
13. www.openfoam.com (last access on 28.03.2024)
14. **Patankar S.** Numerical Heat Transfer and Fluid Flow (Hemisphere Publ. Corp., New-York, 1980. 197 p.

DOI 10.53954/9785604990148_41

SPECIFICS OF NUMERICAL SIMULATION OF VORTEX STRUCTURE IN WING-BODY JUNCTION FLOW

I.S. Bosnyakov, A.V. Wolkov, N.A. Klyuev

FAU Central Aerohydrodynamic Institute named after prof. N.E. Zhukovsky
140180, Zhukovsky, Russia

The flow near the junction of the wing and a flat surface is considered. An air flow with a speed of 27 m/ s forms a thick boundary layer near a flat surface. A wing is installed perpendicularly to the flow. Wing is symmetrical with thickness T = 71.7 mm, wing chord is 4.254 T.

A complex system of vortices is formed near the junction of the wing and the surface. The main horseshoe-shaped vortex bends around the wing and evolves, forming an angular separated flow.

This flow was studied in [1] at $\mathrm{Re}_T \sim 2\times10^5$ experimentally. The phenomenon of bimodality was found – the flow is unsteady, the main horseshoe-shaped vortex "breathes". It alternately occupies two positions – closer and further regarding to the leading edge of the wing (if looking in the symmetry plane in front of the wing).

The problem turned out to be difficult from a computational point of view. The formation of a boundary layer and the flow around a wing far from the joint is resolved readily using modern numerical techniques. At the same time, the flow near the junction is characterized as separation and vortex dominated. Under such condition, industrial turbulence models mispredict the positions of separation and reattachment points.

The flow structure is studied in [2], where one can find the results of direct numerical simulation of the problem at $\mathrm{Re}_T \sim 1\times10^5$. The computational domain is shown in Fig. 1. These results are utilized for numerical schemes validation and tuning purposes.

This paper presents the results of numerical simulations with different turbulence models. The task setup is taken mainly from [2]. Based on the results of experiment and DNS data, an analysis is carried out to study whether practically significant results are within reach with simplified formulations and available computing resources.

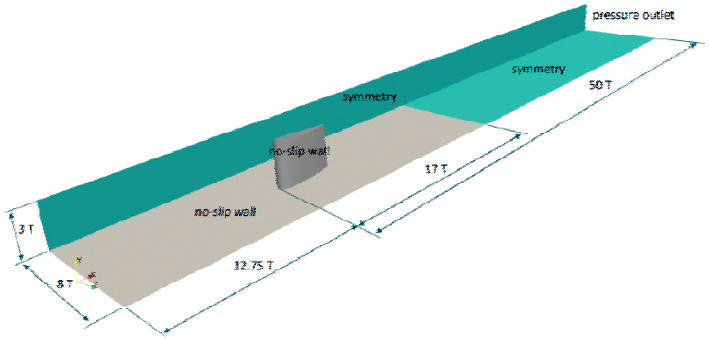

Fig. 1. Scheme of the computational domain for studying the flow

The study was supported by a grant from the Russian Science Foundation No. 23-11-00210, https://rscf.ru/project/23-11-00210/ .

REFERENCES

1. **Devenport WJ, Simpson RL** Time-dependent and time-averaged turbulence structure near the nose of a wing-body junction // J. Fluid Mech. – 1990. – No. 3 (210) – P. 23–55
2. http:// kbwiki . ercoftac.org/w/index . php ?title=DNS_ 1-6_Description

DOI 10.53954/9785604990148_43

DETERMINATION OF AMPLITUDE-FREQUENCY CHARACTERISTICS OF HOT-WIRE ANEMOMETER WITH SENSOR

D.A. Bountin, O.I. Vishnyakov, P.A. Polivanov

Khristianovich Institute of Theoretical and Applied Mechanics SB RAS
630090, Novosibirsk, Russia

The hot-wire method makes it possible to measure average and unsteady flow characteristics with frequencies up to hundreds of kilohertz. However, to obtain correct spectra, it is necessary to know the amplitude-frequency response (AFC) of the sensor + hot-wire/hot-film anemometer system. It is usually determined by applying a rectangular or pulse signal to the Wheatstone bridge of the device. Then, based on the response of the system, the frequency response can be obtained. However, it would be desirable to have a more reliable experimental way to check the frequency response of the system. This method was proposed by the authors in [1]. This work is a continuation of the previous work testing of the proposed method for obtaining the frequency response of the system in the presence of an external flow.

The method is based on obtaining the response of a anemometer sensor to pulsed heating by laser radiation. The laser used in the work creates a pulse with a duration of about 10 ns, which is several orders of magnitude less than the resolution of a hot-wire anemometer and can be considered a delta function, the spectrum of which is well known. In this work, several options for improving the method [1] are considered: changing the width of the laser spot, laser power, and flow speed.

A Litron Lasers NANOL 135-15 laser was used as a thermal source, with a pulse energy of up to 135 mJ and a pulse duration of about 10 ns. The heating area of the sensor's sensitive element was regulated using a slit, the width of which was controlled with an accuracy of 0.05 mm. The tests used constant temperature anemometer (CTA) TPS18-8 (ITPM SB RAS) and AN-1003 (A.A. Lab System, Israel). The CTA response was digitized using a Tie-Pie Handyscope HS6D ADC with a frequency of 650 kHz.

Two types of sensors were used in the work: wire-probe and thin-film probe. The wire-probe was a standard hot-wire sensor made of tungsten wire with a diameter of 10 μm and a wire length of 1.8 mm. Thin-film sensor PDA-10 was developed and manufactured at ITAM SB RAS. The experiments were carried out at overheating Rh/Rc = 1.75 for a wire-probe and 1.4 for a thin-film sensor, where Rc is the resistance of the sensor at room temperature, Rh is the resistance of the heated sensor.

Unlike previous work [1], the sensors were placed in an aerodynamic installation that created an air flow at a speed of 5 m/s. The film sensor was located on the wall of the installation, in the region of a developed turbulent boundary layer with a thickness of about 4 mm, the wire-probe was placed in the center of the cross section of the test section.

In the work the response spectra of the CTA with probe were obtained for various calibration parameters: different heating area, different heating power density, different CTA settings. From the measured spectra, cutoff frequencies were obtained (the frequency at which the amplitude in the signal spectrum drops by 3 dB) and time constants of the system for the wire-probe and surface sensor were derived. The influence of the

Fig. 1. Thin-film surface sensor PDA-10.

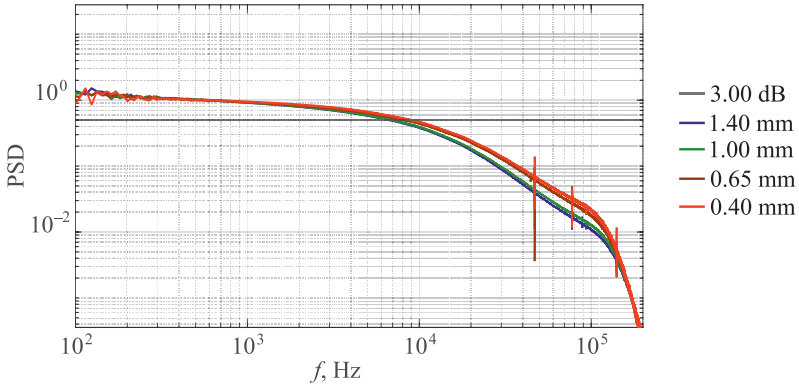

Fig. 2. Change in the power spectrum of the response of the CTA and the PDA-10 sensor to a pulsed thermal effect depending on the width of the laser pulse. Blue line – slit width 1.4 mm; green line – 1 mm; brown line – 0.65 mm; red line – 0.4 mm. Gray line – drop in spectrum amplitude by 3 dB.

above parameters on the frequency response was determined. The frequency characteristics are compared with the standard method for determining the frequency response for CTA.

The study was carried out within the framework of the state assignment of the ITAM SB RAS.

REFERENCES.

1. **Bountin D.A., Vishnyakov O.I., Polivanov P.A., Sidorenko A.A., Gromyko Yu.V.** Determination of the amplitude-frequency characteristics of the anemometer-sensor system using a laser pulse // Thermophysics and aeromechanics. 2024. In press.

DOI 10.53954/9785604990148_45

COMPUTATIONAL-EXPERIMENTAL INVESTIGATIONS THE WING SECTION OF A REGION AIRCRAFT

N.N. Bragin, V. I. Chernousov, E.A. Pigusov, V.S. Zamaraev, E.A. Zavarzina

Central Aerohydrodynamic Institute named after Prof. N.E. Zhukovsky (TsAGI)
140180 Zhukovsky St. 1, Zhukovsky, Moscow Region, Russia

One of the priority growth area of transport link in Russia is design and improvement of region aircrafts. That class of airplanes should be answered modern purposes of safety and environmental friendliness. Additionally, they should be more economically advantageous for high-volume production. One of the service condition of that class airplanes is possibility take-off and landing on a short runway. Solution of this sort of question requires detailed studying of high-lift devices.

The wing section of an aircraft with optimized high-lift devices and the propeller was made for that task execution. At the first stage complex of computational-experimental investigations isolated of the wing section was carried out. The experiment was performed in the TsAGI low-speed wind tunnel in wide range of angles of attack. Test results confirmed high wing lifting efficiency and efficiency of high-lift devices in cruise and landing-and-takeoff regimes which were obtained by numerical investigations.

Data analysis confirms download high aerodynamic and moment characteristics during design.

Offered variation of high-lift devices can be applied on being created region airplanes. Such aircrafts will use different classes runway in so inaccessible regions of our country.

Further work of carrying out of tests with a purpose of obtaining pressure distributions and characteristics of the layout wing section with the active propeller is planned.

DOI 10.53954/9785604990148_46

IDENTIFICATION OF THE MULTIPOLE STRUCTURE OF AEROACOUSTIC SOURCES USING SPECTRAL PROPER ORTHOGONAL DECOMPOSITION

O.P. Bychkov, G.A. Faranosov

Central Aerohydrodynamic Institute named after Professor N.E. Zhukovsky
105005, Moscow, Russia

In aeroacoustic problems, when studying noise generated by turbulent flows, one often deals with sources of various multipole order. Thus, pulsations of mass flow correspond to monopole radiation, pulsations of force correspond to dipole radiation, pulsations of Reynolds stresses correspond to quadrupole radiation [1], and in some flows higher order multipoles may also be significant [2]. Therefore, identification and characterization of multipole noise components of the source can be useful from the viewpoint of non-invasive diagnostics of the physical mechanisms responsible for noise generation.

It is well known [3] that the solution of the wave equation in an infinite stationary medium on a spherical surface surrounding a source of sound can be represented as a decomposition over a complete system of spherical functions $Y_l^n = e^{in\varphi} P_l^{|n|}(\cos\theta)$, where φ and θ are azimuth and polar angles respectively, of the spherical coordinate system, and $P_l^{|n|}(\cos\theta)$ are the associated Legendre polynomials, $l \geq |n|$. For acoustically compact stationary sources located in the center of the spherical coordinate system, there is an unambiguous correspondence between its "physical" multipole components associated with various noise generation mechanisms and spherical functions, i.e. the value l corresponds to the order of the physical multipole: $l = 0$ is monopole radiation containing only an axisymmetric azimuthal component $n = 0$; $l = 1$ is a dipole consisting of two azimuthal components $|n| = 0, 1$; $l = 2$ is a quadrupole containing three azimuthal components $|n| = 0, 1, 2$, etc. The effects of convection and refraction "distort" the directivity of such basic multipoles in the direction of the incoming flow, but their unambiguous relationship with the azimuthal harmonics n is preserved.

It is this interpretation of the azimuthal components of the sound field of aeroacoustic sources that formed the basis of the azimuthal decomposition technique (ADT), developed and implemented in TSAGI [4, 5]. ADT measurements are usually carried out using azimuthal microphone arrays [4, 5], and the number of microphones in each section should not be less than the number of significant azimuthal modes. In some cases none of the above methods of azimuthal decomposition can be implemented due to various geometric limitations (congestion of equipment, proximity of reflective surfaces, etc.). In this case, the task of determining the multipole structure of the source using the most convenient configuration for acoustic measurements: an array of microphones distributed along an arc of a circle around the source (along the polar coordinate θ).

In this work, it is proposed to use spectral proper orthogonal decomposition (SPOD) for such an assessment. In the last decade, SPOD has taken a strong place among the tools used for the investigation of turbulent flows, allowing, for example, to identify spatio-temporal coherent structures in such flows and conduct their detailed analysis [6, 7]. In this paper, in contrast to previous studies, SPOD is designed in such a way that, as a result of its application to the far-field measurements, it is possible to define the type of multipole source and quantify the intensity of its multipole components. The description of the method based

on SPOD is given, the justification for the adequate choice of the inner product for the analysis of an acoustic far field is given. The efficiency of the method is evaluated using the example of model point multipoles, as well as on a set of experimental data obtained in an anechoic chamber AC-2 at TsAGI. The advantages and limitations of the method are compared with those of ADT [4, 5] and beamforming methods [8, 9].

REFERENCES

1. **Curle N.** The Influence of Solid Boundaries on Aerodynamic Sound // Proc. Roy. Soc. (London) Ser. A. 1955. Vol. 231. No. 1187. P. 505–514.
2. **Kopiev V.F., Zaitsev M.Yu., Chernyshev S.A., Ostrikov N.N.** Vortex ring input in subsonic jet noise // Int. J. Aeroacoust. 2007. Vol. 6. No. 4. P. 375–405.
3. **Skudrzyk E.** The foundations of acoustics: basic mathematics and basic acoustics. Springer Vienna, 1971. 790 p.
4. **Kopiev V., Zaitsev M., Chernyshev S.A., Kotova A.** The role of large-scale vortex in a turbulent jet noise // In 5th AIAA/CEAS Aeroacoustics Conference and Exhibit. 1999. AIAA-paper 1999-1839.
5. **Zaitsev M.Y., Kopiev V.F.** Mechanism of sound radiation by turbulence near a rigid body // Fluid Dynamics. 2008. Vol. 43. No. 1. P. 86-96.
6. **Taira K., Brunton S.L., Dawson S., Rowley C.W., Colonius T., McKeon B.J., Schmidt O.T., Gordeyev S., Theofilis V., Ukeiley L.S.** Modal Analysis of Fluid Flows: An Overview // AIAA Journal. 2017. Vol. 55. No. 12. P. 4013–4041.
7. **Towne A., Schmidt O.T., Colonius T.** Spectral proper orthogonal decomposition and its relationship to dynamic mode decomposition and resolvent analysis // Journal of Fluid Mechanics. 2018. Vol. 847. P. 821–867.
8. **Liu Y., Quayle A., Dowling A., Sijtsma P.** Beamforming correction for dipole measurement using two-dimensional microphone arrays // JASA. 2008. Vol. 124. No. 1. P. 182–191.
9. **Bychkov O.P., Demyanov M.A., Faranosov G.A.** Localization of dipole noise sources using planar microphone arrays // Acoustical physics. 2019. Vol. 65. P. 567–577.

DOI 10.53954/9785604990148_48

CONTRIBUTION OF ACADEMICIAN V.V. STRUMINSKY TO THE DEVELOPMENT OF THEORETICAL AND APPLIED MECHANICS

S.L. Chernyshev[1], A.Ph. Kiselev[1], V.I. Shalaev[2]

[1]*Central Aerohydrodynamic Institute,*
140180 Moscowregion, Zhukovsky, Gagarin str., 1

[2]*Moscow Institute of Physics and Technology*
140180 Moscow region, Zhukovsky, Gagarin str., 16

04/29/2024 marks the 110th anniversary of the birth of the outstanding scientist in the field of fluid mechanics Vladimir Vasilyevich Struminsky. His contribution to modern mechanics is difficult to overestimate: he laid the principles of modern high-speed aviation, the foundations of modern research on laminar-turbulent transition and turbulent flows, obtained fundamental results in the kinetic theory of gases, identified ways to study the movements of liquid and gas mixtures as the main process of physic-chemical industrial technologies. His talent covered almost all aspects of scientific and technical activities: from bright theoretical results to their experimental verification and implementation in specific engineering projects, education of young scientists and effective leadership of research teams.

V.V. Struminsky's scientific activity began at the postgraduate school of the Department of Theoretical Physics of the Moscow State University of the name M.V. Lomonosov, where in 1941 he brilliantly defended the thesis of the candidate of physical and mathematical sciences on the quantum theory of metal alloys. His unexpected arrival at the Central Aerohydrodynamic Institute of the name N.E. Zhukovsky and research into the problems of aeromechanics had a completely pragmatic origin, but far-reaching consequences. An excellent education at the Physics Department of Moscow State University and the highest talent of a theorist allowed him to quickly get used to a new field and propose a new solution to the Navier-Stokes equations, which became the basis for studies of the characteristics of viscous gas flows near swept wings – one of the main elements of all modern high-speed aircraft. His engineering talent manifested itself in the development of a method for creating bearing surfaces with optimal characteristics, and the talent of an experimenter – in conducting numerous experiments to verify the proposed approaches.

During the work of V.V. Struminsky as the first deputy head of TsAGI (1952–1961), the existing experimental base was modernized and a new experimental base was created, including aerodynamic installations for hypersonic speeds. With its help, the basic aerodynamic layouts of almost all modern cruise aircraft for various purposes were developed [1].

Being a pioneer by nature, V.V. Struminsky took up new, complex and poorly researched problems: problems of kinetic theory, laminar-turbulent transition and turbulence. Thanks to his work, scientific schools have been established, which currently maintain a high level of research on these problems in Russia. Vladimir Vasilyevich continued to develop these areas at ITPM SB of the USSR Academy of Sciences as director of this institute (1966–1971). Here he began to create a new aerodynamic experimental base and laid down new research directions in which ITPM is now a recognized leader in the world: laminar-turbulent transition, supersonic gorenje, jet streams, kinetic theory, etc. At this institute, he created a team of researchers from graduates of the best universities in the country [1].

In 1972, V.V. Struminsky returned to Moscow and continued his work as the head of the Department of Physical Aeromechanics at the Institute of Problems of Mechanics of the USSR Academy of Sciences. He put forward a completely original idea for the intensification and modernization of technological processes in industry and agriculture through the use of scientific potential and developments in the defense industry. To implement this idea, in 1976, the Presidium of the USSR Academy of Sciences decided to create, under the leadership of V.V. Struminsky, the "Sector of Mechanics of Inhomogeneous Media", which in 1989 It was transformed into the Department "Mechanical and Mathematical methods in technological and economic developments". Significant results were obtained here on the development of methods of the kinetic theory of gases for inhomogeneous media, the construction of the theory of motion and heat transfer in laminar and turbulent multi-dispersed and multiphase media, problems of alternative energy sources were developed, a new concept of safe underground burial of nuclear waste was put forward, well-known and new economic models were developed and their stability was investigated. The Sector and the Department have become the center and the link between fundamental and branch sciences [1].

It is impossible not to note the contribution of V.V. Struminsky to the development of education in the field of physical and technical sciences and the training of young specialists in this field. In fact, since the beginning of the MIPT, he has been a teacher, professor and head of the department of this famous university while working at TsAGI and the USSR Academy of Sciences. In Novosibirsk, he was the head of the university department. His former students speak with gratitude about their teacher [1].

The main stages of the life of V.V. Struminsky, an outstanding mechanical scientist, are reflected in the book of memoirs of his colleagues, students and relatives published by TsAGI for its centennial anniversary [1].

REFERENCES

1. Academician V.V. Struminsky. Outstanding mechanical scientists of TsAGI. (red.-comp.: A.F. Kiselev, V.M. Lutovinov, V.I. Shalaev.) M.: Nauka, 2018. 397 p.

DOI 10.53954/9785604990148_50

COMPARATIVE ANALYSIS OF ACTIVE FLOW CONTROL WAYS IN ROUND JETS

N.V. Demidenko, O.S. Vankova, S.N. Yakovenko

Khristianovich Institute of Theoretical and Applied Mechanics, Siberian Branch of RAS
Novosibirsk 630090, Russia

The study is focused on numerical simulation of submerged round jets by the widely used codes (OpenFOAM, ANSYS Fluent) to solve the Navier–Stokes equations at different forcing types with varied amplitudes, Reynolds ($\mathrm{Re} = UD/\nu$) and Strouhal ($\mathrm{St} = fD/U$) numbers where D is the nozzle diameter, U is the bulk inlet velocity, ν is the molecular viscosity. To simulate a jet, the governing equations are solved at wide ranges of $\mathrm{St} \le 0.5$ and $\mathrm{Re} \le 5\,000$, taking the constant velocity $u(r < D/2) = U$ at the inlet $x = 0$. Computation set-up details are in [1, 2].

The following active ways to control flow are assessed: axial (at frequency $f_a = 2f$), helical ($f_h = f$), flapping ($f_f = f$) oscillations of the inlet velocity profile with amplitudes $A = A_a = A_h = A_f$ [1, 3], transverse vibration of the inlet section at frequency $f_v = f$, amplitude Z [1, 2], oscillations at lateral boundary (mimicking a sound source) [2]. Their combinations are explored too.

The jet splitting is revealed (Fig. 1), as in measurements [4-6], for wide ranges of St, Re, and forcing amplitudes ($A/U \le 0.2$, $Z/D \le 1.0$). The nozzle vibration has the similar effects to those of the transverse acoustic field [1, 2], however the former appears to be a more effective control method, than acoustic forcing, or helical and flapping excitations of the inlet velocity.

The typical thickness d of a jet, the expansion angle α in the bifurcation plane found from the $d(x)$ curve, the mean velocity $\langle u \rangle$ or scalar $\langle c \rangle$ values on the axis can parameterize the mixing enhancement produced by the jet excitations [1–6]. The mixing efficiency grows with larger d and α, relating to wider spreading region and smaller centerline $\langle u \rangle$ and $\langle c \rangle$ values.

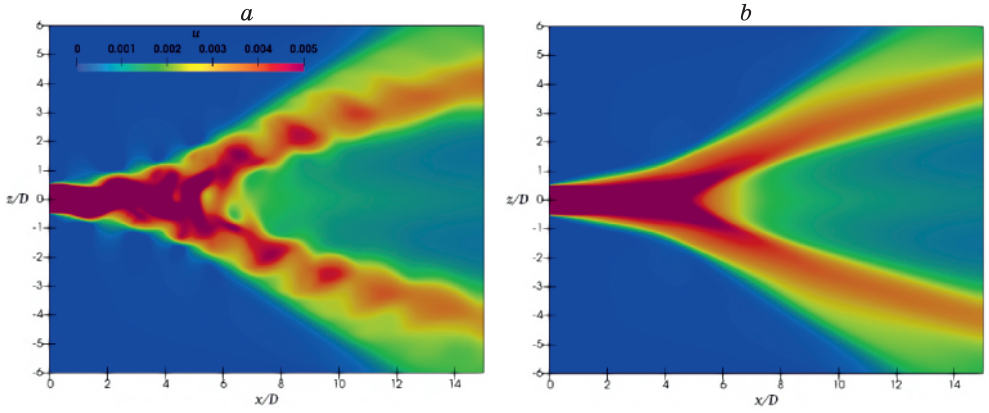

Fig. 1. Instantaneous velocity u (a) and time-averaged velocity $\langle u \rangle$ (a) in the bifurcation plane ($y = 0$) with the combination of nozzle vibrations and axial forcing at $\mathrm{Re} = 500$, $\mathrm{St} = 0.2$, $Z/D = A/U = 0.04$.

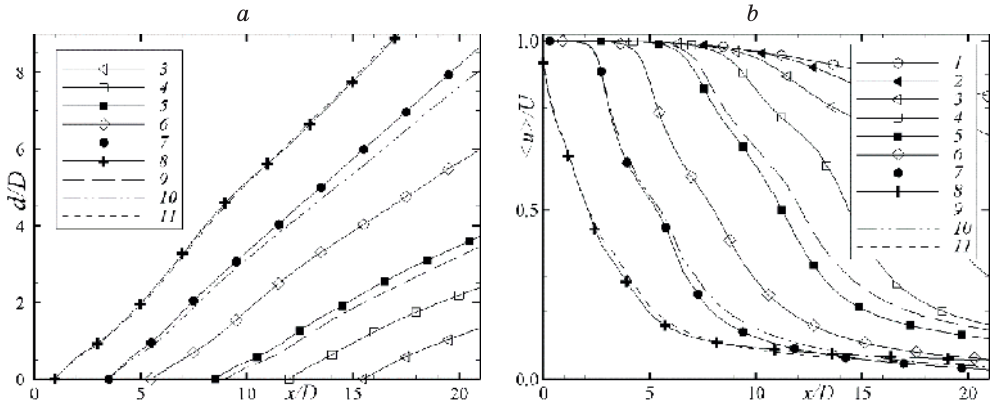

Fig. 2. Thickness $d = z(\langle u \rangle = \langle u \rangle_{max})$ where $\langle u \rangle_{max}$ is the maximum velocity at x = const (*a*); values of $\langle u \rangle / U$ along the jet axis $y = z = 0$ at Re = 500, St = 0.15 and varied amplitudes of the inlet vibration (*b*).

1–8 – fine mesh, Z/D = 0, 0.001, 0.0025, 0.005, 0.010, 0.025, 0.100, 0.500; *9–11* – coarse mesh, Z/D = 0.01, 0.10, 0.50.

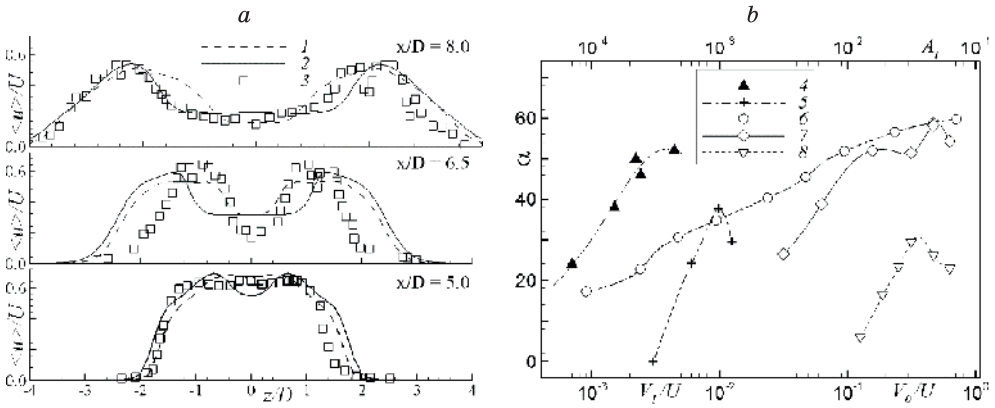

Fig. 3. Comparisons for the axial mean velocity profiles at different sections (*a*), and the bifurcation angle α in degrees (*b*) as a function of the transverse velocity amplitude A_t estimated in [6], or the transverse velocity amplitude V_1/U at $x/D = 2.5$, $y = z = 0$ [2], or the amplitude V_0/U at the inlet section $x = 0$ [1, 2].

Axial + transverse vibration, Re = 500, St = 0.2, $Z = 0.04D$, $A = 0$ (*1*), $0.17U$ (*2*); *3* – axial + orbital forcing, Re = 4300, $0.2 \le$ St ≤ 0.3, $A = 0.17U$, $Z = 0.04D$ [5]; *4* – $\alpha(A_t)$, acoustic forcing, Re = 10^4, St = 0.275 [6]; *5* – $\alpha(V_1)$, sound source, Re = 500, St = 0.07 [2]; $\alpha(V_0)$, inlet vibration, Re = 500, St = 0.15 (*6*); Re = 250, St = 0.1 (*7*); Re = 100, St = 0.1 (*8*).

To study the vibration amplitude effect, the value of St = 0.15 is fixed to ensure the highest α value, and runs at $Z/D \le 1.0$ are performed (Fig. 2). At $Z/D \sim 0.001$ the jet begins to split from $x/D \approx 22$. At $0.001 \le Z/D \le 0.1$ the effect grows steadily: the bifurcation point drifts closer to the inlet; values α and d increase with Z; the centerline velocity demonstrate opposite trends. At $0.1 < Z/D \le 1.0$ the forcing effect saturates (Fig. 2, 3). Verification and validation of codes show good mesh convergence (Fig. 2) and agreement with the measurement data [5–6] (Fig. 3).

Study is supported by RSF grant No. 23-27-00310, https://rscf.ru/en/project/ 23-27-00310/.

REFERENCES

1. **Shevchenko A.K., Yakovenko S.N.** Numerical study of flow control methods and splitting effects in a round submerged jet // Thermophysics and Aeromechanics. 2021. Vol. 28, Is. 3. P. 353–368.
2. **Vankova O.S., Yakovenko S.N.** Numerical simulations of a subsonic round jet with transverse acoustic and mechanical forcing // E3S Web Conf. 2023. Vol. 459. Paper # 03002. P. 1–6.
3. **Tyliszczak A., Geurts B.J.** Parametric analysis of excited round jets – Numerical study // Flow, Turbul. Combust. 2014. Vol. 93. P. 221–247.
4. **Kozlov V.V., Grek G.R., Litvinenko Yu.A., Kozlov G.V., Litvinenko M.V.** Subsonic round and plane macro- and microjets in a transverse acoustic field // Vestnik NGU. Ser. Fiz. 2010. Vol. 5, Iss. 2. P. 28–42. (in Russian)
5. **Reynolds W.C., Parekh D.E., Juvet P.J.D., Lee M.J.D.** Bifurcating and blooming jets // Annu. Rev. Fluid Mech. 2003. Vol. 35. P. 295–315.
6. **Reynolds W.C., Parekh D.E., Mungal M.G.** Bifurcation of round air jets by dual-mode acoustic excitation // AIAA Paper 87-0164. 1987.

DOI 10.53954/9785604990148_53

ON THE INFLUENCE OF WAVY RIBLETS ON THE STABILITY OF INCOMPRESSIBLE LAMINAR BOUNDARY LAYERS

K.V. Demyanko[1, 2], A.V. Boiko[2], Yu.M. Nechepurenko[1, 2]

[1]*Keldysh Institute of Applied Mathematics of RAS, 125047, Moscow, Russia*

[2]*Marchuk Institute of Numerical Mathematics of RAS, 119333, Moscow, Russia*

A turbulent boundary layer significantly increases the aerodynamic drag compared to a laminar boundary layer. Therefore, the laminarization of the boundary layer over structural elements of aircraft is one of the possible ways for drag reduction. The possibility of controlling the laminar-turbulent transition in incompressible boundary layers with the help of streamwise-oriented grooves of the flow exposed surface was first demonstrated experimentally by V.V. Kozlov with coauthors [1, 2]. Namely, the triangular riblets, which height and period were of the order of the laminar boundary layer thickness, enhance the growth of Tollmien-Schlichting waves, promoting the natural laminar-turbulent transition [3]. At the same time, such riblets reduce the energy growth of various streamwise vortices, thereby delaying the so-called subcritical (bypass) transition [3]. Later, for the Poiseuille flow in a streamwise ribbed channel, the authors of this report showed numerically for the first time [4, 5] that with the help of wavy riblets it is possible to simultaneously delay or promote both the subcritical and natural laminar-turbulent transition in the channel flow.

This report discusses the results of a numerical study of the temporal stability of the laminar boundary layer over a streamwise ribbed flat plate with a blunt leading edge, with the plate being placed in a homogeneous viscous incompressible flow at zero angle of attack and zero sweep angle. In this case, the flow around the plate was computed with the help of

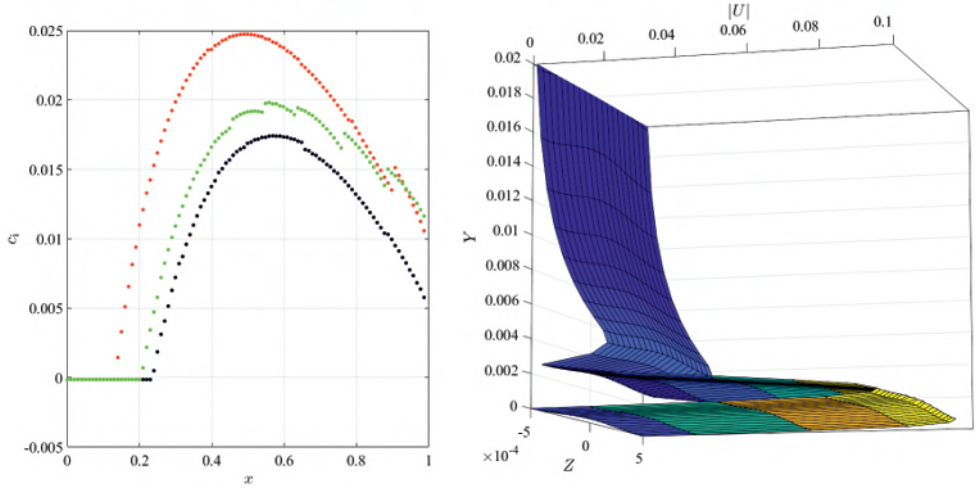

Fig. 1. Left: the dependence of the growth rates of Tollmien-Schlichting waves on the streamwise coordinate for flat (black) and ribbed plates with the period of riblets L_z = 2.5 mm (green) and 0.5 mm (red) and the amplitude of riblets ϵ = 0.25 mm. Right: a typical view of the magnitude of the streamwise amplitude of Tollmien-Schlichting wave velocity in the region of the formed boundary layer.

the OpenFOAM package, while the stability of the boundary layer was studied within the framework of the locally parallel approach [3] based on the technology [6] developed by the authors for channel flows. In particular, it is shown that reducing the period of wavy riblets increases the growth rates of Tollmien-Schlichting waves in the considered range of parameters (Fig. 1).

This research is supported by the Russian Scientific Foundation (grant No. 22-71-10028).

REFERENCES

1. **Grek G.R., Kozlov V.V., Titarenko S.V.** Study of the influence of surface ribbing (riblett) on the development of two-dimensional disturbances (Tollmien-Schlichting waves) in a laminar boundary layer // Sib. Phys.-Tech. J. 1993. V. 35, No. 6, P. 26–30. (In Russian)
2. **Grek G.R., Kozlov V.V., Titarenko S.V.** An experimental study on the influence of riblets in transition // J. Fluid Mech. 1996. Vol. 315, P. 31–49.
3. **Boiko A.V., Dovgal A.V., Grek G.R., Kozlov V.V.** Physics of transitional shear flows. 2011. 271 p.
4. **Boiko A.V., Klyushnev N.V., Nechepurenko Yu.M.** On stability of Poiseuille flow in grooved channels // EPL (Europhysics Letters). 111:1 2015. 14001p1–14001.p6.
5. **Boiko A.V., Klyushnev N.V., Nechepurenko Yu.M.** Stability of fluid flow over a ribbed surface. Moscow: KIAM RAS. 2016. 123 p. (In Russian)
6. **Boiko A.V., Nechepurenko Yu.M.** Technique for the numerical analysis of the riblet effect on temporal stability of plane flows // Comp. Math. Math. Phys. 2010. V. 50, P. 1055–1070.

DOI 10.53954/9785604990148_55

PULSE DISCHARGE IN GAS DYNAMIC FLOW

D. Dolbnya, I. Znamenskaya

Lomonosov Moscow State University, Faculty of Physics
119991, Moscow, Russian Federation

The results of an experimental study on directed pulsed high-energy effects on gas-dynamic structures characteristic of high-speed gas flows achieved, in particular, in aircraft of various types, including internal combustion chambers [1]. The results of the study provide an understanding of the methods and mechanisms of influence on gas-dynamic structures, such as shock waves, laminar-turbulent transition zones, separation zones [2], as well as the possibilities for optimizing the ignition and combustion of fuel in internal combustion chambers, which are components of high-speed aircraft [3]. They also provide new information on the possibilities of controlling high-speed gas-dynamic flows in channels based on new physical effects that are realized when initiating pulsed (submicrosecond) self-localizing electrical discharges in discontinuous flows.

The experimental equipment is a shock tube (channel) with a section where, in a 100-mm section, a pulsed volume discharge with ultraviolet preionization can be initiated from plasma sheets, which are sliding discharges that are formed across the flow on the horizontal walls of the channel. The duration of the discharge current was 0.2–0.3 μs with an amplitude of up to 1.4 kA, the duration of the glow did not exceed 2 μs, the characteristic gas-dynamic time was about 10 μs (the minimum value for the incident shock wave).

The influence of an insert installed in the discharge initiation zone (on the wall of a rectangular channel) on a high-speed gas-dynamic flow is investigated. The main modes of localization of a submicrosecond volume discharge initiated in a high-speed flow of various speeds (up to 1 km/s) are identified. It was shown that the change in the self-localization region of the pulsed discharge in the flow was associated, first of all, with a change in the structure of the gas-dynamic flow created near the obstacle as a result of a change in the speed of the oncoming flow.

REFERENCES

1. **Bulat M., Bulat P., Denissenko P. Esakov I.I., Grachev L.P., Lavrov P.V., Volkov K.N., Volobuev I.A.** Plasma-assisted ignition and combustion of lean and rich air/fuel mixtures in low- and high-speed flows // Acta Astronautica. 2020. Vol. 176. P. 700–709. doi.org/10.1016/j.actaastro.2020.04.028**.**
2. **Mursenkova I., Ivanov I., Liao Y. Kryukov I.** Experimental and Numerical Investigation of a Surface Sliding Discharge in a Supersonic Flow with an Oblique Shock Wave // Energies. 2022. V. 15(6). P. 2189. doi.org/10.3390/en15062189.
3. **Feng R., Huang Y., Zhu J. Wang Z., Sun M., Wang H., Cai Z.** Ignition and combustion enhancement in a cavity-based supersonic combustor by a multichannel gliding arc plasma // Experimental Thermal and Fluid Science. 2021. V. 120. P. 110248. doi.org/10.1016/j.expthermflusci.2020.110248.

DOI 10.53954/9785604990148_56

ON EFFECT OF SOME PARAMETERS ON PERFORMANCE OF THERMAL PROTECTIVE RESPIRATORS BASED ON GRANULAR PHASE CHANGE MATERIALS

S.S. Fetsov, N.A. Lutsenko

Institute of Automation and Control Processes FEB RAS
690041, Vladivostok, Russia

This paper considers the use of granular phase change materials (PCM) as a thermal storage element in prospective thermal-protective respirators for cooling inhaled air. These devices are necessary to protect the human respiratory system from thermal damage caused by inhalation of hot air during indoor fires. Respiratory burns are a major cause of injuries and fatalities in indoor fires, affecting 20–36% of victims; they can lead to an increased incidence of pneumonia (38–77%) and mortality (31–45%) [1–3]. When mortality from subsequent pneumonia is included, the maximum expected mortality from inhalation burns can be as high as 60% [1]. Despite advances in firefighting equipment, the statistics on mortality from inhalation-burn injuries in fires remain unchanged [3]. The use of personal protective equipment can improve this situation by cooling the hot air before it reaches the respiratory system.

We introduced the concept of a thermal-protective respirator that uses granulated PCM in [4]. The respirator is a mask that is equipped with a cooling unit (filter) containing granular PCM. During inhalation, air flows through the filter and is cooled by thermal contact with the granules (see Fig. 1). The granules can either be a fusible substance encapsulated in hermetically sealed capsules or a special adsorbent matrix, or a material with a solid-solid phase transition. An advantage of using granular PCMs is that they combine the high heat absorption density characteristic of phase transitions with the large contact surface area characteristic of granular media, resulting in efficient air cooling.

To model the processes that occur in the cooling unit of a thermal-protective respirator, we use an original solver for the OpenFOAM package [5], which has been validated using a wide range of experimental data. This paper presents the results of a numerical parametric study of the thermal-protective respirator. The study analyses the influence of unit dimensions, the melting temperature of PCM, the type of time dependence of the inhaled air flow rate, as well as the partial closure of the outlet on the cooling process of the filtered air [6]. Commercially available PCM have been shown to effectively cool air within a time frame suitable for human evacuation. With a total material mass of 130 g, it is possible to cool air from 177 °C to below 50 °C within 10 minutes. The study found that increasing the melting

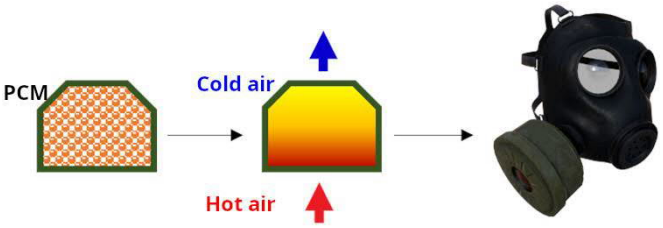

Fig. 1. Schematic representation of air cooling with granular material in a thermal protective respirator.

point of PCM while keeping other parameters unchanged worsens the thermal performance of the thermal-protective respirator. The efficiency of cooling is also reduced when the cooling unit is narrowed, or its outlet is partially closed, as this results in an increase in the maximum temperature of the inhaled air. It has been found that the functional dependence of the flow rate of inhaled air on time, which is set in the calculations of the thermal-protective respirator, should be close to the parameters of real human respiration. The use of an assumption of a constant air flow rate is inadmissible for modelling as it can significantly overestimate the final calculated characteristics of the respirator.

The research was supported by the grant of the Russian Science Foundation No. 22-29-01129, https://rscf.ru/en/project/22-29-01129/.

REFERENCES

1. **Shirani K., Pruitt B., Mason A.** The influence of inhalation injury and pneumonia on burn mortality // Ann. Surg. 1987. Vol. 205, No. 1. P. 82–87.
2. **Smith D.L., Cairns B.A., Ramadan F., Dalston J.S., Fakhry S.M., Rutledge R., Meyer A.A., Peterson H.** Effect of inhalation injury, burn size, and age on mortality // J. Trauma. 1994. Vol. 37, No. 4. P. 655–659.
3. **Charles W.N., Collins D., Mandalia S., Matwala K., Dutt A., Tatlock J., Singh S.** Impact of inhalation injury on outcomes in critically ill burns patients: 12-year experience at a regional burns centre // Burns. 2022. Vol. 48. P. 1386–1395.
4. **Lutsenko N.A., Fetsov S.S.** A Thermal Protective Respirator Based on Granular Phase Change Materials // Dokl. Phys. 2022. Vol. 67. No. 12. P. 486–490.
5. **Fetsov S.S., Lutsenko N.A.** A novel computational model and OpenFOAM solver for simulating thermal energy storages based on granular phase change materials: Advantages and applicability // J. Energy Storage. 2023. Vol. 65. Article 107294.
6. **Fetsov S.S., Lutsenko N.A.** Numerical analysis of thermal performance of breathing air cooler based on granular phase change material // Int. J. Heat Mass Transf. 2024. Vol. 223. Article 125288.

DOI 10.53954/9785604990148_58

METHOD FOR CALCULATING LIFT CHARACTERISTICS OF TWIN-FUSULAGE AIRCRAFT

V.A. Frolov

Samara National Research University
34, Moskovskoye Shosse, Samara, Russia, 443086

Most works devoted to fuselage-wing interference issues only mention wing arrangements with a single fuselage [1]. However, at the present stage of development of aircraft manufacturing, numerous examples of aerodynamic designs of aircraft have appeared in which the wing is articulated with two fuselages. Without going into an analysis of the advantages and disadvantages of the twin-fuselage aircraft, the article proposes an approximate method for calculating the lifting characteristics of such scheme. Based on the author's works [1-4], the proposed method involves solving the problem of transverse flow around two fuselages of circular cross-section in the presence of two point vortices. A model of potential flow of an ideal gas is considered, in which two symmetrically located vortices simulate the tip vortices from the wing. As an example, the work considers a rectangular wing, however, taking into account the wing taper does not cause any fundamental difficulties and can be done with subsequent modifications of the mathematical model. The geometric scheme of the problem of transverse flow around two round fuselages in the presence of two symmetrical vortices is shown in Fig. 1.

Using the theory of the function of a complex variable, we can write down the complex potential (CP) of the flow, which ensures that the normal component of velocity on two circles is equal to zero. The author's work [4] presents a CP for a flow around two cylinders in the presence of a pair of symmetric point vortices. The CP consists of the sum of three terms: the first term represents the CP for an unperturbed flow and two isolated dipoles located at the centers of the circles; the second term is CP, which ensures the conditions of the impermeability of circles when they flow together; the third term is the CP for the flow formed by a pair of symmetrical point vortices near two cylinders. The second and third CP are written in the form of infinite converging series based on the theorem of reflection of dipoles and vortices from circles. The derivative of the CP $W_\Sigma(z)$ with respect to the complex variable z determines the conjugate velocity. By isolating the imaginary part with a minus

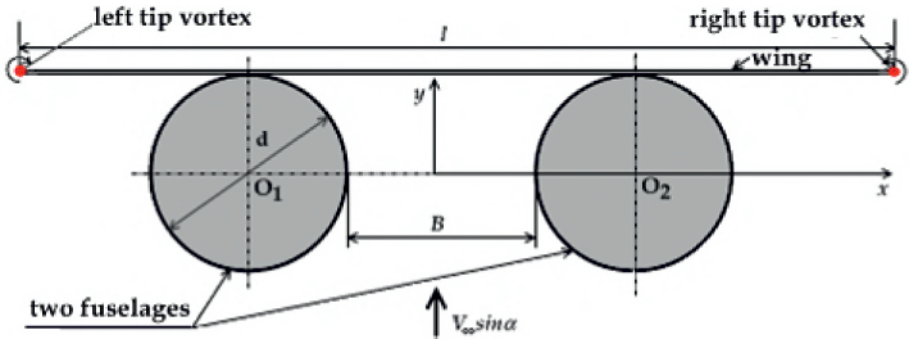

Fig. 1. Transverse flow around two cylinders in the presence of a pair of point vortices

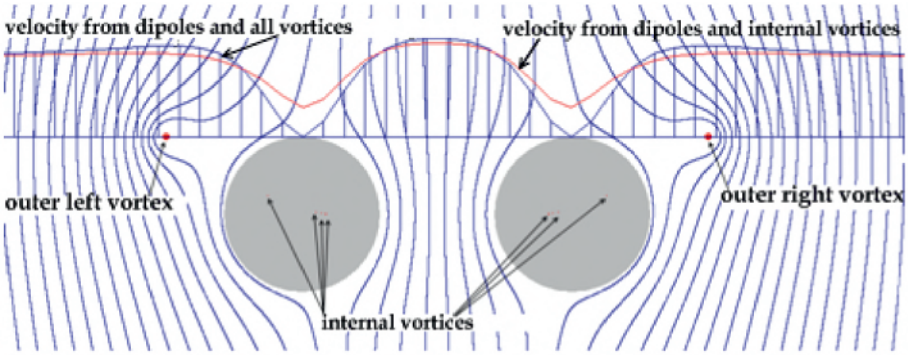

Fig. 2. Streamlines of flow around two cylinders in the presence of a pair of symmetric vortices

sign from the conjugate velocity, we will have a velocity component along the ordinate axis. In Fig. 2 shows cross-flow streamlines around two cylinders in the presence of a pair of external symmetrical vortices (red circles).

The lifting characteristic of the twin-fuselage aircraft combination for small angles of attack ($\alpha \ll 1$) is the derivative of the normal force coefficient with respect to the angle of attack, which, based on the element-by-element calculation method, is written by the formula

$$C_{L_\alpha} = 2C_{L_{\alpha f}} \frac{S_{m.f}}{S} + K_{f+w} C_{L_{\alpha w}}, \tag{1}$$

where $C_{L\alpha}$, $C_{L\alpha\,f}$, $C_{L\alpha\,w}$ are lift-curve slope of the aircraft, fuselage and wing; S, $S_{m.f}$ – wing area and fuselage midsection area; K_{f+w} – total interference coefficient, taking into account the influence of the fuselage on the wing and the wing on the fuselage. Lift-curves slope valuates $C_{L\alpha\,f}$, $C_{L\alpha\,w}$ for the fuselage and wing can be calculated using methods for isolated bodies. According to the strip method [1–3], the coefficient K_{f+W} is equal to the sum of two interference coefficients

$$K_{f+w} = K_{w(f)} + K_{f(w)}; \quad K_{w(f)} = \int_0^1 \bar{V}_y d\bar{x}; \quad K_{f(w)} = K_{w(f)}(K_{w(f)} - 1), \tag{2}$$

where $\bar{V}_y = V_y \big/ \left(V_\infty \sin\alpha\right)$ – dimensionless vertical velocity (red curve in Fig. 2); $\bar{x} = 2x/l$ – dimensionless coordinate along the wing span. Calculation of integrals (2) and further calculation using formula (1) allows us to determine the desired value $C_{L\alpha}$.

REFERENCES

1. **Frolov V.A.** Optimization of Lift-Curve Slope for Wing-Fuselage Combination //In *Aerodynamics*, edited by Mofid Gorji-Bandpy and Aly-Mousaad Aly (IntechOpen, London, 2021). P. 81–97.
2. **Frolov V.A.** Approximate calculation of maximum lifting properties of wing-body combination. //In Int. Conf. High-Energy Processes in Condensed Matter (HEPCM 2021): AIP Conference Proceedings 2504, 030013 (2023). https://doi.org/10.1063/5.0132775
3. **Frolov V.A.** Influence of fuselage on lift capacity of wings of high-wing aircraft structure. XIII All-Russian Congress on Theoretical and Applied Mechanics, // Saint Petersburg, 2023. P. 467–469 (in Russian).
4. **Frolov V.A.** Model of potential flow around a combination of two circular contours in the presence of a pair of discrete stationary vortices // Rocket and Space Technology, series XII, no. 1, Samara, 2001. P. 194–201 (in Russian).

DOI 10.53954/9785604990148_60

ON SUPERSONIC BOUNDARY LAYER STABILITY WITH DIFFUSIVE COMBUSTION

S.A. Gaponov

ITAM SB RAS, 630090, Novosibirsk, Russia

The author and his colleagues' research on hydrodynamic boundary layer instability with diffusion flames are outlined.

In the Dann-Lin-Alexeev approximation [2, 3] with Lewis numbers equal to one the stability problem is reduced to solution the eighth order system equations, as in the stability problem of a one-component gas. The main difference is that in the boundary layer stability problem with combustion, the coefficients of the equations depend not only on temperature and velocity, but also on the molecular weight of the mixture. For perturbations $q = \tilde{q}(y)\exp[i\alpha(x-ct)+\beta z)]$ stability equations have the form:

$$\rho(i\alpha(u-c)\tilde{u}+u'\tilde{v}) = -i\alpha\pi' + \mu\tilde{u}''/\mathrm{Re},\quad \rho i\alpha(u-c)\tilde{v} = -\pi',$$

$$\rho(i\alpha(u-c)\tilde{w}) = -i\beta\tilde{\pi} + \mu\tilde{w}''/\mathrm{Re},$$

$$\rho i\alpha(u-c)\tilde{\theta} - (\rho'/\rho)\tilde{v} = (\gamma-1)\mathrm{M}^2 i\alpha(u-c)\tilde{p}/m + \mu\tilde{\theta}''/\mathrm{PrRe},$$

$$i\alpha(u-c)(\gamma\mathrm{M}^2\tilde{\pi} - \rho\tilde{\theta}) + (\rho'/\rho)\tilde{v} + i\alpha\tilde{u} + i\beta\tilde{w} + \tilde{v}' = 0,$$

Here: *x, z, y* and *u, w, v* – coordinates and velocities in longitudinal, lateral and normal to the plate directions; *t* – time; ρ, π, θ – density, pressure and ratio of temperature to the mixture molecular weight; μ – dynamic viscosity; α, β – wave numbers; M, Re – Mach and Reynolds numbers. The prime denotes differentiation along the normal coordinate and the wavy line marks the perturbation amplitudes

As a result of studies [4], it has been shown that at constant molecular mass of a gases mixture, the equations of «non-viscous» instability do not depend on concentrations, but are determined only by the density ($\rho = 1/T$) and velocity distributions of the main flow. In this case, the boundary layer stability problem with diffusive combustion is reduced to the analogous problem of a one-component gas with internal heating. At different Schmidt numbers, it is possible to approximate modeling of the boundary layer stability problem with diffusion flame by the corresponding problem of one-component gas with heating. The error of such modeling is of the order $(\alpha\mathrm{Re})^{-2/3}$.

Calculations were performed under external airflow conditions with hydrogen injection through a porous insert of plate.

The stationary flow parameters were obtained by direct numerical simulation of the Navier-Stokes equations using the ANSYS Fluent software package. The flow parameters correspond to the free flow with a stagnation temperature T_0 = 300K at the entrance of the computational domain and on its upper boundary. The porous insert had a length of 400 mm and a thickness of 20 mm. There was a 20 mm thick area without porosity under the porous insert. At the lower boundary of this region the mass flow rate of hydrogen with temperature T_{H2} = 300, 600, 900K was set. The mixture was not ignited at T_{H2} = 300K. Therefore the main attention was paid to cases T_{H2} = 600K and 900K.

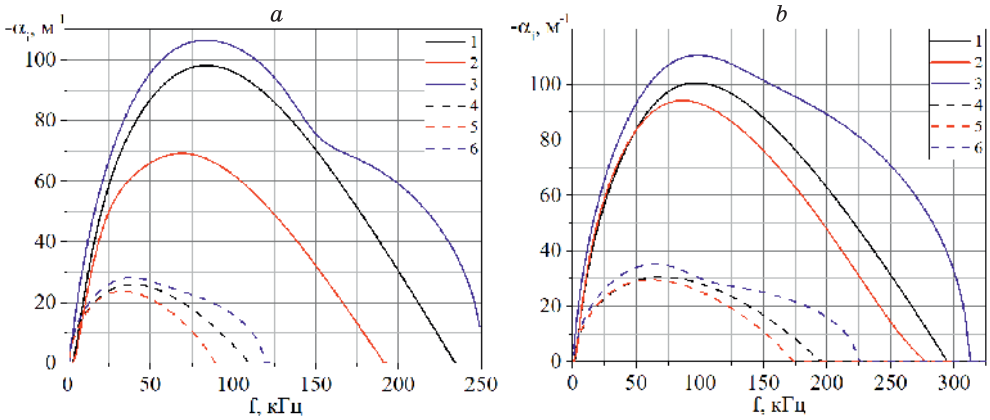

Comparison of amplification rates of different models at T_{H2} = 600 (a) and 900K (b).

Dann-Lin-Alekseev model with taking into account molecular mass perturbation −1,4 and without taking it into account −2,5; inviscid model – 3,6.

The figure shows amplification rates at T_{H2} = 600K (a) and T_{H2} = 900K at different distances from the leading edge (a: x = 0.05m (1–3), 0.2m (4–6); b: x = 0.05m (1–3), 0.1m (4–5)). Results were obtained on the basis of the Dann-Lin-Alekseev model taking into account the molecular mass perturbation (line 1, 4), without taking it into account (line 2,5), as well as in the inviscid approximation (line 3.6).

Comparison of dependences 1 and 2 at T_{H2} = 600K (x = 0.05m) shows that accounting of molecular mass perturbation leads to an increase in the amplification rate. Its influence decreases downstream (see a similar comparison at x = 0.2m (4.5)). The temperature increase in a boundary layer explains this decrease. Therefore, at a sufficiently high temperature the perturbation of the molecular weight can be ignored. The influence of viscosity on the boundary layer stability is demonstrated by comparing dependences 1 and 3. It can be seen that the effect of viscosity is negligible.

At T_{H2} = 900K (Fig. b), a weak influence of molecular mass disturbance is observed already at x = 0.05m (cf. curves 1 and 2), this is more noticeable at x = 0.1m (cf. 4 and 5).

REFERENCES

1. **Gaponov SA, Morozov S.O., and Semenov A.N.** A laminar supersonic boundary layer under the conditions of diffusive hydrogen-air flame and its stability // Thermophysics and Aeromechanics. – 2023. – Vol. 30. No. 6. – P. 1095–1110. DOI: 10.1134/S0869864323060124
2. **Dunn D.W., Lin C.C.** On the stability of the laminar boundary layer in a compressible fluid // J. Aeronaut. Sci. 1955. Vol. 22. No. 7. P. 455–477.
3. **Alekseev M.A.** On Asymptotic Approximations in the Problem of Stability of the Laminar Boundary Layer at Supersonic Velocities. Tr. TsAGI. 1972. No. 1420. 27p.
4. **Gaponov S.A.** Approximate formulation of the problem of boundary layer stability with diffusion combustion // Combustion, Explosion, and Shock Waves. – 2023. – Vol. 59, No. 2. – P. 215–223. DOI: 10.1134/S0010508223020120

DOI 10.53954/9785604990148_62

WIND-TUNNEL WALL INTERFERENCE AND EXPERIMENTAL DATA CORRECTIONS IN SUBSONIC FLOWS

S.A. Glazkov, A.V. Semenov

Central Aerohydrodynamic Institute
140180 Zhukovsky, Russia

The problem of comparing the results of wind tunnel experiments with the real conditions has been relevant for the whole history of wind tunnels. Traditionally, two aspects are distinguished here. The first aspect is related to the influence of flow boundaries. These can be solid, permeable (perforated or slotted) wind tunnel (WT) walls, or jet boundaries in case of an open test section. The second aspect relates to the simulation of viscous effects, since the Reynolds numbers in the model flow in a WT are usually much lower than in the flow of a real aircraft. In this study, only the first aspect is considered. It is also assumed that the position of the laminar-turbulent transition (LTT) does not depend on the presence of flow boundaries (usually in tests, the LTT position on the model is fixed with the help of transition strips).

The classical method developed in the first half of the last century for solving the problem of flow boundary effects in an aerodynamic experiment consisted of testing several (at least two) geometrically similar models. Based on the results of these tests, an extrapolation of the aerodynamic coefficients to the "zero size model" is performed and then the integral interference corrections are determined. This approach, in addition to being expensive and labor-intensive, contains additional uncertainties, and the corrections themselves may depend on the type of aircraft model. Thus, for example, for a subsonic WT with an open test section, according to the test results for a series of several types of geometrically similar models, the dimensionless downwash variation was in range $\delta_0 = 0.18 \div 0.24$ about 30%. Accordingly, the value of the correction to the angle of attack will vary in this range as well.

In this study, a universal approach is considered to analyze the effect of flow boundaries in WTs. The problem is solved in terms of the linearized subsonic small perturbation theory. The obtained solution allows calculating the fields of induction velocity components (the algorithm is implemented in the PANEL128 program package [1]), which [2, 3] are used to determine integral corrections to the flow parameters (to the angle of attack of the model and Mach number of the incident flow). Further, the dynamic pressure and total aerodynamic coefficients are corrected. Darcy's law [4] is used as a boundary condition on the wind tunnel walls. In the cases of solid walls and open test section, we obtain the flow tangency condition and a free streamline (zeroing of the longitudinal perturbed velocity component).

The application of this method in the T-128 WT (TsAGI) is illustrated with an example of the «TEST» control model. The detailed procedure for calculating the distributed interference parameters in the model location region and their interpretation in the form of corrections is described. As an example, Fig. 1 shows a comparison of pressure distributions (c_p) obtained in design and experiment for M = 0.85, Cya = 0.5, $\alpha = 2.3°$, f = 6% (perforation ratio on the test section walls). The unique feature of the T-128 Wind Tunnel is the adjustable perforation of the test section walls. The maximum perforation ratio is f = 18%. The factor confirming the correctness of the proposed methodology is also the substantial con-

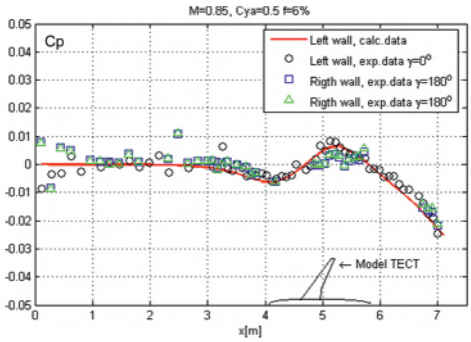

Fig. 1

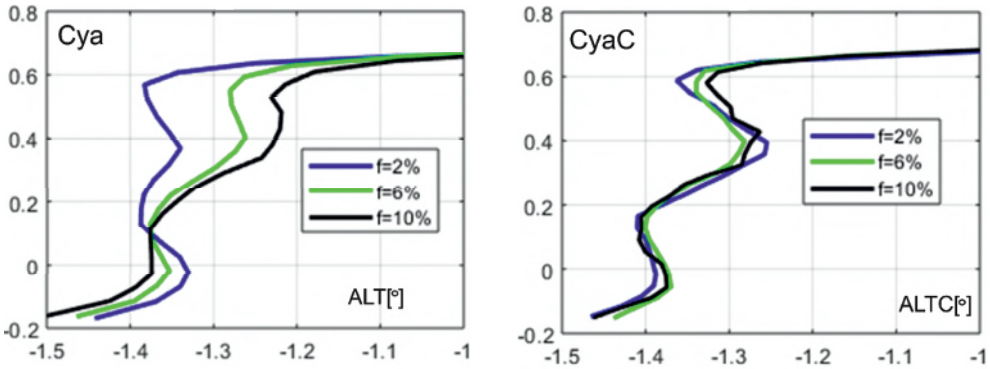

Fig. 2

vergence of the corrected characteristics of the models obtained at different f values. Fig. 2 shows the relation Cya (ALT = α – kCya) for f = 2, 6, 10% with no corrections as well as with the wall effect corrections.

The study also presents the results of verification of the PANEL128 program package on the true numerical solutions (RANS) obtained using the EWT-128-TsAGI program package [5].

The proposed method was also implemented in the MKB «Raduga» WT [6]. A necessary condition for the correctness of the applied method is the convergence of the corrected data in different wind tunnels. To verify this, the test results for the same control model in two wind tunnels were compared. Blockage for the WT test section with solid walls made up the value of $\sigma_1 = S_{mod}/S_{WT\text{-}1}100\% \approx 13.3\%$, and for the WT with an open test section – $\sigma_2 \approx 5.5\%$, i.e. in the WT with solid walls the blockage is 2.4 times greater than in the WT with an open test section. Application of the calculated corrections for wall induction improved significantly the similarity of the test results in two wind tunnels for the control model in the Mach number range $M_\infty = 0.15 \div 0.24$. The difference in Cya(α) decreased by a factor of five and reached the level of 0.07°, expressed in terms of angle of attack. For the drag coefficient Cxa(Cya), the difference decreased by more than 10 times and the maximum discrepancy was no more than 0.0003.

REFERENCES

1. Program for analysizing the effect of flow boundaries on model aicraft flow in a wind tunnel (T-128) at subsonic velocities (PANELT128). Certificate of State Registration of Computer Program No. 2022661713, June 24, 2022.

2. **Pindzola M., Lo C.F.** Boundary interference at subsonic speeds in wind tunnels with ventilated walls, Air Force Systems Command Arnold Air Station, Tennessee, May 1969, AEDC-TR-69-47.
3. **Glazkov S.A., Gorbushin A.R., Ivanov A.I., Semenov A.V.** Recent experience in improving the accuracy of wall interference corrections in TsAGI T-128 wind tunnel. // Progress in Aerospace Sciences // Pergamon Press, Vol. 37, No.3, 2001, P. 263–298.
4. **Glazkov S.A., Gorbushin A.R., Semenov A.V.** Experimental study of boundary conditions on the perforated walls of test sections No 1 and 2 of T - 128 transonic wind tunnel, XIX ICMAR International conference on the methods of aerophysical research, August 13–19, 2018, Novosibirsk, Russia, https://doi.org/10.1063/1.5065299
5. EWT-T128-TsAGI software package for simulating the flow in a transonic wind tunnel. Certificate of State Registration of Computer Program No.2021663575, August 19, 2021.
6. **Glazkov S.A., Goloborodko V.E., Goncharenko V.V., Gorbushin A.R., Kudriavtsev D.A., Makarov P.A., Marusiach E.E., Semenov A.V.** Implementation of the method for considering the influence of flow boundaries in AU-1 and AU-2 wind tunnels, Proceedings of the XXII Scientific and Technical Conference on Aerodynamics of TsAGI, March 3–4, 2011.

DOI 10.53954/9785604990148_65

NUMERICAL SIMULATION OF FLOW AROUND A POORLY STREAMLINED BODY AT NEAR-SONIC VELOCITIES

S.A. Glazkov, A.V. Semenov, E.V. Streltsov

Central Aerohydrodynamic Institute named after Prof. N.E. Zhukovsky, 140180, Zhukovsky, Russia

Nowadays the problem of improving the accuracy and reliability of determination of aerodynamic characteristics for poorly streamlined bodies (e.g., reentering spacecraft) at near-sonic velocities remains actual. Considerable research experience shows that the discrepancy between the results obtained in computational studies and in the wind tunnel experiment may be up to 15% in range of near-sonic Mach numbers, leading to erroneous prediction of aerodynamic characteristics [1, 2]. For this reason, it is important to improve the methodology of aerophysical experiment and to develop the methodology of numerical studies.

In TsAGI a program package "Electronic Wind Tunnel" (EWT-TsAGI) [3] has been developed to perform numerical simulation and complement the results of wind tunnel tests. This software package is based on the solution of the Reynolds-averaged Navier-Stokes equations (RANS). Multi-block structured hexahedral meshes are used for the calculations. EWT-TsAGI software uses a zonal approach, which includes an implicit numerical scheme for sensitive physical phenomena (such as interior part of boundary layer) and an explicit scheme for the rest of computational domain. This approach provides both a high level of resolution and acceptable computational time. The features of the EWT-TsAGI software package are described in detail in [4]; the results of verification and validation of this software are given in [5].

The present work focuses on the methodological aspects of numerical simulation of the flow around complex (in terms of aerodynamics) bodies at near-sonic velocities using the EWT-TsAG software package. Additional validation of the program module was performed using test case for axisymmetric body streamline at similar flow conditions [6].

Numerical simulation of the "unbounded" flow around the model of a reentering spacecraft at Mach numbers in near-sonic velocities range (M = [0.95÷1.05]) have been performed. The following factors are determined within the framework of the study:

– influence of the size of computational grid (calculations were performed on 1/8 of the model on multigrids of 1.7, 13.6 and 109 million cells);

– influence of the size of computational domain;

– influence of turbulence model (SST, SST-NL, SA, DRSM);

– results of numerical research with simulation of the test section walls of the wind tunnel and the supporting device are given.

Further numerical studies are planned to be carried out with simulation in a wide range of permeability of the wind tunnel test section using a specialized boundary condition of the "Darcy" type, which will make it possible to draw conclusions about the influence of flow boundaries and supporting devices on the streamline around a poorly streamlined body at near-sonic velocities. Within the framework of the concept of "Electronic wind tunnel", the obtained results can be further used to determine corrections to the results of experimental studies.

REFERENCES

1. **Pradeep R.** CFD for Aerodynamic Flight Performance Prediction: From Irrational Exuberance to Sobering Reality, 5th Symposium on Integrating CFD and Experiments in Aerodynamics, JAXA, Tokyo, (2012)
2. **Fertig M., Neeb D., Gülhan A.** Windtunnel Rebuilding and Extrapolation to Flight at Transonic Speed for Exomars. ESA Communications. 7th European Symposium on Aerothermodynamics for Space Vehicles, Brügge, Belgien (2011)
3. **Bosnyakov S.M., Vlasenko V.V., Yengulatova M.F., Zlenko N.A., Matyash S.V., Mikhailov S.V.** Program complex for creating the aircraft geometry, creating a multi-block 3-dimensional calculation grid, obtaining the flow fields by solving the system of Euler equations and the system of Navier-Stokes equations, and processing the calculation results (EWT) // Register of computer programs. Certificate of state registration of computer program No. 2008610227 dated January 9, 2008.
4. **Kursakov I.A., Gorbushin A.R., Bosnyakov S.M. et al.** A numerical approach for assessing slotted wall interfernce using the CRM model at ETW, CEAS Aeronaut J 9: 319 (2018). https://doi.org/10.1007/s13272-017-0248-1
5. **Bosnyakov S.M., Gorbushin A.R., Kursakov I.A., Matyash S.V. Mikhailov S.V. Podaruev V.Yu.** About verification and validation of computational methods and codes on the basis of Godunov. TsAGI Science Journal, 48(7):597-615 (2017). DOI: 10.1615/TsAGISciJ.2018026173
6. **Kayser L.D. and Whiton F.** Surface Pressure Measurements on a boattail projectile shape at transonic speeds, Ballistics Research laboratory memorandum Rept. ARBRL-MR-03161, March 1982.

DOI 10.53954/9785604990148_67

THERMOACOUSTIC INSTABILITY AT COMBUSTION OF PRELIMINARY UNPREPARED HYDROGEN-AIR MIXTURE

M.A. Goldfeld

Khristianovich Institute of Theoretical and Applied Mechanics SB RAS Novosibirsk, 630090 Russia, Institutskaya str., 4/1.

The creation of highly efficient heat-stressed combustion chambers and combustion devices involves solving a number of difficult problems that arise when adding heat to a air flow. One such problem is high-frequency oscillations that occur in combustion chambers and industrial furnaces. These oscillations can disrupt the combustion process and lead to the destruction of heating devices and engines. Despite the fact that these complex phenomena have been known for a long time, at present the processes of instability of flows with heat release remain insufficiently studied and are far from their deep understanding and generalization. The dominant factors that determine the thermoacoustic characteristics of the reacting flow are the conditions at the entrance to the channel, non-stationary ignition, and the interaction of acoustic waves with the flame. When acoustic waves begin to interact with combustion processes, thermoacoustic instabilities arise. As the pressure in the combustion zone increases, the separation of the boundary layer intensifies and the intensity of the shock waves increases, which, together with the separation zones, affect the flow in the combustion chamber and change the conditions of mixing and heat release.

The purpose of the work was to determine the spectral characteristics of the flow at high speed at the entrance to the channel under conditions of self-ignition of the mixture and the intense influence of variable acoustic pulsations on the frequency response of the flow. The experiments were carried out on a model in the form of a rectangular channel, consisting of a supersonic nozzle, an isolator and a channel with a transverse dimension of 100×100 mm. with a flame stabilizer in the form of a rear-facing ledge. The model was equipped with optical glasses to visualize the flow. Fuel was supplied in front of the backward facing step (BFS) on the upper and lower walls through 8 round holes with an angle of 90°. The tests were carried out at a static pressure from 0.08 to 0.12 MPa, a total temperature from 1760 ± 35 K and a equivalence ratio coefficient of 0.6–0.98. A description of the model and experimental methodology is given in [1].

During the process of self-ignition, as well as during the transition to stationary combustion, the acoustic characteristics change over time and along the length of the channel. Preliminary measurements showed that the acoustic parameters of the flow at the entrance to the channel vary significantly depending on the initial turbulence, Reynolds number, and fuel supply pressure. At the same time, it was established that in a flow without combustion, the acoustic characteristics remain unchanged throughout the entire regime along the entire length of the channel (Fig. 1). At the ignition and combustion, the pulsation structure changes (Fig. 2). Firstly, the amplitude increases by 5–7 times (depending on the intensity of the heat release). Secondly, local zones of increased amplitude appear during ignition in the interval of 20–30 ms, during the transition to intense combustion (48–58 ms) and when the channel is blocked or at the end of the installation operating mode (here the channel is choked for about 108 ms). These results indicate that pressure fluctuations under complex conditions of thermo-acoustic interaction are very different from those without combustion

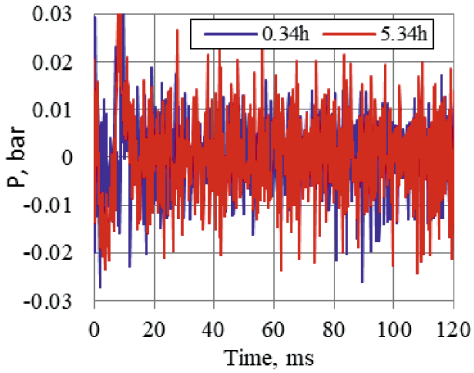

Fig. 1. Pressure oscillations in the flow without combustion.

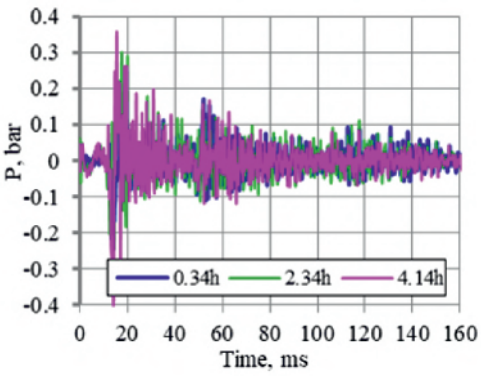

Fig. 2. Pressure oscillations in the flow without combustion at. $\beta = 0.92$.

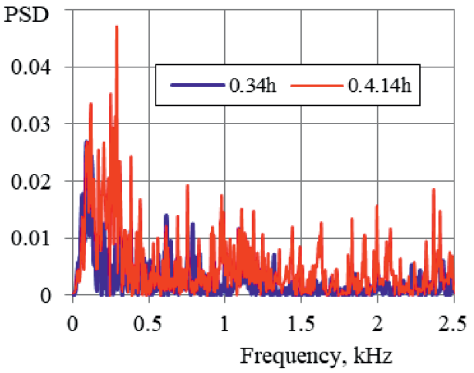

Fig. 3. Comparison of spectral characteristics at various points along the channel length.

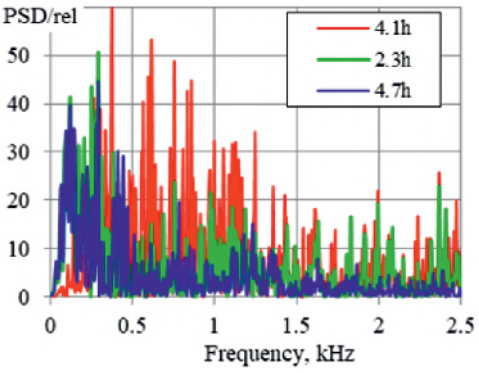

Fig. 4. The influence of heat release on the relative change in the oscillation spectrum.

or at local combustion. Fig. 3 shows the frequency spectra for a fuel excess ratio of 0.92, where it can be seen that frequencies are shifted to lower levels due to combustion and an increase in the spectral power of pressure oscillations (PSD) occurs.

From the data in Fig. 3 it also follows that the most significant increase in PSD occurs in the ignition zone, where the maximum level of average pressure is achieved [2]. It can be seen that the spectral power of oscillation in the ignition zone is approximately by 3–4 times higher than at the beginning of the channel behind BFS. To quantify the effect of heat supply, Fig. 4 shows the spectral power value normalized by the maximum PSD value at the channel entrance, which was calculated taking into account the fuel injection. Compared to an undisturbed flow, PSD can increase by an order of magnitude or more, which confirms the decisive influence of thermo-acoustic interaction on the appearance of flow instability.

Spectral analysis of the flow showed that the intensification of combustion leads to an increase in thermo-acoustic interaction, which is accompanied by an increase in pressure pulsations and, as a result, an improvement in mixing and a corresponding increase in heat release.

The research was carried out within the framework of the Program of Fundamental Scientific Research of the state academies of sciences (project No. 121030500162-7) and conducted at Joint Center «Mechanics» of ITAM SB RAS

REFERENCES

1. **Goldfeld M.A.** Evolution of the ignition and combustion process at high velocity at the channel entrance // Int. J of Hydrogen Energy. 2023. Vol. 48, N. 53. P. 20483–20494. DOI: org/10.1016/j.ijhydene.2023.02.114
2. **Goldfeld M.A.** Processes of fuel self-ignition and flame stabilization with transverse hydrogen fuel injection into a supersonic combustion chamber // Thermophysics and Aeromechanics. 2020. V. 27, N. 4. 573–584. DOI: 10.1134/S0869864320040101

DOI 10.53954/9785604990148_70

NUMERICAL STUDY OF FLOW STABILITY IN FLAT CHANNEL WITH VISCOELASTIC WALLS

E.S. Golub[1], A.V. Boiko[2], A.P. Chupakhin[1]

[1] Lavrentyev Institute of Hydrodynamics of the Siberian Branch of the RAS, Novosibirsk, 630090

[2] Khristianovich Institute of Theoretical and Applied Mechanics SB RAS, Novosibirsk, 630090

The study of the impact of the viscoelastic characteristics of channel walls on the flow stability is a significant problem in fundamental hydrodynamics with practical implications. The results of the study can be used in medicine in describing the flow of blood in vessels, in industry in describing the movement of liquids in pipelines. The main task is to control the laminar-turbulent transition by varying the wall elasticity and viscosity. Laminarization of the flow can significantly reduce wall friction, while turbulization can accelerate heat transfer in the fluid.

The work presents a numerical study of the stability of the Poiseuille flow of a viscous incompressible liquid in a channel with malleable walls made of various model viscoelastic materials. Previously, this problem was solved for fluid flows over a multilayer viscoelastic coating [1]. The propagation of three-dimensional perturbations in the flow is described by the Navier-Stokes equations. The perturbations are divided into symmetric and antisymmetric with respect to the central axis of the channel. A feature of the work is the use of a volume-type model based on the Navier equations to describe small fluctuations in coating. The viscoelastic properties of the coating materials are described using the Kelvin-Voigt model. The numerical calculation is based on the collocation method. Numerical modeling of the dependence of the critical Reynolds number on the properties of wall materials and different coating thicknesses is carried out. The influence of viscoelasticity properties of walls on the flow stability is investigated.

REFERENCES

1. **Darzhain A.E., Boiko A.V., Kulik V.M., Chupakhin A.P.** Analysis of stability of the boundary layer on a flat plate under a finite-thickness two-layer compliant coating // J. Appl. Mech. Tech. Phys., 2019, Vol. 60, No. 4, P. 620−630.

DOI 10.53954/9785604990148_71

HYPERSONIC CHEMICALLY REACTING BOUNDARY LAYER STABILITY AT AEROBRAKING IN MARS ATMOSPHERE

Yu.N. Grigoryev, I.V. Ershov

Federal Research Center for Information and Computational Technologies
630090, Novosibirsk, Russia

Spacecraft flights to Mars initiated the study of the problems of aerothermodynamics of entry and flight in the Martian atmosphere [1–3]. To date, research has been conducted by relatively small unmanned vehicles moving with high overloads along ballistic trajectories [4]. At the same time, flights of the manned spacecraft are planned for the next decade. The prospective projects of future spacecrafts are structures with dimensions of tens of meters [1–3], during landing of which aerobraking will be used. In this case, hyper- and supersonic boundary layers should develop on their extended surfaces of small curvature behind the bow shock wave.

When designing control systems and thermal protection of a spacecrafts, it is necessary to carry out boundary layer stability calculations to assess the position of the transition zone to turbulence, where the heat flux peak occurs.

In calculations it is necessary to use the real characteristics of the Martian atmosphere, 96% of which is carbon dioxide CO_2. It should be noted that the physicochemical kinetics of CO_2 is significantly more complex than the kinetics of the diatomic components of air. Despite the rarefaction and low temperature of the Martian atmosphere, high velocities along the landing trajectory within the range of 2–6 km/s determine high temperatures in the boundary layer behind the shock wave. In the upper part of the trajectory, these temperatures significantly exceed the temperature of complete dissociation of CO_2. In this case, a multicomponent thermochemical nonequilibrium mixture of atoms, radicals and vibrational excited molecules appears in the boundary layer. To take into account the properties of such a mixture, it is necessary to use an adequate physical – mathematical model.

In the report calculations of the position of the beginning of the laminar–turbulent transition zone based on the e^N-method are presented. Two characteristic flow regimes of the hypersonic boundary layer, corresponding to the 66-th second (flow regime 1) and 87-th second (flow regime 2) of the "Pathfinder" spacecraft landing on Mars [4] are considered. The calculations used a three-component model of a thermochemical nonequilibrium mixture CO_2/CO/O. Solutions of the locally self-similar boundary layer equations were taken as stationary flow profiles. The frequency spectrum of spatial disturbances was found using the neutral curves of temporary disturbances at the same wavelengths. The neutral instability curves are shown in Fig. 1*a*. The shape of neutral curves at the hypersonic regime with the characteristic merging instability domains of the first and second modes [5] is completely determined by the Mach number of the flow.

The transition Reynolds number Re_{xT} was determined from the envelopes of the *N*-factor curves families at $N_T = 8$. It is shown that in the hypersonic flow regime 1 at M = 12.6, taking into account the developed thermochemical nonequilibrium leads to a significant decrease of the static gas temperature in the lower part of the boundary layer. As a result, the beginning of the laminar–turbulent transition shifts downstream by approximately 10% compared to the case of a perfect gas. The *N*-factors curves and position of the laminar–tur-

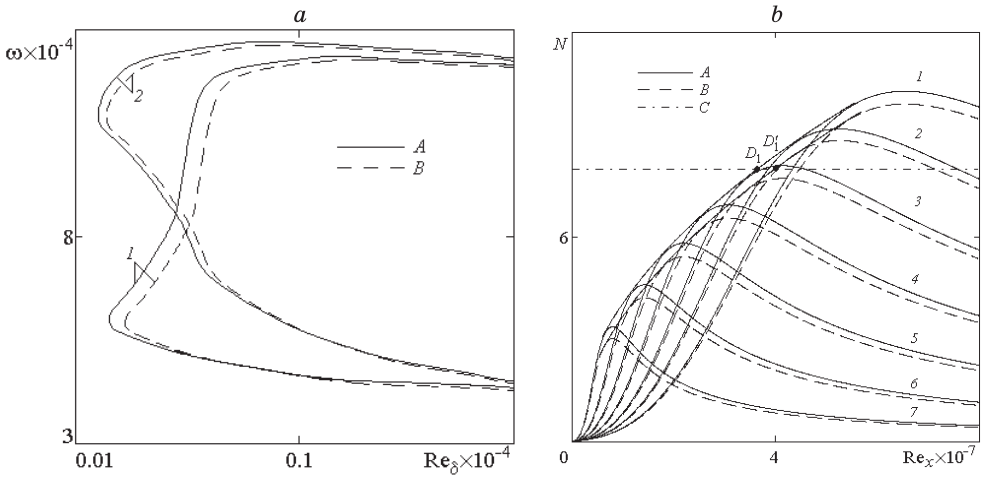

Fig. 1. *a* – neutral stability curves of the most unstable first modes of temporary disturbances; *b* – curves of *N*-factors and position of the laminar–turbulent transition.

1 are flow regime 1; *2* are flow regime 2; *A* is a perfect gas; *B* is a thermochemically nonequilibrium gas; *C* is line $N = 8$; D_1 и D'_1 are the points of transition for flow regime 1; D_2 и D'_2 are the points of transition for flow regime 2; $\omega = 4.25\times10^{-4}$ (*1*), 4.375×10^{-4} (*2*), 4.5×10^{-4} (*3*), 4.625×10^{-4} (*4*), 4.75×10^{-4} (*5*), 4.875×10^{-4} (*6*), 5×10^{-4} (*7*).

bulent transition are shown in Fig. 1*b*. The hypersonic regimes under consideration are characterized by a monotonically increasing dependence of the transition Reynolds number Re_{xT} on the Mach number. Therefore, the Reynolds number Re_{xT} for flow mode 2 at M = 6.9 is approximately four times less than for flow mode 1.

The work is supported by Russian Science Foundation (grant No. 23–11–00027).

REFERENCES

1. **Reynier Ph.** Survey of aerodynamics and aerothermodynamics efforts carried out in the frame of Mars exploration projects // Progress in Aerospace Sciences. 2014. Vol. 70. P. 1–27.
2. **Park Ch., Howe J.T., Jaffe R.L., Candler G.V.** Review of chemical-kinetic problems of future NASA missions. II: Mars entries // J. Thermophysics and Heat Transfer. 1994. Vol. 8, No. 1. P. 9–23.
3. **Armenise I., Reynie Ph., Kustova E.** Advanced models for vibrational and chemical kinetics applied to Mars entry aerothermodynamics // J. Thermophysics and Heat Transfer. 2016. Vol. 30, No. 4. P. 705–720.
4. **Milos F.S., Chen Y.-K., Congdon W.M., Thomas J.M**. Mars Pathfinder entry temperature data, aerothermal, and heatshield material response // AIAA Paper 98-2681. June 1998. 16p.
5. **Mack L.M.** Boundary layer stability theory // Preprint of JPL Technical Report, Document 900–277, Rev. A. Pasadena: California Inst. Technology, 1969. 272 p.

DOI 10.53954/9785604990148_73

SPECTRAL AND STATISTICAL METHODS OF PROCESSING LASER IMAGING DATA

Yu.V. Gromyko, I.S. Tsyryulnikov

Khristianovich Institute of Theoretical and Applied Mechanics, Siberian Branch of RAS, 630090, Novosibirsk, Russia

Experimental practice in the field of fluid mechanics uses the panoramic non-contact method of measuring the velocity field – PIV [1]. An accompanying source of information in the PIV method is the visualization of the particle field in the flow, reflecting all the inhomogeneities of the seeding flow. Since the appearance of seeding inhomogeneities is associated with local flow features, the texture of seeding inhomogeneities observed in the image will also be associated with these features. The analysis of this information can make it possible to evaluate the properties of the flow, which can be useful in research both on their own (for example, the position of the laminar-turbulent transition) and in the context of adapting cross-correlation PIV algorithms. In this paper, methods of image processing for laser visualization of gas dynamic flows based on spectral and statistical analysis are considered.

Experiments on laser visualization of flows in the boundary layer (BL) on a plate model were obtained in a pulse wind tunnel ITAM SB RAS with electric arc heating of the working fluid at a unit Reynolds number $Re_1 = 4 \div 23 \cdot 10^6$ m^{-1}. The plate was exposed at zero angle of attack. The illumination of the particles was carried out with a laser knife with a thickness less than 2 mm (parallel to the plane of the plate). The visualization area is shown in Figure 1a. The laser imaging system included an NdYAG Vilite-Hi-100 laser with a wavelength of 532 nm, providing a pulse generation frequency of up to 100 Hz with an energy of up to 100 MJ and a high-speed FASTCAM NOVA S9 digital video camera with a resolution of 1024 × 1024 pixels, providing an inter-frame delay of 2.3 microseconds.

The electric arc energy supply in the wind tunnel work chamber forms a dusting of the flow by particles. The frames obtained by laser illumination of plate BL (Fig. 1b) show that

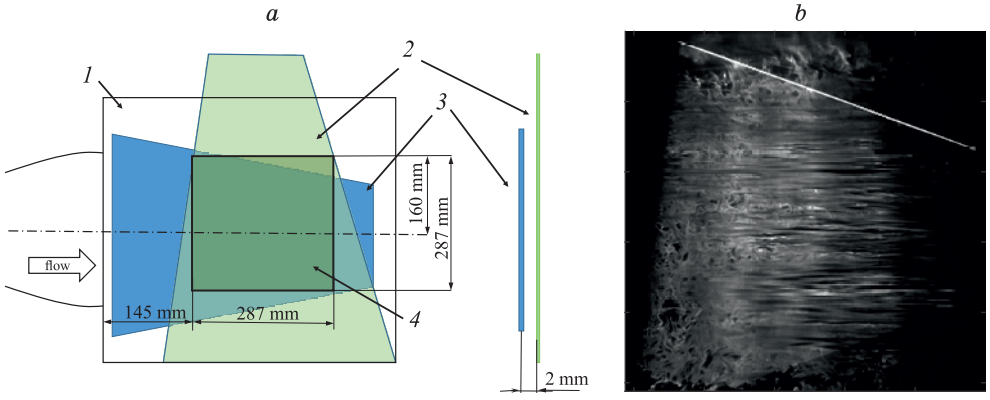

Fig. 1. Location(a) and image (b) of the flow velocity measurement area with the plane of the laser knife:

1 – the working chamber, 2 – the laser knife, 3 – the plate model, 4 – the field of view of the camera

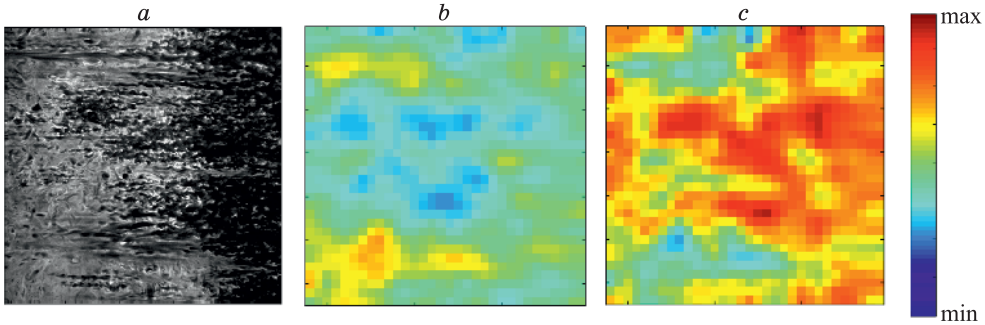

Fig. 2. Laser visualization of the boundary layer on the plate (a), and the result of using texture templates to detect laminar (b) and turbulent (c) flows.

the seeding of the flow in the plane of the laser knife is heterogeneous. Experimental results of laser visualization of the structure of seeding by particles of the flow and the boundary layer of the plate in laminar, transient and turbulent flow regimes were obtained. The dependence of the spectral characteristics of the inhomogeneity of particle seeding on the Reynolds number was demonstrated in experiments. At the same time, the spectral characteristics of the field of this inhomogeneity of seeding in the incoming flow do not depend on the choice of the direction in which the spectral decomposition is performed, i.e., the field of inhomogeneity of seeding of particles in the incoming flow is isotropic. In the case of an uneven average flow velocity field in the plate BL, the isotropy of the seeding inhomogeneity is violated. Once in the region of the longitudinal velocity gradient of the laminar BL, the inhomogeneities experience "stretching", forming extended longitudinal structures. It is shown that the spectral method can isolate such an anisotropic component of the seeding inhomogeneity field (by using Fourier filters).

A statistical approach to the analysis of laser imaging of the inhomogeneity of particle seeding in the plate BL was performed using GLCM (Gray-Level Co-occurrence Matrix). The main types of distributions of the elements of these matrices for various flows in the incoming flow and boundary layer are revealed. The dependence of GLCM on the spatial resolution and image size, the location of adjacent pixels is investigated. The dependence of the textural features of GLCM on the state of the flow in the boundary layer is shown and the principle of constructing special texture templates that allow to identify certain types of flows in visualizations is proposed. Fig. 2 shows examples: the initial image (a) containing the area of turbulent flow and the results of applying texture patterns (b, c).

The results of the study can be used for automated detection of the flow state and laminar-turbulent transition.

The work was carried out within the framework of the state task of ITAM SB RAS. The experiments were carried out on the basis of the Shared-Use Center "Mechanics".

REFERENCES

1. **Akhmetbekov E.K., Bilsky A.V., Lozhkin Yu.A. Markovich D.M, Tokarev M.P., Tyuryushkin A.N.** Software for experiment management and processing of data obtained by digital flow visualization techniques (ActualFlow) // Numerical Methods and Programming. 2006. V. 7. №. 3. P. 79–85.
2. **Haralick R.M.** Statistical and structural approaches to texture // Proceedings of the IEEE, 1979. Vol. 67, № 5, P. 768–804.

DOI 10.53954/9785604990148_75

ACCELERATION OF THE CONVERGENCE OF THE ITERATIVE SOLUTION FOR THE AIRCRAFT'S SIZING EQUATION WHEN OPTIMIZING ITS PARAMETERS

V.H. Hoang, O.E. Lukyanov

Samara National Research University,
443086, Samara, Russian Federation

This paper proposes a new method for the convergence of the aircraft's sizing equation to calculate take-off mass when optimizing parameters at the initial stages of design, allowing to speed up the solution. The proposed methodology operates in conjunction with a differential evolutionary optimization algorithm (Successful-History based Adaptive Differential Evolution (SHADE)) [1], characterized by the inclusion of the desired take-off mass of the aircraft in the vector of design variables when optimizing other parameters. During the optimization process, not only the considered design variables but also the take-off mass are involved in the mutation and crossover processes. Based on the results of obtaining a new population, the individuals with the lowest take-off mass will be selected. The value of the take-off mass of the previous optimization step, entered into the vector of design variables based on the selection result, and the value of the output take-off mass at the current optimization step will approach convergence. Thus, this approach ensures the convergence of the sizing equation in the general optimization cycle and does not require an internal iterative solution at each optimization step, which significantly reduces the calculation time.

The optimization problem of the key technical parameters of an aircraft in the general case is formulated [2]:

$$m_0\left(X^*\right) \le m_0\left(X\right) \forall X \in \Omega \tag{1}$$

$$\left\{X : g_j\left(X\right) \le 0, j = 1,2,\ldots,k\right\}$$

where: $m_0\left(X\right)$ – objective function; $X = \left\{x_1, x_2, ..., x_n\right\}$ – vector of design variables; Ω – range of permissible values determined by a set of restrictions:

– Restriction on the maximum value of the lift coefficient:

$$g_1\left(X\right) = c_{ya}\left(X\right) \le c^*_{ya} \tag{2}$$

– Restriction on the value of the horizontal tail volume coefficient to ensure the required UAV controllability characteristics [3]:

$$g_2\left(X\right) = A_{\text{ro}}\left(X\right) \in \left[A_{\text{ro\_min}}, A_{\text{ro\_max}} \right] \# \tag{3}$$

Aircraft trim is taken into account during all three phases of flight: climb, cruise, descent and landing as follows:

$$m_z\left(X\right) = 0 \tag{4}$$

$$c_{ya}(X) = c_{ya_{bal}}(X) \tag{5}$$

where: c_{ya} – lift coefficient; c^*_{ya} – permissible lift coefficient at a given flight mode; A_{zo} – horizontal tail volume coefficient; m_z – pitching moment coefficient relative to the center of mass; $c_{ya_{bal}}$ – lift coefficient in trim condition.

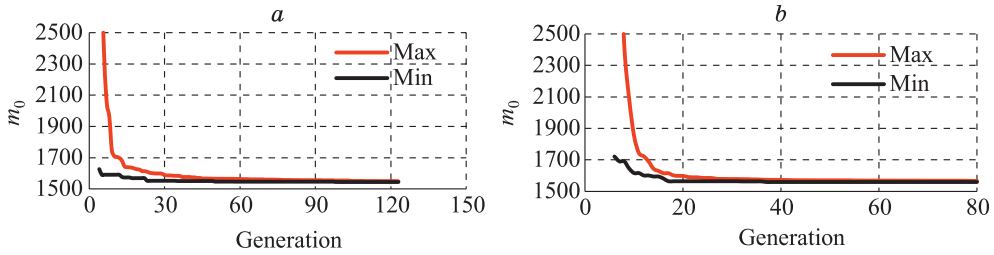

Fig. 1. Objective function convergence process proposed solution (a) and traditional solution (b)

The implementation of restrictions is carried out by the method of penalty functions. The methodology is implemented on the Python platform with the connection of the AVL open source code for aerodynamic calculations.

To demonstrate the advantages of the convergence speed of the proposed approach, the optimization problem of choosing the parameters of the geometric appearance of a heavy UAV and some flight parameters is considered, including: aspect ratio of forward (λ_1) and backward surface (λ_2); sweep along the leading edge of the forward (χ_1) and backward surface (χ_2); taper of the forward (η_1) and backward surface (η_2); installation angle of forward surface (δ_1); relative distance between two surfaces ($\overline{L}$); relative area between two surfaces ($\overline{S}$); velocity (V); specific wing load (p_0) and first approximation take-off mass (m_0^{in}). In addition, the proposed model also takes into account parameters: installation angle of the backward surface (δ_2) and angle of attack (α) as design parameters that are optimized indirectly through a balancing algorithm [3].

To assess the effectiveness of the proposed method, a method for determining m_0 is implemented based on the traditional method, where m_0 will not be considered as the initial calculated parameter, but will be fixed at a sufficiently large value for all individuals, then it is necessary to introduce an internal loop for solving the sizing equation for each individual.

Fig. 1 shows the process of optimization convergence using the proposed method for solving the sizing equation and the traditional method. It should be noted that both convergence methods lead to the same objective function value and combination of design variables.

Table presents comparative characteristics of optimization convergence in the case of using a traditional solution to the sizing equation and the proposed solution in the general optimization cycle.

The number of iterations in the overall optimization cycle of the traditional method is reduced, since the number of input variables is reduced by one (input mass m_0^{in}) and the accuracy of the output mass m_0^{out} at the current optimization iteration increases, but the calcula-

Comparison of parameters between two methods

Parameters	Convergence of traditional method	Convergence of proposed method
Number of iterations of calculating the sizing equation at each optimization step for each individual (average)	6	1
Time to calculate the sizing equation for one individual [s] (average)	14	2,4
Number of iterations	80	123
Total optimization time [h]	3,48	1,04
Convergence accuracy of take-off mass	0,5%	0,5%

tion time increases significantly due to the time spent on additional iterations of solving the sizing equation. At the same time, the proposed method achieves similar convergence accuracy at the end of the optimization process while consuming less time.

REFERENCES

1. **Tanabe R., Fukunaga A.** Success-history based parameter adaptation for Differential Evolution // IEEE Congress on Evolutionary Computation, Cancun, Mexico, 2013. P. 71–78. doi: 10.1109/CEC.2013.6557555.
2. **Lukyanov O.E.** Development of a Methodology for Selecting the Shape of Cargo Aircraft Using Multidisciplinary Optimization; Candidate of engineering sciences thesis; Samara National Research University: Samara, Russia, 2019. 154 p.
3. **Balakin V.L., Lazarev Yu.N.** Aircraft flight dynamics: stability and controllability of longitudinal motion. Samara State Aerospace University, 2011. 48 p.
4. **Pioquinto J.G.Q., Shakhov V.G.** Acceleration of Evolutionary Optimization for Airfoils Design with Population Size Reduction Methods // Proc. of 20 Int. Conf. on the Aviation and Cosmonautics. Samara. 2021. P. 22–26.

DOI 10.53954/9785604990148_78

NUMERICAL SIMULATION OF NONLINEAR DISTURBANCE PROPAGATION OVER UNSWEPT PARABOLIC AIRFOIL IN SUPERSONIC FLOW

I.M. Ilyukhin[1, 2], I.V. Egorov[1, 2]

[1]Moscow Institute of Physics and Technology
141701, Dolgoprudny, Russia

[2]Central Aerohydrodynamic Institute
140180, Zhukovsky, Russia

Turbulent spots appear to be the final stage in the development of the disturbances in the boundary layer [1]. In the intermittency region, their interaction leads to a transition from a laminar boundary layer to a turbulent boundary layer as the area occupied by the spots expanding downstream grows [2]. Additionally in this region, a maximum in the distribution of skin friction coefficient and heat fluxes on the surface of the body is observed [3], which can play a crucial role in the design of supersonic aircraft.

The paper presents the results of numerical simulation of the excitation and development of nonlinear disturbances in the boundary layer of an unswept parabolic airfoil. The computation is performed using the in-house code [4], previously successfully used for the calculation of turbulent spots development [5]. The peculiarity of the parabolic profile is an almost constant pressure gradient. The computational regime is chosen in accordance with [6] and approximately corresponds to flight conditions at an altitude of 20 km. The temperature of the impinging flow $T^*_\infty = 230$K, the Reynolds number based on the impinging flow parameters and the profile length $Re_\infty = 2.72 \times 10^7$. It is shown that the critical amplitude of pressure disturbances on the wall, at which the nonlinear stage of perturbation development began, is equal to 0.58% relative to the local pressure at the outer boundary of the boundary layer. The critical amplitude of longitudinal velocity pulsations on the grid line, approximately corresponding to 40% of the boundary layer thickness, related to the value of longitudinal velocity at the outer boundary of the boundary layer, is equal to 7.5%.

In the nonlinear regime, the interaction of oblique waves with equal frequencies and equal but opposite in sign transverse wave numbers lead to the formation of harmonics corresponding to longitudinal structures in the disturbance spectrum of the longitudinal velocity. The interaction of these harmonics with each other and with the initial perturbations fills the perturbation spectrum of the boundary layer and leads to a sharp increase in the amplitude of the zero harmonic, which indicates the formation of a turbulent spot. The dominant mechanism of nonlinear breakdown is an oblique breakdown, which is shown to be the most probable scenario on the plate at Mach number 1.6 [7].

The evolution of a single spot is compared with the evolution of two interacting spots. The evolution of the isolated spot is well described by correlations for the spots constructed for flows without pressure gradient [8]. On the overlap regime, new perturbations (Fig. 1), not previously observed by other researchers [9], are formed behind the interaction region of the spots. In the distribution of the instantaneous skin-friction coefficient in the interaction region of two spots, the maximum value is reached behind the initial spots (Fig. 2).

Acknowledgments. The authors are grateful to A.V. Fedorov of MIPT for productive discussions and valuable comments. The research was funded by the Russian Science Foundation (project No. 23-79-10072).

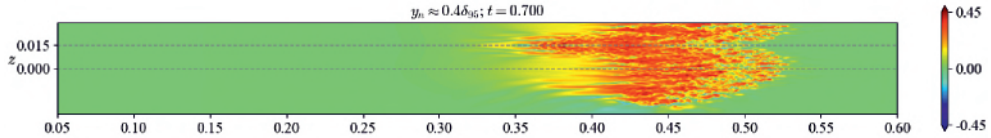

Fig. 1. Perturbations of the longitudinal velocity at 40% of the boundary layer thickness. Two overlapping spots are presented in the upper half-plane, single spot is shown in the lower half-plane

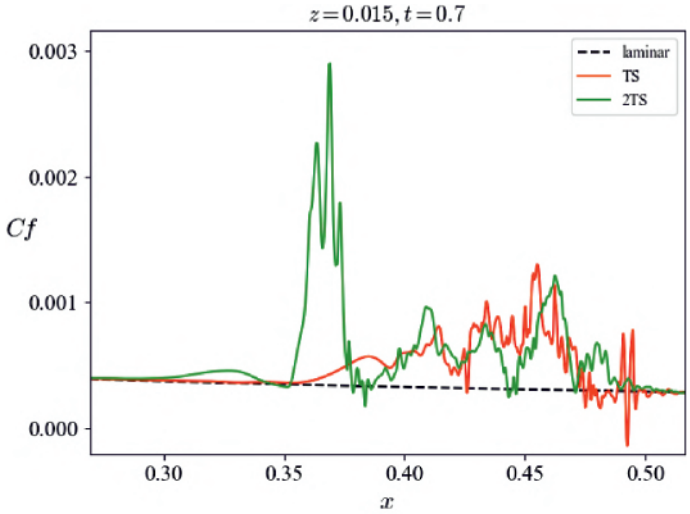

Fig. 2. Instantaneous skin-friction coefficient distribution along z = 0.015 for single spot (TS) and two interacting spots (2TS)

REFERENCES

1. **Fedorov A.V.** Transition and Stability of High-Speed Boundary Layers // Annual Review of Fluid Mechanics. Annual Reviews, 2011. Vol. 43, 2011. P. 79–95.
2. **Narasimha R.** The laminar-turbulent transition zone in the boundary layer // Progress in Aerospace Sciences. 1985. Vol. 22, № 1. P. 29–80.
3. **Egorov I.V. et al.** Simulation of the Laminar–Turbulent Transition by Applying Dissipative Numerical Schemes // Comput. Math. and Math. Phys. 2021. Vol. 61, № 2. P. 254–266.
4. **Bashkin V.A., Egorov I.V.** *Numerical Simulation of Viscous Perfect Gas Dynamics*. Begell House Inc., 2016.
5. **Egorov I.V., Novikov A.V., Chuvakhov P.V.** Numerical Simulation of the Evolution of Turbulent Spots in a Supersonic Boundary Layer over a Plate // Math Models Comput Simul. 2023. Vol. 15, № 1. P. 118–124.
6. **Chuvakhov P.V., Ilyukhin I.M., Fedorov A.V.** Stability of supersonic boundary layer over an unswept wing with a parabolic airfoil // Theor. Comput. Fluid Dyn. 2023.
7. **Chang C.-L., Malik M.R.** Oblique-mode breakdown and secondary instability in supersonic boundary layers // J. Fluid Mech. 1994. Vol. 273. P. 323–360
8. **Van den Eynde J., Steelant J**. Compressibility and temperature effects on turbulent spot growth // Proceedings of HiSST. CEAS, 2018.
9. **Krishnan L., Sandham N.D.** On the merging of turbulent spots in a supersonic boundary-layer flow // International Journal of Heat and Fluid Flow. 2006. Vol. 27, № 4. P. 542–550.

DOI 10.53954/9785604990148_80

VORTEX HEAT TRANSFER ENHANCEMENT IN STRUCTURED MICROCHANNELS AND TUBES DURING THE MOVEMENT OF INHOMOGENEOUS VISCOUS MEDIA

S. Isaev[1, 2], D. Nikushchenko[1], E. Nikushchenko[1], E. Osyuk[2], A. Klyus[2]

[1]*Saint-Petersburg State Marine Technical University, 190121, Saint-Petersburg, Russia*
[2]*Novikov's Saint-Petersburg State University of Civil Aviation, 196210, Saint-Petersburg, Russia*

The intensification of heat transfer during the movement of inhomogeneous media in structured microchannels and pipes with surface generators of intense spiral vortices - inclined oval-trench dimples (OTD) [1] and protrusions is being studied, a calculation methodology is being developed using original multi-block technologies, and domestic methods are being developed and verified. software (parallelized package VP2/3 – "speed-pressure, 2D/3D"). The emphasis in the working media used is on oil (M20 and transformer), for which the thickness of the thermal boundary layer is radically less than the thickness of the dynamic layers, which determines the effectiveness of small-scale discrete roughness at very moderate velocities of the medium. For comparison, air, water and a model liquid with constant physical properties and a high Prandtl number are also considered.

Parametric numerical modeling of laminar heat transfer in round pipes with structured walls was carried out. Databases have been generated for a comparative analysis of traditional symmetrical and weakly asymmetrical shapes of dimples and oval-trench dimples in order to justify the preference of extended dimples – surface vortex generators.

Both the limiting characteristics of laminar convective heat transfer in dimpled pipes with a corridor arrangement of dimples in the stabilized section, and the characteristics of the dimpled pipe section in the initial hydrodynamic section are predicted.

The angle of inclination of the OTD has a significant effect on the thermal and thermohydraulic efficiency of the dimpled pipe in the stabilized section of the laminar flow of transformer oil. The highest thermal efficiency reaches almost 30, and the thermal-hydraulic efficiency reaches 20 at an inclination angle of 55 degrees. Spherical dimples are significantly (one and a half to two times) inferior to OTD at the optimal angle of inclination, but are close in heat transfer characteristics at an inclination angle of 30 degrees.

The intensification of laminar heat transfer in the initial hydrodynamic section of a round pipe is analyzed when pumping a coolant with a fixed large Prandtl number (Pr = 327) at a Reynolds number of 2000, determined by the diameter of the pipe (Fig. 1). We are considering a seven-row corridor package with 8 OTDs evenly spaced around the circumference, applied with a pitch of 0.275 on an dimpled section 1.925 long and inclined at an angle of 45 degrees. The distributions of the relative values of the friction components, local and integrated over the transverse stripes of Nusselt numbers on the scan of the irradiated pipe wall demonstrate a gradual intensification of flow and heat transfer in the longitudinal stripes as the rows of dimples increase in the longitudinal direction. Local values of relative friction towards the end of the irradiated section reach values of the order of 3, and the values of relative Nusselt numbers exceed 25 on the windward slopes of the last row of dimples. The maximum Nusselt numbers averaged over the bands reach 8–10. The thermal efficiency of

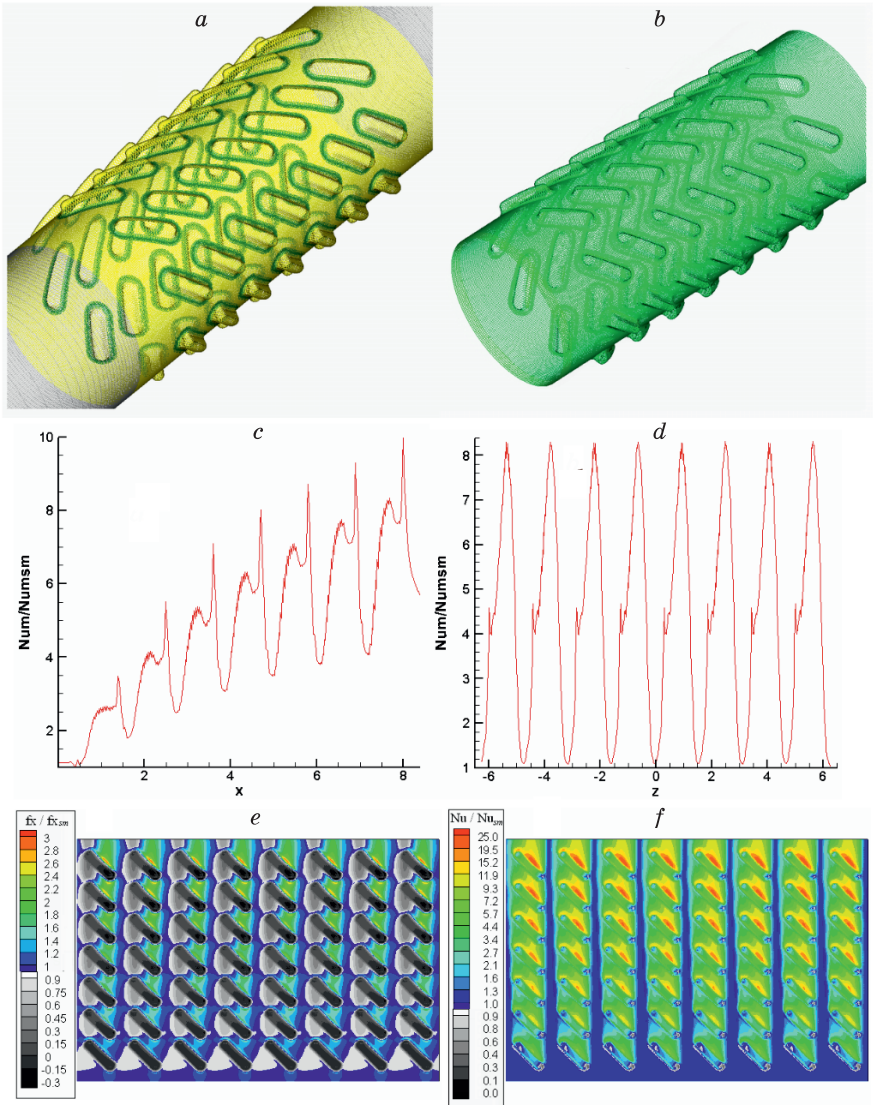

Fig. 1. A tube with a package (7×8) of oval-trench dimples (a) and a selected dimpled middle section (b), distributions along the longitudinal (c) and transverse (d) coordinates of the relative Nusselt numbers integrated along the transverse and longitudinal stripes of the dimpled section of the tube, scan of the fields of relative x-components of friction (e) and Nusselt numbers (f) on the dimpled section of the tube

the dimpled area is 4.676 with practically unchanged hydraulic losses (increase by 1.022 times). The thermal-hydraulic efficiency of the section is 4.575.

The investigations are partially supported by the RSF (grant No 23-19-00083, testing and grant No 22-19-00056, calculations).

REFERENCES

1. Isaev S.A. Genesis of anomalous intensification of separation flow and heat transfer in inclined grooves on structured surfaces // Fluid Dynamics. 2022. Vol. 57 (5). P. 558–570.

DOI 10.53954/9785604990148_82

NEW PERSPECTIVES OF AEROPHYSICS OF THE XXI CENTURY

M.Ya. Ivanov

Research Institute of Mechanics, Moscow State University
119192, Moscow, Russia

Experimental achievements of the 21st century allow us to consider new prospects for the use of aerophysical methods in the study of natural and technical processes. In terms of natural ones, we will indicate a wide range of processes occurring on various scales (from the characteristic nuclear scale – about 10–15 m and to the galactic scale of our Universe). Vivid examples here are the structure of the gold ion registered using tomography methods [1] (Fig. 1, a), high-speed registration of superluminal photon motion [2] (Fig. 1, c), registration of superluminal cosmic jets [3] (Fig. 1, c) and a photograph of the center of our Milky Way galaxy [4] (Fig. 1, d).

The presented report examines such prospects. At the same time, the analysis is based on the ideas of the famous scientific school of Academician G.G. Cherny [5] and his students. The theoretical part of the study uses the laws of conservation of continuum mechanics, the classical theory of the electromagnetic field and Faraday's field lines recorded in experiments. When obtaining the corresponding systems of equations for modeling aerophysical processes in a generalized approximation, in particular, an analogy with the hydrodynamic methodology of vortex motions in the Gromeka-Lamb form was used [6, 7]. We present here, as a demonstration, Euler's basic equation for the vortex motion of a compressible gas in generally accepted notation

$$\frac{\partial \vec{V}}{\partial t} + \vec{\omega} \times \vec{V} = -grad\ H,$$

where $\omega = \mathrm{rot}V$, H is the so-called Lamb function introduced for polytropic gas. Applying the rot operation to this equation, we arrive at an equation that describes the change in time of the vorticity vector ω.

Lamb in his book [7] notes the complete analogy of the analytical relationships between aerophysical and electromagnetic relationships, on which this study is based.

A wide class of processes is considered both in the traditional linear approximation and taking into account nonlinear effects leading to the formation of solitons and the presence of intense transition fronts. As typical examples of promising directions, we indicate the mod-

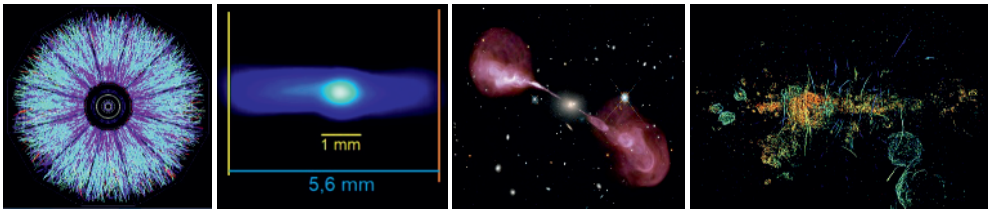

Fig. 1. (a). Polarized space of the gold ion (outer electron shell) [1]; (b) – photograph of a superluminal photon [2]; (c) – photograph of the superluminal jet of the quasar GW170817 [3]; (d) – cosmic jets in the Milky Way galaxy [4].

eling of processes that are illustrated in Fig. 1. In terms of technical applications of aerophysics, examples of solving problems in engines with spin detonation, high-temperature foreign jet engines and ground-based gas turbine engines are given.

The performed theoretical and experimental analysis allows us to confirm the fact of the presence in nature of only one physical interaction – an electrodynamic force field. All other force fields – gravitational, strong and weak – are special cases of the electrodynamic force field. In the absence of charge movement, only purely electrostatic Faraday lines of force (electric potential gradient lines) are clearly demonstrated. The general case of a vortex electrostatic field is analyzed. A magnetic field appears only when charges move and can also be represented in the form of magnetic lines of force, introducing its potential and vortex parts into consideration. In the stationary case, the theory is reduced to the unified Hooke-Newton-Coulomb law in the form of the quasilinear Poisson-Boltzmann equation, which unifiedly models gravitational, strong and weak force interactions [8]. In the non-stationary case, the theory leads to an extended system of Maxwell's electromagnetic equations.

REFERENCES

1. Tomography of ultrarelativistic nuclei with polarized photon-gluon collisions. // STAR 2023. Collaboration. Sci. Adv. No. 9.
2. **Kazuhiro Morimoto, Ming-Lo Wu, Andrei Ardelean, Edoardo Charbon.** Superluminal Motion-Assisted 4-Dimensional Light-in-Flight Imaging. arXiv:2007.09308, v1, 2020.
3. **Mooley K.P., Deller A.T., Gottlieb O.** et al. Superluminal motion of a relativistic jet in the neutron-star merger GW170817. Nature 561, 355–359 (2018).
4. **Yusef-Zadeh F., Arendt R.G., Wardle M.** The Population of Galactic Center Filaments: Position Angle Distribution Reveals a Degree-scale Collimated Outflow from Sgr A* along the Galactic Plane. The As trophysical Journal Letters, 949:L31 (14pp), 2023.
5. **Cherny G.G.** A word about eternally new mechanics. Lecture on the "Knowledge" society program, Moscow Polytechnic Museum, March 20, 2008. Institute of Mechanics, Moscow State University. – 68 p.
6. **Gromeka I. S.** Collected Works. – M.: Publishing House of the USSR Academy of Sciences, 1952. – 296 p.
7. **Lamb G.** Hydrodynamics. M.-L., OGIZ, 1947. – 928 p.
8. **Ivanov M.Ya.** On the classical theory of a unified force field with modeling of near and far Interactions. Phys. images in universities. 2022, 28, No. 1, – pp. 43–61.

DOI 10.53954/9785604990148_84

RETURN FLOWS STRUCTURE ANALYSIS IN THE INTERACTION ZONE OF STRONGLY UNDEREXPANDED JETS WITH STRUCTURAL ELEMENTS

A.V. Kashkovsky[1], M.S. Antipova[2], A.V. Beloshitsky[2], Yu.I. Gerasimov[2], A.N. Krylov[2], Y.S. Pyatakova[2], A.A. Rodicheva[2]

[1] Khristianovich Institute of Theoretical and Applied Mechanics, SB RAS
630090 Novosibirsk, 4/1 Institutskaya str.

[2] RSC Energia,
141070 Korolev, Moscow region, 4a Lenin Street

Numerical methods for calculating jet flows are widely used in the development of new spacecraft, which significantly reduce the amount of experimental testing. One of these tasks is to determine the force and thermal effects of blocky strongly underexpanded jets on the structural elements of the spacecraft in the orbital flight.

This paper presents the results of numerical studies of the flow fields of multiblock jets of engines that meet at large angles and form intense zones of continuous medium and transient flow regimes.

To solve this problem, a multi-zone approach is used, implying the division of the entire flow region into several zones, in each of which flow modeling is performed using the most appropriate method, depending on the gas flow regimes. The Navier-Stokes equations are solved for the continuous medium regime, and the direct statistical modeling (PSM) method is used for transient and free molecular regimes [1, 2]. Modeling in zones is performed sequentially, and the calculation results in each zone are used as boundary or initial data in the next zone. This approach has been repeatedly applied to simulate flow into vacuum [3, 4, 5].

As preliminary calculations have shown, it is difficult to use a multi-zone approach to assess the impact of the jet on structural elements located close to the engines. A noticeable part of the jet is reflected from the structural elements and of return flows appear. In fact, the boundary of the continuum and transition zones lies behind the nozzle section, but the transition from zone to zone is complicated by return flows, which greatly affects results accuracy. Therefore, in this study, it was decided to make zones boundary in nozzle exit and to model the flow inside nozzle based on solving the Navier-Stokes equations using the commercial FloEFD package. The distribution of gas dynamic parameters along the nozzle section serves as initial data for flow modeling using the PSM method. With this approach, another problem arises: modeling the flow using the PSM method from the nozzle exit at a distance of several meters requires significant computing resources. This problem was solved by using graphics processing units (GPUs) in the PSM method [6, 7].

Calculations have been performed for the cases of interaction of jets from 2 to 8 engines. The results of calculating the distribution of convective heat flows over the surface of structural elements during operation of 8 engines are shown in Fig. 2.

The analysis of the influence of the calculation area size on the calculation results is carried out. Based on the results of the work performed, restrictions were set on the number of simultaneously operating engines and recommendations were issued for installing additional thermal protection in areas of maximum jets thermal impact.

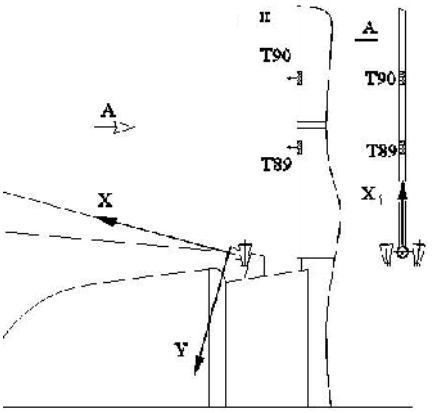

Fig. 1. Placement of calorimeters on Soyuz-T

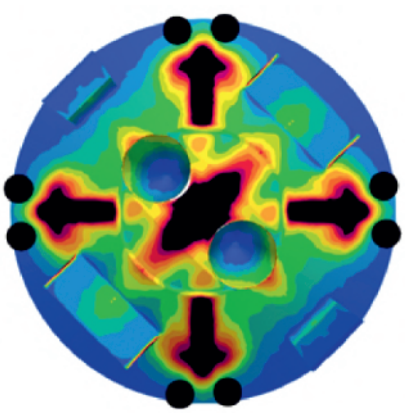

Fig. 2. Heat flows distribution on structural elements

REFERENCES

1. **Bird G.A.** Molecular gas dynamics and the direct simulation of gas flows .Clarendon Press, Oxford, 1994.
2. **Ivanov M.S., Rogazinsky S.V.** Analysis of the numerical techniques of the direct simulation Monte Carlo method in the rarefied gas dynamics. Soviet J. Numer. Anal.Math. Modelling, Vol.3, No.6, 1988, P.453–465.
3. **Giordano D., Ivanov M., Kashkovsky A., Markelov G., Tumino G., Koppenwallner G.** Application of DSMC to the Study of Satellite Thruster Plumes. Atlanta, AIAA Paper 97-2538.
4. **Ivanov M., Markelov G., Kashkovsky A., and Giordano D.** Numerical analysis of thruster plume interaction problems // Second Europian Spacecraft Propulsion Conference, ESA SP-398, August 1997, P. 603–610.
5. **Giordano D., Ivanov M.S., Kashkovsky A.V., Markelov G.N., Tumino G., and Koppenwallner G.** Application of the numerical multizone approach to the Studyof Satellite Thruster Plumes. J. Spacecraft and Rockets, Vol. 35, No. 4, 1998, P. 502–508.
6. **Kashkovsky A.V. Vashchenkov P.V. Shershnev A.A. Shevyrin A.A.** Parallelization of the DSMC method for simulation of high-altitude aerothermodynamics on hybrid supercomputers./ 17th International Conference on the Methods of Aerophysical Research (ICMAR'2014) (Russia, Novosibirsk, 30 Jun. – 6 Jul., 2014): abstracts. Pt. II. – Novosibirsk, 2014. – P. 90–91.
7. **Kashkovsky A.V.** 3D DSMC computations on a heterogeneous CPU-GPU cluster with a large number of GPUs. 29th International Symposium on Rarefied GasDynamics (RGD) (China, Xian, 13–18 Jul., 2014: Proceedings AIP Conference. – Vol. 1628. – Melville; New York, 2014. – P. 192–198. – (AIP Conference Proceedings, V. 1623). DOI: 10.1063/1.4902592.

DOI 10.53954/9785604990148_86

IDENTIFICATION OF VORTICES ON THE BACKGROUND OF A NOISY FLOW FIELD.

A.V. Kashkovsky

Khristianovich Institute of Theoretical and Applied Mechanics SB RAS,
630090 Novosibirsk, Russia

One of the aspects of using the Direct Simulation Monte Carlo (DSMC) method [1] is studying the flow instability [2–6]. Due to its stochastic nature, this method allows instability to be excited without introducing additional disturbances. As a result, the mechanism of instability initiation and development can be studied in more detail.

Flow simulation by the DSMC method is based on using particles that move and collide like gas molecules. The number of particles and their velocities in each cell are accumulated in counters that are subsequently used to calculate the gas-dynamic parameters of the flow. Obviously, the longer the accumulation period, the "smoother" the flow fields. However, the accumulation period in unsteady calculations is rather short, resulting in large fluctuations of the gas-dynamic parameters.

A fragment of the vertical velocity field in the problem of a mixing layer of two flows with Mach numbers of 1.5 and 2.5 are shown in Fig. 1. Although the vortices are "captured," it is rather difficult to obtain their sizes and coordinates of their centers due to the "spotty" nature of the flow field. Standard analysis schemes (Q-criterion, entropy field, etc.) use derivatives, which makes the picture even more "spotty" and does not facilitate the analysis.

To analyze vortices in noisy flows, an algorithm based on integration of rotation velocities in a given neighborhood is proposed. Integration can significantly reduce the statistical noise.

The result of applying this algorithm is shown in Fig. 2. The maximum and minimum of the criterion (called the "vox" criterion) correspond to the centers of vortices with positive (clockwise) and negative rotation.

The flow pattern looks smoother, and vortices are visible even at the very beginning of flow mixing (at the left boundary), which is practically impossible to resolve in Fig. 1. This criterion allows one not only to find the vortex center positions, but also to estimate their sizes and rotation intensity. It seems that this criterion can be used not only to analyze flows obtained by the DSMC method, but also to analyze experimental results.

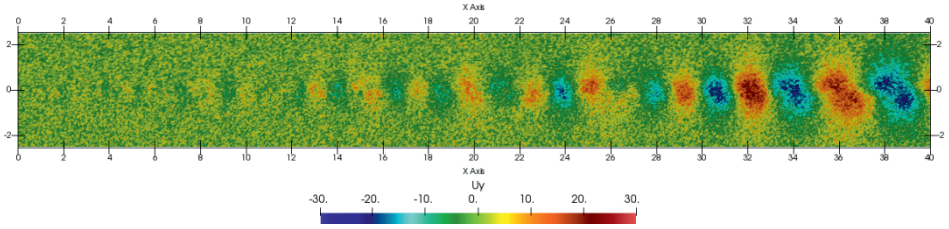

Fig. 1. Vertical velocity, m/s.

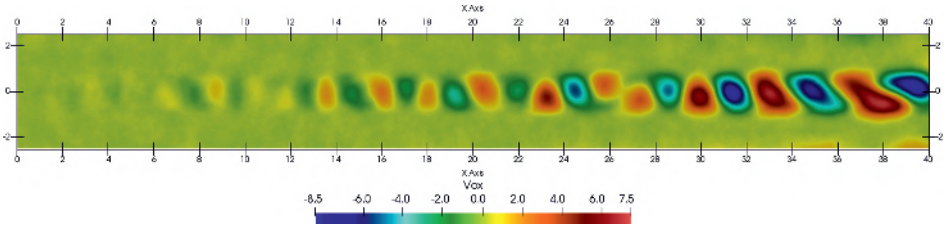

Fig. 2. Proposed “vox” criterion.

The research was supported by the Russian Science Foundation (grant No. 23-11-00258). The study was conducted at the Equipment Sharing Center “Mechanics” of ITAM SB RAS.

REFERENCES

1. **Bird G.A.** Molecular gas dynamics and the direct simulation of gas flows .Clarendon Press, Oxford, 1994.
2. **Gallis M.A., Koehler T.P., Torczynski J.R., Plimpton S.J.** Direct simulation Monte Carlo investigation of the Richtmyer-Meshkov instability // Phys. Fluids. 2015. Vol. 27, No. 084105. doi: 10.1063/1.4928338
3. **Gallis M.A., Koehler T.P., Torczynski J.R., Plimpton S.J.** Direct simulation Monte Carlo investigation of hydrodynamic instabilities in gases // AIP Conference Proceedings. 2016. Vol.1786. No. 050002. doi: 10.1063/1.4967552
4. **Kashkovsky A.V., Kudryavtsev A.N., Shershnev A.A.** Investigation of the Kelvin-Helmholtz instability with the DSMC method // Proc. of the XXVI Conf. on High-Energy Processes in Condensed Matter (HEPCM–2019): AIP Conference Proceedings. 2019. – Vol. 2125. No. 030028(5). doi: 10.1063/1.5117410
5. **Kashkovsky A.V., Kratova Y.V., Shershnev A.A.** Initiation of Richtmyer–Meshkov instability by a detonation wave // XVI All-Russian Seminar with international participation “Dynamics of Multiphase Media”: IOP Publishing, 2019. Vol.1404. pp. 012058(6). doi: 10.1088/1742-6596/1404/1/012058
6. **Kashkovsky A.V., Kudryavtsev A.N., Shershnev A.A.** Numerical simulation of the Rayleigh-Taylor instability in rarefied Ar/He mixture using the Direct Simulation Monte Carlo method // XXXV Siberian Thermophysical Seminar: IOP Publishing, 2019.Vol. 1382. pp. 012154(5). doi: 10.1088/1742-6596/1382/1/012154

DOI 10.53954/9785604990148_88

KINETIC AND CONTINUUM SIMULATIONS OF A REVERSE FLOW BEHIND THE MACH DISC IN AN UNDEREXPANDED SUPERSONIC JET

A.V. Kashkovsky, A.N. Kudryavtsev, A.A. Shershnev, L.P. Trubitsyna, V.I. Zapryagaev

Khristianovich Institute of Theoretical and Applied Mechanics SB RAS, 630090, Novosibirsk, Russia

In the present paper the emergence of a recirculation region behind the Mach disc of the first shock cell of an underexpanded jet is studied using different numerical approaches. This phenomenon was observed in many numerical simulations using a wide variety of computational approaches, including the Euler equations [1], laminar Navier-Stokes (NS) equations [2, 3, 6], Reynolds-averaged Navier-Stokes equations (RANS) [5], the so called quasigasdynamic (QGD) equations and recently it was studied numerically using kinetic approach based on the Direct Simulation Monte Carlo (DSMC) method [6]. In [6] it was shown that NS and DSMC produce similar solutions with reverse flow behind the Mach disc and the sizes of recirculation regions are in reasonable agreement. At the same time, there is no experimental evidence of the natural occurrence of the reverse flow behind the Mach disc, see e.g. [7, 8]. Any emergence of this phenomenon in experiments was induced by some external action on the jet, such as thin jet of a low-pressure gas was injected along the jet axis from the nozzle [9] or when an upstream-directed thin spike was placed along the axis [7].

In attempts to explain these discrepancies between numerical solutions and experimental data we carried out a series of computations of underexpanded circular jet of argon with jet Mach number $M_j = 1.2$ and nozzle pressure ratio $n = 8$, using three different CFD codes: in-house code HyCFS-R based on the Navier-Stokes equations and modern shock-capturing schemes, popular commercial software suite Ansys Fluent and SMILE++/SMILE-H software systems based on the DSMC method. Initially the computations were performed for the axisymmetric case, where all approaches showed close results with a recirculation region in the flow pattern.

However, it should be noted that the axisymmetric formulation is usually associated with computation of terms containing $1/r$ factor, poor approximation of which can lead to numerical artifacts near the jet axis. This affects all three approaches used, and as a result obtained solutions could be physically unviable. To factor out the approximation near the axis as potential source of errors, fully 3D computations were performed using HyCFS-R and SMILE-H codes. The results are presented in Fig. 1, where the local Mach number isolines are shown. As can be seen both computations once again yield close results in terms of flowfields and shockwave configurations with reverse flow present in both solutions. This result confirms that the emergence of a reverse flow behind the Mach disc is not caused by numerical errors in approximation of axisymmetric terms near the axis. Further investigation of the phenomenon would require additional numerical simulations, experiments and more detailed analysis of new and available data.

This study was supported by the Russian Science Foundation (Grant No. 23-11-00258). All computations were performed at the Equipment Sharing Center «Mechanics» of ITAM SB RAS.

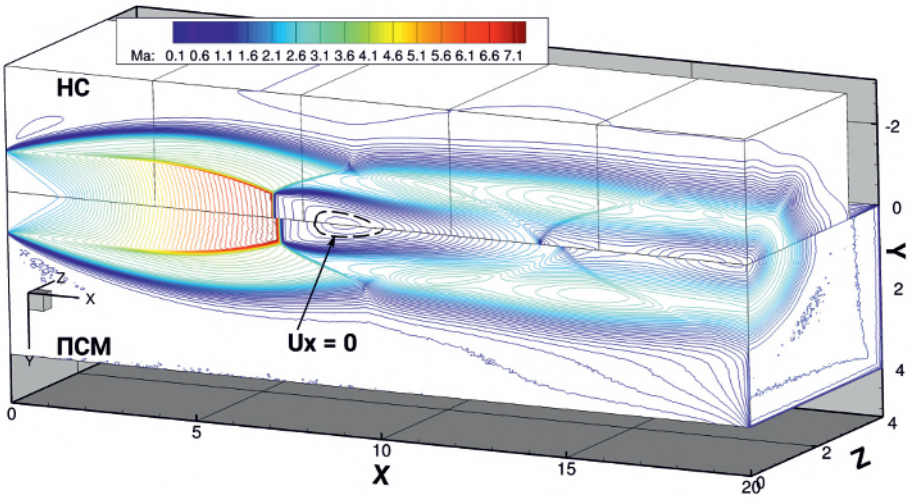

Fig. 1. Mach isolines in 3D Navier-Stokes (top) and Direct Simulation Monte Carlo (bottom) computations. Dashed line indicates the boundary of recirculation region.

REFERENCES

1. **Goryainov V.A.** Some possibility of reverse phenomenon for supersonic flows in free jets // Matem. Mod. 2003. Vol. 15. No. 7. P. 86–92.
2. **Gribben B.J., Badcock K.J., Richards B.E.** Numerical study of shock-reflection hysteresis in an underexpandedjet // AIAA J. 2000. Vol. 38, No. 2. P. 275–283.
3. **Skovorodko P.A.** About the nature of the recirculation zone behind a Mach disk in an underexpanded jet // AIP Conf. Proc. 2011. Vol. 1333. P. 601–606. doi: 10.1063/1.3562713.
4. **Kashkovsky A.V., Kudryavtsev A.N., Shershnev A.A.** Numerical investigation of the rarefied supersonic underexpanded jet structure using the DSMC method // Thermophysics and Aeromechanics. 2023. Vol. 30, No. 1. P. 29–36.
5. **Reijasse P., Bouvier F. and Servel P.** Experimental and numerical investigation of cap-shock structure in overexpanded thrust-optimized nozzles // West East High Speed Flow Fields. Aerospace applications from high subsonic to hypersonic regime / ed. by D.E. Zeitoun, J. Périaux, J.A. Désidéri, M. Marini. CIMNE, Barcelona, Spain. 2003. P. 338–345.
6. **Maté B., Graur I.A., Elizarova T., Chirokov I., Tejeda G., Fernández J.M., Montero S.** Experimental and numerical investigation of an axisymmetric supersonic jet // J. Fluid Mech. 2001. Vol. 426. P. 177–197.
7. **Zapryagaev V.I., Boiko V.M., Kavun I.N., Kiselev N.P., Pivovarov A.A.** Flow structure behind the Mach disk in supersonic non-isobaric jets // AIP Conf. Proc. 2016. Vol. 1770, P. 030029-1–030029-8.
8. **Edgington-Mitchell D., Honnery D.R., Soria J.** The underexpanded jet Mach disk and its associated shear layer // Phys. Fluids. 2014. Vol. 26, No. 9. P. 096101-1–096101-5.
9. **Glotov G.F.** Local subsonic zones in supersonic jet flows // Fluid Dynamics. 1998, Vol. 33. P. 117–123.

DOI 10.53954/9785604990148_90

IMPLEMENTATION OF DYNAMIC SORPTION MODE ON SELECTIVELY PERMEABLE MICROSPHERES FOR HELIUM RECOVERY

I.V. Kazanin, V.N. Zinovyev, A.S. Vereshchagin, V.M. Fomin

Khristianovich Institute of Theoretical and Applied Mechanics SB
630090, Novosibirsk, Russia

At the Institute of Theoretical and Applied Mechanics of the Siberian Branch of the Russian Academy of Sciences, work is underway to develop a membrane-sorption method for extracting helium from gas mixtures for further use in the gas production industry. A distinctive feature of the method is the use of hollow spherical microparticles as membrane elements, the wall of which is selectively permeable to helium [1]. The use of hollow microspherical particles as membrane elements makes it possible to solve some of the features associated with silicate materials and membranes based on them, which are characterized by low permeability parameters and high selectivity coefficients, namely: significantly increase the total gas exchange area, while the spherical shape and small dimensions ensure high hydrostatic strength, which is directly related to the performance parameters of separation plants. As a result, such particles can be used as microballoons, into the internal volume of which helium from the mixture penetrates and is retained in it. Microspheres behave as adsorbents for helium, and the separation of the mixture is based on the selectivity of their shell. To separate the gas mixture, a short-cycle operating mode of the installation is used. At the first stage of the cycle, the helium-containing mixture is poured into the adsorber and the sorption process begins, helium penetrates into the internal volume of the microspheres, this process continues until the partial pressures outside and inside the microspheres are equalized. Next, the lean mixture is removed from the adsorber and, by creating a reverse helium pressure difference outside and inside the microspheres, the desorption process begins – helium from the internal volume of the microspheres enters the free volume of the adsorber and is pumped using compressor pumps into a special container. The lean mixture is sent to the next adsorber, where the separation stages described above take place – sorption and subsequent desorption, the cycles continue until the required degree of helium extraction from the mixture is achieved.

As various types of microspheres and granular sorbents based on them were studied, samples were discovered that had high permeability coefficients for helium. The characteristic times of sorption processes for which range from 5–6 minutes at a temperature of ~ 20 C to 60 seconds at a temperature of 110 C. At such high rates of absorption processes, it becomes possible to implement a dynamic mode of separation of helium-containing gas mixtures, similar to the short-cycle adsorption (SCA) method. In this case, the helium-containing mixture is passed through a sorbent located in an extended adsorber, such that the gas flow times exceed the characteristic times of sorption processes. Sorption process occurs, and the concentration of helium in the mixture decreases. As the sorbent becomes saturated, the supply of the mixture is switched to the next adsorber, while the original adsorber is put on regeneration – the absorbed helium is pumped out and pumped into a special container.

The goal of this work was to implement a dynamic sorption mode on selectively permeable microspheres for the release of helium. Determination of mixture separation parameters.

This required the creation of an experimental stand to study changes in the concentration of the components of a gas mixture as it flows through a selectively permeable layer of microspheres in the modes of the PSA method. To be able to obtain information directly at the pace of the experiment about changes in the concentration of components in the gas mixture, a concentration sensor developed at ITAM SB RAS for binary gas mixtures based on the hot-wire anemometric method was used. The operating principle of this sensor is based on determining heat loss on the sensitive element, which is proportional to the change in the thermal conductivity of the gas mixture, depending on the concentration of its constituent components and gas flow parameters.

The work was carried out with financial support from the Russian Science Foundation and the Government of the Novosibirsk Region (project code 23-29-10068).

REFERENCES

1. **Fomin V.M., Zinovyev V.N., Kazanin I.V., Lebiga V.A., Pak A.Y., Vereshchagin A.S., et al.** The method of separation of a multicomponent vapor-gas mixture. 2014 R.F. Patent No. 2508156014.
2. **Zinovyev V.N., Kazanin I.V., Pak A.Yu., Vereshchagin A.S., Lebiga V.A. and Fomin V.M.** Journal of Engineering Physics and Thermophysics 89, 25–37, (2016).

DOI 10.53954/9785604990148_92

NUMERICAL SIMULATION OF THE DEVELOPMENT OF DISTURBANCES AND TRANSITION TO TURBULENCE IN SUBSONIC AND SUPERSONIC ISOBARIC JETS

D.V. Khotyanovsky, A.N. Kudryavtsev

Khristianovich Institute of Theoretical and Applied Mechanics SB RAS, Novosibirsk, 630090, Russia

Based on the numerical solution of the Navier–Stokes equations, simulations of the development of disturbances and transition to turbulence in an isobaric jet exhausting from a circular nozzle have been carried out. The eddy-resolving simulations are carried out in a three-dimensional formulation for two values of the jet Mach number and several values of the Reynolds number. The calculations were carried out using the HyCFS computational code [1] developed at the Laboratory of Computational Aerodynamics of the ITAM SB RAS with spatial discretization of the convective terms of the Navier-Stokes equations based on the WENO shock-capturing scheme of the 5th order [2]. The computational domain had the form of a truncated pyramid of square section with a height $L_x = 40\ d$ along the streamwise axis x, and the dimensions $L_y = 10\ d$, $L_z = 10\ d$ along the normal axes y, z at the initial section $x = 0$. Here d, hereafter used as the length scale, is the diameter of the jet at the initial cross-section. The angle of expansion of the pyramidal computational domain in the streamwise direction was 7.5°. The computational grid was condensed in the region of the core and the near field of the jet. Calculations were performed on the grid $N_x = 1152$, $N_y = 330$, $N_z = 330$ (125 million cells in the entire computational domain). At the inflow boundary of the computational domain, at $x = 0$, the jet profile for the streamwise velocity component was set in the form:

$$U(r) = \frac{U_j + U_a}{2} + \frac{U_j - U_a}{2} \tanh\left(\frac{r_0 - r}{2\theta}\right) \qquad (1)$$

where U_j, U_a are respectively velocities of the jet and the ambient stream; $r_0 = 0{,}5$ is the jet radius at the initial cross-section; θ is the jet thickness at the initial section, which was assumed to be equal to $\theta = 0{,}01$. The temperature profile at the initial cross-section was set from the Crocco–Busemann relation for a gas with a Prandtl number Pr = 1. The pressure at the inflow boundary was assumed to be constant, which corresponds to the case of the isobaric jet. For better posedness of the numerical boundary-value problem, the boundary conditions at the inflow boundary corresponding to the ambient gas were set with an addition of a background co-flow of a low velocity U_a corresponding to the Mach number 0.05.

The first considered computational case corresponds to the experimental conditions [3] for a supersonic isobaric jet with the Mach number M = 2.12 and the Reynolds number determined by the diameter d of the nozzle exit section, Re = 70,000. The second computational case for a subsonic jet with the Mach number at the outlet of the nozzle M = 0.9 corresponds to the conditions of numerical simulations carried out in [4]. In all cases, disturbances develop in the annular mixing layer bounding the jet, and then gradually spread to the jet core. At M = 0.9, the disturbances at the initial stage are axisymmetric; at M = 2.12, both axisymmetric and three-dimensional disturbances are present in the flow. The numerical simulation results obtained for the case M = 2.12 are shown in the Figure. At some dis-

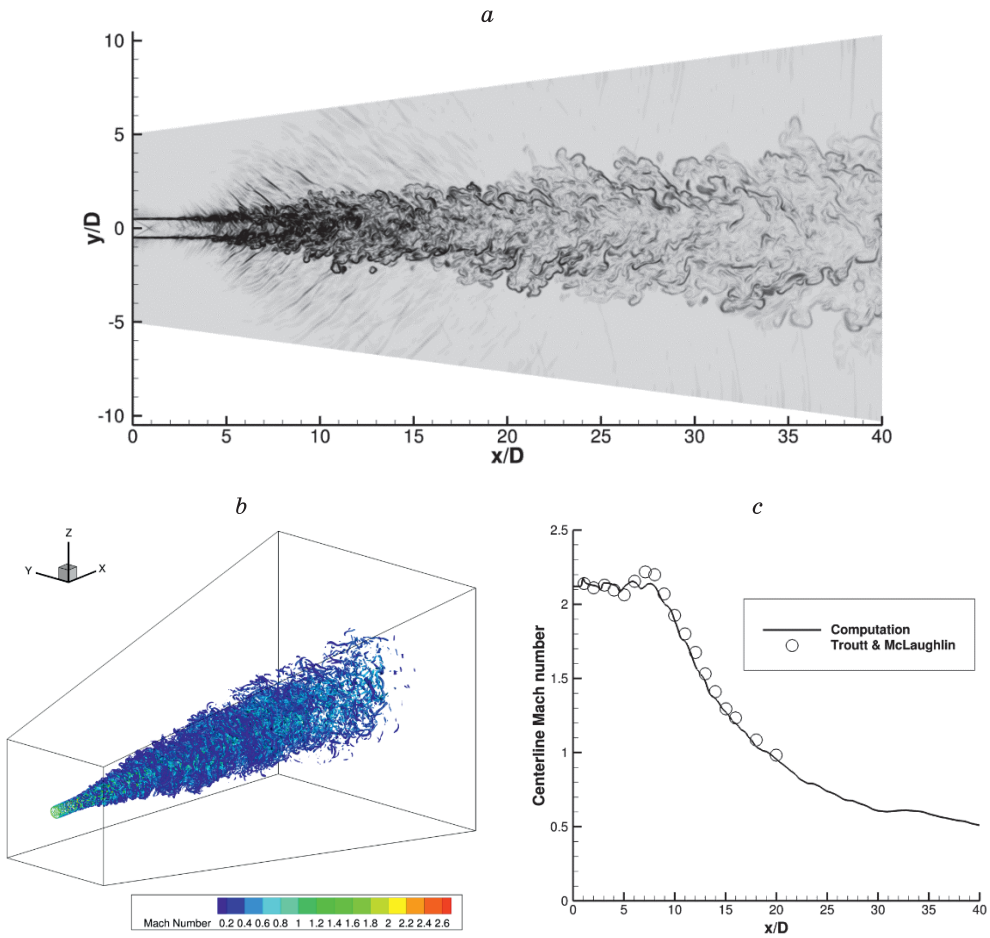

Fig. Numerical schlieren visualization in plane $z = 0$ (a), Q-criterion isosurface (b), and Mach number axial distribution in the computations and the experiment [3] (c).

tance from the nozzle exit, rapid growth of small-scale three-dimensional fluctuations begins, after which the transition to turbulence occurs. For a jet with M = 2.12, this happens at the value of the non-dimensional streamwise coordinate $x/d \approx 10$. Immediately after that, the mean flow velocity on the axis starts to fall rapidly, and at $x/d \approx 18$ it becomes less than the speed of sound.

A comparison of the axial distribution of the mean flow Mach number shows very good agreement with the experimental measurements [3]. A remarkable detail of the development of the supersonic isobaric jet flow was the intense emission of sound into the ambient space in the form of inclined Mach waves. This radiation occurred in a certain area, starting from the stage when large-scale vortex disturbances appeared in the mixing layer, including the entire zone of transition to turbulence and ending shortly before the jet velocity decreased to sonic.

This work was supported by the RSF grant 23-11-00258. Numerical simulations were performed at the hybrid computing cluster of the CCU «Mekhanika» of the ITAM SB RAS, and also at the cluster of Information-Computational center of the NSU.

REFERENCES

1. **Shershnev A.A., Kudryavtsev A.N., Kashkovsky A.V., Khotyanovsky D.V.** HyCFS, a high-resolution shock-capturing code for numerical simulation on hybrid computational clusters // Proc. of 18 Int. Conf. on the Methods of Aerophys. Research (ICMAR2016): AIP Conf. Proc. 2016. Vol. 1770. Art. 030076. 11 p.
2. **Jiang G.S., Shu C.-W.** Efficient implementation of weighted ENO schemes // J. Comput. Phys. 1996. Vol. 126. P. 202–228.
3. **Troutt T.R., Mclaughlin D.K.** Experiments on the flow and acoustic properties of a moderate-Reynolds-number supersonic jet // J. Fluid Mech. 1982. Vol. 116. P. 123–156.
4. **Bogey C., Bailly C.** Influence of nozzle-exit boundary-layer conditions on the flow and acoustic fields of initially laminar jets // J. Fluid Mech. 2010, Vol. 663, P. 507–538.

DOI 10.53954/9785604990148_95

EMPIRICAL MODELING OF ENERGY EXCHANGE IN RAREFIED FLOWS USING MOLECULAR BEAM DIAGNOSTICS

V.E. Khudozhitkov, A.E. Zarvin, V.V. Kalyada, A.S. Yaskin

Novosibirsk State University
630090, Novosibirsk, Russia

When gases (or mixtures of gases) flow out of the source (sound or supersonic nozzle), a sharp drop in density and temperature occurs in the supersonic flow, accompanied by a departure from the equilibrium between vibrational, rotational and translational degrees of freedom of molecules. Also, with a certain set of initial gas dynamic parameters, clusters are formed in the flow. Therefore, the use of low-density supersonic jets in various physical and chemical studies is accompanied by significant deviations from the calculated parameters performed under conditions of isentropic flows. The main attention in this work is paid to the molecular beam method. The simulation conditions on laboratory stands do not allow to reach temperatures at which the natural glow of the gas can be used to visualize the flows. At the same time, the low local density of the gas in the supersonic flow make it difficult to use shadow or laser methods. Therefore, the main method of initiating the glow of a gas detected by optical equipment is a high-voltage and well-focused electron beam. To simulate the processes of outflow and interaction of jets behind the nozzles of spacecraft in deep vacuum, to study the mechanisms of formation of cluster flows under conditions of nonequilibrium energy exchange at the LEMPUS-2 gas dynamic stand of Novosibirsk State University [1], a set of diagnostic techniques discussed in this report has been developed and tested.

1. Mass spectrometry of mixtures and flows with clusters. The molecular beam method has traditionally been used for non-invasive sampling for mass spectrometry.
2. The combination of electron beam ionization of the flow with mass spectrometry. To implement the technique, the transport of ions from the jet to the mass spectrometer detector through a skimmer and a collimator of the molecular beam system has been debugged.
3. Excitation and ionization of gas by discharge in a supersonic nozzle. An appropriate gas source has been developed for this purpose.
4. Visualization of flows. The paper provides examples of photofixation and photo scanning of processes in gas streams.

An illustration of the use of these diagnostic methods, partially developed again, partially debugged on the stand based on available descriptions and literature data, is given by examples of the results obtained.

The work was performed using the equipment of the NSU Applied Physics Research Center with the financial support of the Ministry of Education and Science of the Russian Federation (project FSUS-2020-0039).

REFERENCES

1. **Zarvin A.E., Kalyada V.V., Madirbaev V.Zh., Korobeishchikov N.G., Khodakov M.D., Yaskin A.S., Khudozhitkov V.E., Gimelshein S.F.** Condensable Supersonic Jet Facility for Analyses of Transient Low-Temperature Gas Kinetics and Plasma Chemistry of Hydrocarbons // IEEE Transact. Plasma Sci. 2017. Vol. 45, No. 5. P. 819–827. DOI: 10.1109/TPS.2017.2682901

DOI 10.53954/9785604990148_96

THE INFLUENCE OF BLOWING A GAS JET ON THE CHANGE IN THE CYLINDRICAL BODY AERODYNAMIC CHARACTERISTICS IN SUPERSONIC TRANSVERSE FLOW

V.A. Kislovskiy

Khristianovich Institute of Theoretical and Applied Mechanics SB RAS, 630090, Institutskaya str., 4/1 Novosibirsk, Russia

As a result of the oncoming flow interaction with the jet, significant changes in the flow occur on the streamlined body surface, as well as in the flow downstream from the interaction place. These flow changes are a combination of many complex gas-dynamic processes, including the formation of shocks and vortex structures, which significantly affect the redistribution of pressure on the streamlined body surface and heat transfer during the flow interaction with the streamlined body surface [1,2].

The study examined the transverse flow around a cylinder with a diameter D = 25 mm by a supersonic flow (V_∞ = 616 m/s, P_{st} = 13611 Pa, T_{st} = 106 K) in various cases blowing.

Several positions of the blowing hole along the streamlined cylinder circumference were considered: 0° (blowing against the oncoming flow); 45°; 90°; 135°; 180°. For all cases, the blowing parameters remained unchanged (b = 2 mm, V_∞ = 313 m/s, P_{st} = 660000 Pa, T_{st} = 290 K).

In case of transverse flow around the considered cylinder without jet blowing, the drag coefficient of this cylinder was C_{x0} = 0.0446. The jet blowing, depending on its version, led to various changes in drag, which is shown in Fig. 2.

Thus, it was shown that in the jet blowing first case, against the direction of the oncoming flow, there is a significant reduction in drag. Which is the expected result, the jet blowing since against the oncoming flow is a known way to reduce drag. The second variant of the jet blowing direction led to a slight increase in drag. The transverse direction of the jet blowing (option 3) did not affect the change in drag. The fourth and fifth variants of jet blowing reduced the drag by approximately half as much as with the first variant of jet blowing.

The work was carried out within the framework of the project supported by the Russian Science Foundation, No. 23-79-01057.

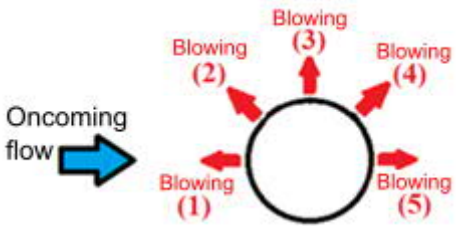

Fig. 1. Jet blowing options.

(1) – χ = 0°; (2) – χ = 45°; (3) – χ = 90°; (4) – χ = 135°; (5) – χ = 180°

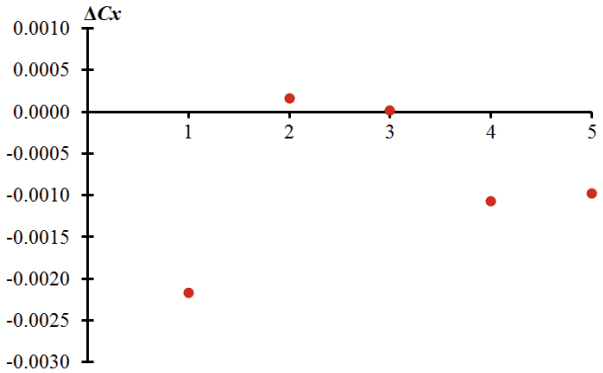

Fig. 2. The influence of the jet blowing option on the change in drag force.

REFERENCES

1. **Bashkin V.A., Egorov I.V., Ezhov I.V.** Circular cylinder in a transonic flow at high reynolds numbers: thermal problem// High Temperature, 2016. Vol. 54, No 4, pp. 547–554.
2. **Kornilov V.I., Lysenko V.I.** Study of aerodynamic characteristics of cylindrical bodies in a supersonic flow // Bulletin of NSU. Series: Physics, 2011, Vol. 6, No. 4, pp. 16–24.

DOI 10.53954/9785604990148_98

SUPERSONIC FLOW PAST A BLUNT CYLINDRICAL BODY IN A REFLECTED SHOCK TUNNEL

E.V. Kolesnik[1], T.A. Lapushkina[1, 2], N.A. Monakhov[2], P.A. Popov[2]

[1]Peter the Great St.Petersburg Polytechnic University, 195251, Saint Petersburg, Russia

[2]The Ioffe Physical-Technical Institute of the RAS, 194021, Saint Petersburg, Russia

The study of the flow structure caused by interaction of a supersonic flow with any structural elements fixed on the streamlined surface is important for many practical applications. Such problems arise, in particular, in the aerospace industry, when designing various aircraft elements [1]. The interaction of the boundary layer with a three-dimensional obstacle leads to a complex flow structure near the junction region, which is characterized by the presence of a system of shocks and compression waves, the formation of a frontal separation region with a system of horseshoe-shaped vortices, and strong non monotonicity of the parameters in front of the body [2-4]. Such flows can be studied using long-term or pulsed experimental facilities. Recently, with the increase in computing power, numerical simulation of the experimental configuration has become popular, allowing not only to obtain a complete three-dimensional flow structure, but also to evaluate the influence of the walls of the experimental stand [4].

An experimental study of the supersonic flow past a blunt cylindrical body was carried out using reflected shock tunnel in the Laboratory of Physical Gasdynamics of the Ioffe Institute. Experimental stand scheme is shown in Fig. 1: a shock-compressed gas plug created in the shock tube is decelerated at the end of the low-pressure chamber and enters the expanding nozzle 29 cm long through a slot of 6 mm high (the angle is 15° from the nozzle axis). A streamlined body with a leading edge of radius 1 cm is located at the nozzle exit (Fig. 1), the distance between the side walls of the nozzle is 4 cm. Nitrogen was used as the working gas. The Mach number of the flow at the nozzle exit (without a streamlined body) is 5, the unit Reynolds number is $7.5 \cdot 10^5$ [1/m].

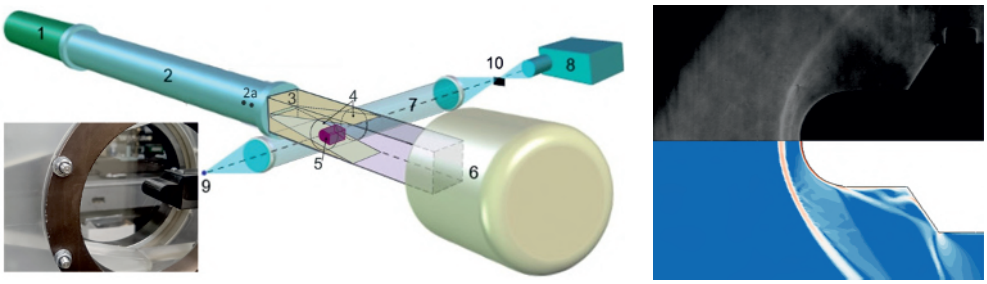

Fig. 1. Experimental stand scheme and shock-wave flow pattern.

1 – high-pressure chamber, *2* – low-pressure chamber, *3* – working chamber with nozzle, *4* – viewing windows, *5* – aerodynamic model, *6* – damper tank, *7* – Schlieren system, *8* – digital camera, *9* – pulse laser, *10* – optical knife.

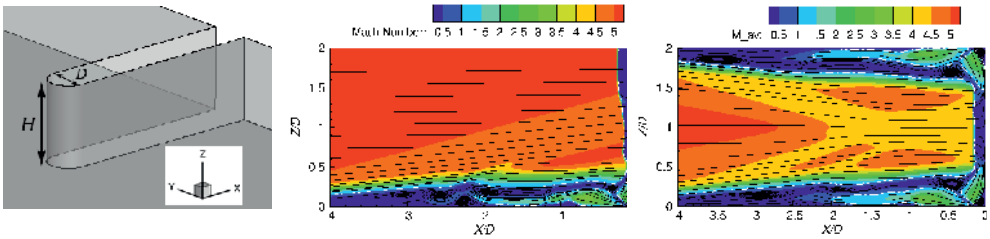

Fig. 2. Problem definition and flow structure in middle plane for $H = \infty$ and $H = 4$ cm.

The schlieren system was used to obtain the flow pictures illustrating the shock wave pattern near the body. Pressure signals at several points on the frontal line of the body (at different distances from the nozzle wall) and on the surface of the plate in the middle longitudinal plane in front of the streamlined body were measured during the experiment.

Experimental pressure oscillograms reveal a significantly unsteady flow pattern near the junction of the body and the nozzle walls. It is assumed that this is due to the complex structure of interaction between the boundary layers and the forming shock waves.

Numerical simulation was used to conduct a detailed analysis of the flow features. Calculations were performed using the SINF/Flag-S program code developed at St. Petersburg Polytechnic University; the resources of the supercomputer center of St. Petersburg Polytechnic University (www.scc.spbstu.ru) were used. The Navier-Stokes equations for a perfect gas were solved. The AUSM scheme of the second order of accuracy was used to convective fluxes evaluation.

To study the gas-dynamic flow structure without taking into account the influence of boundary layers on the nozzle walls, calculations were performed using a two-dimensional formulation. Fig. 1 illustrates the consistency of the calculated and experimental shock wave flow patterns.

The influence of the nozzle walls on the flow structure was studied for a model configuration (Fig. 2); calculations were performed using three-dimensional formulation, assuming uniform incoming flow. Blunt body diameter is $D = 2$ cm, the distance between walls was varied: $H = \infty$ (one wall), 8 cm, 6 cm и 4 cm (corresponds to the experimental stand). The computational meshes contained about 15 million cells.

The Mach number fields in the middle longitudinal plane in front of the streamlined body are shown in Figure 2 for the cases $H = \infty$ and $H = 4$ cm. An extended separation region is formed near the junction of the body and walls. The flow is stationary in the case $H = \infty$, whereas the flow pattern is significantly unsteady in the case $H = 4$ cm (Fig. 2 shows the time-averaged field). In this case, one can see intense oscillations within the separation region in front of the body, which are not symmetrical near the lower and upper walls; the bow shock wave is located closer to the streamlined body than for the case $H = \infty$.

This research was funded by the Russian Scientific Foundation, grant number 23-29-00286.

REFERENCES

1. **Korkegi R.H.** Survey of viscous interactions associated with high Mach number flight // AIAA Journal. 1971. V. 9. No. 5. P. 771–784.
2. **Tutty O.R., Roberts G.T., Schuricht P.H.** High-speed laminar flow past a fin-body junction // J. Fluid Mech. 2013. V. 737. P. 19–55.
3. **Kolesnik E.V., Smirnov E.M.** Numerical Analysis of Vortex Structures and Heat Transfer in a Supersonic Flow Past the Junction of a Blunt-Fin Body and a Plate // Technical Physics. 2020. V. 65. No. 2. P. 174–181.
4. **Sabnis K., Babinsky H.** A review of three-dimensional shock wave–boundary-layer interactions // Progress in Aerospace Sciences. 2023. V. 143. No. 1. P. 100953

DOI 10.53954/9785604990148_100

DEVELOPING STATISTICAL METHODS OF THE INTERMITTENCY PROCESSING AT LAMINAR-TURBULENT TRANSITION CAUSED BY CROSS-FLOW INSTABILITY

A.Ya. Kotvitskii[1], A.A. Abdullaev[1], I.A. Moralev[1]

[1]Joint Institute for High Temperatures RAS, 125412, Moscow, Russia

To evaluate quality control in a laminar-turbulent transition delay application intermittency processing techniques performed by defined flow diagnostic method are required. Classical methods for intermittency processing are based on spectral analysis of the hot-wire signal the laminar-turbulent transition in which is associated with an increase in the amplitude velocity pulsation of the high-frequency component. However, the threshold amplitude is determined empirically depending on the flow class and depends on the measurement po-

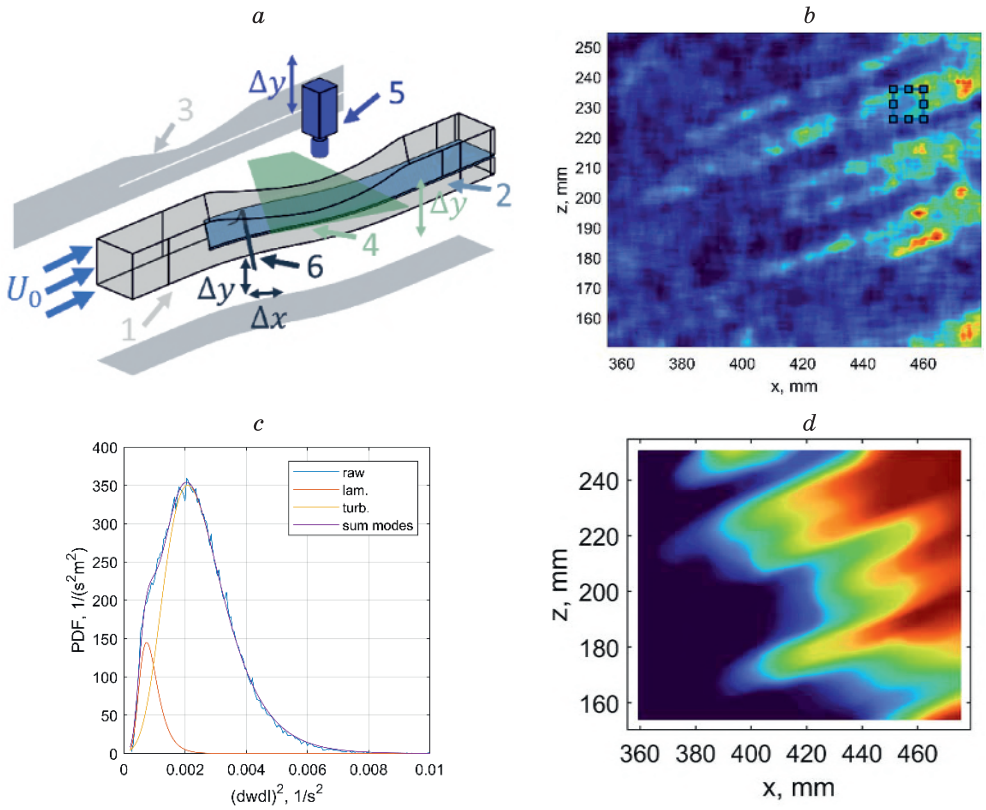

Fig. 1. Schema of the test section and measurement configuration (a): 1 – test section, 2 – swept plate, 3 – displacement body, 4 – laser plane, 5 – double-frame digital camera, 6 – hot-wire; turbulent wedges caused by secondary instability (b); statistical distribution of filtered velocity field (c); intermittency filed (d)

sition. This paper presents intermittency processing methods based on spatial, temporal and spatial-temporal statistical analysis of velocity fields measured by both low-speed PIV acquisition system in the planar configuration and single channel hot-wire (fig. 1a).

Investigations were carried out in the a subsonic low-turbulent wind tunnel with an open test section at an oncoming flow velocity 25 m/s. The three-dimensional boundary layer is created by a swept plate with 40 degree and induced pressure gradient. Laminar-turbulent transition investigation are performed at various amplitude relation natural stationary and travel mode instability. External flow conditions were created by a turbulizing grid and distributed roughness.

It is shown that the indicator function for detecting laminar-turbulent transition can be the directional derivative of the velocity along the primary vortex and the invariants of the velocity gradient tensor (fig1.b) as well time derivative of time-resolved signal. It is established that statistical distribution of the filtered instantaneous velocity fields selected by all implementation in the local flow region is bimodal in the transition domain (fig1.c) that turns out similar for time filtered signal. Methods for intermittency processing are based on spatial clustering of the flow domain into laminar and turbulent regions. Separation of statistical modes was performed both by k-means clustering methods and by models of fitting of a given distribution. Results of intermittency processing by statistical analysis of the PIV data were compared with hot-wire measurements. Testing of methods were carried out at various external flow conditions. It is shown that the accuracy of the determining the transition location consists 5-10mm or 0.9-2% model chord.

The work was supported by Russian Science Foundation, grant # 24-19-00627

REFERENCES

1. **Walker G.J., Solomon W.J.,** Turbulent Intermittency Measurement on an Axial Compressor Blade. Elev Australas Fluid Mech Conf. 1992:1277-1280
2. **Zhang D.H., Chew Y.T., Winoto S.H.б** A proposed intermittency measurement method for transitional boundary layer flows. Exp Fluids. 1995;19(6):426-428.
3. **Zhang D.H., Chew Y.T., Winoto S.H.,** Investigation of Intermittency Measurement Methods for Transitional Boundary Layer Flows. Exp Therm Fluid Sci. 1996;12(4):433-443.

DOI 10.53954/9785604990148_102

TRANSITION CONTROL IN A SWEPT WING BOUNDARY LAYER BY A MULTICHANNEL PLASMA ACTUATOR IN A CLOSED LOOP MODE

A.Ya. Kotvitskii[1], A.A. Abdullaev[1], M.V. Ustinov[2], I.A. Moralev[2]

[1] Joint Institute for High Temperatures RAS, Moscow, Russia
[2] Central Aerohydrodynamic Institute, Zhukovskii, Russia

Turbulent drag is responsible for the 80% of the total airplane drag at cruise conditions, with wing boundary layer laminarization able to diminish this value by at least 10%. Transition to turbulence in the swept wing boundary layer is driven by two instabilities: Tollmien-Shliechting waves and cross-flow vortices. The latter dominate in the accelerating part of the flow. At low turbulence of the oncoming flow, CF vortices are excited by surface roughness and thus are stationary.

Swept wing boundary layer was modeled on a flat plate with 40° sweep angle with an external induced pressure gradient. Oncoming flow velocity was 25 m/s, turbulence level 0.05%. Plasma actuator was installed at the position 70–110 mm from the leading edge. In the transition control experiments, stationary disturbances were artificially excited by applying roughness elements near the leading edge of the plate.

Closed-loop control of the vortices is realized using multichannel (16) plasma actuator based on a multielectrode surface barrier discharge system. Actuator was assempled on a 0.5 mm thick alumina ceramic plate. Each section was powered independently by sinuous voltage of frequency 50–65 kHz and amplitude less than 4 kV. Spanwise separation of the sections was chosen to provide spatial resolution of ¼ wavelength of the most unstable stationary mode (7 mm), according to the recommendations of [1]. Control of the actuator was performed using the microprocessor unit based on ESP32. Flow measurements were performed using PIV, with the laser sheet oriented in parallel with the plate surface, and by single hotwire.

Properties of the disturbances, induced by the discharge, were studied at various amplitude of the supply voltage. It was shown that actuator can create 2D disturbances with the initial amplitude within 2% of the oncoming flow. It was shown that main secondary disturbances, induced by actuator itself during the operation, correspond to the low frequency III type secondary instability mode of the vortex packet. It was shown that the disturbances generation problem is linear up to the peak-to-peak amplitude of 10% of local freestream velocity.

A control problem formulated is shown in fig.1. An approach for the optimal control was developed, both in open-loop and closed-loop operation of the system. For the open loop case, boundary layer was excited by individual actuator sections, forming the matrix of boundary layer responces to stationary forcing. After that, a minimization problem was solved for the amplitude of the transversal velocity profile, using the gradient descent algorythm. In the closed-loop mode, spanwise velocity profile in the boundary layer at a given distance form the leading edge was used as system exit. Optimization was performed in situ, with the voltage distribution across the electrodes updated at each step.

Boundary layer control was tested for the two types of the artificial disturbances: stochastic roughness, distributed near the plate leading edge, and a single cilyndrical roughness element. For the distributed roughness, reduction of the cross-flow vortices amplitude was

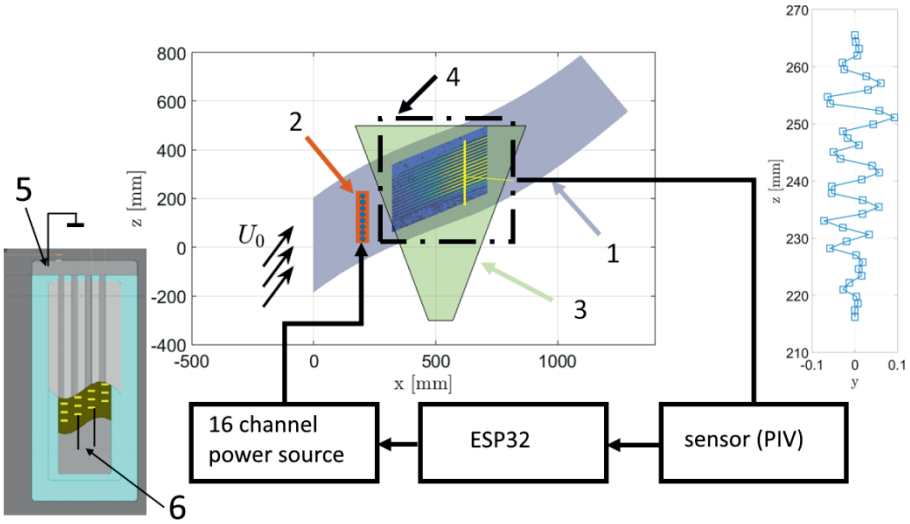

Fig. 1. Principal scheme of the experiment

1 – swept plate, *2* –plasma actuator, *3* – laser sheet, *4* – region of measurements, *5* – grounded actuator electrodes, *6* – high voltage electrodes

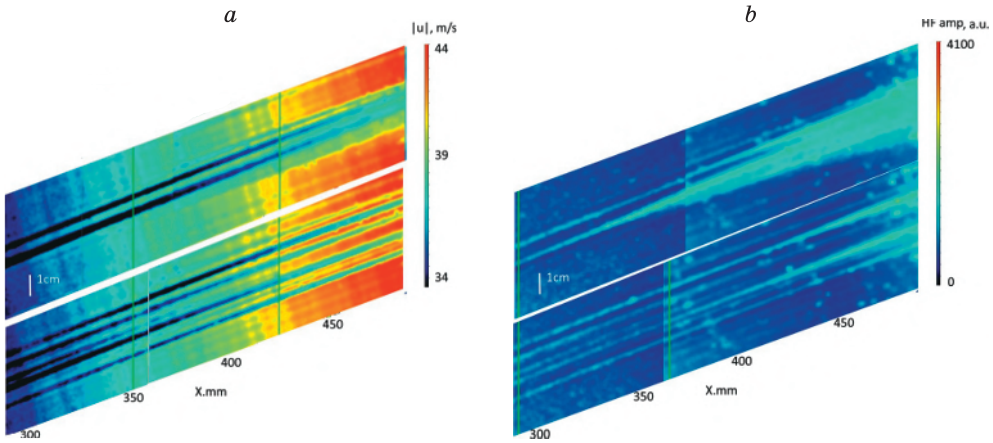

Fig. 2. a) vortex packet, induced in the boundary layer by a single roughness in reference (upper image) and controlled (bottom image) case, b) Amplitude of the short-wavelength disturbances in the boundary layer, same to (a)

demonstrated along the whole length of the disturbances evolution, however, transition shift was not obtained due to the narrow control region. For the single roughness with high enough amlitude, the reduction of the CF vortex packet was shown to reduce the transition length. It is assumed, however, that in this case the transition is delayed due to the mechanism of the nonlinear interaction of the natural and artificial instability vortices.

The work was supported by Russian Science Foundation, grant # 24-19-00627

REFERENCES

1. **Abdullaev A., Kotvitskii A., Moralev I., Ustinov M.** On the Possibility of Cross-Flow Vortex Cancellation by Plasma Actuators // Aerospace., 2023. V. 10. No 5. P. 469

DOI 10.53954/9785604990148_104

RESONANT MODE OF GAS OSCILLATIONS IN THE HEAT EXCHANGER OF A ROTARY-BLADE MACHINE

V.Yu. Koyokin, S.V. Bulovich

Peter the Great St. Petersburg Polytechnic University
195251, St. Petersburg, Russia

The efficiency of heat exchangers in engines with external heat supply is related to the nature of the movement of the working fluid in them. In a rotor-blade engine with an external heat supply (RBEEHS) [1] mass transfer with the working chambers leads to a pulsating movement of the working fluid in the heat exchanger. In the proceedings of the conference [2] the results of numerical simulation of RBEEHS are presented, the work indicates the presence of wave processes in the heat exchanger. The purpose of this work is to determine the conditions for the excitation of gas oscillations in a heat exchanger at its natural frequency.

The RBEEHS scheme is shown in Figure 1a. The size designations on the diagram, as well as the geometric parameters of the engine itself correspond to the data used in the work [2]. The hot heat exchanger is a group of U-shaped pipes of circular cross-section 5 (one pipe is shown in the figure), which contacts the engine chambers through manifolds 11, 12. The cold heat exchanger has a similar design and is subsequently omitted from consideration.

The task statement includes an engine element of the same type in width which accounts for one tube of the heat exchanger. The length of the heat exchanger tube is $L = 2.17$ m, the tube radius is $r = 1$ cm. The volume of collectors, also based on the proportion per tube, is 50 cm^3. The width of the calculated area (Fig. 1b) is equal to the radius of the tube. The condition of the plane of symmetry is set at the end boundaries that determine

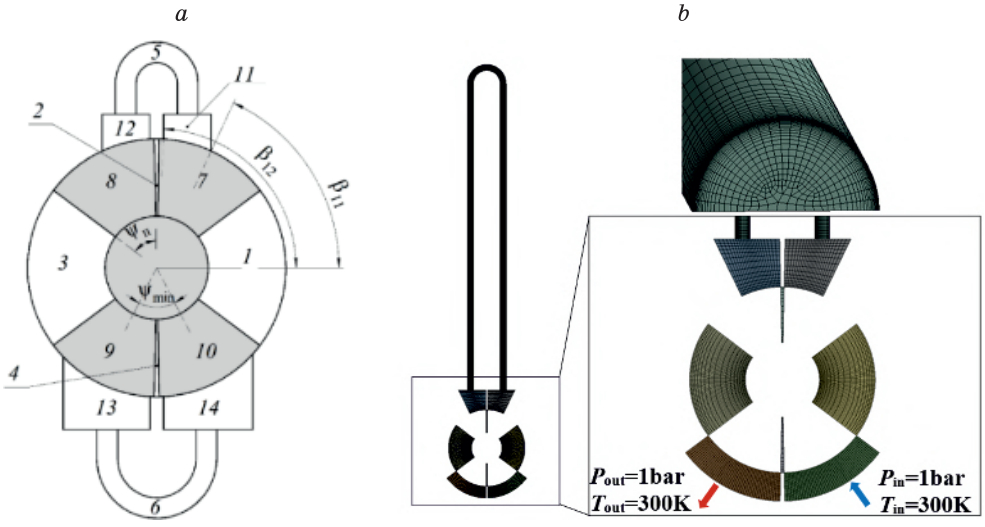

Fig. 1. Scheme of a rotor-blade engine with external heat supply (*a*), calculation area and grid (*b*)

the width of the calculated area. The boundary conditions of entry and exit are indicated in Figure 1b by arrows. The no-slip condition and thermal insulation are imposed at the remaining boundaries. The simulation of the unsteady turbulent flow of an ideal gas was carried out in the Ansys Fluent package in a 2.5D formulation. A quasi-three-dimensional calculation grid is being built in the engine chambers, and a three-dimensional calculation grid is being built in the collectors and tube (Fig. 2b). The total number of cells is approximately 140 thousand. The URANS Realizable k-e model with the enhanced wall treatment option was used to simulate turbulence.

The work determines the natural frequency of oscillations in a system consisting of collectors and a heat exchanger tube, which is $f_n = 70$ Hz. The frequency of external action for the oscillating system in the heat exchanger is determined by the frequency of its contact with the chamber. The considered engine design has four equivalent working chambers. Thus, the frequency of external action will be 4 times higher than the rotation frequency of the rotor of the engine $f_1 = 4 \cdot f_0$.

The excitation of gas oscillations at its own frequency can be achieved if the supply and extraction of mass from collectors are synchronized with the phases of the wave process. The intensive supply of mass to the inlet collector must coincide with the phase of pressure increase as a result of the wave process. Similarly, mass extraction from the outlet collector should occur when the pressure in it decreases. In the design under consideration, supply and extraction of mass from collectors do not occur simultaneously. Therefore, it is necessary that one period of gas exchange takes place between the supply of mass to the inlet and the selection of mass at the outlet. Then, in order to achieve resonance, the period of external action must be twice as long as the period of oscillations at the natural frequency, i.e. $f_1 = f_n/2$.

The calculation results are shown below at the rotor speed $f_0 = 8.75$ Hz. Then the frequency of external exposure will be $f_1 = 35$ Hz, and the period $T_1 \approx 0.028$ s.

Mass extraction (first half-period) and mass supply (second half-period) to the heat exchanger leads to a periodic change in the average mass pressure in the pipe (green curve) (Fig. 2a). It can be seen from Fig. 2a that intensive mass supply occurs during the phase of pressure increase ($0.5T_1$-$0.75T_1$) in the inlet collector (blue curve). Similarly, part of the mass extraction occurs during the pressure reduction phase (0-$0.25T_1$) in the outlet collector (red curve). This mode of gas oscillations in the pipe leads to the fact that the amplitude of the harmonic corresponding to the natural frequency exceeds the amplitude of the harmonic at the frequency of external action (Fig.2b), which indicates the correctness of the qualitative reasoning given earlier.

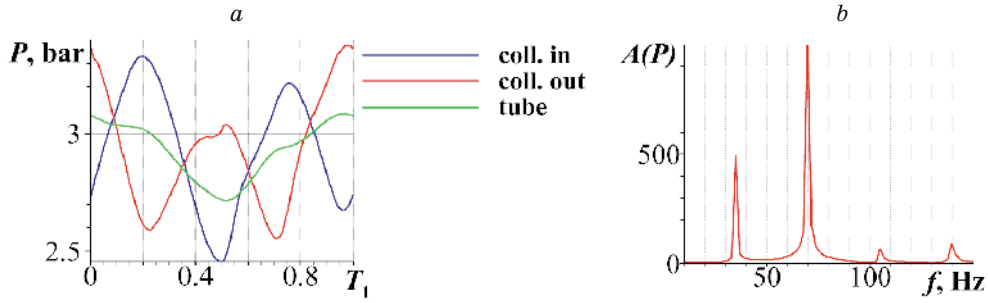

Fig. 2. Change in the average mass pressure in the collectors and the heat exchanger pipe during the period of interaction with the working chamber (*a*), Fourier spectrum of oscillations of the average mass pressure of the gas in the inlet collector (*b*)

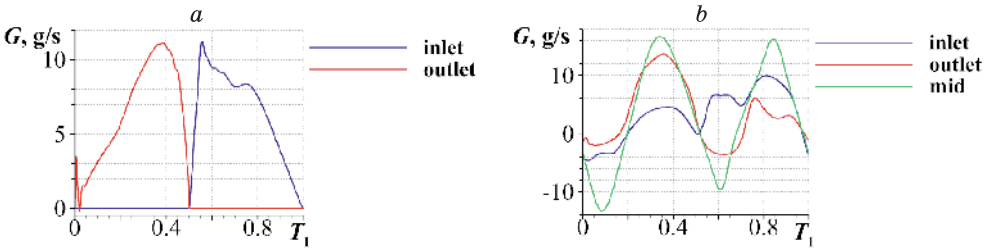

Fig. 3. The change in gas flow at the boundary between the collectors and the working chamber (a) and gas flow in the characteristic cross sections of the pipe (b) over the period

The resonant oscillation mode in the heat exchanger leads to the fact that the maximum mass flow values in the control sections of the tube (Fig. 3b) exceed the maximum flow values at the interface of the chamber and collectors (Fig. 3a). Such a flow regime can lead to a significant intensification of heat transfer. The flip side of the considered resonant gas flow regime is the energy expended by the engine to maintain oscillations.

REFERENCES

1. **Koyokin V.Yu., Bulovich S.V.** Simulation of thermophysical processes in a rotor-blade engine with external heat supply by nodal analysis, St. Petersburg State Polytechnical University Journal. Physics and Mathematics. 16 (3) (2023) 49–58. DOI: https://doi.org/10.18721/JPM.16305
2. **Koyokin V.Yu., Bulovich S.V.** Numerical simulation of the thermo-gas dynamics of a rotor-blade engine with external heat supply / Physics Science Week: collection of articles of the All-Russian Scientific Conference. April 3–7, 2023. St. Petersburg, Russia. P. 93–96.

DOI 10.53954/9785604990148_107

WING AERODYNAMIC CHARACTERISTICS CONTROL USING A VARIOUS FORM SECTIONAL SURFACE

A.V. Kryukov[1, 2], I.D. Zverkov[1, 2], V.P. Chekhov[1]

[1] KhristianovichInstitute of Theoreticaland Applied Mechanics SB RAS
630090, Novosibirsk, Russia

[2]Novosibirsk State Technical University
630073, Novosibirsk, Russia

Abstract. This paper presents the results of weight measurements of the aerodynamic characteristics of a wing with a variform-sectional surface. During the aerodynamic experiment, the characteristics of a wing with a special elastic surface, the shape of which changed with the help of external influences, were measured. Characteristic measurements were carried out using six-component aerodynamic balances in the T-324 aerodynamic installation of the ITPM SORAN at a Reynolds number of 1.5×10^5

Currently, aircraft with low flight Reynolds numbers are experiencing a period of rapid development; these include not only small-sized drones, but also promising stratospheric global communications vehicles. In some countries, the main funds for providing communications and the Internet are directed to the development of precisely these types of repeaters (1). As a rule, the repeater is installed on a high-altitude glider-type apparatus with a renewable energy source. High aerodynamic quality and low specific wing load give such devices the ability to stay in the air around the clock through the use of solar energy and current batteries. On the other hand, the operation of such devices goes into the region of low Reynolds numbers (2). This is due to the fact that there is a simultaneous decrease in flight speed, due to the low specific load on the wing, as well as a decrease in the wing chord due to the need to provide greater aspect ratio to increase the aerodynamic quality. In these conditions, from the point of view of aerodynamics, ensuring stability and controllability of the flow on the wing comes first. There are several expressed objectives within this issue. On the one hand, this is a delay in separation and elimination of hysteresis of characteristics when reaching the critical angle of attack (3), while the more laminated the profile, the more negatively these effects affect the flight. Moreover, it is necessary to ensure efficient maneuvering with a low specific weight of the control wiring. In addition, there is a separate task that is relevant for any profile shape – combating icing of the leading edge of the wing. Previous studies have shown that the use of flow-longitudinal waviness on the wing surface, at low Reynolds numbers, significantly improves its aerodynamic characteristics in the region of critical angles of attack (3, 4). On the other hand, within the framework of work on the study of wavy wings, the concept of a VFS wing with an elastic skin capable of changing the undulation parameters during flight was proposed (5). This method allows not only to control the flow on the surface but also to change the pressure distribution on the wing, being essentially a mechanism for controlling aerodynamic forces and moments. A previous study assessed the effectiveness using calculations (6).

As part of this work, a series of experiments were carried out to determine the real effectiveness of the proposed method for use on a stratospheric aircraft. The studies were carried out using six-component strain gauge aerodynamic balances on a T-324 ITAM installation at a Reynolds number of 1.5×10^5.

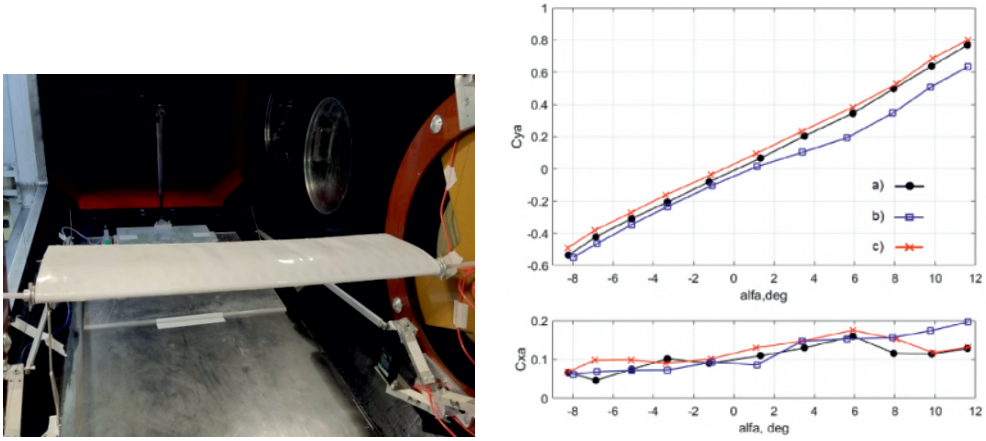

Fig. 1. Experimental setup with VFS wing and Cya(alfa) and Cx(alfa) diagram for four case:
a – without pressure, b – top deflated bottom inflated, c – top inflated bottom deflated

In the experiment, a specially developed VFS wing with an elastic skin was studied, which allows the sole to create excess pressure and vacuum in the wing sections to create the waviness configuration necessary for the study.

As a result of a series of experiments, it was found that the maximum change in force occurs in the configuration of inflated lower sections and deflated upper sections and is 16%, which corresponds to the deflection of the aileron of conventional mechanization by approximately 10 degrees. In view of the requirements for maneuverability and restrictions on overloads for stratospheric vehicles with a large wing aspect ratio, the efficiency of the VFS wing will be sufficient for flight control, and the use of the effects of a wavy wing will reduce the negative impact of flow separation when reaching critical angles of attack. Moreover, the deformable surface of the wing VFS makes it possible to successfully combat icing of the leading edge of the wing.

Work supported by a grant RNF 24-29-00329

REFERENCES

1. **Dantsker O. D., Haviland S.T., Allford R., Daley D., Danowsky B.P., Haplin D., Kendall G., Lisoski D.L., Liu Z.T., Mukherjee J., Peltz A., Price B., Sano G., Warner R.B. and Bershadsky D**. "Flight Testing of Tailless Subscale HAPS Aircraft," AIAA Paper 2023-3780, AIAAAviation Forum, Virtual Event, Jun. 2023
2. **Pelletier A., Mueller T.J.** Aerodynamic Force Moment Measurement at Very Low Reynolds // Proceedings of the 46th Annual Conference of the Canadian Aeronautics and Space Institute. Montreal, 1999. P. 59–68.
3. **Zverkov I.D., Kryukov A.V.** Impact onto the boundary layer on the airfoilof a small-sized flying vehicle with the use of a wavy surface. Problems and prospects (review) // Journal of Applied Mechanics and Technical Physics, 2021, Vol. 62, No. 3, P. 180–198
4. **Zverkov I.D., Kozlov V.V. and Kryukov A.V.** Prospects for research in the field of small-sized aircraft // NSU Bulletin, Series: Physics, 2014, Vol. 9, Iss. 2, P. 95–115
5. **Zverkov I.D., Kryukov A.V. Evtushok G.Yu.** Methods of determining the boundary layer characteristics of the varioform section wing // AIP Conference Proceedings 2027, 030097 (2018); doi: 10.1063/1.5065191
6. **Kryukov A.V., Zverkov I.D., Chubrikov A.E., Kulikov V.V.** Morphine wing as the basis of the aircraft of the future // AIP Conference Proceedings 2288, 030059 (2020); https://doi.org/10.1063/5.0028416

DOI 10.53954/9785604990148_109

NUMERICAL SIMULATION OF THE UNDEREXPANDED JET EXHAUSTING FROM THE ROUND NOZZLE

A.N. Kudryavtsev, D.V. Khotyanovsky, V.I. Zapryagaev

Khristianovich Institute of Theoretical and Applied Mechanics SB RAS, Novosibirsk, 630090, Russia

Based on the numerical solution of the Navier–Stokes equations, simulations of the development of disturbances and transition to turbulence in an underexpanded jet exhausting from a convergent (sonic) nozzle with the Mach number at the nozzle exit M = 1 have been carried out at two ratios of the total pressure to the ambient pressure $N_{pr} = p_0/p_a = 5$ and 9. The calculation parameters correspond to the conditions of the experiment conducted at the Laboratory of Experimental Aerogasdynamics of the ITAM SB RAS. Eddy-resolving numerical simulations are performed in a three-dimensional formulation. The calculations were carried out using the HyCFS computational code [1] developed at the Laboratory of Computational Aerodynamics of the ITAM SB RAS, with spatial discretization of the convective terms of the Navier–Stokes equations based on the shock-capturing WENO scheme of the 5th order [2]. The computational domain had the form of a truncated pyramid of square section with a height $L_x = 20\ d$ along the jet axis x and the dimensions $L_y = 8\ d$, $L_z = 8\ d$ along the normal axes y, z at the initial cross-section $x = 0$. Here d, hereafter used as the length scale, is the diameter of the jet at the initial cross-section. The angle of expansion of the pyramidal computational domain in the streamwise direction is 7.5°. The computational grid was condensed in the region of the core and the near field of the jet. Calculations were performed on a grid $N_x = 864$, $N_y = 430$, $N_z = 430$ (160 million cells in the entire computational domain). At the inflow boundary of the computational domain, at $x = 0$, a piecewise-constant top-hat jet profile was set: at $|y|, |z| \le d/2$, the values of the gas dynamic variables corresponding to the flow at the nozzle exit were set; at $|y|, |z| > d/2$, the values corresponding to the ambient gas were set. The parameters of the jet and the ambient gas correspond to the experimental conditions for the underexpanded jets with N_{pr} =5 and 9. For better posedness of the numerical boundary-value problem, the boundary conditions at the inflow boundary corresponding to the ambient gas were set with an addition of a background co-flow of a low velocity corresponding to the Mach number 0.05.

The visualizations of the flow fields shown in Fig. 1 for the $N_{pr} = 5$ case show that the numerical simulation reproduces the main details of the mean and pulsation motion. The disturbances begin to grow rapidly downstream from the section coinciding with the Mach disk in the first shock cell of the jet. The flow is rapidly turbulized, and the growth of instability, as might be expected, begins at the boundary of the jet and also in the inner mixing layer, emanating from the line of intersection of the incident intercepting shock, the Mach disk and the reflected shock. Such characteristic features of the flow observed in the experiment as intense vortex motion and large-scale vortex structures are also present in the numerical results.

The calculated and experimental Pitot pressure profiles shown in Fig. 2 agree very well at cross-sections close to the nozzle exit (Fig. 2a). Downstream, however, the agreement begins to deteriorate, with the greatest differences being observed on the jet axis (Fig. 2b). If we compare the distributions along the axis (Fig. 2c), it appears that the data agree very well up to the cross-section $x/d = 2$. Then the Pitot pressure in the experiment begins to grow. In the numerical simulation, however, the pressure increase begins only starting from the cross-

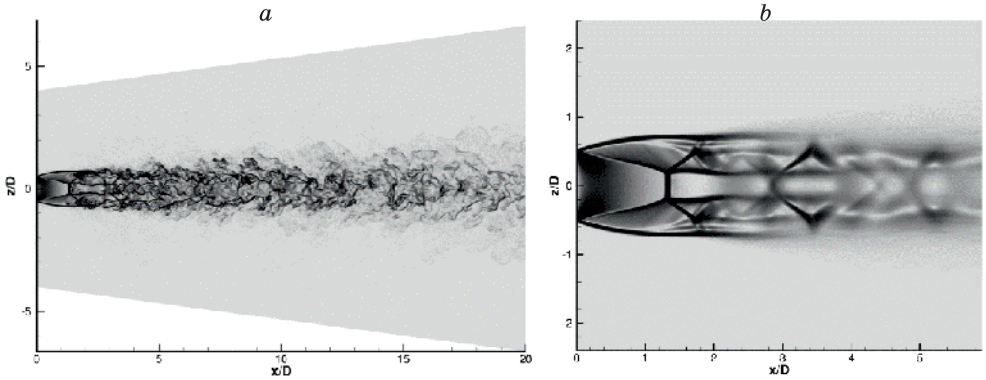

Fig. 1. Numerical schlieren visualizations of the instantaneous (a) and time-averaged (b) flow field in the plane $y = 0$.

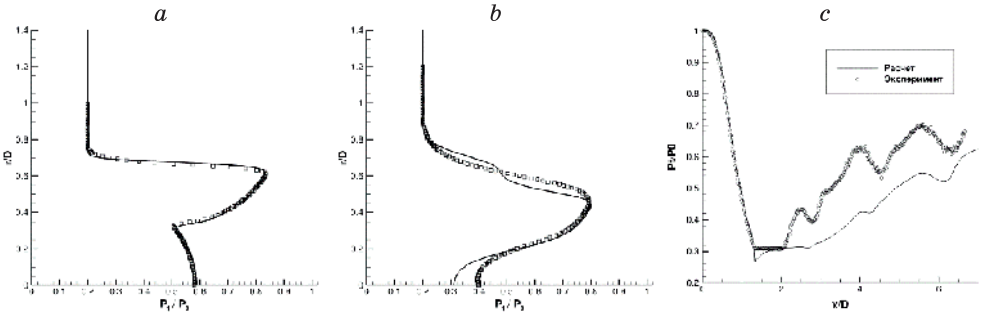

Fig. 2. Experimental and numerical Pitot pressure profiles: a) at cross-section x/d = 0,833; b) at cross-section x/d =2,66; c) along the jet axis.

section $x/d = 2.7$. In the experiment, the initial Pitot pressure increase, at $2.1 \le x/d \le 2.5$, occurs significantly faster than in the calculation. In addition, significant Pitot pressure oscillations along the jet axis observed in the experiment, compared with the simulation results, are noteworthy.

The reason for the discrepancy between the calculation and experimental data may be that after the transition to turbulence, all dynamic scales of vortex motions are not resolved in the calculation, and, thus, the role of small-scale fluctuations in turbulent mixing is ignored. The Reynolds number in this case is very large, so the direct numerical simulation is probably under-resolved and in fact we perform modeling using the LES method without an explicit subgrid-scale model; more precisely, the role of such a model is played by the inherent numerical viscosity of the shock-capturing scheme used. Perhaps, introduction of a subgrid-scale model could improve agreement.

This work was supported by the RSF grant 23-11-00258. Numerical simulations were performed at the hybrid computing cluster of the CCU «Mekhanika» of the ITAM SB RAS, and also at the cluster of the Information-Computational center of the NSU.

REFERENCES

1. **Shershnev A.A., Kudryavtsev A.N., Kashkovsky A.V., Khotyanovsky D.V.** HyCFS, a high-resolution shock-capturing code for numerical simulation on hybrid computational clusters // Proc. of 18 Int. Conf. on the Methods of Aerophys. Research (ICMAR2016): AIP Conf. Proc. 2016. Vol. 1770. Art. 030076. 11 p.
2. **Jiang G.S., Shu C.-W.** Efficient implementation of weighted ENO schemes // J. Comput. Phys. 1996. Vol. 126. P. 202–228.

DOI 10.53954/9785604990148_111

NUMERICAL STUDY OF UNSTEADY REFLECTION OF SHALLOW WATER BORE WAVES

A.N. Kudryavtsev[1], A.A. Kudryavtseva[2], G.V. Shoev[1]

[1]Khristianovich Institute of Theoretical and Applied Mechanics, Siberian Branch of the Russian Academy of Sciences, 4/1 Institutskaya St., Novosibirsk, 630090, Russia

[2]Novosibirsk State University, 2 Pirogova St., Novosibirsk, 630090, Russia

The shallow water equations are commonly used to describe free-surface fluid flows when solving problems in open-channel hydraulics, modeling sea tides, storm surges and tsunamis [1]. It is well known, that they are equivalent to the isentropic compressible Euler equations with the ratio of specific heats $\gamma = 2$. The Froude number $\mathrm{Fr} = u / \sqrt{gh}$ where u is the flow velocity, h is the water depth and g is the acceleration of gravity, is a counterpart of the Mach number. For supercritical flows, $\mathrm{Fr} > 1$, the shallow water equations allow discontinuous solutions, shock waves and contact discontinuities. Shallow water shock waves are usually called bore waves or hydraulic jumps. When an oblique bore wave reflects from a solid wall regular reflection is not always possible and, as well as in gas dynamics, irregular reflection with a triple point and an additional strong wave, a Mach stem, can occur. It was shown [2] that the transition between steady regular and irregular configurations can be accompanied by a hysteresis.

In the current paper, unsteady reflection of bore waves is investigated numerically. Numerical simulations are performed using a shock-capturing TVD scheme for the Froude numbers of the incident wave from 1.5 to 7.5 and various angles of its incidence on the solid wall. It is shown that irregular reflection is observed if the angle of incidence exceeds the value predicted by the theoretical detachment criterion. It is found out, for the first time, that, in addition to the known single Mach reflection (SMR), other irregular bore wave configurations exist such as the transitional Mach reflection (TMR) and the double Mach reflection (DMR). These reflection types are well studied at unsteady reflection of shock waves in gas dynamics but have never been observed before for shallow water waves. They are shown in Fig. 1 for the Froude number of the incident shock $\mathrm{Fr}_s = 5$ and the wall slopes $\theta = 20^\circ$ and 45°.

Reflection of a bore wave from a curvilinear wall with a gradually changing slope is also investigated. A dynamical transition from irregular reflection to regular one and back to irregular reflection (shown in Fig. 2) is observed on the wall whose slope first increases and then, after a rectilinear wall section, decreases. Generally speaking, an analogue of hysteresis when direct and reverse transitions happen at different angles of incidence can be expected here. However, it seems that preliminary results give evidence that both the transitions occur at the same angle. Nevertheless, it cannot be considered as a final conclusion. It is possible that the transition to regular reflection on the rectilinear part of the wall happens because the grid resolution is not sufficient to resolve a very small Mach stem. Thus, new numerical simulations with a higher resolution are planned to solve this problem.

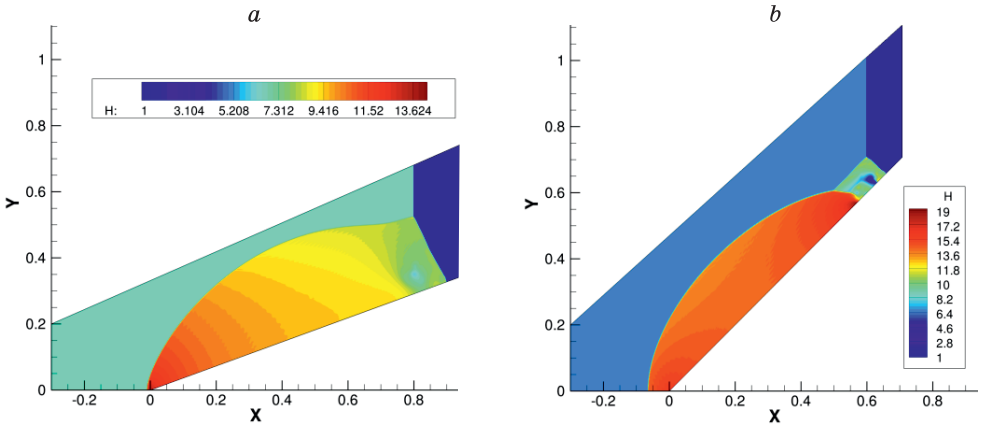

Fig. 1. Transitional Mach reflection (a) and double Mach reflection (b).

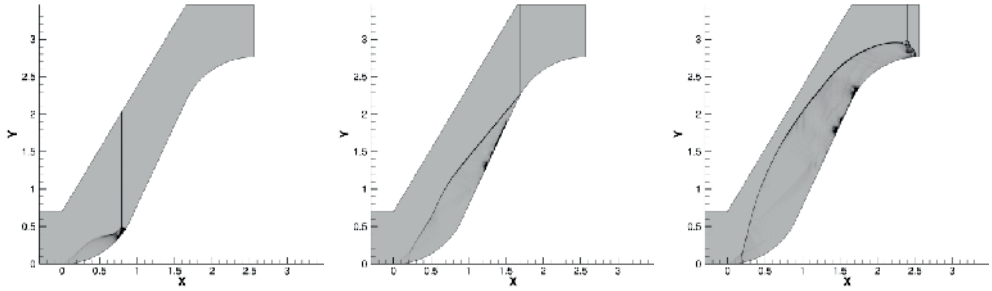

Fig. 2. Dynamical transition on curvilinear wall at $Fr_s = 5$.

The work was supported by the Russian Science Foundation (Grant No. 23-11-00258).

REFERENCES

1. **Castro-Orgaz O., Hager W.H.** Shallow water hydraulics. Springer, 2019. 563 p.
2. **Kudryavtsev A.N., Mikhailova U.V.** Hysteresis induced by interaction of oblique hydraulic jumps on shallow water // Thermophysics and Aeromechanics. 2023. Vol. 30, No. 6. P. 1073–1082.

DOI 10.53954/9785604990148_113

TURBULENCE MODEL OF PENETRATIVE CONVECTION AND POLLUTANT DISPERSION IN THE URBAN HEAT ISLAND IN STABLY STRATIFIED ENVIRONMENT

L.I. Kurbatskaya

Institute of Computational Mathematics and Mathematical Geophysics, Russian Academy of Sciences, Siberian Branch, 630090 Novosibirsk, RUSSIA

It is well-known that the elevated temperatures in cites arise due to anthropogenic heat generation and retardation of the nocturnal cooling of urban surfaces in contrast to rural surfaces, which causes higher temperatures over the city relative to its vicinity (the urban heat island effect). A plume of warm air that appears over the city promotes the development of circulation due to the difference in temperature of the urban heat island and its surrounding environment, which has a lower temperature.

RANS approach of the second order closure used to the study of structural features of the penetrative convection above the urban heat island in the stably stratified atmosphere at a weak wind. For description of atmospheric dispersion of a passive air contaminant, the three-parameter $E-\varepsilon-\overline{\theta^2}$ turbulence model [1] (the turbulence kinetic energy E, is its dissipation ε, the dispersion on turbulent temperature fluctuations $<\theta^2>$) should be added by the equation for mean concentration $C(x_i,t)$, the equation for turbulent flux of a contaminant $f_j \equiv <u_i c>$ and the equation for correlation $<c\theta>$ [2].

Euler's model was formulated to describe the propagation of a passive pollutant in a stably stratified atmospheric boundary layer. The fully explicit algebraic expressions for the components of the vector of turbulent pollutant fluxes correctly describe the anisotropy of the turbulent transfer and the effect of buoyancy on the transport of pollutants. The equation for mean concentration

$$\frac{\partial C}{\partial t}+\frac{\partial}{\partial x}C\cdot U+\frac{\partial}{\partial z}C\cdot W=-\frac{\partial}{\partial z}\langle wc\rangle-\frac{\partial}{\partial x}\langle uc\rangle\,. \qquad (1)$$

The main goal of the numerical simulation was to take into account the effects of buoyancy on the distribution of the average concentration passive pollutant in the mixed and inversion layers above the urban heat island. The height of the inversion layer z_i is determined from the profile the turbulent flux heat $\langle w\theta\rangle$ and corresponds to the height at which $\langle w\theta\rangle$ reaches its maximum negative value. At the same height, an entrainment layer with negative buoyancy is formed, which characterizes the transition from unstable stratification to stable stratification. The height of the inversion layer depends on the temperature at the lower boundary of the region under consideration [3].

This paper discusses modeling results of passive pollutant dispersion from the continuous surface source for the critical meteorological period (stably stratified atmosphere and suppressive inversion).

A numerical experiment is implemented for the case of dispersion of a pollutant from an urbanized surface (city) with a time variation typical for traffic emissions (high values in the period 07:00 am to 18:00 pm and low values during the night) to obtain a realistic behavior of concentration profiles. Since most of the air pollution over urbanized surfaces comes

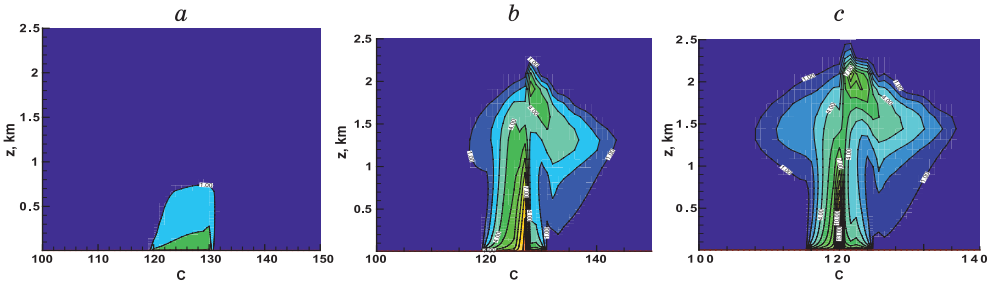

Fig. 1. Isolines of average concentration fields at 09-00, 12-00, 13-00 hours.

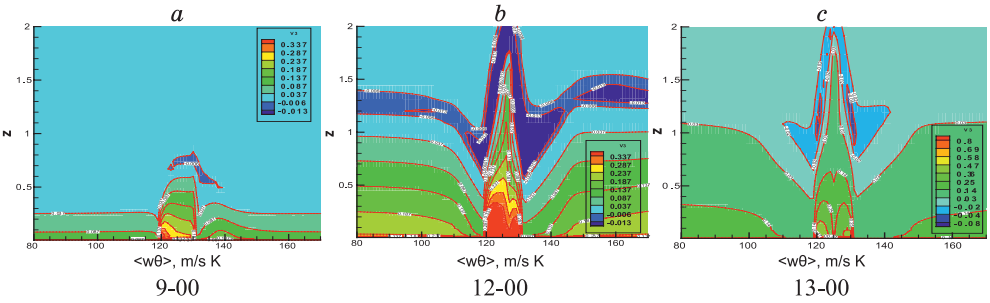

Fig. 2. Isolines of fields turbulent heat fluxes at 09-00, 12-00, 13-00 hours.

from numerous distributed sources, as a surface boundary condition for the equation (1) of a passive pollutant transfer at the lower level of the model ($z = z_1$), a uniform concentration distribution is specified, which is close to the distribution used in the numerical experiment [4].

Figures 1, 2 show average concentration the fields and the turbulent heat fluxes at 9:00, 12:00, 13:00, respectively. The blue to dark blue areas in the figures for the turbulent fluxes correspond to negative heat fluxes. The results shown in Figures 1, 2, give an idea of the behavior of a passive pollutant from the beginning of the ABL evolution. When the earth's surface is heated, turbulence develops, which contributes to the destruction of the stable stratification and the formation of positive heat fluxes, which leads to a rise in the upper boundary of the inversion layer.

The modeling of the dispersion of a passive pollutant from a continuous surface source over a heat island using the described above three-parameter model for the turbulent transfer of momentum, heat, and mass made it possible to obtain results that are qualitatively consistent with the laboratory measurements of the distribution of passive pollutants in a convective boundary layer [5]. In particular, the model reproduces well the penetration of pollutants from the mixing layer into the inversion layer.

«This work was carried out under state contract with ICMMG SB RAS FWNM-2022-0003».

REFERENCES

1. **Kurbatskii A.F. and Kurbatskaya L.I.** " $E - \varepsilon - \overline{\theta^2}$ turbulence closure model for an atmospheric boundary layer including the urban canopy // Meteorol. Atmos. Phys. 2009. Vol. 104, No. 1–2, P. 63–81.

2. **Kurbatskii A.F. and Kurbatskaya L.I.** Urban aeromechanics: Turbulent circulation and contaminant dispersion above city in stably stratified environment // AIP Conference Proceedings. 2027, 030024 (2018)
3. **Kurbatskaya L.I.** Influence of inversion on the diffusion of a passive impurity over a heat island with large-scale roughness // Proceedings. Vol. 12780, 29th International Symposium on Atmospheric and Ocean Optics: Atmospheric Physics; 127805G.
4. **Martilli A.** Numerical Study of Urban Impact on Boundary Layer Structure: Sensitivity to Wind Speed, Urban Morphology, and Rural Soil Moisture // J. Appl. Meteor. 2002. Vol. 41, No. 12, P. 1247–1266.
5. **Snyder W.H., Lawson R.E., JR., Shipman M.S., Lu J.** Fluid Modeling of Atmospheric Dispersion in the Convective Boundary Layer. // Bound. -Layer Meteor. 2002. Vol. 102. P. 335–366.

DOI 10.53954/9785604990148_116

TURBULENT BOUNDARY LAYER OVER PERFORATED SURFACE AT THE EARLY STAGES OF DEVELOPMENT

A.S. Kuznetsov, A.R. Gorbushin, D.S. Sboev

Moscow Institute of Physics and Technology
141701, Dolgoprudny, Russia

Turbulent boundary layers (TBL) over the perforated walls is of importance in many applications, e.g. for transonic wind tunnels. A brief account has given in [1] of series experiments undertaken on its structure in two wind tunnels. The main attention in [1] was devoted to the details of near-wall structure of mean flow in this TBL and some interesting its features had been reported. By comparison with known data [2, 3] the conclusion was that the TBL under study was far from equilibrium (fully rough conditions). The present communication provides further data on the initial stages of development of TBL on perforated surface. The approach used is common for roughness studies, when the near-wall details of flow are neglected.

The hot-wire measurements (a 5 μm single wire with length about 1 mm) were conducted in the AT-1 wind tunnel at MIPT at free-stream velocity U_e = 36 m/sec. The perforated surface was a steel plate with circular perforations arrayed in a hexagonal pattern. The perforations were 6 mm in diameter spaced about 10 mm between centers giving an openness ratio of about 65%. The plate was 6 mm thick that gives roughness Reynolds number ku_τ/ν about 500-800 depending on the u_τ values determined. The wind tunnel floor's TBL was additionally tripped by sandgrain paper placed at the nozzle exit (X = 0). The perforation starts at X = 485 mm and could be replaced by a smooth wall to comparative measurements. Below the data at X = 710 mm is reported that corresponds to 225 mm length over the rough surface. In this position the smooth wall TBL was at almost equilibrium zero pressure gradient conditions (Fig. 1) with the form parameter H = 1.33, the Clauser parameter G = 6.51, the wake parameter Π = 0.46 and Re_θ = 6269. The skin friction determined by the Clauser plots was $C_f = 2.93\times10^{-3}$.

The mean velocity profile in a full rough conditions usually expressed in form

$$U^+ = \frac{U}{u_\tau} = \frac{1}{\kappa}\ln\left(\frac{(Y-d)u_\tau}{\nu}\right) + B - \Delta U^+ + \frac{2\Pi}{\kappa}w\left(\frac{Y-d}{\delta}\right),$$

where w is the wake function, the ΔU^+ is the roughness function and d is so called zero plane displacement. The equivalent form (e.g. [2]) is

$$U^+ = \frac{1}{\kappa}\ln\left(\frac{Y-d}{Y_0}\right) + \frac{2\Pi}{\kappa}w\left(\frac{Y-d}{\delta}\right).$$

This equation was fitted to the data to obtain the u_τ, d and Y_0 (Fig. 1). As it seen from the plot, the TBL over rough wall shows the extended logarithmic region in comparison to the smooth wall case. The ΔU^+ value is comparable with the ones reported in [3], but the wake parameter is almost zero, while the Clauser parameter lows to the G = 5.13 and H rises to 1.42. All these effects are confirmed by the PIV measurements [1] in the wind tunnel of completely different construction. This is in a strike contrast to the results [2, 3], when it was shown that the wake parameter increases to 0.6–0.7 in a full rough conditions. Castro [2]

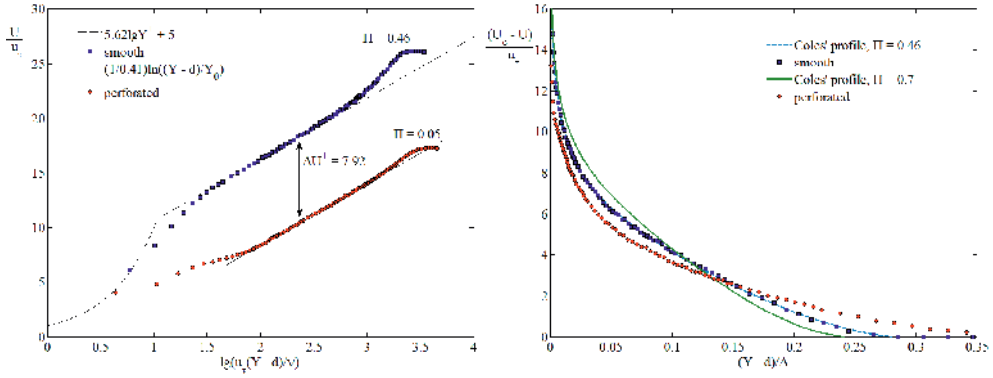

Fig. 1. The mean velocity profiles at $X = 710$ mm in wall units (left) and in a deficit velocity form (right).

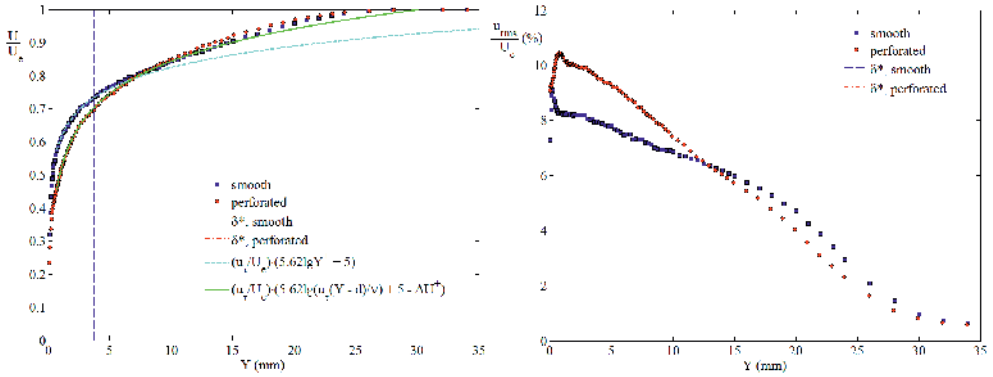

Fig. 2. The mean velocity profiles (left) and the fluctuation profiles (right) at $X = 710$ mm.

was able to correlate the mean flow data over a wide range of roughness geometry to the velocity deficit profile with $\Pi = 0.7$. As it shown in Fig. 1, it is not the case for our measurements of the non-equilibrium TBL developing over the perforations. The tendency observed is quite contrary. In Fig. 2 the wall-normal coordinate is intentionally given as dimensional units to show by comparison with the fitted profiles the enlargement of log-region at the same free-stream conditions. While at the smooth wall the visible wake region starts about $Y = 5$ mm, over the perforated wall the almost pure log-region extends to over 10 mm. It is interesting to note that the streamwise velocity fluctuations are much greater in the log-layer over perforations, while they are decreased in the outer region in comparison to the smooth wall case. It means that the motion in the outer part of TBL is undergoing through the significant changes during the evolution of TBL to the equilibrium state. Probably, this effect could be related to the observed decrease in the wake parameter. The further investigations of the TBL relaxation process over perforated surface are strongly needed.

This work was supported by the RSF grant 20-11-20006.

REFERENCES

1. **Gadjimagomedov G.G., Gorbushin A.R., Kuznetsov A.S., Sboev D.S.** Some properties of turbulent boundary layer over perforated surface // Proc. of XIII Russian Congress on Theoretical and Applied Mechanics. 2023. Vol. 2, P. 341–343. (in Russian)
2. **Castro I.P.** Rough-wall boundary layers: mean flow universality // J. Fluid Mech. 2007. Vol. 585, P. 469–485.
3. **Bergstrom D.J., Kotey N.A., Tachie M.F.** The effects of surface roughness on the mean velocity profile in a turbulent boundary layer // J. Fluids Eng. 2002. Vol. 124, No. 9. P. 664–670.

DOI 10.53954/9785604990148_118

DYNAMICS OF PUFF-TYPE SUPERSTRUCTURES IN JETS. EXPERIMENT AND NUMERICAL SIMULATION

V.V. Lemanov, V.A. Ivashchenko, V.V. Lukashov, R.I. Mullyadzhanov, K.A. Sharov

Kutateladze Institute of Thermophysics SB RAS
630090, Novosibirsk, Russia

For the purpose of intensifying heat and mass transfer processes, large-scale vortex structures formed in jets under the effect of various types of instabilities are widely used. In this regard, one of the main tasks in such flows is still the study of vortex structures, which is due to both their applied significance and importance for solving fundamental issues of the transition to turbulent flow. To describe this kind of vortex formations, terms such as large-scale vortices and coherent structures are most often used, which usually include vortex structures in the mixing layer, toroidal vortices, streak structures in jets, etc. [1]. In the last decade, the term "superstructures" has appeared in wall flows and convection [2]. The main difference between this object and coherent structures is its significantly larger size. Previously such superstructures were registered by researchers of IT SB RAS in the near field of round subsonic jets (M < 0.1) [3]. Their longitudinal size can reach l/d = 20–30 (d is the initial diameter of the jet), which is significantly larger than the size of coherent structures l/d = 2–4, characteristic of jet flows. These superstructures were observed for jets which outflow from long tubes (L/d > 100) in laminar-turbulent transition regimes through intermittency, in the range of Reynolds numbers Re = 2000–4000. Large-scale turbulent structures with a longitudinal size l/d = 10–20 are formed inside the tube, which are called puffs in foreign literature. As our experiments have shown, superstructures are stable in the near field of jets (x/d < 20) for inert and reactive jet flows [3] (x is the distance to the beginning of the jet). This work is devoted to the study of the behavior and characteristics of vortex turbulent superstructures (puffs) in the near field of a jet as it flows out of a pipe.

The jet flowed from a long (L = 1.6 m) axisymmetric pipe with a diameter of d = 8 mm into the air space at low Reynolds numbers of 2000–4000 and atmospheric pressure. Air and carbon dioxide (CO_2) were used as the working fluid. During the experiment, no artificial disturbances were introduced either in the tube or in the jet. The main focus was on measuring velocity fields using high-speed 2D-PIV at 7 kHz in a plane passing through the jet axis with a measurement area of 63x63 mm, which included the origin of the CO_2 jet.

The experimental results are compared with the results of direct numerical simulation (DNS) of a jet flow with similar flow parameters. A unique feature of the calculation part is the use of a combination of two computational codes, the N.V. Nikitin code. (Research Institute of Mechanics, Moscow State University) [4] and DNS in the open package Nek5000, for analyzing the transient flow regime in a jet (scenario with intermittency) when superstructures are formed.

The instantaneous velocity fields obtained by the PIV technique made it possible to obtain instantaneous velocity distributions over time, with a time resolution of 143 μs, at any point in space of the measuring region covering the jet near field. In Fig. 1 shows the time distribution of the instantaneous longitudinal velocity on the jet axis when passing the puff superstructure at distances of 6 and 60 mm from the tube outlet. As you can see, in the jet the puff maintains a very flat leading front and a steep trailing one, which is typical for these

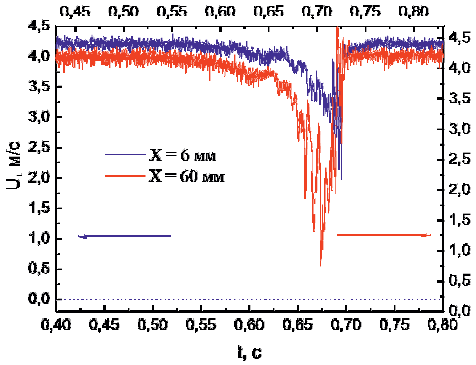

Fig. 1. Distribution of axial instantaneous velocities over time in two sections when puff passes through the jet. Re = 2400, x = 0.75*d*; 7.5*d*

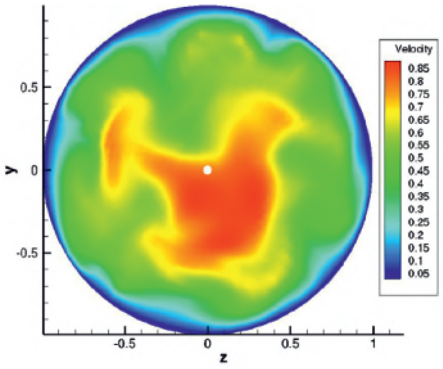

Fig. 2. Instantaneous field of longitudinal velocity of tube flowing in cross-section x = 12.5*d*

vortex structures when they move inside the pipe. In this case, as follows from the figure, with an increase in the distance from the nozzle exit to 7–8 calibers, its length and the amplitude of pulsations inside this superstructure increase. The resulting distributions of instantaneous velocities made it possible to calculate autocorrelation functions and frequency spectra.

To calculate flow with intermittency and generate puff-type superstructures in a pipe, the turbulent flow regime was set as the initial one, then the Reynolds number was reduced to transition values. The puff superstructure arose when the number Re = 2400 → 2200 was switched. The calculation was carried out in a pipe section 40*d* long with periodic boundary conditions at the ends; a jet flow was calculated downstream. At the tube flow, in the instantaneous velocity field in the cross section, not far from the trailing front, one can see the formation of three large vortices inside the puff (Fig. 2). The calculation showed that, as in a physical experiment, superstructures have a strong effect on the flow of the jet, while maintaining their internal structure at some distance from the tube outlet. The instantaneous velocity fields in puff show a smooth decrease in velocity on the axis and a steep trailing edge.

A comparison of the results obtained from a physical experiment and direct numerical simulation showed satisfactory agreement.

The work was supported by the Russian Science Foundation, grant No. 23-29-00584

REFERENCES

1. **Ginevsky A.S., Vlasov Y.V., and Karavosov R.K.** Acoustic Control of Turbulent Jets. Berlin, 2004. 235 p. https://doi.org/10.1007/978-3-540-39914-8
2. **Schumacher J., Eckhardt B., Haller G.** Turbulent superstructures in closed and open flows // Proceedings of the Euromech Colloquium. 2017. Art. 586. 2 p.
3. **Lemanov V., Lukashov V., Sharov K.** Turbulent superstructures in inert jets and diffusion jet flames // Fluids. 2021. Vol. 6, No 459. https://doi.org/10.3390/fluids6120459
4. **Nikitin N.** Finite-Difference Method for Incompressible Navier-Stoks Equations in Arbitrary Orthogonal Curvilinear Coordinates // Journal of Computational Physics. 2006. Vol. 217. P. 759–781. https://doi.org/10.1016/j.jcp.2006.01.036

DOI 10.53954/9785604990148_120

FORMATION OF A SECONDARY JET IN THE COLLISION OF TWO LAMINAR MICROJETS

Yu.A. Litvinenko, A.A. Smyatskikh

Institute of Theoretical and Applied Mechanics of the Siberian Branch of the Russian Academy of Science, 630090, Novosibirsk, Russia

The results of experimental studies of the process of diffusion combustion during the collision of two axisymmetric laminar propane microjets are presented in this paper. The studies were carried out using hot-wire measurements and the shadow method. The flowing out of gas through round nozzles is carried out at equal velocities. During the experiment, the transverse position of the nozzles relative to each other is varied while keeping the angle between them. The option of full overlap corresponds to the position when the symmetry axes of both jets are in the same plane. As a result, a flame formation scenario is shown for various positions of the nozzles. The features of the development of the torch at intermediate positions of the nozzles are presented. It has been established that when the outflowing jets are completely blocked, the torch deforms with the formation of an orthogonal torch. This process has common features with a similar outflow of air jets. With an increase in the exhaust velocity, a region of local gap of the flame front was found.

The development of jet currents is associated with the appearance of various types of hydrodynamic instability [1]. In the presence of combustion processes, the gas-dynamic jet structure significantly affects the processes of heat and mass transfer, flame stabilization, etc. In the case of interaction of two jets, the flow pattern becomes significantly more complicated. At the same time, the use of counter jets allows, for example, to control the speed parameters of the resulting jet and shape the shape of the flame, thereby influencing the combustion process. A feature of these studies is that the symmetry axes of the colliding jets are located at an acute angle to each other, and the transverse position of the nozzles changes from complete overlap of the jets, when the symmetry axes are in the same plane, to complete divergence of the jets, when the nozzles diverge in the transverse direction.

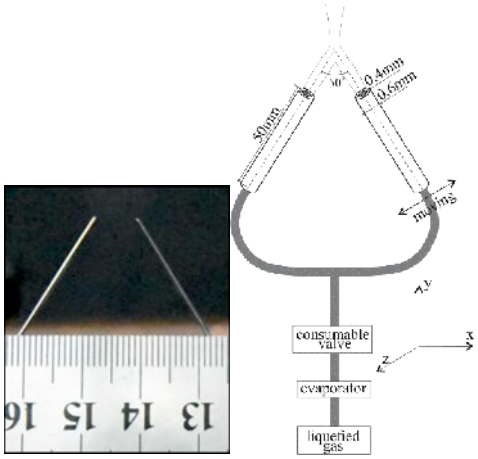

Fig. 1. Setup

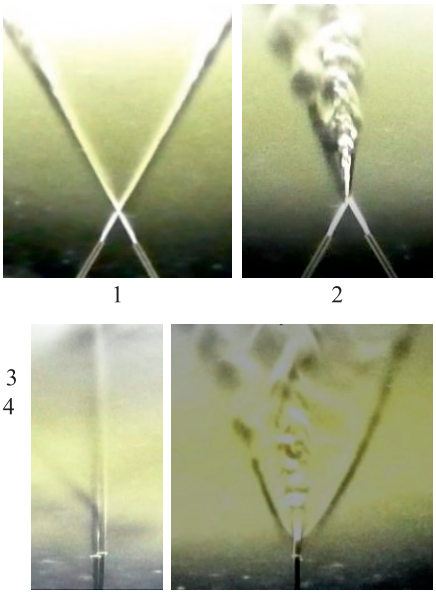

Fig. 2. Shadow images

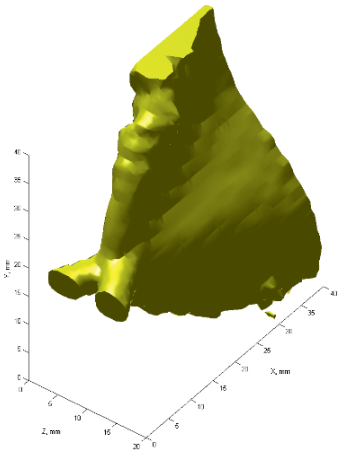

Fig. 3. Hot-wire isosurface

The experiments were carried out on a jet facility at the Khristianovich Institute of Theoretical and Applied Mechanics SB RAS. The setup consists of two identical cylindrical tubes 50 mm long and 0.4 mm in inner diameter, located at an angle of 50° between the axes of symmetry of the nozzles. The distance between the ends of tubes is 7mm. The experimental setup is shown in Fig.1. The used gas was a propane/butane mixture in a percentage ratio of 70/30. Liquefied gas was supplied from the balloon through the evaporator to the reducer, then to the mass flow controller, then it was divided into two parts. The gas flow rate through each nozzle corresponded to ½ of the set flow rate on the flow meter and was equal to 1.0×10^{-7} m^3/s. The calculated velocity of the gas flowing through each nozzle is $U_1 = U_2 = 0.39$ m/s, which corresponded to $Re_{propane} = 42$, at the nozzle diameter 400 μm. At the current Reynolds number, the flame was laminar. When the velocity reaches $U \geq 0.53$ m/s ($Re \geq 55$), the flame becomes turbulent and detaches from the nozzle exit. Fig. 2 shows shadow photographs of the development of two colliding gas jets without combustion at different overlap. Photo 1 and 3 (Fig. 2) correspond to xy and yz planes, respectively, for case when the jets do not interact. Photo 2 and 4 (Fig. 2) show the same planes, for the case of overlap of the jets is ~ 100% of the cross-sectional area of each nozzle. Figure 3 shows the isosurface of velocity fluctuations at 100% jet overlap. As a result, characteristic features of the formation of the resulting jet and flame during diffusion combustion were obtained.

The research was supported by the Russian Science Foundation No 22-19-00151, https://rscf.ru/project/22-19-00151/

REFERENCES

1. **Kozlov V.V., Grek G.R., Litvinenko Yu.A.** Visualization of Conventional and Combusting Subsonic Jet Instabilities. Book Springer Briefs in Applied Sciences and Technology, 2016, 1 – 126, ISBN: 978-3-319-26957-3 (Print), 978-3-319-26958-0 (Online).

DOI 10.53954/9785604990148_122

SURFACE PROCESSES ON SILICA IN THE DIRECT MONTE CARLO SIMULATIONS OF HIGH-ENTHALPY FLOWS

A.S. Litvintsev, A.N. Molchanova, Ye.A. Bondar

Khristianovich Institute of Theoretical and Applied Mechanics SB RAS
630090, Novosibirsk

Development of thermal protection system of reusable spacecraft requires accurate prediction of thermal loads on its surface in various flow regimes along the descent trajectory. The main tool of re-entry aerothermodynamics research is numerical simulation because of high complexity of such investigations in ground-based test facilities. At altitudes below 80 km, the flow is usually modeled with the Navier–Stokes equations. At altitudes above 80 km, it is necessary to employ the kinetic approach based on the Direct Simulation Monte Carlo (DSMC) method because of significant rarefaction effects.

Surface catalytic processes involving components of a high-temperature air mixture strongly affect the heat flux to the vehicle. Ignoring these processes leads to significant underestimation of heat loads. There are a numerous works where finite-rate surface reactions sets were obtained using different approaches. In classical approach the rate constants are obtained from an experimental data at certain conditions. Such curve fitting of experimental data can ignore effects of complex interplay of surface processes and make incorrect predictions in extension to other conditions. Additionally this approach causes the simplification of surface catalytic mechanism with neglecting some surface processes. In our work we consider the more complete and consistent detailed macroscopic catalytic mechanism recently developed in [1] which describes the processes on the surface of β-cristobalite. The authors calculated the rate constants using the quantum-mechanical approach and the transition state theory in a wide range of parameters for a large set of surface processes: atomic and molecular adsorption and desorption, dissociation on a surface, Eley–Rideal and Langmuir–Hinshelwood recombination.

The present work is dedicated to the implementation of this detailed macroscopic model in the DSMC method using the approach described in [2, 3] and further investigation of effect of surface processes to the heat flux in a wide range of parameters. The report presents details of the numerical implementation of this mechanism into the SMILE++ software system [4, 5]. Verification of such implementation is difficult because of the aforementioned surface processes' interplay. Thorough analysis of all processes is performed in order to make a better selection of calculation parameters. The report will also present the results of a numerical study of the effect of surface catalytic processes on the aerothermodynamics of a generic vehicle in a wide range of flow regimes.

The research was carried out within the state assignment of Ministry of Science and Higher Education of the Russian Federation.

REFERENCES

1. **Kroupnov A.A., Pogosbekian M.Ju.** Interaction of dissociated air with the surface of β-cristobalite material // Acta Astronautica. 2023. Vol. 203. P. 454(68).
2. **Molchanova A.N., Kashkovsky A.V., Bondar Ye.A.** Surface recombination in the direct simulation Monte Carlo method // Physics of Fluids. 2018. Vol. 30, no. 10. P. 107105(18).

3. **Litvintsev A.S., Molchanova A.N., Bondar Ye.A.** Effects of heterogeneous NO production on the aerothermodynamics of high-altitude re-entry // AIP Conference Proceedings, Vol. 2288, No. 1, 2020
4. **Kashkovsky A., Bondar Y., Zhukova G., Ivanov M., Gimelshein S.** Object-oriented software design of real gas effects for the DSMC method // 24th Int. Symp. on RGD, Pp. 583–588, 2005
5. **Ivanov M., Kashkovsky A., Vashchenkov P., Bondar Y.** Parallel object-oriented software system for DSMC modeling of high-altitude aerothermodynamic problems // 27th Int. Symp. on RGD, AIP Conf. Proceedings 1333, Pacific Grove, California, Pp. 211–218, 2011

DOI 10.53954/9785604990148_124

LES INVESTIGATION OF PRECESSING VORTEX ROPE IN FRANCIS TURBINE AIR MODEL AND MITIGATION STRATEGIES

I.I. Lutchenko[1, 2], E.V. Palkin[1], M.Yu. Hrebtov[1, 2], R.I. Mullyadzhanov[1, 2]

[1]Institute of Thermophysics SB RAS, 630090, Novosibirsk, Russia

[2]Novosibirsk State University, 630090, Novosibirsk, Russia

Hydroelectric power plants are a renewable and reliable source of energy, as water is constantly replenished by the natural water cycle. While they can provide a consistent electricity source, they also adjust electricity production based on continuously changing consumer demands. Therefore, hydro turbines have to operate at high and partial load conditions. However, operating at partial loads leads to the high residual swirl of the runner outflow resulting in vortex breakdown in the draft tube. This phenomenon is characterized by as an extensive recirculation zone and its interaction with the main flow gives rise to a spiral vortex structure - precessing vortex rope (PVR). It results in increased pressure pulsations in the draft tube wall, power swings [1]. Since about the middle of the 20th century, a lot of techniques have been developed to mitigate this phenomenon: passive [1–3] and active flow controls [4].

In this work we present the numerical investigation of active flow control application to the swirling flow in a Francis turbine air model. This allowed to avoid significant computational costs and focus on high-fidelity numerical simulations of the PVR [5]. Large-eddy simulations (LES) with dynamic Smagorinsky model were carried out on hexagonal mesh with non-comformal interfaces by the open-source code OpenFOAM-11. The base flow under partial load condition $Q/Q_{\text{bep}} = 0.50$ was verified against the experimental PIV data. A flow control strategy was based on the recent study [6] and applied to the $Q/Q_{bep} = 0.35$ case. Axial and radial jets injection were employed to suppress the PVR dynamics. While the previous study was focused on the spectral characteristics of pressure pulsations, this work expands upon it by analyzing the control effect on the PVR's velocity field data, pressure isosurfaces, and other relevant parameters.

The work is supported by the state contract with IT SB RAS.

REFERENCES

1. **Rheingans W.J.** Power swings in hydroelectric power plants // Transactions of The American Society of Mechanical Engineers. – 1940. – T. 62. – No. 3. – P. 171–177.
2. **Kurokawa J., Imamura H., Choi Y.D.** Effect of J-groove on the suppression of swirl flow in a conical diffuser. – 2010.
3. **Lückoff F., Naster M., Müller J.S., Sieber M., Litvinov I., Oberleithner K.** Impact of runner crown shape modifications on the onset of the precessing vortex core // IOP Conference Series: Earth and Environmental Science. – IOP Publishing, 2022. – Vol. 1079. – No. 1. – P. 012051.
4. **Shtork S., Suslov D., Skripkin S., Litvinov I., Gorelikov E.** An overview of active control techniques for vortex rope mitigation in hydraulic turbines // Energies. – 2023. – Vol. 16. – No. 13. – P. 5131.
5. **Skripkin S.G., Suslov D.A., Litvinov I.V., Gorelikov E.U., Tsoy M.A., Shtork S.I.** Comparative analysis of air and water flows in simplified hydraulic turbine models // Journal of Physics: Conference Series. – IOP Publishing, 2022. – Vol. 2150. – No. 1. – P. 012001.
6. **Litvinov I., Suslov D., Tsoy M., Gorelikov E., Shtork S., Alekseenko S., Oberleithner K.** Active Control of the Vortex Induced Pressure Fluctuations in a Hydro Turbine Model via Axial and Radial Jets at the Crown Tip // International Journal of Fluid Machinery and Systems. – 2023. – Vol. 16. – No. 4. – P. 320–331.

DOI 10.53954/9785604990148_125

LASER AND ELECTRON BEAM ADDITIVE TECHNOLOGIES

A.G. Malikov[1], V.M. Fomin[1], A.A. Golyshev[1], E.A. Kolubaev[2], A.V. Chumaevsky[2]

[1] S.A. Khristianovich Institute of Theoretical and Applied Mechanics, SB RAS, 630090, Novosibirsk, Russia

[2] Institute of Strength Physics and Materials Science SB RAS, 634055, Academichesky Ave, 2/4, Tomsk, Russia

In recent years, additive manufacturing (AM), also known as 3D printing, has attracted significant attention due to its wide range of applications in various industries such as aerospace and automotive, biomedicine, nuclear production, etc. Currently, AM is revolutionizing the manufacturing industry due to its ability to produce complex-shaped products in a short period of time and with virtually no material waste. Additive manufacturing of metal materials plays a key role in the aerospace industry due to the widespread use of metal components in almost all areas of technology.

In the Siberian Branch of the Russian Academy of Sciences, two organizations have been actively involved in fundamental research on additive technologies in the last decade – the ITAM SB RAS and ISPMS SB RAS.

The ITAM SB RAS focuses on laser micro-metallurgy, aiming to achieve a desired structural-phase composition and mechanical properties of materials after laser processing.

Laser micro-metallurgy is based on a comprehensive approach that has allowed to establish general physical regularities describing the final characteristics of the material depending on the alloying system and thermophysical properties of the material, solidification regimes and type of molten metal flow, rapid local non-equilibrium heating, melting and subsequent material crystallization, cooling rate, optimal post-processing and material phase composition diagnostics using synchrotron radiation on the "Megasience" class facility at the Siberian Synchrotron Radiation Center of the Institute of Catalysis of the Siberian Branch of the Russian Academy of Sciences.

Based on the results of fundamental research, applied technologies are being implemented: direct laser growth of metal-ceramic coatings based on aviation titanium, high-temperature nickel, and promising aluminum alloys, as well as ceramics such as carbides (boron carbide B4C, tungsten carbide WC, titanium carbide TiC, etc.) and borides (boron B, titanium boride TiB, titanium diboride TiB2, etc.), technology for restoring blade tips in a gas turbine engine.

Composite materials with a metallic matrix are being developed at the ITAM SB RAS. Similar metal matrix composites are classified depending on the nature of reinforcement formation during their manufacturing, ex-situ and in-situ. Novel metal matrix composites reinforced by in-situ method have been developed, in which reinforcing particles are synthesized in the metallic matrix as a result of a chemical reaction between elements during the composite manufacturing process (for example, Ti+B4C→2TiB2+TiC). These composites allow achieving better physical and mechanical properties due to better control of the size and level of reinforcement, as well as the matrix-reinforcement interface. The mechanical and physical properties of composites are primarily determined by the properties of the matrix, reinforcement dispersion, interfacial bonding between the matrix and reinforcement, and the processing method. The use of laser irradiation for the formation of metal matrix

composites with in-situ reinforcement opens up new horizons for creating multifunctional composites with a metallic matrix that are difficult to obtain using traditional manufacturing processes.

The main direction of research in the field of 3D printing at the ISPMS SB RAS is the study of patterns and mechanisms of structure formation of products made of various metals and alloys using wire-based electron beam additive technology. The development of the equipment was carried out in cooperation with the industrial partner "Cheboksary Enterprise "Sespel", which received an installation for electron beam wire printing with a chamber volume of 8 cubic meters. The equipment produced during the project was the first domestic samples of this type of equipment, and after their development, the Russian Federation became the third country in the world after the USA and China to master the technology of wire-based electron beam 3D printing. Electron beam printing equipment allows the production of large-sized products from aluminum, titanium, copper alloys, steels, and composite materials based on them with high productivity. Printing is possible using refractory and high-alloy materials that cannot be printed by other methods (high-alloy nickel superalloys, refractory intermetallic alloys, steels, multi-component composites). For example, using electron beam printing, the institute was able to produce experimental samples of nickel heat-resistant superalloys ZhS6U and ZhS32 with high mechanical properties and a defect-free structure for the first time. Additionally, the institute was one of the first to develop techniques for printing multi-component composites or modified alloys based on copper, nickel, titanium, aluminum alloys, and steels by feeding two or more components into the melt bath in the form of wire filament or a combination of wire and powder.

During the printing process of products using wire electron-beam technology, it is possible to change the structure of the resulting products by applying heat-physical, thermomechanical, physico-chemical, and other methods of control. The heat-physical method involves the use of additional thermal breaks to increase cooling rate, regulation of beam current to change the heat contribution to the sample, application of cooling systems to dissipate excess heat, etc. The thermomechanical method involves the use of additional mechanical, vibrational, or impact actions during printing, as well as after the completion of product formation (ultrasonic treatment, shock-wave treatment, friction-stir processing). The physico-chemical method allows to control the composition of the material in different areas of the details through the use of developed methods of multi-wire or combined wire-powder printing, which is difficult with other printing methods. The application of control methods is part of the concept of non-stationary local metallurgy developed at the institute, which considers the printing zone as an analog of a metallurgical process occurring in a molten bath, moving along the sample and forming the product layer by layer. The developments of the ISPMS SB RAS in relation to wire additive electron-beam printing allow to regulate the structure and properties of products directly during their production. Fine control of the structure in local regions of the detail allows for optimizing the product not only in terms of size and shape, but also in terms of internal structure by using the necessary alloying elements only in those areas where they are required in operating conditions. This makes electron beam printing technology relevant for obtaining intricately structured parts with high performance in industry.

This work was carried out as part of the state assignment of the ITAM SB RAS. The equipment of the Centre for Collective Use "Mechanics" of the ITAM SB RAS was used in this work.

DOI 10.53954/9785604990148_127

GAS RELAXATION BEHIND REFLECTED SHOCK WAVES: SIMULATION, COMPARISON AND MODEL VALIDATION BASED ON EXPERIMENTS

M.Yu. Melnik[1, 2], D.S. Kravchenko[1, 2], A.A. Isakov[1], E.V. Kustova[1, 2]

[1]Saint Petersburg State University,
7/9 Universitetskaya nab., St. Petersburg, 199034, Russia

[2]Federal Research Center "Computer Science and Control" of the Russian Academy of Sciences, 44-2 ul. Vavilova, Moscow, 119333, Russia

Modern research in aerospace, environmental, and low-temperature plasma applications require deep understanding and accurate modeling of highly nonequilibrium gases. They are characterized by complex interactions between the processes of vibrational, electronic excitation and chemical reactions. This creates significant difficulties for their theoretical description and requires large resources for accurate modeling. Therefore, the development of the kinetic schemes incorporating models that are optimal in terms of accuracy and computational costs is relevant. Such analysis is conveniently carried out on the basis of simple problems, for instance, gas relaxation behind shock waves. The present study is devoted to the analysis and validation of a number of theoretical models within the framework of the state-to-state approach [1]. Validation was carried out on the basis of recent high-precision experimental measurements behind reflected shock waves [2, 3, 4].

The approach used to simulate relaxation behind reflected shock waves is developed in [5]; in this paper, models describing various nonequilibrium processes were varied, and all possible combinations were considered. Thus, to describe the dissociation process, the Marrone-Treanor [6] model with the values of the parameter $U = 3T$, $D/6k$ and ∞ was used. For vibrational energy exchanges, the widely used models SSH [7], FHO [8] as well as the recent FHO-FR-reg model developed using regression analysis [9] are considered. The latter model is based on the FHO-FR model [10, 11], which takes into account the three-dimensional nature of particle collisions and the free rotation of molecules. In our studies prior to [5] it was anticipated that a more accurate FHO-FR model could improve agreement with experiments; however, this assumption was not assessed due to high computational costs of the model. This was tested using the FHO-FR-reg model.

The use of this approach made it possible to accurately describe the relaxation of gas behind reflected shock waves in the considered mixtures of O_2/Ar, NO/Ar, NO/N_2/Ar and N_2/O_2/NO. Particular attention was paid to taking into account the partial relaxation between the incident and reflected shock waves. In the interpretation of early experiments, the authors neglected relaxation between waves. However, this work shows the importance of taking into account relaxation and its influence on the internal energy and relaxation behind the reflected shock wave.

The study ran more than 700 simulations for various initial conditions and model combinations. The result of a typical simulation for NO concentration is shown in Fig. 1. Analysis of the results allowed us to deeply explore the validity of various combinations of rate coefficients for vibrational transitions, dissociation and exchange reactions. Including partial relaxation between shock waves in the simulation was found to significantly improve the agreement between calculated and measured pressures in O_2/Ar mixtures, including pure

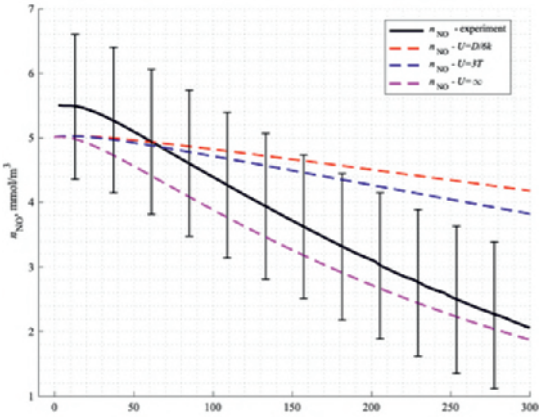

Fig. 1. Evolution of NO concentration behind reflected shock wave. 1% NO in argon. Gas temperature T just behind the reflected shock wave is 5580 K. FHO-FR-reg with various values of U.

oxygen. However, for mixtures containing NO, turning on relaxation does not have a noticeable effect on the results.

Based on our analysis, we recommend to use the SSH model in combination with the Marrone-Treanor model with the parameter $U = D/6k$ for the O_2/Ar mixture. For mixtures containing NO, if one expands the acceptable error to 5–10% at the initial moments of time, using a combination of the FHO model and the value of $U = \infty$ is preferable. For the considered conditions ($T < 14\ 000$ K) the hypothesis that using the FHO-FR model considerably improves the agreement with experiments was not confirmed. However, the approach used in the development of the FHO-FR-reg model speeds up calculations several times even in comparison with the ordinary FHO model. Moreover, a recent study [12] showed that the main advantages of FHO-FR are revealed at temperatures above 10 000 K. This makes FHO-FR-reg attractive for use in resource-intensive problems.

This study is supported by the Russian Science Foundation, project 22-11-00078.

REFERENCES

1. **Nagnibeda E., Kustova E.** Nonequilibrium Reacting Gas Flows. Kinetic Theory of Transport and Relaxation Processes, Springer Verlag, Berlin, Heidelberg, 2009.
2. **Streicher J., Krish A., Hanson R.** Coupled vibration-dissociation time-histories and rate measurements in shock-heated, nondilute O2 and O2-Ar mixtures from 6000 to 14000 K // Phys. Fluids. 2021. Vol. 33, No. 5. P. 056107.
3. **Streicher J., Krish A., Hanson R.** High-temperature vibrational relaxation and decomposition of shock-heated nitric oxide. I. Argon dilution from 2200 to 8700 K // Phys. Fluids. 2022. Vol. 34, No. 11. P. 116122.
4. **Streicher J., Krish A., Hanson R.** High-temperature vibrational relaxation and decomposition of shock-heated nitric oxide: II. Nitrogen dilution from 1900 to 8200 K // Phys. Fluids. 2022. Vol. 34, No. 11. P. 116123.
5. **Kravchenko D., Kunova O., Kustova E., Melnik M.** Reflected shock waves in air components and their mixtures: Validation of theoretical models // Acta Astronautica. 2024. Vol. 218. P. 47–58.
6. **Marrone P., Treanor C.** Chemical relaxation with preferential dissociation from excited vibrational levels // Phys. Fluids. 1963. Vol. 6, No. 9. P. 1215–1221.
7. **Schwartz R., Slawsky Z., Herzfeld K.** Calculation of vibrational relaxation times in gases // J. Chem. Phys. 1952. Vol. 20. Art. 1591.
8. **Adamovich I., Macheret S., Rich J., Treanor C.** Vibrational energy transfer rates using a forced harmonic oscillator model // J. Thermophys. Heat Transfer. 1998. Vol. 12, No. 1. P. 57–65.
9. **Isakov A.A., Gorikhovskii V.I., Melnik M.Yu.** Regression Models for Calculating State-to-state Coefficients of the Rate of Vibrational Energy Exchanges // Vestnik St. Petersburg University, Mathematics. 2024. Vol. 57, No. 2. P. 226–235.

10. **Adamovich I., Rich J.** Three-dimensional nonperturbative analytic model of vibrational energy transfer in atom-molecule collisions // J. Chem. Phys. 1998. Vol. 109, No. 18. P. 7711–7724.
11. **Adamovich I.** Three-dimensional analytic model of vibrational energy transfer in molecule-molecule collisions // AIAA J. 2001. Vol. 39, No. 10. P. 1916–1925.
12. **Gimelshein S.F., Wysong I.J., Adamovich I.V.** Application of the 3D Forced Harmonic Oscillator Model in the DSMC Method // Journal of Thermophysics and Heat Transfer. 2018. Vol. 32, No. 4. P. 882–891.

DOI 10.53954/9785604990148_130

THE EFFECT OF CHANGING THE ANGLE OF ATTACK ON THE FLOW STRUCTURE BEHIND A SEMICIRCULAR CYLINDER WITH A SLIT

D.S. Mironov, V.N. Zinoviev, V.A. Lebiga, A.Yu. Pak

Khristianovich Institute of Theoretical and Applied Mechanics SB RAS
630090, Novosibirsk, Russia

One of the most popular areas of aerodynamics is flow control. For aircraft, this is necessary to improve flight characteristics, in various technological facilities to intensify or reduce heat and mass transfer or reduce noise levels. Despite the prospects and effectiveness of active methods of flow control with the development of technologies, including MEMS, the use of passive methods also remains attractive due to the simplicity of implementation and has been actively studied in recent years [1]. The development of computational technologies and methods for processing non-stationary data makes it possible to analyze the results obtained in experiments under continuously changing conditions.

The presented work is a continuation of the experimental investigation [2]. In this paper, the aim was to study the effect of the presence of a slit in a semicircular cylinder on the characteristics of the flow behind it at a non-stationary angle of attack, as well as the effect of the rigidity of the model itself on the nature and level of the flow fluctuations in the wake.

All experiments were carried out in the T-325M wind tunnel of ITAM SB RAS. The test section is a 40×40 mm^2 square channel. Two types of models were used: metal and plastic, made using 3D printing technology, with and without slits. The model consisted of a half round cylinder with a diameter of D = 8 mm, with a length of 40 mm for the entire width of the test section. A slit with a width of s = 1 mm was located perpendicular to the flat side of the semicircular cylinder in the center of the diameter. The cylinder model was mounted on a rotary mechanism based on a stepper motor, which allows you to change the angle of attack with an accuracy of 0.1°. The scheme of the experiment and the determination of the angle of attack are shown in Fig. 1.

The longitudinal component of the velocity was measured using a constant temperature thermoanemometer CTA-5 developed in ITAM SB RAS using a hot wire probe. The probe was located at a distance of x = 32 mm downstream from the axis of the model on a coordinate device, driven by a stepper motor, allowing it to be moved in a transverse direction to the main stream in the range ±15 mm along Y axis.

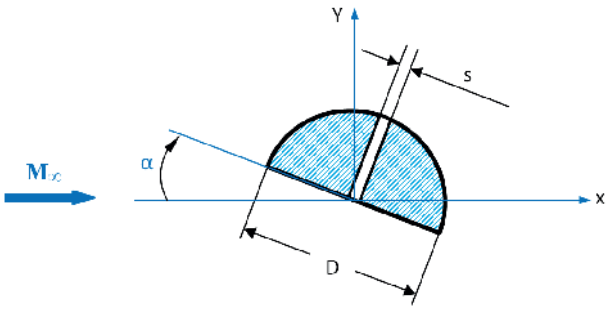

Fig. 1. Scheme of experiment.

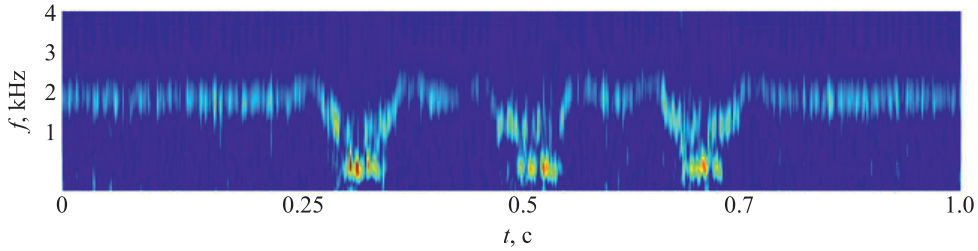

Fig. 2. Wavelet spectrum of velocity fluctuations.

The Mach number of the incoming flow in all series of experiments was M = 0.15, which corresponds to the Reynolds number on the diameter of the model $Re_D = 4.8 \cdot 10^4$. The range of change in the angle of attack in each case was 20° in a positive or negative direction relative to some initial angle, the values of which were set to –10°, 0 or +10°. At the same time, different speeds of rotation and the number of cycles of changing the angle of attack were used. An example of the obtained wavelet spectrum of velocity fluctuations obtained with a three-fold change in the angle of attack from +10° to –10° and vice versa is shown in Fig. 2.

Based on the results of measurements in the wake behind the semicircular cylinder, averaged and instantaneous profiles of the average and fluctuation components of the longitudinal velocity were obtained at a varying angle of attack, and time-frequency spectra of velocity fluctuations were obtained. It is shown that in the presence of a slit, the characteristic frequencies of vortex shedding behind a semicircular cylinder depend non-linearly on the effective width of the cross-section of the model. It was found that at low angles of attack in the presence of a slit, there is a noticeable difference in the flow around the semicircular cylinder compared to the case without a slit. The most pronounced changes in the frequency and intensity of velocity fluctuations occur at a negative angle of attack close to zero.

The work was performed within the framework of the State Assignment (registration number 121030500154-2).

REFERENCES

1. **Isaev S.A., Lebiga V.A., Sudakov A.G., Nikuschenko D.V., Chung K.-M.** Control of vortex structures to reduce the drag of blunted bodies and to increase the lift of thick carrying surfaces // XXI International conference on the methods of aerophysical research (ICMAR 2022). Abstracts. Part I. Novosibirsk, 2022. P. 68–69. DOI: 10.53954/9785604788967_68
2. **Zinovyev V.N., Lebiga V.A., Mironov D.S., Pak A.Yu.** Experimental investigation of the wake behind the semicircular cylinder with a slit in subsonic flow under unstable angle of attack// XXI International conference on the methods of aerophysical research (ICMAR 2022). Abstracts. Part II. Novosibirsk, 2022. P. 183–184. DOI: 10.53954/9785604788974_183

DOI 10.53954/9785604990148_132

INVESTIGATION OF SHOCK WAVES REFLECTION FROM HIGHLY–POROUS MATERIALS

S.G. Mironov, T.V. Poplavskaya, S.V. Kirilovskiy

Khristianovich Institute of Theoretical and Applied Mechanics, Siberian Branch of the Russian Academy of Sciences, 630090, Novosibirsk, Russia

The study of the interaction of shock waves (SW) with various materials is of significant practical interest. Most of the research into such interaction is devoted to the problem of protecting buildings and structures from the effects of pressure pulses in SW. However, there are tasks where it is necessary to minimize the effect of wave reflection. In particular, the use of coatings with low SW reflection makes it possible to reduce the risk of detonation of mixtures of flammable dispersed particles or gases with air, which often occur in a number of technological processes.

In this work, we carried out experimental and numerical modeling of the interaction of weak flat shock waves during their normal incidence on obstacles made of gas-permeable, highly porous materials. The results of parametric studies of the influence of the defining flow parameters on the characteristics of waves reflected from obstacles are presented: the size of the cells of the porous material, the thickness of the obstacles, the Mach number of SW and the length of the buffer volume between the obstacle and the tough wall, as well as a combination of layers of highly porous materials.

The experiments were carried out in a low-pressure shock tube with air inlet from the atmosphere (Fig. 1*a*). By varying the initial pressure in the tube channel, shock waves were created in the range of Mach numbers from 1.2 to 1.8. In the experiments, the time dependence of the static pressure P(t) in front of the obstacles was recorded using a PCB113B28 piezoelectric sensor. Based on the time difference between the signals of two piezoelectric sensors, the speed of the front and the Mach number of the shock wave were calculated. The unit Reynolds number Re1 in the flow behind the incident shock wave was not constant and varied in the range from $\cong 4\times10^6$ 1/m to $\cong 6\times10^6$ 1/m depending on the Mach number and the initial air pressure in the channel of the shock tube.

The experiments used gas-permeable porous inserts made from stacks of triangular meshes and layers of cellular porous nickel. The triangular meshes had a cell side length l from 12 to 4 mm, cellular porous nickel had a porosity of 95 % and an average pore diameter of d = 1 and 3 mm. Cylindrical porous inserts were attached to thin-walled cylinders of various lengths L with a capped end, which were tightly inserted into the channel of the shock tube and played the role of a buffer volume behind the obstacle.

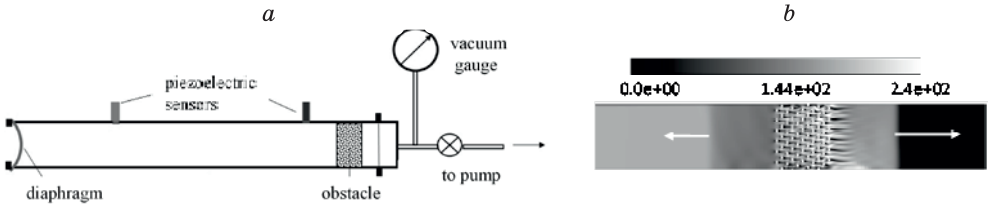

Fig. 1. Scheme of the experimental setup (*a*) and an example of the calculated velocity field near the gas-permeable insert in the shock tube (*b*)

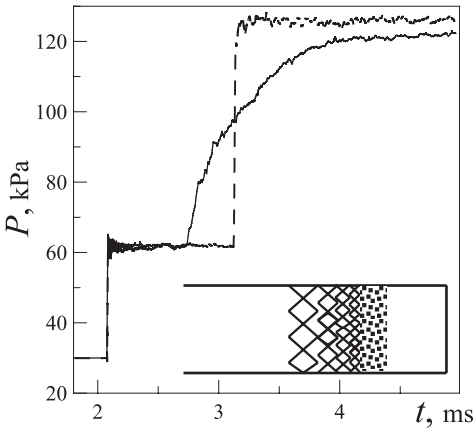

Fig. 2. Examples of experimental dependences of static pressure on time:

A combined obstacle made of triangular meshes and cellular-porous nickel (solid curve), consisting of 4 layers of meshes with a thickness of h = 15 mm with the side length of the mesh cells l = 10; 8; 6; 4 mm and a layer of cellular porous nickel with a thickness of h = = 20 mm with pour diameter of d = 1 mm. The length of the buffer volume behind the obstacle is L = 25 mm, the Mach number of the SW is M = 1.39. The dotted curve is the P(t) dependence in the absence of the obstacle.

The experiments were supported by numerical modeling of the problem of interaction of shock waves with obstacle made of highly porous cellular material (HPCM). This made it possible to visualize the flow inside and outside the porous obstacle (Fig. 1*b*) and understand the process of generation of reflected waves. Numerical modeling was performed using the ANSYS Fluent package based on solving the unsteady Reynolds-averaged Navier-Stokes equations using the k-ω SST turbulence model. The gas-permeable cellular-porous insert was modeled within the framework of a toroidal skeletal model [1].

It has been shown (see, for example, [2]) that gas-permeable cellular-porous inserts create a pressure jump reflected from the target that is weaker in amplitude compared to the shock wave reflected from the back wall of the shock tube in the absence of an insert. In this case, an HPLM with a smaller pore diameter, although it has a higher level of reflection from the insert, shows a smooth (without jumps) increase in pressure when gas flows from the region between the insert and the back wall of the shock tube. This led to the idea of constructing combined obstacles with weakly reflect shock waves.

It was found that the greatest efficiency in attenuating reflected shock waves is achieved in the case of using combined obstacles consisting of a package of triangular meshes with decreasing cell sizes as they go deeper into the barrier, and a final layer of HPCM with a small pore size. For example, in Fig. 2 shows the dependence of P(t) in the incident and reflected waves for such a combined obstacle and without it, where one can see a significant “extension” of the dependence of static pressure on time compared to the case of the absence of a highly porous obstacle.

This study was performed within the framework of the Project of the Basic State Order. The experiments were performed at the Collective Use Center “Mekhanika” (Mechanics) at ITAM SB RAS.

REFERENCES

1. **Kirilovsriy S.V., Poplavskaya T.V., Mironov S.G. et. al** Three-dimensional models of gas-permeable skeleton high-porosity cellular materials for supersonic aerodynamics // Thermophysics and Aeromechanics. 2022. Vol. 29. No. 5. P. 741–752.
2. **Mironov S., Kirilovsriy S., Poplavskaya T., Tsyryulnikov I.** Interaction of weak shock waves with highly porous materials // E3S Web of Conference 04007 (2023).

DOI 10.53954/9785604990148_134

INFLUENCE OF ENVIRONMENTAL PARAMETERS ON THE INTENSITY OF SOUND BOOM FROM SUPERSONIC TRANSPORT

P.A. Mishchenko, T.A. Gimon

Khristianovich Institute of Theoretical and Applied Mechanics, Siberian Branch of Russian Academy of Sciences, 630090, Novosibirsk, Russia

One of the restrictions that determines the right to operate supersonic passenger aircraft and their market competitiveness is the need to ensure an acceptable level of sonic boom when the aircraft flies at supersonic speed [1]. The nature of the transformation of a sonic boom wave when propagating in the atmosphere is influenced by such atmospheric effects as nonlinearity, stratification of the atmosphere, dissipative, dispersion effects and the presence of environmental inhomogeneities (wind). To more accurately predict a sonic boom, a thorough study of the influence of environmental parameters on the intensity of the sonic boom and other characteristics of the disturbed flow is necessary.

When recalculating the initial profile of the disturbed pressure from the near zone to the far zone, the quasi-linear problem of pressure profile propagation was solved using the one-dimensional augmented Burgers equation [2] in the form:

$$\frac{\partial p}{\partial x}=\frac{\beta}{2\rho_0 c_0^3}\frac{\partial p^2}{\partial t`}-\frac{1}{2A}\frac{\partial A}{\partial x}p+\frac{1}{2\rho_0 c_0}\frac{\partial(\rho_0 c_0)}{\partial x}p+\frac{\delta}{2c_0^3}\frac{\partial^2 p}{\partial t`^2}+\sum_j\frac{(\nu c)_j\tau_j}{c_0^2}\left(1+\tau_j\frac{\partial}{\partial t`}\right)^{-1}\frac{\partial^2 p}{\partial t`^2}, \quad (1)$$

where $p(x, t')$ – pressure, x – curvilinear coordinate along the wave propagation ray, A – ray tube area, $t'=t-\int_0^x\frac{1}{c_0}\mathrm{d}x$ – retarded time, c_0 – equilibrium speed of sound, ρ_0 – ambient density, β – nonlinearity coefficient, δ – sound diffusion coefficient due to both viscosity and thermal conductivity. The splitting method allows sequentially solving the system of equations. The solution was implemented as a computational program in Python.

The work involved calculating the intensity of a sonic boom at various wind speeds and directions. The initial one-dimensional profile of the disturbed pressure (Fig. 1(a)) corresponds to the pressure values in the near zone of the aircraft model when an oncoming supersonic air flow with Mach number M = 1.4 flows around it. The model represents the layout of a supersonic passenger aircraft with a mass G = 70 tons and a length L = 40 m. In the simulation, the aircraft flies east at a cruising altitude of 16.46 km. Sonic boom waves travel

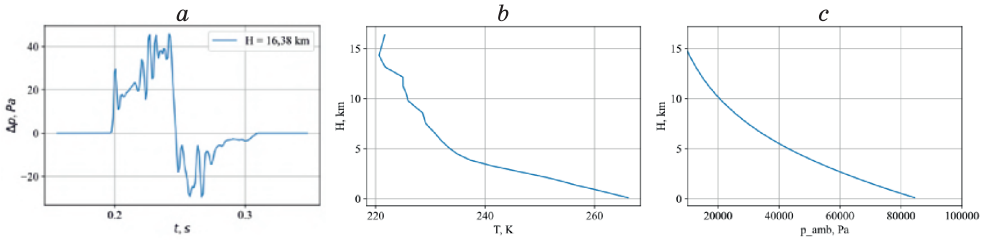

Fig.1 Initial profile of the disturbed pressure (a), parameters of the environment (b)–(c)

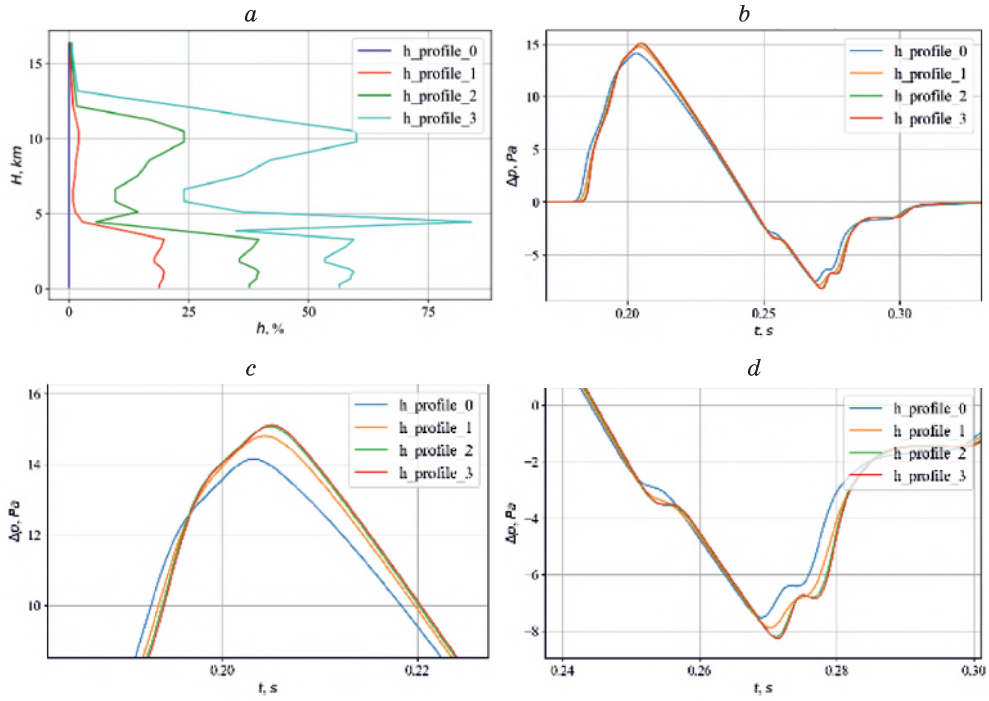

Fig. 2. Relative humidity (a), the result of recalculation of the disturbed pressure profile from an altitude of 16.46 km to 101 m at different relative humidity (b)–(d)

in a stratified atmosphere. In Fig. 1(b), (c) shows the distribution of ambient temperature and pressure over altitude. The calculation was carried out with a computational grid of 384 by 7707 angles.

The altitude distribution of relative humidity is presented in Fig. 2(a), in Fig. 2(b)-(d) are the results of recalculation of the initial profile of the disturbed pressure into the far zone at different relative humidity. With an increase in relative humidity, the front of jumps in the disturbed pressure profile increases in steepness and their amplitude increases.

The research was carried out within the state assignment of Ministry of Science and Higher Education of the Russian Federation (project No. 121030900260-6).

REFERENCES

1. **Chernyshov S.L.** Sonic boom. M: Sciense, 2011.
2. **Cleveland R.O.** Propagation of sonic booms through a real, stratified atmosphere: PhD thesis. – The University of Texas at Austin, 1995.

DOI 10.53954/9785604990148_136

SEPARATION OF SWIRLING FLOWS IN CHANNELS AT MODERATE REYNOLDS NUMBERS

V.M. Molochnikov, N.D. Pashkova, A.A. Paereliy

Federal Research Center "Kazan Scientific Center of the Russian Academy of Sciences", Kazan 420111 Russia

Separation of swirling flows is interesting from the standpoint of both the basic science and numerous engineering applications. Swirling flows in general and separated flows in particular are essentially three-dimensional and unsteady. Therefore, they are rather challenging to study. Swirling is typically accompanied by precession of the vortex core and vortex breakdown [1]. Large number of experimental and computational studies focus on separation of swirling *turbulent* flows, but the problem of their description is far from being solved. Separation of swirling flows at low and moderate Reynolds numbers is studied less. Swirling is known to delay laminar-turbulent transition or, vice versa, promote earlier transition of separated flows compared to non-swirling flows. Turbulizing or stabilizing effect of swirling in separated flows can be employed for enhancement of heat transfer and mixing, for reduction of sizes of separation regions behind obstacles, discrete roughness elements, etc. Biomechanics of blood circulation is a critical research field of laminar-turbulent transition in swirling separated flows in channels. Normally, the flow mode in blood vessels is laminar. Turbulization of flow behind a local narrowing of the vessel (stenosis) or around the attachment of bypass circumventing the diseased part of the artery (anastomosis) to the host artery is unfavorable for hemodynamics in these regions. Moreover, it is one of the reasons for intense proliferation of the inner surface of vessel leading to its obstruction. Forced swirling of flow can benefit hemodynamics, and hence, result in reduced risk of repeated surgical intervention. The research dealing with this problem has only started, and publications are scarce. Besides, swirling of blood flow in large arteries is a well-known fact [2]. However, this phenomenon is not taken into account when studying hemodynamics in diseased vessels; therefore, practical recommendations for prevention of proliferation of inner surfaces in diseased vessels are not fully reliable.

The present paper describes experimental research into the structure of steady swirling flows behind axisymmetric sudden expansions in channels and in regions of channel branching (fig. 1) at the Reynolds number Re = 1500. The authors designed a dedicated experimental setup for this purpose. The research included flow visualization and SIV measurement of instantaneous vector fields of velocity. Swirling flow was generated by a blade swirler mounted at the distance of 5d upstream of the expansion (branching). The integral swirl ratio upstream of these regions was Y = 0.145. Fully developed laminar velocity profile (Poiseuille law) was provided upstream of the swirler. Evolution of profiles of flow statistics was analyzed, including the distributions of circumferential velocity component and the swirl ratio of flow in the smooth channel before the expansion (branching). It was found that profiles of streamwise velocity in the channel behind the sudden expansion are distorted under the impact of swirling, and the streamwise size of the separation region decreases by almost three times. The swirling curve plotted along the channel has two local peaks. Large-scale vortices start forming in the mixing layer at the boundary of recirculation region closer to the reattachment zone. These vortices promote fluctuations of velocity components. The

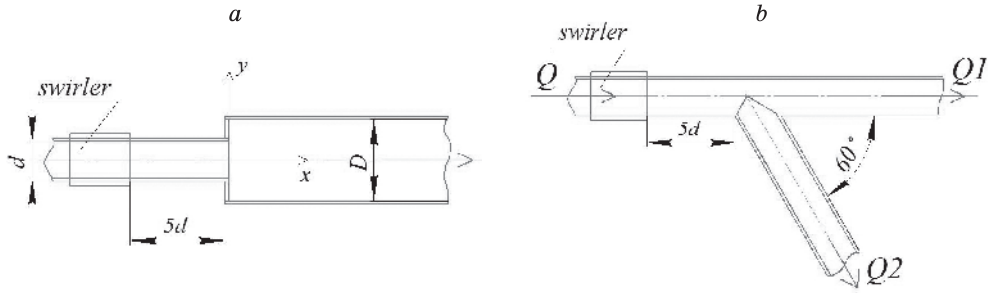

Fig. 1. Test sections: *a* – axisymmetric sudden expansion of the channel; *b* – region of channel branching

maximum of these fluctuations is observed in the vicinity of reattachment zone, but no signs of laminar-turbulent transition are documented in this zone. Downstream of the reattachment zone, the high-frequency range of the spectrum of velocity fluctuation becomes fuller, and inertial range emerges in the spectra indicating the onset of turbulence in the flow.

Without swirling, the flow in the branching region features steady separation regions in both branches (Q1 and Q2) (fig. 1,b). Large-scale vortices are formed in the mixing layer at the boundaries of these regions. These vortices are regularly swept downstream. Swirling eliminates the separation region in Q1 branch. However, the zone of velocity distortion is formed immediately behind the branching near its symmetry axis. The size of this velocity distortion zone is (1.6 – 2.4)*d* in streamwise and 0.3*d* in transverse direction. Downstream of this zone, large-scale vortices are formed. Oscillograms of the transverse velocity component near this zone indicate the precession of the vortex formed in this branch. The precession frequency is approximately 37 Hz. Despite relatively high intensity of streamwise velocity fluctuation, no signs of laminar-turbulent transition are observed in Q1 branch. The effect of swirling on the flow structure in Q2 branch is significantly weaker. The separation region persists. Its size changes, as well as the shape of velocity profiles in the high-speed jet above the separation region. Similar to the case with no swirling, the inertial interval is observed in the spectrum of velocity fluctuation in Q2 branch. Together with high level of velocity fluctuation, this can be indicative of the onset of turbulence in the flow.

The study was financially supported by the Russian Science Foundation, project no. 22-10-00507.

REFERENCES

1. **Alekseenko S.V., Kuibin P.A., Okulov V.L.** Introduction to the theory of concentrated vortices. Moscow; Izhevsk: Institute of Computer Studies. 2005. 503 p.
2. **Agafonov A.V., Talygin E.A., Bockeria L.A., Gorodkov A.Y.** The hydrodynamics of a swirling blood flow in the left heart and aorta //Acta Naturae, 2021. Vol. 13 (4). P. 4–16.

DOI 10.53954/9785604990148_138

ON USING THE SPECTRAL PORTRAITS IN THE NUMERICAL STUDY OF BOUNDARY-LAYER STABILITY

Yu.M. Nechepurenko, A.V. Boiko, K.V. Demyanko, G.V. Zasko

Marchuk Institute of Numerical Mathematics RAS,
119333, Moscow, Russia

The hydrodynamic stability theory deals with external disturbances of a main flow, whose stability is of interest. It studies their propagation in space or evolution in time. Stability characteristics, such as the growth rate, and the phase and group velocities, allow one to describe the propagation of the most unstable disturbances. The computation of the stability characteristics is usually reduced to that of the eigenvalues of parameter-dependent matrices. Then, the leading eigenvalues are selected and the corresponding eigenvectors are computed [1, 2]. Along with the external main-flow disturbances propagating against the background of the main flow, there might exist internal main-flow perturbations, which should be treated as perturbations of the parameters of the stability problem. Such a main-flow perturbation leads to a perturbation of entries of the matrix, whose eigenvalues are computed within the stability analysis. The present report deals with such internal perturbations. In what follows, we assume that the relative perturbations of the main-flow velocity components are independent random variables taking values in the interval $[-\delta,\delta]$ where $0 < \delta < 1$ In the present report, we propose to estimate the eigenvalue sensitivity to the main-flow perturbations, using spectral portraits based on the structured pseudospectrum [4–6] instead of those based on the widely used unstructured pseudospectrum [3, 7–9]. As an example, it is considered the flow of a viscous incompressible fluid over a concave surface of small curva-ture with the parameters are favorable for either the Goertler vortices (G) or the Tollmien-Schlichting waves (TS). It is shown that a proper structuring the pseudospectra leads to much more accurate estimates.

Figure 1 compares the unstructured spectral portrait (subfigures (a) and (b)) with the structured spectral portrait (subfigures (c) and (d)) for configuration G. For each point of the considered part of the complex plane, these portraits show the value δ smaller than which this point cannot be an eigenvalue of a perturbed matrix. In addition, the eigenvalues of the unperturbed matrix (black dots) are compared with those of perturbed matrices (white dots) for 100 random main-flow perturbations at $\delta = 10^{-3}$ The leading eigenvalue, which corresponds to the Goertler instability, is marked with the black cross. Subfigures (a) and (c) show spectral portraits near the physically relevant leading eigenvalue; while subfigures (b) and (d) show spectral portraits in a broader region of the complex plane that includes two eigenvalues with the imaginary part approximately equal to –100. These eigenvalues are well-separated from the leading part of the spectrum and correspond to physically insignificant modes. The white lines for the unstructured spectral portrait correspond to $\ddot{a} = 10^{-8}$ The white lines for the structured spectral portrait correspond to $\delta = 10^{-4}$ These lines are geometrically close. Thus, the structured pseudospectrum leads to a significantly (by four orders of magnitude) more accurate estimate for the eigenvalue sensitivity to the main-flow perturbations. At the same time, the eigenvalues of perturbed matrices do not reach the white lines plotted on the structured pseudospectrum, despite they are computed at $\delta = 10^{-3}$ i.e., for

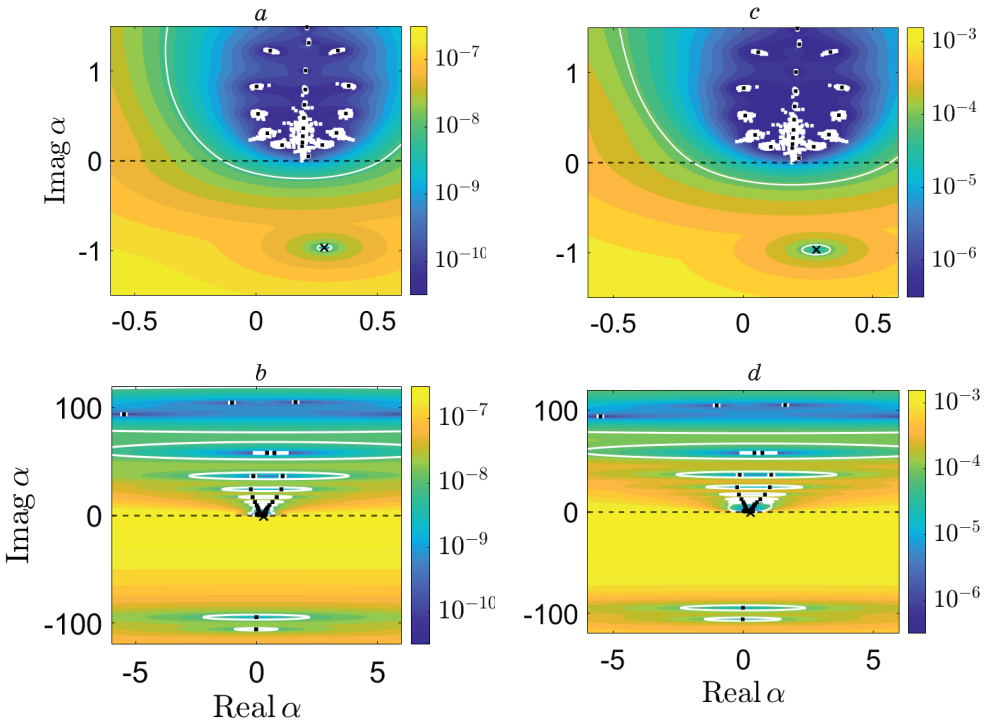

Fig. 1. Unstructured (a), (b) and structured (c), (d) spectral portraits for configuration G.

perturbations an order of magnitude larger. This suggests that the estimate based on the structured pseudospectrum is still an overestimate and able to be improved. The present report shows similar results for configuration TS.

The present research is supported by the Russian Scientific Foundation (grant No. 22-11-00025).

REFERENCES

1. **Boiko A.V., Dovgal A.V., Grek G.R., Kozlov V.V.** Physics of Transitional Shear Flows: instability and laminar-turbulent transition in incompressible near-wall shear layers. Berlin: Springer–Verlag. 2011. 272 p.
2. **Schmid P.J., Henningson D.S.** Stability and Transition in Shear Flows. New York: Springer. 2000. 558 p.
3. **Godunov S.K.** Modern aspects of linear algebra / TransL of Math. Monographs Amer. Math. Soc. V. 175, 1998.
4. **Hinrichsen D., Kelb B.** Spectral value sets: a graphical tool for robustness analysis // Systems Control Lett., 1993, V. 21, P. 127–136.
5. **Gallestay E., Hinrichsen D., Pritchard A.J.** Spectral value sets of closed linear operators // Proc. Roy. Soc. London Ser. A., 2000, V. 456, P. 1397–1418.
6. **Nechepurenko Yu.M.** The regularly structured pseudospectrum // Russ. J. Numer. Anal. Math. Model., 2004. V. 19. N. 3. P. 265–288.
7. **Trefethen L.N., Embree M.** Spectra and Pseudospectra: The Behavior of Non-normal Matrices and Operators. Princeton: Princeton University Press, 2005. 606 p.
8. **Trefethen L.N., Trefethen A.E., Reddy S.C., Driscoll T.A.** Hydrodynamic stability without eigenvalues // Science, 1993. V. 261. P. 578–584.
9. **Foster R.C.** Structure and energetics of optimal Ekman layer perturbations // J. Fluid Mech., 1997. V. 333. P. 97–123.

DOI 10.53954/9785604990148_140

VALIDATION OF A COMPUTATIONAL MODEL FOR SOLVING THE PROBLEM OF TURBULENT SUPERSONIC COMBUSITON OF HYDROGEN-AIR MIXTURE

A.M. Nikonov, N.A. Kharchenko

TSAGI
104181, Zhukovsky, Russia

Nowadays a topical task is the development of computational models and software tools for numerical modeling of supersonic turbulent combustion processes, which could more adequately describe complex processes, since conducting experiments in this area is associated with many economic and technical difficulties, as well as rather low informativeness of the results obtained. It is also worth noting the importance of the correct description of physicochemical processes, which makes it necessary to analyze the use of correct models of chemical kinetics.

This paper presents the developed computational model [1, 2], which is intended for modeling the processes of turbulent supersonic combustion of hydrogen-air mixture. The model is based on the numerical solution of the three-dimensional system of Navier-Stokes equations by the finite volume method [3, 4], which describes the motion of a viscous, compressible, chemically reacting gas. The system of gas dynamics equations is augmented with a two-parameter differential RANS model of k-ω SST turbulence [5]. The approximation of the system of equations is based on the modified AUSM+ method [6, 7], which is a method of splitting the flows into convective and acoustic components depending on the Mach number. This approach is an alternative to the methods based on the idea of calculating the fluxes through finite volume faces from the solution of the arbitrary gap decay problem proposed by S.K. Godunov [8]. A two-step method is used to solve the system of chemical kinetics equations, in which a semi-implicit scheme for approximating the source terms is applied at

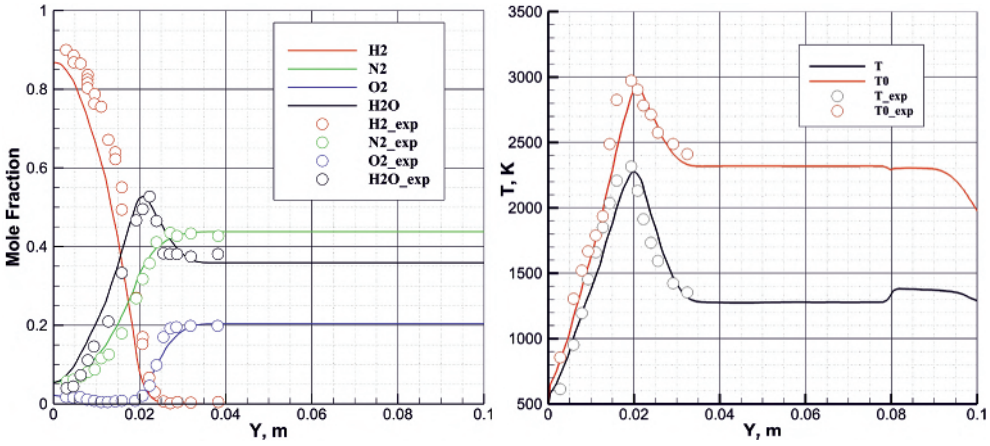

Fig. 1. Distributions of mole fractions of gas mixture components and temperature in the outlet section of the channel

a separate step. Numerical integration of the systems of equations of gas dynamics and chemical kinetics was carried out until a stationary solution was established.

Due to the high computational complexity of solved physical problems, special requirements are imposed on numerical modeling tools and their software implementation. Namely, it is necessary to apply parallel computing technologies to tasks of this type. The hybrid method OpenMP + MPI [9] is realized in this work.

The paper presents the results of numerical modeling of the processes of turbulent combustion of a hydrogen jet in a supersonic flow of moist air. A good agreement of the numerical simulation results with the experimentally obtained distributions (see Fig. 1) of the mole fractions of the gas mixture components, static temperature profiles, and stagnation temperature in the outlet section of a flat channel is shown [10]. In addition, the paper compares the results of numerical simulations with different kinetic mechanisms of hydrogen combustion, and evaluates the change in the location of the ignition point and the distributions of flow parameters in the channel.

REFERENCES

1. **Kharchenko N.A., Nikonov A.M.** Determination of the distributed aerodynamic characteristics of an axisymmetric body of the SOCBT configuration at turbulent flow with a transonic flow // Mathematical modeling and numerical methods. 2023. No. 2. P. 100–128.
2. **Kharchenko N.A., Nosenko N.A.** Numerical modeling of streamline by a high-speed flow of a cylindrical-conical body and a double cone // Mathematical modeling and numerical methods. 2022. No. 3. P. 33–46.
3. **Nikonov A.M., Gerber M.Yu., Nosenko N.A. Kharchenko N.A.** Numerical solution of the problem of turbulent combustion of hydrogen jet in supersonic flow of hot moist air // XXXIV Scientific and Technical Conference on Aerodynamics. TSAGI. 2024. P. 78–79.
4. **Bosniakov S.M., Berezko M.E., Deryugin Y.N., Duben A.P., Zhuchkov R.N., Kozelkov A.S., Kozubskaya T.K., Matyash S.V., Mikhailov S.V., Okulov M.K., Talyzin V.A., Utkina A.A., Kharchenko N.A., Shevyakov V.I.** Accuracy estimation of modern codes by comparing computational and experimental data on the example of the problem of tandem wedge flow of rarefaction and compression by supersonic flow of viscous turbulent gas // Mathematical Modeling. 2023. V. 35. No. 10. P. 69–112.
5. **Menter F.R., Kuntz M., Langtry R.** Ten Years of Industrial Experience with the SST Turbulence Model // Turbulence, Heat and Mass Transfer 4. 2003. P. 625–632.
6. **Liou M.-S.** A sequal to AUSM: AUSM+ // J. Comput. Phys. Vol. 129, 1996 p. 364–382
7. **Chen SS, Cai FJ, Xue HC, Wang N., Yan C.** An improved AUSM-family scheme with robustness and accuracy for all Mach number flows // Appl. Math. Model. Vol. 77, 2020. p. 1065–1081.
8. **Godunov S.K.** A difference method for numerical calculation of discontinuous solutions of hydrodynamic equations // Matem. sb. 1959. V. 47. No. 3. P. 271–306.
9. **Bessonov O.A., Kharchenko N.A.** Software platform for supercomputer modeling of aerothermodynamics problems // Software Engineering. 2021. V. 12. No. 6. P. 302–310.
10. **Burrows M.C., Kurkov A.P.** An Analytical and Experimental Study of Supersonic Combustion of Hydrogen in Vitiated Air Stream // AIAA J. 1973. Vol. 11. No. 9. P. 1217–1218.

DOI 10.53954/9785604990148_142

INFLUENCE OF INPUT AREA ON THE COUETTE FLOW IN A SEMICIRCULAR CHANNEL

A.Yu. Pak, V.A. Lebiga, D.S. Mironov, A.A. Aleksandrov

Khristianovich Institute of Theoretical and Applied Mechanics SB RAS, Novosibirsk, pak@itam.nsc.ru

One of the simplest classical flows is the flow between coaxial cylinders, first proposed and used by Couette to determine the viscosity of a liquid. Later, the flow in the gap between flat plates was called the Couette flow, in which the relative velocity of the plates plays a decisive role. This flow has been well studied both theoretically and experimentally for different conditions, such as laminar, turbulent flow conditions, the influence of heat transfer, etc. [1–2]. Due to its importance for practice, much attention is paid to the study of the Couette flow in the annular channel, and there are numerous results obtained by theoretical, computational methods that require verification.

Unlike a flat flow, the nature of the Couette flow in an annular channel depends not only on the relative velocity of the walls and the viscosity of the process fluid, but also on the action of centrifugal forces leading to the appearance of Taylor-Görtler vortices.

Application of experimental methods to study such annular flows is very limited even for the simplest cases. These are optical methods requiring transparent walls and visualization of surface current lines on the walls, which provide some, mostly qualitative information about the flow structure, mainly for liquids, in addition, it is practically impossible to study non-stationary flow characteristics. The introduction of any sensors into the flow leads to the creation of disturbances by them, occupying the entire volume in the channel and distorting the entire flow.

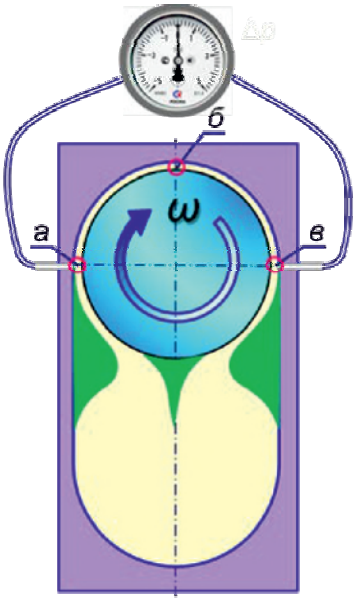

Fig. 1. Test bench schematic

In this paper, the flow is considered in a channel formed by a concentric fixed wall in the form of a semicylinder and a rotating cylinder with a diameter of $D = 2R = 200$ mm and a height of $H = 100$ mm (Fig. 1). The gap between the cylinder surfaces was $\delta = 4$ mm.

The maximum rotation speed of the cylinder could reach 60 rpm, and the linear velocity of the cylinder surface could reach ~40 m/s. The internal volume of the stand was sealed, which made it possible to change the pressure during the Couette flow. A hot-wire probe with a wire of 5–10 microns could be inserted into the flow and moved across the channel in several places at the beginning, end and middle of the channel using a coordinate device created on the basis of a measuring micrometer. The degree of difference between the flow in a fully annular channel and the flow in a semicircular channel and the effect of the initial section of the semicircular channel due to the possible pressure difference between the inlet and outlet of the semicircular channel and the boundary layer on the rotating cylinder were studied in this work.

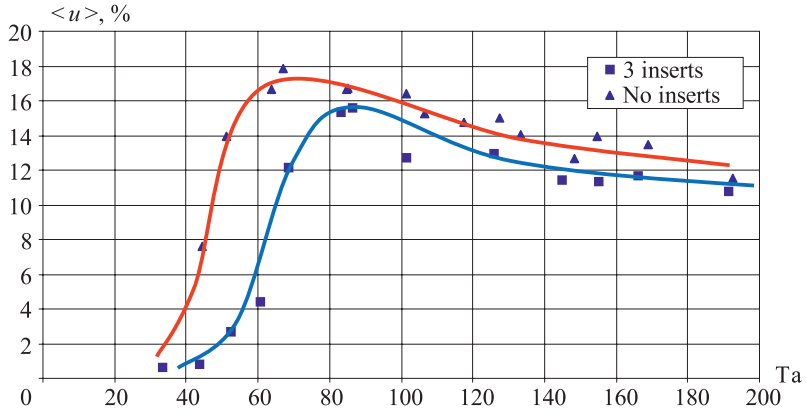

Fig. 2. The dependence of the relative velocity pulsations on the Taylor number for the case of a cylinder without inserts and in the presence of 3 inserts.

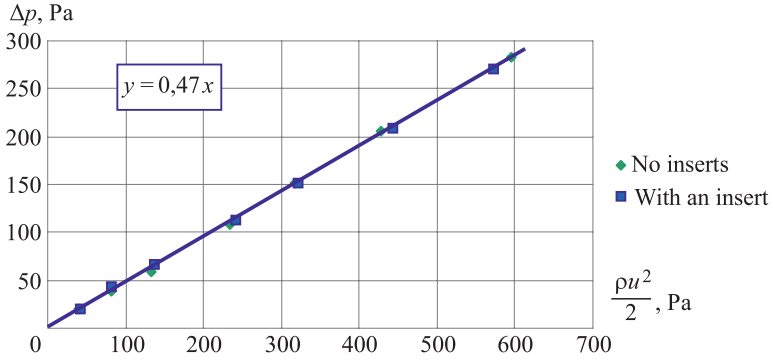

Fig. 3. Pressure difference at the inlet and outlet of the Couette flow in a semicircular channel.

In order to determine the influence of the inlet section on the Couette flow in the semi-annular channel, the inlet and outlet parts were changed using two special symmetrical inserts (Fig. 1), whereas, to remove the influence of the boundary layer on the wall of the inner cylinder, a central additional insert was added.

The pressure drop between points *a* and *b* was measured (Fig. 1), as well as the profiles of the average and fluctuation velocity components at point *b*. The dependences of the relative velocity fluctuations on the Taylor number Ta for various combinations of inserts and without them were obtained (Fig. 2). The pressure difference at the inlet and outlet was measured without inserts and with inserts for different revolutions of the cylinder (see Fig. 3).

The installation of inserts does not affect the pressure drop between the beginning and the end of the semi-annular channel, but affects the development of disturbances in the channel.

REFERENCES

1. Schlichting G. // Theory of the boundary layer. Moscow: Nauka, 1974. 712p.
2. Coles D. // Transition in circular Couette flow. J. Fluid Mech. 1965. Vol. 21. P. 385–425.

DOI 10.53954/9785604990148_144

INVESTIGATION OF THE EFFECT OF CELL HEIGHTS AND PERFORATION DIAMETERS ON THE ACOUSTIC CHARACTERISTICS OF SOUND-ABSORBING STRUCTURES

P.V. Pisarev, K.A. Akhunzyanova

Perm National Research Polytechnic University
614990, Perm, Russia

Modern aircraft engines use two- and three-layer sound-absorbing structures, which allow noise reduction in a wide frequency range due to the operation of resonators (cells) tuned to different frequencies [1–3]. However, multilayer sound-absorbing structures have a number of disadvantages, particularly not great acoustic characteristics, high density, high workload and high manufacturing cost, large weight and dimensions.

To create a more efficient design of the sound-absorbing structures, it is necessary to study the properties of a separate resonant cell. However, the efficiency of the resonant cell is limited by a narrow frequency band, which is in the range between two resonant frequencies [1, 4]. In this regard, the development of resonant cell systems capable of effectively absorbing sound in a wide range of operating frequencies is relevant.

In this work, the results of experimental studies of the influence of resonator heights and perforation diameters on the acoustic characteristics of the sound-absorbing structures are presented. Experimental studies were carried out on an interferometer with a normal sound wave attenuation at a sound pressure level of 130 dB.

Four types of sound-absorbing structures with prismatic resonators are considered as objects of this study. The first sample is a standard uniform structure (Fig. 1, a), the second is a multi–height structure (Fig. 1, b), the third and fourth are uniform structures with different perforation diameters. The perforations diameter varies from 1.4 mm to 2.6 mm, for the third sample the diameter of the central perforation is 1.4 mm, while for the fourth sample the diameter of the central perforation is 2.6 mm (Fig. 1, c, d).

Based on the results of the experimental studies, the dependence of the sound absorption coefficient on frequency was obtained (Fig. 2).

The analysis of the results showed that the sound-absorbing structure with a uniform honeycomb filler (sample 1) is less effective compared to the presented modifications (samples 2–4).

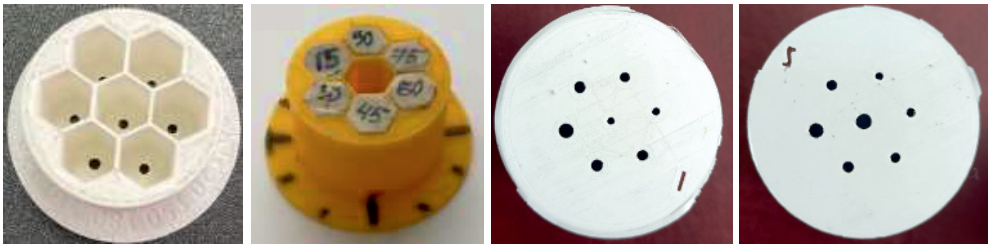

Fig. 1. General view of the studied samples

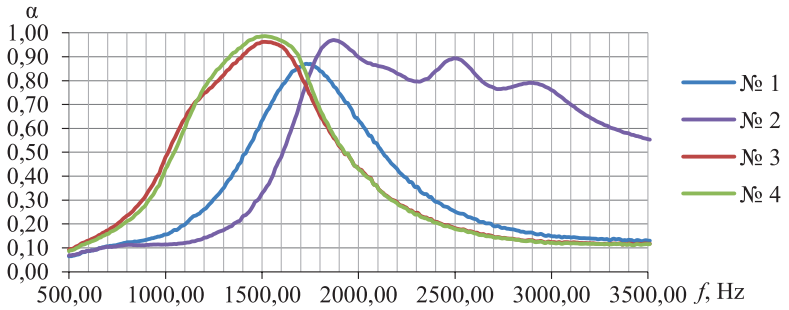

Fig. 2. Dependence of the sound absorption coefficient on the frequency (130 dB)

Several peaks were observed for sample 2. The peak with the highest sound absorption coefficient has a value of 0.97 at a resonant frequency of 1880 Hz. The operating frequency range of the resonant cells was 1696÷3100 Hz with a sound absorption coefficient of 0.7. Analysis of the dependence of the sound absorption coefficient on the frequency of sample 1 revealed that the sound absorption coefficient of 0.87 at a resonant frequency of 1736 Hz. The operating frequency range of the resonant cells was 1544÷1944 Hz with a sound absorption coefficient of 0.7. An analysis of the results obtained for samples 3 and 4 showed that the acoustic efficiency was almost identical. Thus, for sample 3, the sound absorption coefficient was 0.96 at a resonant frequency of 1504 Hz, for sample No. 4 it was 0.99 at a frequency of 1520 Hz.

Based on the results of the performed research, a broadband sound-absorbing structure was developed, consisting of cells (Helmholtz resonators) of various volumes and heights. To increase the acoustic efficiency of the structure, it is proposed to use an irregular in area perforation of sound-absorbing structure. It has been experimentally confirmed that the developed design has the highest sound absorption coefficient and provides a wide operating frequency band compared to a uniform structure. When developing highly efficient aircraft noise reduction systems, it is recommended to combine different volumes of resonant cells and perforation diameters to ensure maximum acoustic efficiency and broad frequency range coverage of these structures.

The research was conducted at Perm National Research Polytechnic University with the support of a state assignment (project No. FSNM-2023-0006).

REFERENCES

1. **Zaharov A.G., Anoshkin A.N., Pan'kov A.A., Pisarev P.V.** Akusticheskie rezonansnye harakteristiki dvuh i trekhslojnyh sotovyh zvukopogloshchayushchih panelej // Vestnik PNIPU. Aerokosmicheskaya tekhnika. – 2016. – No. 46. – S. 144–159.
2. **Sobolev A.F., Ushakov V.G., Filippova R.D.** Homogeneous sound-absorbing structures for aircraft engine ducts // Acoustical Physics. – 2009. – Vol. 55, No. 6. – P. 805–815. – DOI 10.1134/S1063771009060153.
3. **Baklanov V.S., Postnov S.S., Postnova E.A.** Raschyot rezonansnyh zvukopogloshchayushchih konstrukcij' dlya sovremennyh aviacionnyh dvigatelej // Matematicheskoe modelirovanie. 2007. Vol. 19, No. 8. S. 22–31.
4. **Pisarev P.V., Pankov A.A., Anoshkin A.N., Akhunzyanova K.A.** Modeling Acoustic Processes of the Interaction of Cells of Sound-Absorbing Structures of Aircraft Engines / // Acoustical Physics, 2023, Vol. 69, No. 6, pp. 853–862. DOI: 10.1134/S1063771023600912.

DOI 10.53954/9785604990148_146

TRANSIENT HEAT FLUX MEASUREMENT USING SENSORS ON ANISOTROPIC THERMOELEMENTS AND METAL HETEROGENEOUS STRUCTURES IN SHOCK TUNNEL EXPERIMENTS

P.A. Popov[1], A.V. Pavlov[2], S.A. Poniaev[1], N.A. Monakhov[1], V.A. Sakharov[1], T.A. Lapushkina[1, 2], R.O. Kurakin[1], A.B. Podlaskin[1]

[1] Ioffe Institute,
194021, Saint Petersburg, Russia

[2] Peter the Great St. Petersburg Polytechnic University,
195251, Saint Petersburg, Russia

Heat flux measurement is one of the basic types of diagnostics in a gas-dynamic experiment. Sufficiently complete modeling of the conditions of real high-speed flight is possible only on impulse high-enthalpy facilities [1]. Short working time, not exceeding $10\,ms$ intense heat fluxes $\sim 1\,MW/m^2$ intense erosive action of a gas flow containing fragments of diaphragms, impose stringent requirements on measuring instruments in terms of their speed, thermal and mechanical strength. This leads to the need to develop new materials and designs of sensors that correspond to the modern level of gas-dynamic experiment.

Ioffe Institute, together with the St. Petersburg Polytechnic University, is developing and implementing new approaches for measuring unsteady heat fluxes in shock tube experiments. Currently, thermoelectric sensors based on bismuth anisotropic thermoelements (Fig. 1a) and copper–nickel heterogeneous metal structures (Fig. 1b) are successfully used [2].

The principle of operation is based on the generation of a thermoelectric field in a sensitive element that has thermoEMF anisotropy when a temperature gradient appears in it [3]. Based on a detailed analysis of thermal and thermoelectric processes, the method for heat flux calculating from the electrical signal of sensors has been developed, tested and successfully used in experimental practice [4]. This also made it possible to obtain estimates of measurement uncertainty for sensors with different length-to-thickness ratios at different characteristic times of thermal loads. The calibration technique has been developed using a reflected shock wave to determine the volt-watt coefficient [5] and check for the presence of internal defects in anisotropic thermoelements made of a bismuth monocrystal. The features

Fig. 1. Structure of a heat flux sensor based on anisotropic thermoelements (a) and on heterogeneous structure of a copper-nickel (b).

of measurements in inert gases and air at heat fluxes up to $10 MW / m^2$ ave been studied. The accumulated experience shows that even with the same size of anisotropic thermoelements, the volt-watt coefficient of sensors can differ noticeably, which is caused by manufacturing features. For sensors on metal heterostructures, it practically coincides and does not change over time even with slight damage to the working surface during experiments.

Due to the high sensitivity $\sim 1 mV / W$ nd short response time to thermal influence $\sim 0.1 \mu s$ sensors based on anisotropic thermoelements make it possible to measure small heat fluxes $\sim 100 kW / m^2$ ith a duration of $1 \mu s$ Due to the fragility of bismuth single crystal, they should be installed in areas where the likelihood of mechanical damage from collision with solid particles is minimal. Sensors based on metal heterostructures have the greatest mechanical strength. The existing technology for mounting the sensitive element in the model body allows measurements to be taken near the critical point at a stagnation temperature of up to $5000 K$ However, due to the low sensitivity $\approx 10 \mu V / W$ it is necessary to use intermediate low-noise amplifiers in the recording system.

Using sensors based on anisotropic bismuth thermoelements and metal heterogeneous structures, measurements were taken on the surface of models of various shapes. Comparison of the obtained results with known theoretical dependencies and numerical simulation data showed the applicability of the sensors, the reliability of their calibration and signal processing techniques. The results obtained allow us to assert that the presented sensors with complementary characteristics make it possible to carry out measurements at any points of the models in a wide range of heat flux densities from $100 kW / m^2$ o $10 MW / m^2$ nd various characteristic times from $1 \mu s$ o $10 ms$ 6].

REFERENCES

1. **Sapozhnikov S.Z., Mityakov V.Yu., Mityakov A.V.** Heatmetry: The Science and Practice of Heat Flux Measurement. 2020. 209 p.
2. **Rowe D.M.** Thermoelectrics Handbook: Macro to Nano. 2006. 954 p.
3. **Popov P.A., Bobashev S.V., Reznikov B.I., Sakharov V.A.** A Method of Nonstationary Heat Flux Calculation Using the Signal of a Sensor Based on Anisotropic Bismuth Single-Crystal Thermoelements // Technical Physics Letters. 2018. Vol. 44, No. 4. P. 316–319.
4. **Popov P.A., Monakhov N.A., Lapushkina T.A., Poniaev S.A., Kurakin R.O.** Calibration of heat flux sensors based on anisotropic thermoelements and heterogeneous metal structures using a reflected shock wave // Technical Physics Letters. 2022. Vol. 48, No. 10. P. 46–48.
5. **Popov P.A., Sakharov V.A., Lapushkina T.A., Poniaev S.A., Monakhov N.A.** Heat-Flux Measurement by Sensors Based on Anisotropic Thermoelements in a Gas-Dynamics Experiment Shock Tubes // Fluid Dynamics. 2023. Vol. 58, No. 4. P. 779–786.

DOI 10.53954/9785604990148_148

EXPERIMENTAL INVESTIGATION BY THE SHADOW METHOD OF WATER DROPLETS BREAKUP IN AN ADJUSTABLE SUPERSONIC NOZZLE

S.S. Popovich, A.G. Zditovets, Y.A. Vinogradov

Lomonosov MSU Institute of Mechanics
119192, Moscow, Russia

It is known that when the initially compressed gas expands in the channel, its static temperature decreases due to the transition of the internal energy of the gas into the kinetic energy of the flow. The question arises: is it possible to create conditions in the flow in which the temperature of the streamlined wall would be close to the minimum temperature in the system – the static temperature of the flow. The solution of this problem is possible through the use of the properties of gas droplet flows with a low mass concentration (up to 1%) of the liquid phase. In this case, the liquid phase practically does not affect the properties of the carrier flow, while the droplets can be cooled to the thermodynamic temperature of the flow [1–3]. By focusing of cooled droplets on the wall, it is possible to achieve a decrease in surface temperature.

As a result of previously conducted experimental studies [4–6], a system for preparing and injecting liquid into a supersonic flow through a single and multi-nozzle system in the pre-chamber of the wind tunnel was created and tested. A series of thermal imaging measurements of the cooling rate of a plate streamlined by supersonic air and air-droplet flows has been carried out. The effects of the formation of ice growths on the streamlined wall with a decrease in temperature by 10–13 C compared with a single-phase flow were found. The method of aerodynamic focusing of particles along the front of the shock wave has been tested when installing a wedge shock wave generator in front of the model. The purpose of this work is to study the dynamics of droplet breakup and droplet size distribution along the nozzle length.

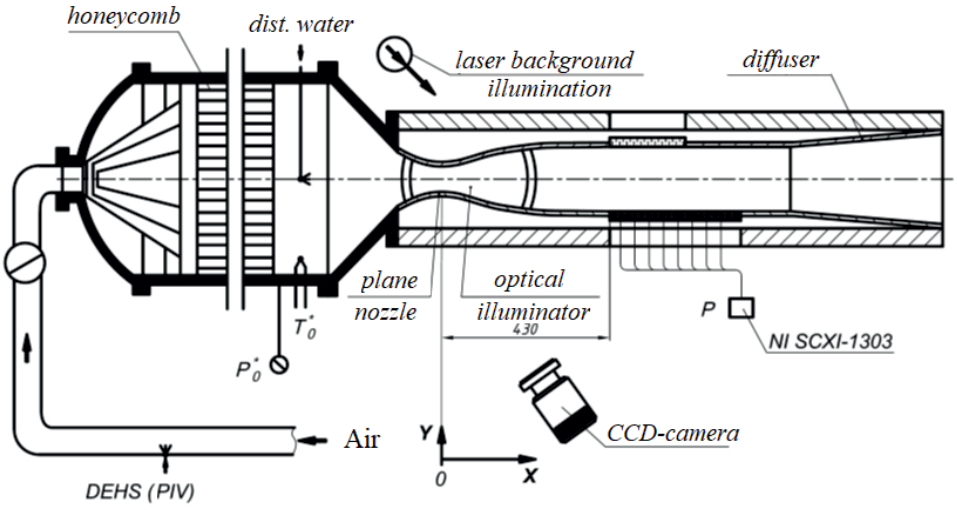

Fig. 1. The scheme of conducting an experimental study on supersonic wind tunnel

Experimental studies were carried out on the AR-2 supersonic wind tunnel (Fig. 1). The working channel of the installation has a rectangular cross-section with dimensions of 70×98 mm. The nozzle is formed by two flat flexible plates, which provide the possibility of adjusting the Mach number on the nozzle section by preloading the critical section using an electric drive. Optical glasses are mounted on the side walls of the working part of the channel to visualize the flow pattern. When studying the size distribution of droplets in a supersonic flow, the SSP (shadow photography) method was used [7–9], which includes: a flow illumination system based on a Beamtech double pulsed Nd:YAG laser with a wavelength of 532 nm, a digital CCD camera with a frequency of up to 15 Hz and a Polis SP-10.0 synchronizing processor. A series of measurements of the distribution of water droplets in an atmosphere was carried out preliminarily.

A series of snapshots of the instantaneous state of droplets breakup process in the critical section area and in the expanding part of the nozzle was obtained. The SSP method obtained a series of lognormal droplet size distributions for a number of values of the current Mach number at the nozzle exit section.

The work is carried out within the framework of the state budget theme AAAA16-116021110200-5 of Lomonosov Moscow State University Institute of Mechanics.

REFERENCES

1. **Leont'ev A.I., Osiptsov A.N., Rybdylova O.D.** The boundary layer on a flat plate in a supersonic-gas-droplet flow: Influence of evaporating droplets on the temperature of the adiabatic wall // High Temperature. 2015. Vol. 53, No. 6. P. 866–873.
2. **Leontiev A.I., Lushchik V.G., Makarova M.S., Popovich S.S.** The temperature recovery factor in a compressible turbulent boundary layer // High Temperature. 2022. Vol. 60, No. 3. P. 409–431.
3. **Zditovets A.G., Kiselev N.A., Popovich S.S., Vinogradov U.A.** Adiabatic wall temperature in the supersonic flow of moist air with spontaneous condensation // Experimental Thermal and Fluid Science. 2024. V. 150, N. 111057.
4. **Popovich S.S., Zditovets A.G., Vinogradov Y.A., Kiselev N.A., Medvetskaya N.V.** Measurement of the adiabatic wall temperature of a flat plate in a supersonic air-droplet flow // Fluid Dynamics. 2020. Vol. 55, No. 5. P. 701–707.
5. **Popovich S.S., Zditovets A.G., Kiselev N.A., Vinogradov Y.A.** Experimental study of the shock wave influence on adiabatic wall temperature in a supersonic air-droplet flow // Journal of Physics: Conference Series. 2020. doi.org/10.1088/1742-6596/1683/2/022064.
6. **Popovich S.S., Leontiev A.I., Zditovets A.G., Kiselev N.A., Vinogradov Y.A.** Experimental study of the flow around the plate by a supersonic air flow with an admixture of finely dispersed water droplets // Material of Russian national heat transfer conference RNKT-8. MPEI. 2022. V. 1. P. 428–431.
7. **Popovich S.S., Vinogradov Y.A. Zditovets A.G.** Experimental study of the thermogasodynamics of the flow of an airborne droplet in a flat supersonic nozzle // XIII Russian Congress on Theoretical and Applied Mechanics: abstracts. SPbPU, 2023. P. 1051–1052.
8. **Bilsky A.V., Gobyzov O.A., Markovich D.M.** Evolution and recent trends of particle image velocimetry for an aerodynamic experiment (review) // Thermophysics and Aeromechanics. 2020. Vol. 27, No. 1. doi.org/10.1134/S0869864320010011.
9. **Znamenskaya I.A.** Methods of panoramic visualization and digital analysis of thermophysical fields. Review // Scientific Visualization. 2023. Vol. 13, No. 3. P. 125–158. doi.org/ 10.26583/sv.13.3.13.

DOI 10.53954/9785604990148_150

ASPECTS OF HEAT PROPAGATION INDUCED BY HEATING OF A FREE LIQUID SURFACE WITH IR LASER

Yu.K. Rudenko, A.V. Pushtaev, Yu.Yu. Plaksina, N.A. Vinnichenko, A.V. Uvarov

Lomonosov Moscow State University,
Faculty of Physics, 119991, Moscow, Russia

Of special interest is the laser IR-heating of the liquid surface in terms of testing the composition of the surface layer and investigation of its properties.

It is important to set suitable boundary conditions on the liquid surface in the simulations of heat transfer tasks including the liquid-gas interface. Temperature and velocity fields, relief surface are depended on these boundary conditions. Even with small amounts of contaminants in liquids with high surface tension coefficient (distilled water, glycerol) the classical slip boundary conditions on the surface are not correct [1]. In these liquids there is a «weak» film on the surface which is not prevent evaporation and tangential stress but the thermocapillary convection is blocked by it. At the same time another group of liquids can be distinguished (ethanol, isopropanol, silicone oil, deionized water) in which thermocapillary convection takes place. The disruption of film is possible due to the strong heating. In this case more complicated boundary conditions should be considered. Aside from the thermocapillary convection the concentration convection [2] takes place in solutions and it can stand in opposition with thermocapillary mechanism.

Different boundary conditions on the surface lead up to different temperature and velocity distributions both near the surface and in the volume of liquid and affect the surface relief. In the absence of the film the Marangoni convection plays a main role while in its presence the pressure redistribution on the surface and the horizontal Rayleigh convection are the main mechanisms. The features of the resultant boundary layer (the propagation velocity, characteristic thickness) can be described in universal form by similarity solutions. In work [3] similarity solutions were proposed for the 2D task with linear heating source. They enable to estimate the characteristics of the stationary boundary layer for the liquid with the presence of the surface film. In this work the similarity coordinates were obtained for the case of non-stationary cylindrical task of the heat marker propagation. These coordinates differ fundamentally for the liquids with two different boundary conditions. They allow to obtain the universal dependences and investigate the most general properties of the heat boundary layer.

In the work the features of the heat marker propagation from the CO_2 laser with the wavelength 10.6 mcm and low power (0.3 W) are demonstrated on the surfaces of the liquids with two different boundary conditions: in the presence of the film (water, glycerol) and in its absence (ethanol, silicone oil with various viscosity). IR-fields are experimentally measured by the IR-camera. To investigate surface relief the optical method Moon-Glade BOS [4] was used (surface relief allow to obtain the pressure field). Simulation with two boundary conditions was carried out: no-slip boundary condition and the condition considering thermocapillary convection. Experimental data and simulation are in good agreement.

The figure 1 shows the comparison of experimental and numerical radial profiles of IR-camera digital levels from ethanol and water. In the presence of the surface film the heat propagation rate is one order less than in the case of thermocapillary convection.

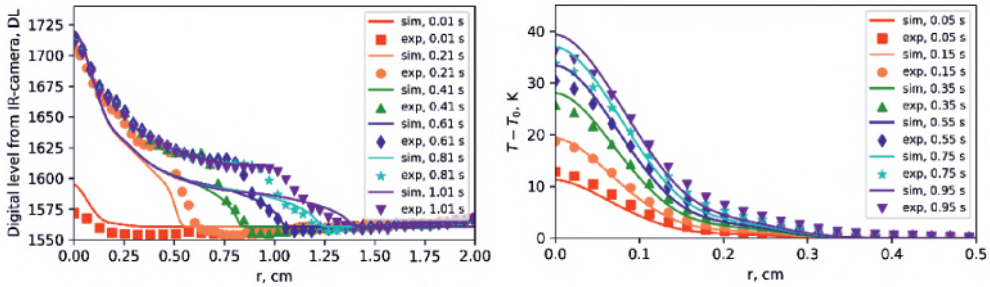

Fig. 1. The comparison of radial profiles of the digital levels from IR-camera in ethanol (to the left) and temperature fields in water (to the right) obtained experimentally and numerically

From the similarity solution the following expressions for the heat propagation rate can be obtained: for the thermocapillary convection: $r = \sqrt{\tau_m \chi t}$, n the presence of the surface film: $r = \tau_f^{3/4} \left(\frac{\rho g \beta q \chi^2}{\eta \lambda} \right)^{1/4} t^{3/4}$. he values of the constants were estimated from the simulation and were equaled: $\tau_m = 15000, \tau_f = 0.6$. t was shown that thermocapillary flow are leading to the fast expansion of the heat spot. In the presence of the «weak» film the heat propagation rate is one order less and the maximum temperature on the surface is significantly higher. Free surface deformation measured by Moon-Glade BOS also strongly depends on the presence of the surface film. Obtained similarity solutions allow estimate the propagation rate of the heat spot.

This work was partially supported by Russian Science Foundation (grant 23-19-00591). Yu.K. Rudenko also acknowledges the Foundation for the Advancement of Theoretical Physics and Mathematics «Basis» for personal financial support (grant 22-2-2-5-1).

REFERENCES

1. **Vinnichenko N.A., Pushtaev A.V., Plaksina Yu.Yu., Rudenko Yu.K., Uvarov A.V.** Horizontal convection driven by nonuniform radiative heating in liquids with different surface behavior // Int. J. Heat Mass Transfer. 2018. Vol. 126. P. 400–410.
2. **Shmyrov A., Mizev A., Demin V., Petukhov, Bratsun D**. On the extent of surface stagnation produced jointly by insoluble surfactant and thermocapillary flow // Adv. Colloid Interface Sci. 2018. Vol. 255. P. 10–17.
3. **Rudenko Yu.K., Vinnichenko N.A., Plaksina Yu.Yu., Pushtaev A.V., Uvarov A.V.** Horizontal convective flow from a line heat source located at the liquid–gas interface in presence of surface film // J. Fluid Mech. 2022. Vol. 944. A35.
4. **Vinnichenko N.A., Pushtaev A.V., Plaksina Yu.Yu., Uvarov A.V.** Measurements of liquid surface relief with moon-glade background oriented schlieren technique // Exp. Therm. Fluid Sci. 2020. Vol. 114. 110051.

DOI 10.53954/9785604990148_152

WHAT IS THE SPIKES IN BYPASS-TRANSITION

D.S. Sboev, T.T. Nguyen

Moscow Institute of Physics and Technology
141701, Dolgoprudny, Russia

In several papers (e.g., [1, 2]) attention was paid to the phenomenon of large pulses, observed in a boundary layer at bypass transition. These pulses looks like rather narrow spikes of negative (positive) velocity fluctuations in the hot-wire signals obtained in upper (near-wall) part of boundary layer subjected to elevated free-stream turbulence. Some attempts were made to connect such spikes to the turbulent spot generation. Present communication reports some findings on spikes' parameters and their spectral content. In following the negative spikes will be referred to as the spikes-down and the positive ones as the spikes-up. To the purpose of present study the hot-wire data measured in zero pressure gradient flat plate boundary layer at several wind tunnels were used. As the results were qualitatively the same in all facilities, the data from the T-324 wind tunnel (ITAM SB RAS) will be presented in the graphs below. Free-stream velocity U_0 was 7.4 m/sec and the grid-generated free-stream turbulence was 1.15%. All data were obtained in streamwise positions with zero intermittency, long before the turbulent spots generation starts.

Examples of signals with spikes are shown in Fig. 1. To obtain the spikes' characteristics by condition averaging process the simple condition was used that implies finding of local extremum of signal above some threshold during specified time interval. The identified spikes were then ensemble averaged. The threshold level was chosen equal to the $3u_{rms}$ at the $X = 290$ mm and corresponding Y/δ_1. This threshold based on the previous analysis of disturbances spectral development in this experimental set-up. The conditionally averaged spikes-down are shown in Fig. 2. The average frequencies f_s of spikes detections were determined at different downstream positions. The increase of f_s was in accordance with growth of asymmetry of probability density functions with X. For $X = 560$ mm the $f_s = 2.48$ and 1.16 Hz

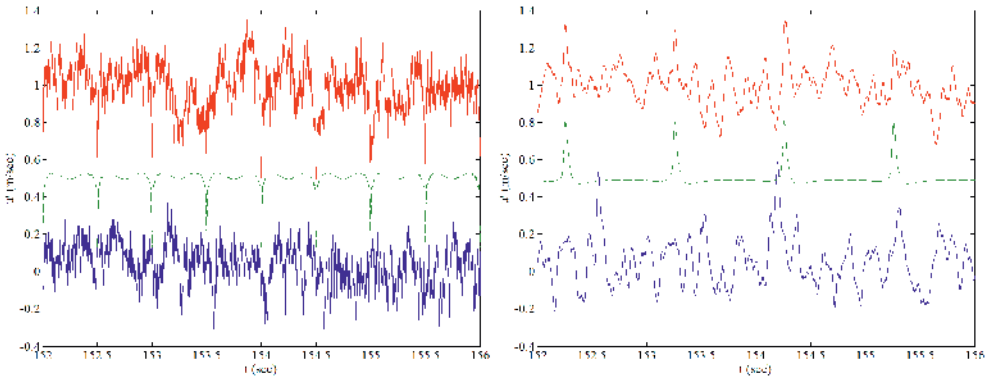

Fig. 1. The hot-wire traces at $X = 560$ mm with spikes-down (left, $Y/\delta_1 = 2.61$) and spikes-up (right, $Y/\delta_1 = 0.43$); the measured (bottom), reconstructed deterministic (middle) and composite (top) signals. Traces are shifted up by 0.5 m/sec.

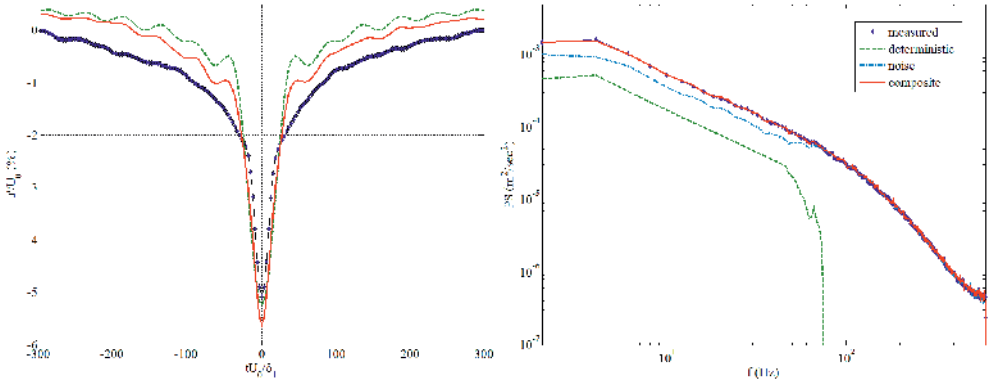

Fig. 2. The conditionally averaged spikes-down (left, $Y/\delta_1 = 2.61$) and power spectra of signals at $X = 560$ mm, measurements (symbols, blue), reconstructed deterministic (dashed, green), noise (dot-dashed, light-blue) and composite (solid, red) signals.

for spikes-down and spikes-up respectively. With τ taken as characteristic spike duration the values τf_s were about 0.06 for both spikes-down and spikes-up in this position.

In order to compare of registered spikes with well-known spikes in the K-regime of transition the various form parameters introduced in [3] were computed. It was concluded that spikes observed were totally different from the spikes in [3]. The first of all, their nondimensional duration was order of magnitude greater than in K-regime. By comparison the spikes parameters at various Y positions with the PIV data [4] it was concluded that spikes registered has strong resemblance with intensive boundary layer streaks.

To gain further understandings of spikes nature the bispectral analysis was used. All signals analysed reveals nonlinear interactions in low-frequency range up to 60 Hz. The bispectral data was used to reconstruct the spikes as model signals. To this end the signals were represented by a sum of deterministic part and random noise. The deterministic part was taken as sum of sine waves with frequencies up to 60 Hz. The dependencies of wave's amplitudes on frequency were taken from the measured power spectra, while their values were adjusted to obtain the same spike's amplitudes (Fig. 2). The phases of sinusoids were determined from the measured biphase distributions. The noise with prescribed spectrum was modelled by the filtering white gaussian noise to obtain the same composite spectrum as in a measured signal. The examples of this modelling are given in Fig. 1 and 2. The good qualitative agreement between the measured and reconstructed composite signals is obvious. It is important to note that events with only 6% fraction of total duration of signals are responsible for almost 25% of total disturbances' energy.

The main conclusion of this work is that the spikes-down and spikes-up observed in the hot-wire traces are represents the strong nonlinear boundary layer streaks and appears in signals long before transition starts.

REFERENCES

1. **Hernon D., Walsh E.J., McEligot D.M.** Experimental investigation into the routes to bypass transition and the shear-sheltering phenomenon // J. Fluid Mech. 2007. Vol. 591, P. 461–479.
2. **Sandborn V.A.** Origin of Surface-Shear-Stress Pulses in Turbulent Boundary Layers // AIAA J. 2008. Vol. 46, No. 10. P. 2646–2649.
3. **Kachanov Y.S., Ryzhov O.S., Smith F.T.** Formation of solitons in transitional boundary layers: theory and experiment // J. Fluid Mech. 1993. Vol. 251, P. 273–297.
4. **Balamurugan G., Mandal A.C.** Experiments on localized secondary instability in bypass boundary layer transition // J. Fluid Mech. 2017. Vol. 817, P. 217–263.

DOI 10.53954/9785604990148_154

INFLUENCE OF AN EXTERNAL ELECTRIC FIELD ON THE VELOCITY AND TEMPERATURE DISTRIBUTION IN A LAMINAR CONE FLAME. MEASUREMENTS BY PIV/PLIF METHOD

D.K. Sharaborin, R.V. Tolstoguzov, A.G. Savitskii, V.M. Dulin

Kutateladze Institute of Thermophysics of the SB RAS, 630090 Novosibirsk, Russia

The influence of external electric fields on the combustion region was observed as early as the 20s and 30s of the last century [1-3], which served to stimulate research interest in the causes of this effect on combustion and methods of controlling the flame stabilisation processes. In particular, the organisation of combustion in an electric field can be used to improve flame stability [4]. While in most papers the authors show that the electric field has a significant effect on the flame propagation rate, there are practically no data in the literature on the change in temperature distribution. The direction of the electric field vector influences the direction of ion migration (in the case of low voltages), which is particularly noticeable in the flame front [5], where a high ion concentration is observed. Thus, by stretching/compressing or deflecting the flame front, it is possible to stabilise or promote flame blow-off.

The study of the structure of a flow, even a burning one, requires more than just the measurement of the velocity distribution in the flow, because of the sudden change in gas parameters behind the flame front. The Planar Laser Induced Fluorescence (PLIF) method allows the measurement of instantaneous temperature distributions in a combustion flow without introducing significant perturbations into the flow under study. Furthermore, the PLIF method can be used to localise the position of the flame front in a laminar flame. Under the condition of applying a low-intensity electric field, this allows the direct visualisation of the effect on the flame front. The work has been carried out to experimentally investigate the effect of a constant transverse electric field on the structure of a laminar premixed conical flame. The focus of the work is to estimate the temperature distribution, velocity and position of the flame front in the presence and absence of the electric field.

A laminar premixed methane/air Bunsen flame was formed by a constricting nozzle with a Vitoshinsky profile, which provided a top-hat velocity profile at the nozzle edge. The electric field was organised by two parallel metal plates mounted near the nozzle in such a way that the electric field intensity lines were perpendicular to the gas flow from the nozzle. A high voltage power supply was used to apply a voltage U = 2.5 kV to the plate electrodes, which corresponds to an electric field E = 62.5 kV/m (at a distance of 40 mm between the electrodes) in the parallel-plate capacitor approximation. The Reynolds number was Re = 1000 and was determined from the bulk velocity and viscosity of air at room temperature. The equivalence ratio was $\varphi = 0.92$.

The experimental study of the flow structure was carried out in the longitudinal section of the flow passing through the nozzle symmetry axis. Velocity field measurements were made by particle image velocimetry using a single ImperX Bobcat IGV-B4820 camera and a Beamtech Vlite-200 double-head pulsed Nd:YAG laser. To estimate the temperature behind the flame front, the Two-line OH PLIF method was used, based on recording the intensities of the fluorescence signals of OH radical molecules obtained under excitation by two laser shots with wavelengths corresponding to the two transitions $Q_1(5)$ and $Q_1(14)$ of the (1-0)

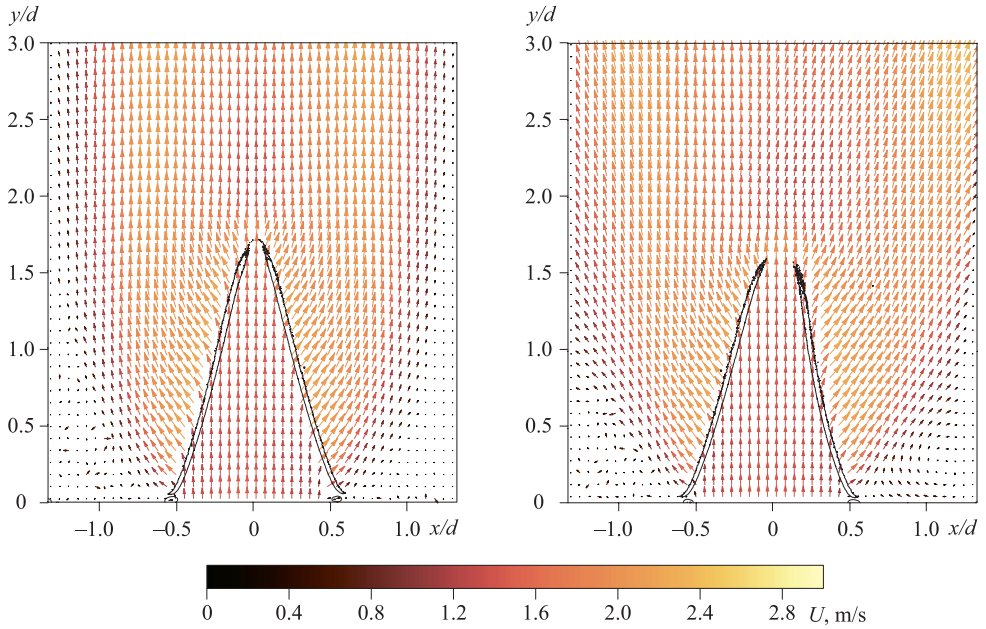

Fig. 1. Spatial distribution of the time-averaged velocity in a laminar Bunsen flame Re = 1000, φ = 0.92, the isoline shows the averaged position of the flame front. Without electric field (left), with electric field E = 62.5 kV/m (right).

band of the $A^2\Sigma^+$–$X^2\Pi$ electronic system. The intensity ratio of the fluorescence signals is correlated with temperature in accordance with the population of energy levels according to the Boltzmann distribution. The visualisation of the position of the flame front is based on the determination of the maximum gradient of the fluorescence signal under excitation of the Q1(5) transition.

Examples of the average velocity field in the cross-section of the Bunsen flame and a visualisation of the average position of the flame front are shown in Figure 1. A change in the shape of the flame cone is observed, particularly in the upper part where rounding occurs, and a deflection of the entire surface towards the cathode. Despite the effect on the position of the flame front and the velocity field, the influence of the electric field has no significant effect on the values of the temperature distribution behind the flame front.

This work was financially supported by the Russian Science Foundation (Project Code 22-19-00803).

REFERENCES

1. **Laughton D., Weinberg F.** Electrical Aspects of Combustion. Moscow: Energia, 1976. C. 186 p.
2. **Lavrov F. A., Malinovsky A. E.** Influence of a longitudinal electric field on the process of combustion of gas mixtures// Zhurnal Fizicheskaya Khimiya [Russian Journal of Physical Chemistry]. 1933. Vol. 4, No. I, P. 104. (in Russian)
3. **Malinovsky A.E., Egorov K.E.** Influence of the electric field on combustion processes at reduced pressures // Zhurnal Eksperimentalnoi i Teoreticheskoi Fiziki [Journal of Experimental and Theoretical Physics]. 1934. Vol. 4, No. 2, P. 208. (in Russian)
4. **Starikovskaia S.M.** Plasma assisted ignition and combustion // Journal of Physics D: Applied Physics. 2006. Vol. 39, No. 16, P. R265.
5. **Tretyakov P.K., Tupikin A.V., Denisova N.V. et al.** Laminar propane-air flame in a weak electric field // Combustion, Explosion, and Shock Waves. 2012. Vol. 48, P. 130–135.

DOI 10.53954/9785604990148_156

COMPUTATIONAL AND EXPERIMENTAL STUDY OF SLUG FLOW REGIME IN A Y-TYPE MICROCHANNEL SIMULATING A PORE

A.A. Shebeleva, A.S. Lobasov, A.V. Minakov

Siberian federal university
660041, Krasnoyarsk, Russia

A computational and experimental study of the slug flow regime of an oil-water suspension of silicon dioxide of various concentrations of 1–10% with an average nanoparticle size of 10 nm was carried out. Experimental study was carried out on a chip with a Y-shaped microchannel simulating a microporous medium. The chip is made of polymer (PDMS), dimensions of input channels are 40 × 40 × 3000 μm, output channels are 40 × 80 × 10000 μm. The experiments were carried out in a wide range of oil flow rates $1 \le Q_0 \le 8$ μl/min, which was supplied through lower entrance to microchannel, and suspension flow rates of $0.5 \le Q_S \le 50$ μl/min, which were supplied through upper entrance to microchannel. Liquids were pumped into microfluidic chip using two syringe pumps. To visualize slug flow regime, a high-speed camera was connected to microscope; recording frequency was constant throughout experiment and equal 1 ms. To model two-phase flow of immiscible liquids in porous media, computational fluid dynamics methods were used; microflows were modeled by solving the Navier–Stokes equations. To model free surface, the VOF method and the CSF algorithm were used; a detailed description of numerical methodology is presented in [1], verification and testing of proposed methodology is presented in [2].

As a result of calculations and experiments, it was found that the slug flow regime, for a given microchannel and sets of liquids under study, exists at oil flow rates of $1 \le Q_0 \le 4$ μl/min.

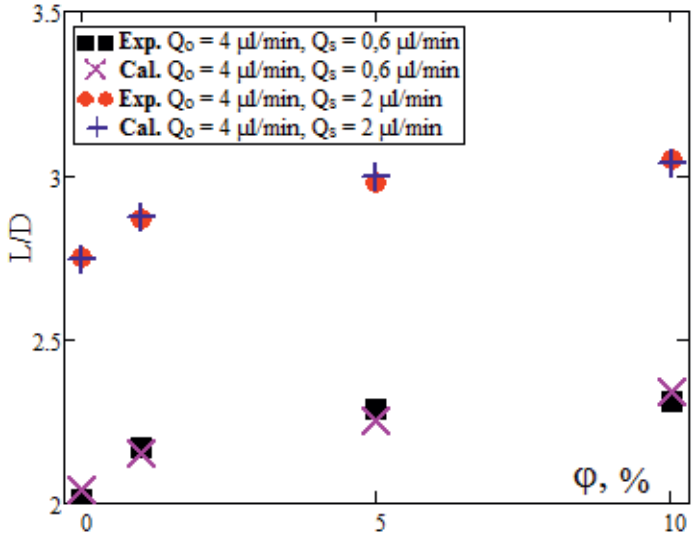

Fig. 1. Dependence of relative size of slugs on concentration of suspension.
Comparison of calculated and experimental data.

A quantitative parameter of slug flow regime is length of slug. To assess effect of suspension concentration on length of slug, relative length of slug was used (a value obtained as arithmetic mean of lengths of all slugs in channel, normalized to hydraulic diameter o microchannel equal 53.3 μm). It was found that addition of silicon dioxide affects size of projectiles and distance between them. As SiO_2 concentration increases, length of slugs increases and distance between them decreases. With increasing suspension consumption, dependence of slug length on concentration of nanoparticles remains unchanged. A comparison of calculated and experimental data was carried out, and it was found that numerical method well describes process of slug formation and its movement along channel at same instants of time.

The work was carried out within framework of the state assignment of the Ministry of Science and Higher Education of the Russian Federation (number FSRZ-2020-0012).

REFERENCES

1. **Minakov A.V., Lobasov A.S., Shebelev A.V., Zaitsev D.V., Kabov O.A.** Flow Regimes of a Liquid Film Carried Away by a Gas Flow in a Flat Horizontal Channel under Isothermal Conditions // J. Appl. Ind. Math. 2022. Vol. 16, P. 490–500.
2. **Lobasov A.S., Minakov A.V.** Numerical investigation of the distance between micropillars effect on the flow characteristics in the microchannel with textured wall // Interfacial Phenomena and Heat Transfer. 2022. Vol. 10, Is. 2, P. 1–10.

DOI 10.53954/9785604990148_158

THE STUDY OF THE INFLUENCE OF SMALL ANGLES OF ATTACK ON THE LAMINAR-TURBULENT TRANSITION ON A SWEPT WING WITH A SUBSONIC LEADING EDGE

S.A. Shipul, A.D. Kosinov, A.N. Semenov, N.V. Semionov, B.V. Smorodsky, A.A. Yatskikh

Khristianovich Institute of Theoretical and Applied Mechanics SB RAS
630090, Novosibirsk, Russia

The investigations of turbulence origin and the development of new engineering approaches to the prediction and control of laminar-turbulent transition in three-dimensional boundary layers on the basis of obtained the experimental data is at the center of attention of the specialists in many countries. Such studies are of practical interest, since similar flows occur when flowing around the swept wing of an aircraft. One of the factors affecting the transition position on a swept wing is the angle of attack. Even a small change in this parameter leads to a significant change in the transition Reynolds number [1]. A review of research on the influence of small angles of attack on the development of disturbances in the boundary layer of swept wings is given in [1].

The experiments were carried out in the low-noise supersonic wind tunnel T-325 of the ITAM SB RAS at Mach numbers M = 2 and 2.5. For these Mach numbers, a low-noise regime of the wind tunnel is [2]. The experimental data obtained in low-noise conditions are in good agreement with the results of calculations using the linear theory of hydrodynamic stability (LTS). The measurements were carried out on a model of a swept wing with a 3% profile at the base with a variable chord length along the span (chord at the base – 498 and 200 mm at the end of the wing). The sweep angle of the leading edge is 72°, that at M = 2 and 2.5 corresponds to the case of a subsonic leading edge.

Disturbances in the flow were recorded with a constant-temperature hot-wire anemometer. The automated data collection system, the data processing procedure and the method for determining the absolute values of mass flow pulsations <m'> are described in more detail in [1]. As a result of the measurements, the dependence of the disturbance amplitude versus the Reynolds number $Re_x = Re_1 \times x$ was defined. The transition point from laminar to turbulent flow was determined by the maximum of mass flow pulsations.

An experimental study of the influence of the angle of attack on the position of the laminar-turbulent transition in a supersonic boundary layer was carried out on a model of a swept wing. Calculations of the mean flow in a supersonic boundary layer and calculations using the LTS were carried out for experimental conditions on the wing, and the values of the growth rate in the amplitudes of disturbances of stationary and non-stationary vortices of crossflow instability were obtained.

Figure 1 shows the experimentally obtained dependence of the transition Reynolds number on the angle of attack at different Mach numbers for two wing models: a swept wing with a subsonic leading edge ($\chi = 72°$) and a supersonic leading edge ($\chi = 45°$) [1].

Figure 2 shows the growth rates of the disturbance amplitudes of the fastest growing stationary vortices of crossflow instability as a function of Re_x on a swept wing with $\chi = 72°$ for Mach numbers 2 and 2.5 and various angles of attack. Here curve is 1, 2, 3 – M = 2, $\alpha = –1°$, 0, 0.3°, and 4, 5, 6 – M = 2.5, $\alpha = –0.46°$, 0, 0.46°.

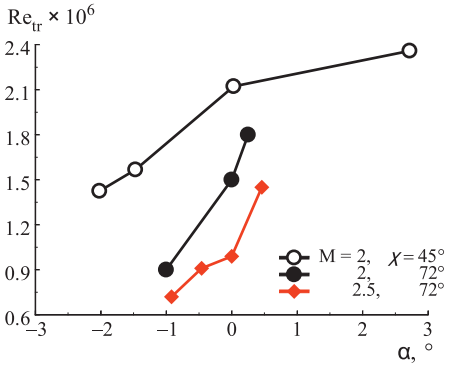

Fig. 1. Dependence of the transition Reynolds number versus the angle of attack for Mach numbers 2 and 2.5.

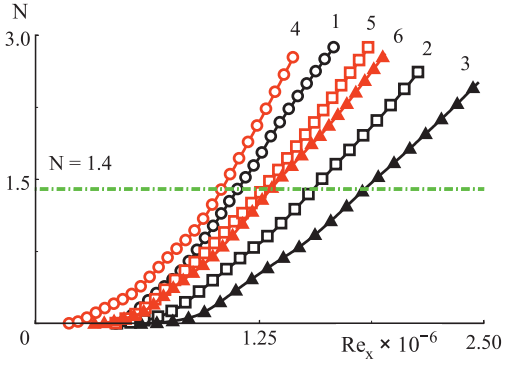

Fig. 2. Growth rates of the disturbance amplitudes for the stationary crossflow instability vortices.

Analyzing the experimental data, it was found that changing the angle of attack has a strong effect on the transition Reynolds number. For a wing model with $\chi = 72°$, changing the angle of attack from approximately –1° to 0.5° leads to a doubling of the transition Reynolds number. At the same time, on a wing with $\chi = 45°$, a change in the angle of attack from –2° to 3° leads to an increase in the transition Reynolds number by approximately one and a half times. It follows that the angle of attack has a stronger effect on the transition position on models with a subsonic leading edge than on swept wing with a supersonic leading edge.

Calculations have shown that the amplitude of stationary vortices increases most rapidly at a negative angle of attack, and with an increase in the angle of attack, the growth rate of stationary disturbances are getting less. The obtained calculation results good correlating with experimental data on the transition on a swept wing with a subsonic leading edge. For non-stationary obtained modes increasing growth rate of with enhancing angle of attack. Analyzing the calculation results and the data obtained as a result of the experiment, we can conclude that the decisive role in the position of the laminar-turbulent transition in the boundary layer of a swept wing is performed by stationary disturbances.

REFERENCES

1. **Kosinov A.D., Semionov N.V., Yermolaev Y.G., Smorodsky B.V., Kolosov G.L., Yatskikh A.A., Semenov A.N.** The influence of moderate angle-of-attack variation on disturbances evolution and transition to turbulence in supersonic boundary layer on swept wing//Journal of Aerospace Engineering: Part G. Proceedings of the Institution of Mechanical Engineers. – 2020. – No 234(1). P. 96–101. DOI: 10.1177/0954410019852804.
2. **Kosinov A.D., Semionov N.V.** The laminar-turbulent transition experiments in supersonic boundary layers // AIP Conference Proceedings: High-Energy Processes in Condensed Matter (HEPCM–2019): Proceedings of the XXVI Conference on High-Energy Processes in Condensed Matter, dedicated to the 150th anniversary of the birth of S.A. Chaplygin (Novosibirsk, 3–5 Apr. 2019). – Vol. 2125, No.030105(5). – S.l.: AIP Publishing, 2019. DOI: 10.1063/1.5117487

DOI 10.53954/9785604990148_160

EXPERIMENTAL STUDY OF THE DISTURBANCES DEVELOPMENT IN THE BOUNDARY LAYER ON THE FLAT PLATE WITH A WAVY SURFACE AT MACH 3

A.V. Shmakova, A.D. Kosinov, Yu.G. Yermolaev, N.V. Semionov

Khristianovich Institute of Theoretical and Applied Mechanics, 630090, Novosibirsk, Russia

This work is devoted to an experimental study of the passive flow control in a supersonic boundary layer using a wavy surface at Mach 3. The research is a continuation of a series of studies carried out within the framework of a state assignment in 2021-2022, and within the framework of the Russian Science Foundation grant 17-19-01289 [1, 2].

The experiments were conducted in T–325 supersonic wind tunnel of ITAM SB RAS at Mach 3. The model of a flat steel plate with a blunt radius of the leading edge r = 0.32 mm was used. In the wind tunnel the model was fixed in the central plane of the test section at approximately a zero angle of attack. Photo of the model with a wavy surface is shown in Fig. 1,*a*. To create a wavy surface on the model, longitudinal roughness elements were applied. They were additionally coated with a film to align the side sections of the roughness and give them a rounded shape. Dimensions of roughness elements: width – 2 mm, length – 150 mm, thickness – 93 microns. Distance between roughness elements 12 mm. To preserve the surface properties in experiments on a model with flat surface, the longitudinal roughness elements were removed from the model and the flat plate was sealed with a film, the same as in the case of a wavy surface of the model. Constant temperature anemometer CTA 2017 was used for mean and pulsating flow quantities measurements [3]. The mean and pulsating characteristics of the flow were obtained after data processing using the standard technique, which is described in [3–6].

To determine the mean flow distortion in the boundary layer created by longitudinal roughness elements, measurements were made with a hot-wire anemometer along a line parallel to the leading edge at x_0 = 127 mm, y_0 = const. The measurements showed that the mean flow is periodically modulated (Fig. 1,*b*), the period of flow modulation corresponding to the distance between the established roughnesses. The minima in the distributions corre-

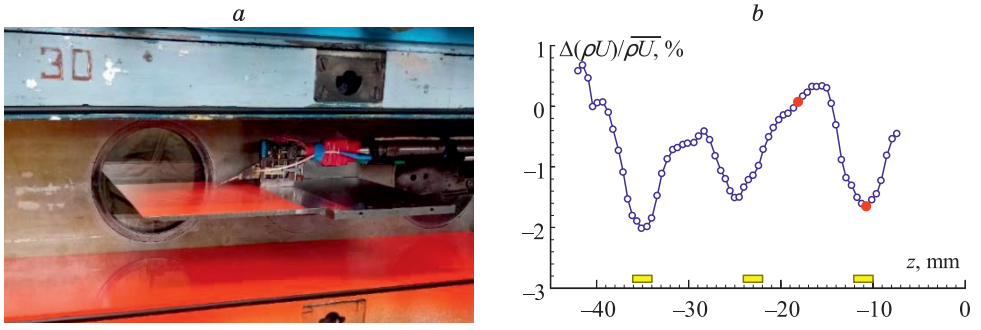

Fig. 1. Photographs of the flat plate with a wavy surface in the test section of T–325 (*a*). Mean flow distortion in the spanwise direction for plate with wavy surface (*b*).

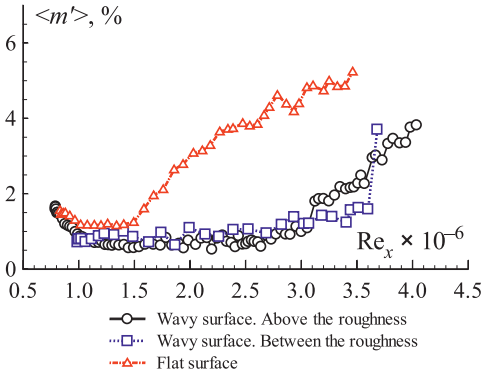

Fig. 2. The RMS mass flux pulsations for the plate with flat and wavy surface

spond to the center of the roughness elements, and in the wake between the roughness there is a plateau in the mean flow distortion. The yellow rectangles schematically indicate the location of the longitudinal roughness elements. The red dots show the areas where the laminar-turbulent transition were measured (z = –11 mm in the area above the center of the roughness elements, z = –18 mm in the area between the roughness).

Measurements of the laminar-turbulent transition in the boundary layer of a plate with a wavy and flat surface (Fig. 2) showed that on a plate with a wavy surface, the Reynolds number of the transition in the region above the roughness is $Re_{tr} = 4.0\times10^6$ and is 14% higher than on the model with flat surface ($Re_{tr} = 3.5\times10^6$).

In measurements in the boundary layer of a plate with a wavy surface in the region between the roughness elements, the transition positions could not be fixed. The area where the transition begins is approximately the same in measurements above and between the roughness elements.

The research was carried out within the state assignment of Ministry of Science and Higher Education of the Russian Federation.

The study was conducted at the Equipment Sharing Center “Mechanics” of ITAM SB RAS.

REFERENCES

1. **Panina A., Kosinov A., Semionov N., Yermolaev Yu.** Experimental study of the natural disturbance development in a supersonic flat plate boundary layer with a wavy surface // AIP Conference Proceedings. Vol. 2125. AIP Publishing, 2019. P. 030107.
2. **Shmakova A., Kosinov A., Semionov N., Yermolaev Yu., Yatskikh A., Kocharin V.** Experimental study of the disturbances development in the boundary layer of a flat plate with a wavy surface at supersonic flow // AIP Conference Proceedings. Vol. 2504. AIP Publishing, 2023. P. 030055. DOI: 10.1063/5.0132422
3. **Kosinov A.D., Semionov N.V., Ermolaev Y.G., Kolosov G.L., Yatskikh A.A., Kocharin V.L.** Hot-wire measurements of the evolution of total temperature and mass flow pulsations in supersonic boundary layer on flat plate with coating permeability // AIP Conference Proceedings. Vol. 2027. AIP Publishing, 2018. P. 040087.
4. **Panina A.V., Kosinov A.D., Yermolaev Y.G., Gorev V.N., Semionov N.V.** // Thermophysics and Aeromechanics. 2014. Vol. 21, No. 1. P. 3–13.
5. **Kosinov A.D., Kolosov G.L., Yatskikh A.A., Semionov N.V., Ermolaev Y.G., Panina A.V.** Hot-wire measurements of the evolution of total temperature and mass flow pulsations in a modulated 3d supersonic boundary layer // AIP Conference Proceedings. Vol. 2027. AIP Publishing, 2018. P. 020016.
6. **Yatskikh A.A., Kosinov A.D., Semionov N.V., Smorodsky B.V., Ermolaev Y.G., Kolosov G.L.** Investigation of laminar-turbulent transition of supersonic boundary layer by scanning constant temperature hot-wire anemometer // AIP Conference Proceedings. Vol. 2027. AIP Publishing, 2018. P. 040041.

DOI 10.53954/9785604990148_162

WING COMPARTMENT ICING STUDY IN THE SMALL ICING WIND TUNNEL SIWT OF ITAM SB RAS

A.S. Shmakov[1], A.A. Sidorenko[1], A.M. Shevchenko[1], A.V. Khalutin[2], A.P. Mokhnachev[2]

[1]Khristianovich institute of theoretical and applied mechanics SB RAS
630090, Novosibirsk, Russia

[2]LLC «CG Silentwings»,
198095, Saint-Petersberg, Russia

The methodology and results of studying the processes and modes of icing of the wing compartment of a small unmanned aerial vehicle (UAV) and the possibilities of using an electric thermal anti-icing system (AIS) for wing de-icing.

The experiments were carried out in the small Icing Wind Tunnel (sIWT) of ITAM SB RAS [1].

The object of research is a model of a wing compartment with a constant chord. In the area of the leading edge of the wing compartment, heating elements are installed inside the model. Thermal AIS occupied 90% of the wing compartment span. To control the surface temperature of the model, two thermocouples are installed.

The experiments were performed at air flow velocities in test section in the range of V = 15 ÷ 36 m/s, flow temperatures T = –3 °C, –7 °C, –11 °C and –20 °C. Water content at different temperatures and flow rates was w = 0.36 ÷ 1.47 g/m^3. In all experiments, the wing compartment was installed at an angle of attack of 4°.

The temperature flow was measured with a K-type thermocouple in the test section at the outlet (behind the model). The shape and size of ice formations were recorded using a RangeVision PRO 3D scanner.

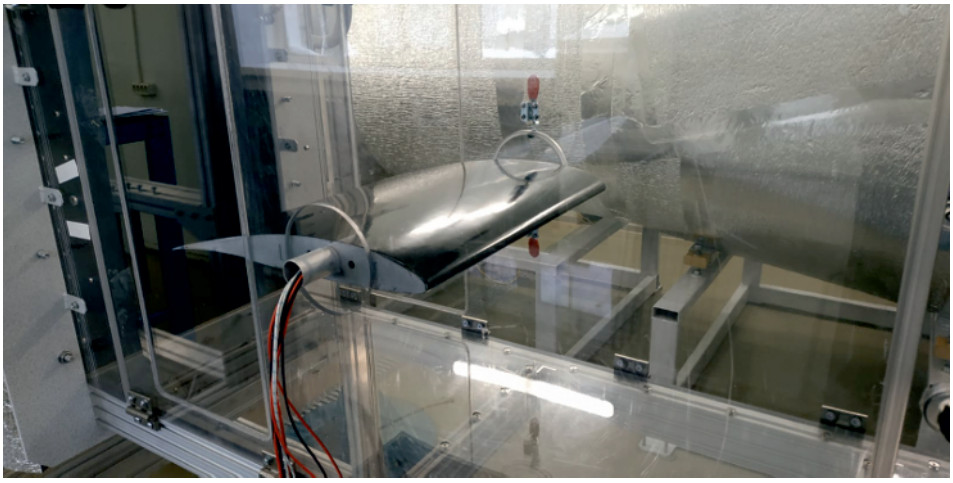

Fig. 1. Wing compartment model in test section of sIWT of ITAM SB RAS

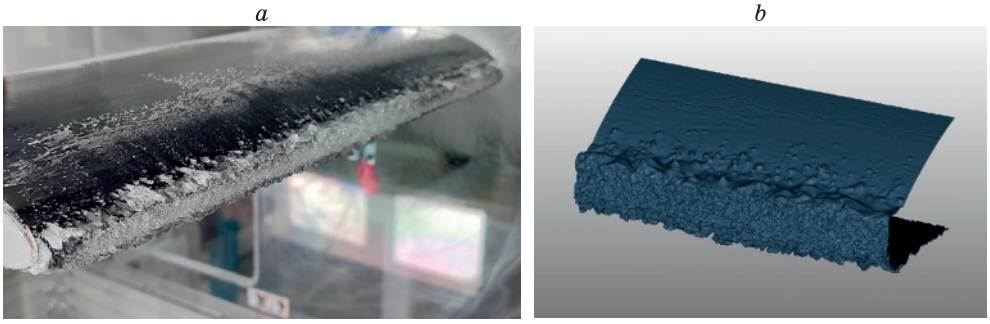

Fig. 2. Icing at V = 36 m/s, T = –3 C, Δt = 6 min: (a) ice formation structure on the model surface; (b) 3D model of ice near the leading edge

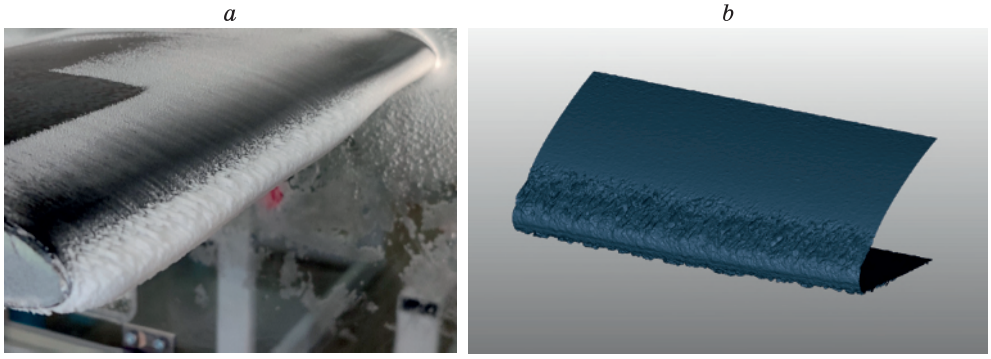

Fig. 3. Icing at V = 36 m/s, T = –20 °C, Δt = 6 min: (a) ice formation structure on the model surface; (b) 3D model of ice near the leading edge

As a result, typical time dependences of temperature during icing process and 3D ice models were obtained. Grlaze and rime icing regimes were recorded.

Tests with thermal AIS showed the possibility of completely eliminating ice formation with an input heater power of at least 5 kW/m^2. At the same time, ice did not form only at the location where the thermal AIS was installed.

The study was conducted at the Equipment Sharing Center «Mechanics» of ITAM SB RAS.

REFERENCES

1. **Prikhodko Yu.M., Sidorenkoa A.A., Shmakov A.S., Shevchenko A.M., Sorokin A.M., Bogdanov A.A., and Shiplyuk A.N.** Small icing wind tunnel based at the khristianovich institute oftheoretical and applied mechanics of the Siberian Branch of the Russian Academy of Sciences // Journal of Applied Mechanics and Technical Physics, 2023, Vol. 64, No. 6, pp. 1015–1024.

DOI 10.53954/9785604990148_164

NUMERICAL SIMULATION OF FLOW AERODYNAMIC IN A VORTEX CHAMBER WITH UNIFORM ROTATION ALONG THE SIDE SURFACE

N.P. Skibina

Kutateladze Institute of Thermophysics of the Siberian Branch of the Russian Academy of Sciences, 630090, Novosibirsk, Russia

Swirling flows is an important part of aero- and gas dynamics and are widely used in various technical devices [1]. Heat and mass transfer processes are enhanced in swirling flows, which ensure the operation of cooling, heating, cleaning and separation systems. The one of relevant problem is the research of the non-stationary structure of swirling flow and the selection of a reliable device geometry that ensures high operating efficiency. Despite fairly extensive and various experimental studies, the results of numerical simulation of vortex chambers flows yield quantitative and qualitative discrepancy.

The purpose of this work is numerical simulation of the flow aerodynamics in a vortex chamber with uniform rotation in a side cylindrical surface [2, 3]. Experimental studies for this vortex chamber and tangential velocity distribution data in a cross section (z/L = 0.5, where z is the coordinate of the plane, L is the length of the chamber) were carried out at the Institute of Thermophysics of the Siberian Branch of the Russian Academy of Sciences. The flow rotation was carried out by path supply of air through four rows of holes drilled tangentially in the side wall of the chamber (Fig. 1a).

For numerical solution of problem finite volume method implemented in the ANSYS Fluent CFD software was used. The Reynolds Averaged Navier-Stokes equations was used for describe of non-compressible gas flow with constant viscosity and specific heat. The internal volume of the vortex chamber discretized by polyhedral mesh (Fig. 1b) with grid refinement near the walls. The boundary layer was resolved hexa-cells. The number of cells in the calculation domain is $5 \cdot 10^6$. The wall surfaces are no slip boundary conditions, for tangential air pipes is velocity inlet boundary condition was used. The air outflow from internal volume of vortex chamber is realized in ambient with pressure and temperature values P = 10^5 Pa and T = 293.15 K.

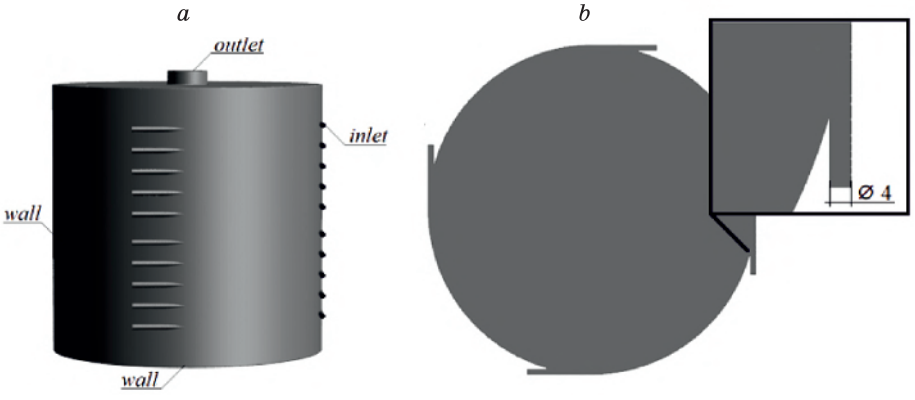

Fig. 1. 3D model of vortex chamber (*a*) and tangential air pipe (*b*)

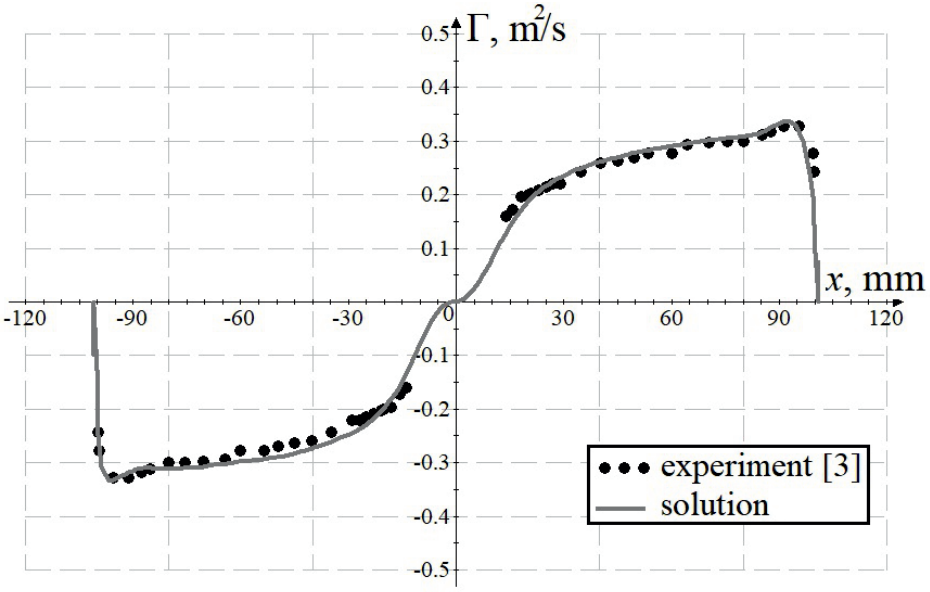

Fig. 2. Tangential velocity circulation in a z/L=0.5 plane, $Re_\varphi = 2.2 \cdot 10^4$

By results of numerical simulation of swirling flow in vortex chamber used by described mathematical model a quantitative and qualitative correspondence of the circulation distribution of the tangential velocity component with experimentally values for a case with $Re_\varphi = 2.2 \cdot 10^4$ was obtained (Fig. 2). Non steady and asymmetric swirling flow structure was obtained for internal volume of vortex chamber with uniform rotating. Precession of vortex structure near the central axis of chamber occurs. In numerical solution also visualization of process of swirling flow formation and dynamic of axial and tangential velocity components, which cause a continuous restructuring of the flow in the vortex chamber are obtained.

The work was carried out with the financial support of the Russian Science Foundation, grant number 24-19-00358.

REFERENCES

1. **Gupta A., Lily D., Syred N.** Swirling flows // Moscow, 1987. 588 p.
2. **Volchkov E.P., Smulsky I.I.** Experimental study of aerodynamics of vortex cylindrical wall injection chamber. –Novosibirsk: Inst. Thermophys., Sib. Branch, Acad. of Sci. of the USSR, 1979. Pre-print № 38-79. 30 p.
3. **Semenov S.V.** Aerodynamics and heat transfer of end-wall boundary layer in a vortex chamber.: diss. cand. tech. sci.: 01.04.14. – Novosibirsk, 1987. – 182 p.

DOI 10.53954/9785604990148_166

APPLICATION OF TOMOGRAPHIC PIV FOR A THREE-DIMENSIONAL CONVECTIVE FLOW

M. Sorokin[1], M. Tokarev[1], Y. Popov[2], E. Kirchanova[1], M. Korotkov[2], V. Dulin[1], A. Vasiliev[3], A. Sukhanovskii [3], R. Stepanov[3]

[1]*Kutateladze Institute of Thermophysics, Siberian Branch of RAS, Novosibirsk 630090, Russia*

[2] *Sigma-Pro LLC, Novosibirsk 630090, Russia*

[3]*Institute of Continuous Media Mechanics of the Ural Branch of RAS, 614000, Perm, Russia*

Particle image velocimetry (PIV) has been successfully used for flow diagnostics over an extended period of time [1–3]. Instantaneous velocity field distributions in a plane obtained by classical 2D PIV have reached reliable accuracy and spatial resolution. However, 2D distributions are not enough to study the dynamics of complex three-dimensional flows. Convective flows, for example, often have a complex three-dimensional structure [4]. Therefore, to achieve a more complete understanding of the dynamics and structure of such flows, it is necessary to use methods that can capture velocity distributions in volume (3D PIV), such as tomographic PIV (Tomo PIV) [5]. It provides the measurement of the instantaneous velocity distributions in a small volume of flow, typically not exceeding 10 cm. This paper reports on the data processing issues and sample results of applying the Tomo PIV for a flow near the heated lower surface in a free convection problem.

The experimental setup is a rectangular cavity with internal dimensions of $576 \times 576 \times 300$ mm^3. The walls of the cavity are made of 12 mm thick acrylic glass. The bottom boundary is made of 10 mm thick copper, which serves as a heater. A silicone heater with a power of 2.0 kW is attached to the outer side of the copper plate. The temperature of the copper plate is kept constant at a set value using a PID controller and monitored by four copper-constantan thermocouples located at the ends of the copper plate. The height of the heater water layer is 143.5 mm. The upper wall is absent.

In the implemented Tomo PIV system, image registration was carried out using four Imperx B2720M cameras equipped with Samyang 100mm lenses. Each camera was

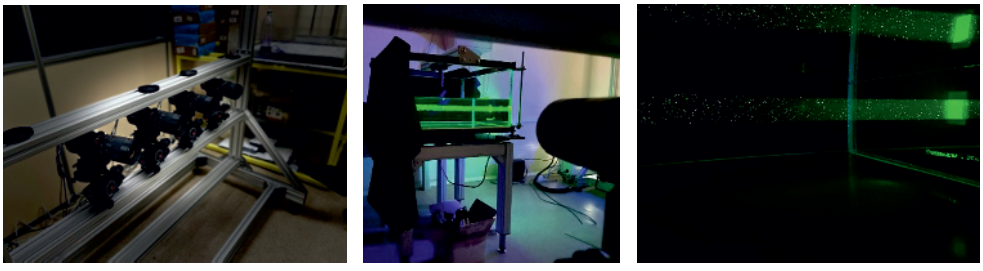

Fig. 1. Camera placement – on the left, working area – in the center, illuminated polyamide particles – on the right.

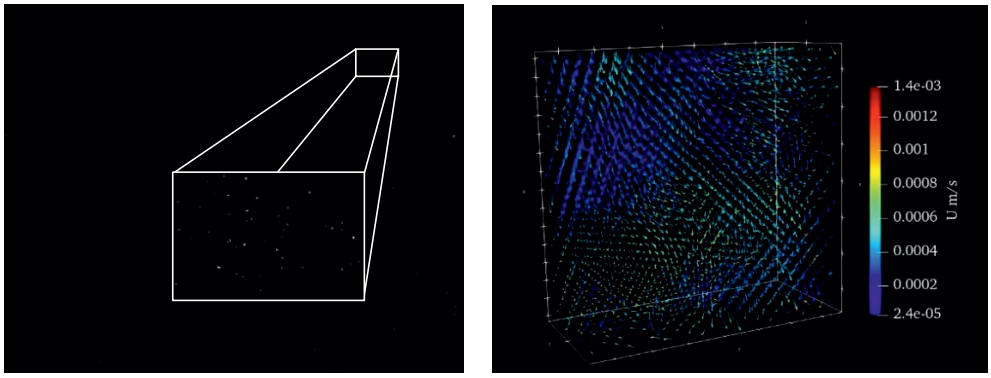

Fig. 2. Example of obtained image of tracer particles from a single camera – on the left, 3D instantaneous velocity field – on the right.

equipped with a Scheimpflug correction platform. The flow was illuminated using a pulsed Nd:YAG laser Beamtech Vlite-200 with a pulse energy of 200 mJ. To create volumetric illumination of the flow, an additional lens was mounted on the laser's output aperture. Spatial calibration of the cameras was performed using a flat calibration target measuring 100×100 mm. The recording was done for a linear configuration of camera placement (see Fig. 1) at a frame rate of 10 Hz in single-frame mode. The working area dimensions were $100 \times 100 \times 50$ mm, and the image resolution was 2700x2200 pixels. Polyamide spherical particles with a diameter of 50 μm were used for seeding the flow.

The measurements provided three-dimensional velocity fields with temporal resolution of the convective flow of water, created by the temperature difference between the heater and the upper boundary of water-air. In the experiments, the temperature difference reached 2 °C, corresponding to the Rayleigh number $Ra = 1.2 \times 10^8$. The paper will present details of the experiment, features of spatial calibration of the cameras and reconstruction of the three-dimensional image, as well as examples of the obtained results on the flow dynamics.

The study was financially supported by the Russian Science Foundation (№21-72-20067).

REFERENCES

1. **Adrian R.J., Westerweel J.** Particle image velocimetry. – Cambridge university press, 2011.
2. **Westerweel J., Elsinga G.E., Adrian R.J.** Particle image velocimetry for complex and turbulent flows //Annual Review of Fluid Mechanics. – 2013. – Vol. 45. – P. 409–436.
3. **Raffel M., Willert C.E., Scarano F., Kähler C.J., Wereley S.T., Kompenhans J.** Particle image velocimetry: a practical guide. – Springer, 2018.
4. **Sakakibara J., Adrian R.J.** Whole field measurement of temperature in water using two-color laser induced fluorescence // Experiments in Fluids. – 1999. – Vol. 26. – No. 1–2. – C. 7–15.
5. **Scarano F.** Tomographic PIV: principles and practice // Measurement Science and Technology. – 2012. – Vol. 24. – No. 1. – P. 012001.
6. **Shestakov M.V. et al.** PIV study of large-scale flow organisation in slot jets // International Journal of Heat and Fluid Flow. – 2015. – Vol. 51. – P. 335–352.

DOI 10.53954/9785604990148_168

NON-DESTRUCTIVE ACOUSTIC QUALITY CONTROL OF COMPOSITE AND NANOCOMPOSITE HETEROGENEOUS AND MULTIPHASE MATERIALS, MEDIA AND STRUCTURES

S.V. Sukhinin

Lavrentyev Institute for Hydrodynamics SB RAS
630090 Novosibirsk, Russia

Background. The homogeneity of a continuous medium is a conditional concept, it depends on or implies the choice of scale and some averaging of properties and parameters. All material environments are heterogeneous. This means that they consist of several components. The presence and number of components can significantly affect the properties of the medium. This makes it important to determine the concentration of components in heterogeneous media. To control the "purity" of continuous media, special standards for quality control or determination are being developed. Determining the concentration of components in heterogeneous media is, as a rule, a difficult and time-consuming and very demanding task, for example, when controlling the production of composite or nanocomposite materials. This determines the relevance of the work.

Examples of heterogeneous media for which quality control is important. Aerosols, mists, foams (styrofoam, styrofoam, polyurethane foam), dust and smoke flows. All porous media, including bricks, ceramics, and oil and gas formations. All composite and nanocomposite materials. Ceramics, liquids, gases. Quality control of meat and other food products. Control of dispersion and completeness of combustion of liquid and solid fuels.

Goal. A fundamental theory for the development of techniques and technologies for non-destructive quality control of inhomogeneous media using acoustic methods. Determination of the concentration of components of heterogeneous media and devices made of composite materials using acoustic methods of non-destructive quality control.

Methods and results. Using the methods of the theory of representation of translation groups in the solution space, a description of wave propagation in heterogeneous multiphase and multicomponent media with translational symmetry conditions has been created, which is valid for composite materials. Based on this theory, software products for non-destructive quality control of these media have been created using numerical and analytical methods [1–4].

Quality control methods make it possible to design new composite materials with increased performance characteristics, for example, with increased vibration isolation, with reduced thermal conductivity.

Methods have been developed and described for determining the transmission and reflection coefficients of acoustic waves from various types of defects in composite materials and heterogeneous media, which are determined by the boundaries of the composite–composite interface (a violation of the composite structure) and composite–homogeneous medium (foreign inclusion) in various combinations [5–7].

A feature of the creation and use of acoustic flaw detection methods by the phonon crystal method is the possible size variation (polydispersity) of the matrix material components and reinforcing components of composite materials and products made from them.

It should be noted that the relative ease of use of quality control methods for heterogeneous media makes it possible to develop and create measuring instruments and systems, components of which are already mass-produced and are freely available.

An example of numerical and analytical studies for a polydisperse two-component water-air mixture. It is assumed that in the SI system at a temperature of +20 degrees Celsius, the speed of sound into the air is 343 meters per second, the air density is 1.2 kilograms per meter in a cube. For water, the speed of sound is 1400 meters per second, and the density of water is 1000 kilograms per meter in a cube.

The main anomaly. For a heterogeneous water–air mixture, there is a minimal acoustic velocity U in the mixture. For the above parameters, this velocity is expressed in meters per second U = 23.75. The value of the minimum sound velocity in the mixture for long waves is achieved at the value of the concentration k* of air in the mixture k* = 0.4994352967. The minimum speed of sound in the mixture is an order of magnitude less than the speed of sound in air and 2 orders of magnitude less than the speed of sound in water.

Fog. Low volume concentration of k water in the air. K = 0.0001 the speed of sound of the mixture is 330 meters per second; k = 0.001 the speed of sound of the mixture is 253 meters per second; k = 0/0015 the speed of sound of the mixture is 229 meters per second.

Carbonated or aerated water layer. This phenomenon occurs in the upper layers of open water (aeration), in the layers of algae or organisms.

Carbonated or aerated water layer. k = 0.9999, the speed of sound of the mixture is 906 meters per second; k = 0.999, the speed of sound of the mixture is 363 meters per second; k = 0.9985, the speed of sound of the mixture is 230 meters per second. It is necessary to note the strong influence of the mixture on the speed of sound.

REFERENCES

1. **Sukhinin S.V.** Wave propagation and resonance phenomena in inhomogeneous media // J. Appl. Mech. Tech. Phys. 2001, Vol. 42, P. 411–419.
2. **Sukhinin S.V., Kondratenko D.A.** Wave transmission trough inhomogeneous chain of transparent obstacles // In Proceedings of the International Conference on Mathematical Methods in Electromagnetic Theory, Kiev, Ukraine, 10–13 September 2002; P. 157–162.
3. **Sukhinin S.V.** Waveguide, anomalous, and whispering properties of a periodical chain of obstacles // Sib. Zh. Indust. Mat. 1998, Vol. 1. P. 175–198.
4. **Sukhinin S.V.** Features of signal propagation in heterogeneous media // In Proceedings of the V International Seminar on Stability of Flows of Homogeneous and Heterogeneous Liquids, Novosibirsk, Russia, 22–24 April 1998. P. 98–103.
5. **Baenova G., Sukhinin S., Zhulamanova, Z., Zhumadillayeva A.** Effect of polydispersity on the bandwidth of transmission and locking in phonon two–component crystals. J. Mech. Eng. Res. Dev. (JMERD) 2021, 44, 79–88.
6. **Konstantinov A.P., Sukhinin S.V., Yurkovskiy V.S.** Wave transmission and reflection at the boundary of phononic crystals. J. Phys. Conf. Ser. 2017, 894, 012094.
7. **Saimanova Z.B., Sukhinin S.V., Zhumadillayeva A.K.** Wave transmission and reflection from the boundary of phononic crystal – homogeneous medium // Eurasian J. Math. Comput. Appl. 2020, Vol. 8. P. 62–75.

DOI 10.53954/9785604990148_170

DETONATION INITIATION UPONINCIDENCE OF A SHOCK WAVE ON A COMBUSTIBLE GAS BUBBLE ADJACENT TO A SOLID WALL

O.G. Sutyrin, P.Yu. Georgievskiy, V.A. Levin

Institute of Mechanics, of Lomonosov Moscow State University, Michurinsky pr. 1, 119192, Moscow, Russia

In recent years, the problem of the interaction of a shock wave with a flammable gas bubble (reactive shock-bubble interaction, RSBI) [1, 2] has been actively studied as a promising method for initiating combustion and detonation in gas mixtures. The key phenomenon is the focusing of secondary shock waves, which strongly depends on the wave intensity, gas density in the bubble and its shape [3, 4]. The phenomenon of significant amplification of a shock wave upon reflection from a wall is also well known, especially in the case of a concave wall profile, which is also a way to initiate gas detonation [5]. In this regard, the problem of initiating detonation through a combination of the effects of wave focusing on a gas bubble and wave reflection from the wall is of great interest.

In this work, we consider the incidence of a shock wave on a flammable near-wall gas bubble in a flat two-dimensional setting. The intensity of the shock wave is specified by the Mach number M, and the shape of the bubble is determined by the ratio of the semi-axes of the cross-section χ. Unsteady two-dimensional gas flows are modeled using the Euler equations for a perfect gas with a non-uniform distribution of thermodynamic characteristics. For numerical modeling, a finite-difference WENO5-JS scheme of the fifth order of approximation is used, supplemented by a special method for approximating the transport equation of the gas heat ratio [6]. The combustion reaction of a gas mixture is modeled using two-stage Korobeinikov-Levin kinetics [7] with reaction parameters corresponding to a hydrogen-oxygen mixture diluted with argon.

Various regimes of detonation initiation during the interaction of a shock wave with a near-wall gas bubble are described (Fig. 1). At sufficiently large Mach numbers of the incident wave, combustion of the mixture is initiated directly due to heating in the shock wave transmitted into the bubble (Fig. 1a). For weaker shocks, ignition can occur when the shock

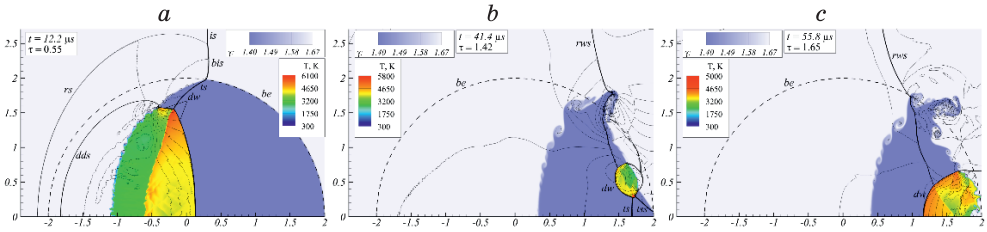

Fig. 1. Regimes of initiation of detonation in a near-wall combustible bubble. Pressure contours.

a – direct initiation (M = 3.0), *b* – initiation during wave reflection from the wall and refraction in a bubble (M = 2.2), *c* – initiation during reflection and focusing on the symmetry plane (M = 1.9). Inert gas and temperature (only in the combustion area) are shown in color. Coordinates in centimeters, dotted line *be*is the initial boundary of the bubble. The lower boundary of the colored drawings is the plane of symmetry, the right boundary is the solid wall. *is*and *bis*are incident shock wave (moves from left to right) and its curved section, *rs*is wave reflected from the bubble, *ts*is wave transmitted into the bubble, *rws*is wave reflected from the wall, *tss*is transverse secondary wave, *dw*is detonation wave, *dds*isdetonation-driven shock wave in the inert gas.

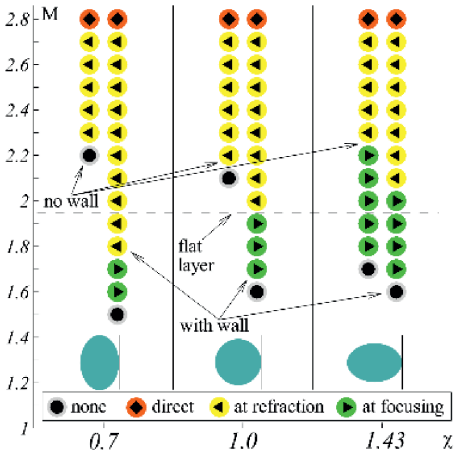

Fig. 2. Detonation initiation regimes dependence on the Mach number of the incident shock and the shape of the bubble.

Flattened ($\chi = 0.7$), round ($\chi = 1.0$) and elongated ($\chi = 1.43$) bubbles. For each value of χ, two flow options are given: without a wall (left column of symbols) and with a wall (right column). The regimes are indicated by symbols on a colored background: diamond on red – direct initiation when a wave passes into a bubble, left triangle on yellow – upon refraction (and, if there is a wall, interaction with a reflected wave), of internal waves in the bubble, right triangle on green –upon shock focusing on the plane of symmetry. The dotted line is the threshold Mach number for a flat layer of combustible gas ($\chi = 0$).

wave *rws* reflected from the wall penetrates the combustible gas and interacts with the longitudinal *ts* and transverse *tss*secondary shocks (Fig. 1b). At lower Mach numbers, the intensity of these waves is not enough, but the required gas temperature is achieved by focusing shock waves on the symmetry plane (Fig. 1c).

Based on a series of simulations, the dependence of detonation initiation regimes on the Mach number of the incident wave and the shape of the bubble was determined (Fig. 2). For all considered bubble shapes, the presence of a wall reduces the threshold Mach number from M = 2.2 to M = 1.7 for a round bubble, from M = 1.7 to M = 1.6 for an elongated bubble, and, especially significantly, from M = 2.3 to M = 1.6 for a flattened bubble. For comparison, the diagram shows the value M = 1.95, starting from which detonation in a layer of combustible gas is successfully initiated without focusing, only due to heating in a plane reflected wave. It can be noted that wave focusing when interacting with an elongated bubble ($\chi = 1.43$) turns out to be more effective than simple reflection of a plane wave, whereas free round and flattened bubbles ignite when an incident wave of higher intensity is refracted. In the presence of a wall, the smallest threshold Mach number M = 1.6 is achieved in the case of a flattened bubble due to slightly better localization of wave focusing directly near the wall.

Such a significant decrease in the threshold intensity of the incident wave due to the presence of local gas inhomogeneity opens up the possibility for the development of new – purely gas-dynamic – methods for the effective initiation of detonation in perspective systems of high-speed combustion of fuel gas mixtures.

The work was carried out at the Institute of Mechanics of Lomonosov Moscow State University using the resources of the supercomputer complex of Lomonosov Moscow State University with financial support from the Ministry of Education and Science of the Russian Federation (Agreement No. 075-15-2024-543)

REFERENCES

1. **Haehn N., Ranjan D., Weber C., Oakley J., Rothamer D., Bonazza R.** Reacting shock bubble interaction // Combustion and Flame. 2012. V. 159. No. 3. P. 1339–1350.
2. **Diegelmann F., Tritschler V., Hickel S., Adams N.** On the pressure dependence of ignition and mixing in two-dimensional reactive shock-bubble interaction // Combustion and Flame. 2016. V. 163. P. 414–426.
3. **Georgievskiy P.Yu., Levin V.A., Sutyrin O.G.** Interaction of a shock with elliptical gas bubbles // Shock Waves. 2015. V. 25, No. 4, P. 357–369.

4. **Georgievskiy P.Yu., Levin V.A., Sutyrin O.G.** Combustible gas cylinder detonation upon incident shock focusing// Technical Physics Letters. 2019. Vol. 45, Iss. 12. P. 1209–1211.
5. **Achasov O.V., Labuda S.A., Penyaz'kov O.G., Pushkin P.M., Tarasov A.I.** Initiation of detonation in reflection of a shock wave from a concave curvilinear surface // Journal of engineering physics and thermophysics. 1994. Vol. 67, Iss. 1. P. 739–744.
6. **He Z., Li L., Zhang Y., Tian B.** Consistent implementation of characteristic flux-split based finite difference method for compressible multi-material gas flows // Computers & Fluids. 2018. V. 168. P. 190–200.
7. **Korobeinikov V.P., Levin V.A.** Strong explosion in a combustible gas mixture // Fluid Dynamics. 1969. Vol. 4. Iss. 6. P. 30–32.

DOI 10.53954/9785604990148_173

METHODS FOR MODELING THE ATMOSPHERIC BOUNDARY-LAYER FLOWS IN THE WIND TUNNELS WITH A SHORT TEST SECTION

J.V. Telkova, A.D. Obukhovskiy, S.D. Salenko

The Federal State Budgetary Educational Institution of Higher Education
Novosibirsk State Technical University
630076, Novosibirsk, Russia

According to the requirements of international [1] and Russian [2] standards, experimental studies of ground-based structures require modeling atmospheric boundary-layer flows corresponding to the natural wind of a certain area in wind tunnels. The rules for calculating and confirming the aeroelastic stability of bridges and other extended structures are set out, and the requirements for wind flow in the test section of the wind tunnel are regulated. In order for the structure of the flow in the experiment to correspond to the natural wind, the similarity of the vertical profiles of velocity, intensity and scale of turbulence must be observed.

In wind tunnels with a long test section (15...30 m), the natural build-up of the boundary layer provides the most stabilized boundary layer along the length. Bluff bodies and turbulators (jagged barriers, spires) installed on the wall or floor at the beginning of the test section are typically used to increase the thickness of the boundary layer. The tests sections must be large enough to carry out studies on large-scale models, taking into account the surrounding buildings or terrain, and observe the similarity in Reynolds numbers. In landscape wind tunnels, all requirements for wind flow parameters and the dimensions of the test section are followed [3, 4].

Universal wind tunnels typically have short test sections with low flow turbulence. It is necessary to use specialized devices that allow intensive expansion of the boundary layer at a short distance to adapt such pipes to the research of engineering structures. The parameters of these devices are changed depending on the type of terrain, features of the surrounding buildings and relief. There are several of the most effective methods for modeling atmospheric boundary-layer flows in wind tunnels with short test section presented in the literature. The methods are [4–7]:

– installation of gratings with horizontal rods installed at the beginning of the test section;

– the use of a horizontal screen with various turbulators in the test section of the wind tunnel;

– the use of spiers (vertical plates) and roughness elements to increase the thickness of the boundary layer.

The grating at the beginning of the test section allows the formation of vertical velocity profiles corresponding to atmospheric profiles. The distance between the rods is variable and increases with distance from the screen. It is possible to obtain the required shape of the vertical profile of flow by changing the distance between the rods. The paper [5] describes an iterative algorithm for calculating the grating parameters depending on the required vertical velocity distribution law, developed and tested in the Industrial Aerodynamics Laboratory of the Novosibirsk State Technical University. The horizontal screen installed in the test section of the wind tunnel models the earth's surface. For the rapid growth of the boundary

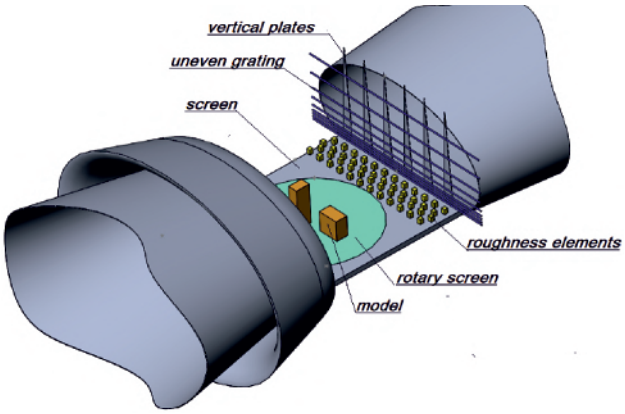

Devices for modeling the atmospheric boundary-layer flows in wind tunnels with short test sections

layer and the provision of turbulence parameters close to full-scale, vortex generators and elements modeling the surface roughness must be placed on the screen in front of the model. Spires or vertical plates create vortex structures that are superimposed on separated flows behind rows of artificial roughness cubes and enable to reproduce the necessary intensity and scale of turbulence. The examples of effective devices for modeling the atmospheric boundary-layer flows in wind tunnels with short test sections is shown in Figure.

The article [8] presents a method for modeling the atmospheric boundary-layer flows using deflecting vortex generators. The author claims that the deflecting of the vortex generators relative to the screen in the angle range from 0 to 90 degrees allows to simulate the different profiles of boundary layer, while the grating at the beginning of the test section is not required.

Carrying out studies of ground-based building structures in wind tunnels with short test sections is possible, but such experiments require the development of specialized devices that provide the characteristics of the simulated flow.

REFERENCES

1. GOST P 59625-2022. Public roads. Bridge structures. Rules for calculating and confirming aeroelastic stability / S.D. Salenko [A.D. Obukhovsky, Yu.A. Gosteev, J.V. Telkova]. – Moscow: Russian Institute of Standardization, 2021. – 61 p.
2. Eurocode 1: Actions on structures. Part 1–4: General actions. Wind actions. EN 1991-1-4:2005 / European Standard. – Brussels, 2005.
3. **Simiu E. Scanlan R.** Wind effects on structures. Translated from the English by B.E. Maslov, A.V. Shvetsova; edited by B.E. Maslov. M.: Stroyizdat, 1984. – 360 p.
4. **John D. Holmes.** Wind Loading of Structures. New York: Taylor & Francis e-Library. – 2007. 433 p.
5. **Salenko S.D.** The methodology of modeling in a wind tunnel of the velocity distribution of the surface boundary layer / S.D. Salenko, A.A. Kuraev // Izvestiya SB AN USSR, a series of technical. – Novosibirsk, 1985. No. 16 (409), issue 3. P. 110 – 114.
6. **Telkova J.V., Pisanova A.L.** Modeling atmospheric turbulence in a wind tunnel using a uniform grid // Aerodynamics and flight dynamics of an aircraft: tez. dokl. X SibNIA school-seminar / edited by A.G. Rumyantsev. – Novosibirsk, 2012. P. 24–26.
7. Wind loads on glass cladding of a tower building/ Zhifu Gu, Yan Li, Minghui Cheg // Wind engineering into 21st Century. – Rotterdam: Larsen, Larose&Livesey, 1999. P. 653–658.
8. **Pavlovskiy R.N., Kuznetsov S.G.** Modelling of atmospheric ground boundary layer in short air dynamic tubes wind tunnels // Modern Industrial And Civil Construction. 2009. Vol. 5. No. 1. P. 15–22.

DOI 10.53954/9785604990148_175

FLOW STRUCTURE IN A FLAT CHANNEL WITH A CYLINDRICAL TRENCH CAVITY

V.I. Terekhov[1, 2], I.A. Chokhar[1], and N. Yang Lun[1, 2]

[1]Kutateladze Institute of Thermophysics SB RAS, 630090, Novosibirsk, Russia

[2] Novosibirsk State Technical University, 630073, Novosibirsk, Russia

A transverse turbulent flow around cavities often occurs in nature and in various technical devices. The most fully studied cavities are square or rectangular [1], as well as with inclined front and rear walls [2]. Flow and heat transfer in cylindrical trenches have been studied in less detail, despite the active use of such configurations to intensify convective heat transfer in tubes [3].

This presentation, which is a further development of the authors' works [4, 5], demonstrates the experimental results on aerodynamics of a turbulent flow around a single semi-cylindrical trench located on the surface of a flat channel. The influence of the trench inclination angle relative to the main flow direction on the wall pressure field and the profiles of longitudinal and transverse velocity components and their pulsations was studied. The pressure was measured in the range of inclination angles φ = 45° – 90°, and velocity distributions were measured at angles φ = 45° and φ = 90° and constant Reynolds number $Re_D = 1.65 \cdot 10^4$.

The nature of pressure coefficient distribution across the trench C_p depends largely on the angle of trench inclination. If the trench is located in the direction of the channel axis (φ = 0°), then the value of C_p is almost unchanged in the trench and is close to the excess pressure in the channel (Fig. 1a).

The flow in the trench at small inclination angles φ < 15° is continuous. As the angle of inclination increases, both the magnitude of rarefaction and its length inside the trench start increasing. The maximum rarefaction is achieved at inclination angle φ = 45°. With a further increase in angle φ > 45°, the level of rarefaction decreases again and with the normal location of an obstacle to the main flow (φ = 90°) it becomes minimal. At the same time, at large

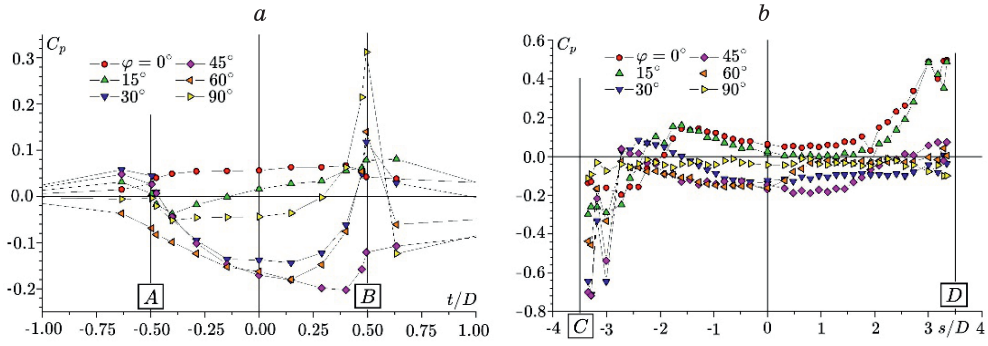

Fig. 1. Distribution of pressure coefficient across (a) and along (b) a trench.

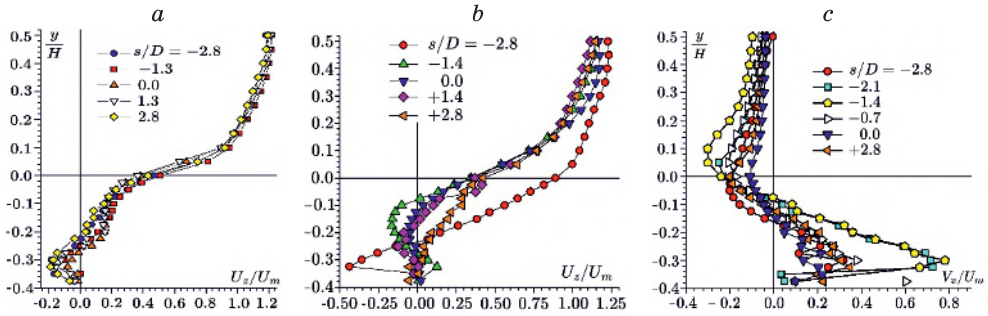

Fig. 2. Profiles of longitudinal velocity (a) at φ = 90°, and profiles of longitudinal (b) and transverse (c) velocity components with cavity inclination by φ = 45° relative to the incident flow $t/D = 0$.

inclination angles in the back edge area, the rarefaction turns into excess pressure due to the impact interaction of the mixing layer with the back zone of the trench (Fig. 1a).

There are three characteristic zones in the static pressure distribution along the trench longitudinal axis (Fig. 1b). In the area where the flow enters the trench, there is a powerful rarefaction, almost reaching the value of the velocity pressure. Further, when moving along the trench, the rarefaction region weakens quickly and does not undergo noticeable changes throughout almost the entire length of the cavity. Only the cases of small inclination angles φ = 0 – 15° do not obey this pattern, when the flow along the trench comes directly onto its hemispherical boundary in the outlet area, due to which the pressure increases there intensively.

If the trench is normal to the flow, the longitudinal velocity profiles measured at various distances from the median cross-section of the trench do not differ much from each other (Fig. 2a). This applies, first of all, to the flow region outside the trench $y/H > 0$. Within this region ($y/H < 0$), one can note a tendency towards a slight increase in the return flow velocity when approaching both edges of the trench. At that, the maximum velocity of gas recirculation movement inside a normally oriented trench does not exceed 20%.

The profiles of longitudinal velocity pulsation depend little on the location along the s axis. The highest value of the pulsation velocity is achieved at the boundary between the channel and the trench, where a mixing layer is formed after flow separation. The maximum value is typical of the shear flows and is ~20%. Further, when moving inside the trench, the level of pulsations drops by more than half.

In the inclined trenches (φ = 45°), the distributions of both longitudinal (Fig. 2b) and transverse (Fig. 2c) velocity components differ significantly depending on the location of the considered cross-section along the big axis of the trench. Thus, in the area of the trench inlet, a powerful circulation flow is observed with a maximum velocity value equal to approximately half of the flow velocity in the channel. The length of the zone of intense rotation in the vicinity of the inlet is small and is about one caliber. Further, when moving along the trench, the rotation velocity drops sharply and at $\Delta/D = 0.5$, the vortex motion of the medium degenerates completely towards the trench outlet, and the flow becomes continuous. In shallow trenches with $\Delta/D = 0.22$, according to the data of [5], the transition to continuous flow occurs much earlier, resulting in $U^*_{max}/U_m > 0$ along most part of the trench, which indicates the absence of return flows inside the trench.

This work was supported by a grant from the Russian Science Foundation RSF 24-19-00358

REFERENCES

1. **Terekhov V.I., Dyachenko A.Yu., Smulsky Ya.J., Bogatko T.V., Yarygina N.I**. Heat transfer in subsonic separated flows// Springer Nature Switzerland AG, 2022, 230 P.
2. **D'yachenko A.Y., Terekhov V.I., Yarygina N.I.** Turbulent flow past a transverse cavity with inclined side walls. 1. Flow structure // J. Appl. Mech. Tech. Phys. 2006. Vol. 47, P. 671–678.
3. **Kalinin E.K., Dreitser G.A., Kopp I.Z., Myakotchin A.S.** Efficient surfaces for heat exchangers. Fundamentals and design. Engl. ed. ed.: A.Bergles and W. Begell. – New York; Wallingford: Begell house, 2002. – XIX, 392 p.
4. **Yan Lun N., Baranov I.N., Terekhov V.I., Chokhar I.A.** Experimental investigation of pressure fields in a single trench dimple// J. Physics: Conf. Ser. 2021.Vol. 2119. 012033.
5. **Terekhov V.I., Terekhov V.V., Chokhar I.A., Yan Lun N.** Experimental investigation of the flow structure in a single trench dimple // Thermophys. Aeromech. 2022. Vol. 29, P. 887–898.

DOI 10.53954/9785604990148_178

ESTIMATION OF FLAME TEMPERATURE FIELD BY PLIF METHOD: DATA PROCESSING, COMPARISON OF RESULTS

R.V. Tolstoguzov, D.K. Sharaborin, A.G. Savitskii, A.A. Ponomarev, V.M. Dulin

Kutateladze Institute of Thermophysics of the SB RAS
630090, Novosibirsk, Russia

The use of modern optical techniques, which allow simultaneous measurements of temperature, velocity and concentration, allows the detailed study of local heat transfer and chemical reaction characteristics in turbulent, often unsteady, three-dimensional flows. Such experimental data are necessary to optimize burner and combustor designs, in particular to increase their efficiency and reduce harmful emissions [1, 2]. Flame temperature plays an important role in the physical and chemical processes that occur during combustion in complex combustion devices. An extensive database of experimental studies is updated annually, providing information on the spatial distribution of mixture components, the position of the flame front, areas of maximum heat release and the temperature of combustion products. Particularly valuable are measurements made using non-contact optical methods. These provide instantaneous two-dimensional distributions of values of interest in the study of combustion processes.

The aim of this work is to carry out a series of experimental studies to estimate the temperature field in conical flames of different configurations using optical methods based on Planar Laser Induced Fluorescence (PLIF). The results obtained can be used for the study of physico-chemical features of combustion, for the development of optical diagnostic methods, as well as for the verification and validation of numerical models and various analytical approaches designed to analyse systems with combustion.

To estimate the temperature field, the PLIF method was used to excite OH molecules. Temperature measurements by the PLIF method are based on the registration of fluorescence intensity images of molecules excited to a higher energy state by laser radiation. In this work, the «Two-line» PLIF method is used, which is described in detail in [3]. An alternative approach for temperature measurement is the «Thermally-assisted» PLIF method. Both of these methods measure fluorescence intensity in the excited state, but the former relates fluorescence to temperature via the Boltzmann distribution of the ground state population, while the latter relates the distribution of excited quantum states to temperature [4].

The work was carried out on an experimental stand which contained a profiled axisymmetric conical nozzle (internal diameter d = 15 mm), with the possibility of feeding a premixed mixture of air with different fuels: methane, propane, ethylene. The equivalence ratio varied from 0.7 to 1, Reynolds number Re = 700 – 1500. The PLIF method was used to record the OH fluorescence signal using digital cameras with electron-optical converters, quartz lenses and optical filters. Pulsed pump lasers and tunable dye lasers were used to excite the fluorescence.

As a result of the work, temperature field estimates have been obtained using the «Two-line» PLIF, «Thermally-assisted» PLIF methods, as well as temperature fields obtained by three-dimensional direct numerical modelling using the OpenFOAM software package. A detailed description of the experimental setup and application of the PLIF method is presented, the main difficulties in interpreting the obtained results, data processing are

considered, the main limiting factors of applicability and advantages of the methods are determined. The methods of temperature field estimation are validated, the measurement results are compared with literature data and results obtained by contact temperature measurement methods. The experimental results were compared with the results obtained by numerical modelling methods. In the course of the work it was found that the temperature field measurements using the two PLIF methods are in good agreement with each other, with RMS ~ 75 K, as well as with the temperature values obtained by numerical modelling.

This work was financially supported by the Russian Science Foundation (Project Code 22-19-00803).

REFERENCES

1. **Bouras F.** Numerical study of turbulent structures for lean premixed prevaporized combustion // Journal of Applied Mechanics and Technical Physics. 2014. V. 55, No 4. P. 614–626.
2. **Veselov K.E., Evdokimov O.A.** Gas dynamics and liquid fuel combustion in a model combustor // Journal of Applied Mechanics and Technical Physics. 2023. V. 64, No 2. P. 266–278.
3. **Cattolica R.J.** OH rotational temperature from two-line laser-excited fluorescence // Applied Optics. 1981. V. 20, No 7. P. 1156–1166.
4. **Copeland C., Friedman J., Renksizbulut M.** Planar temperature imaging using thermally assisted laser induced fluorescence of OH in a methane — air flame // Experimental Thermal and Fluid Science. 2007. V. 31, No 3. P. 221–236.

DOI 10.53954/9785604990148_180

NUMERICAL SIMULATION OF THE FLOW OF THERMALLY NONEQUILIBRIUM SUPERSONIC MICROJETS OF SF6

I.S. Tsyryulnikov, S.G. Mironov, T.V. Poplavskaya, S.V. Kirilovskiy

Khristianovich Institute of Theoretical and Applied Mechanics of SB RAS, 630090, Novosibirsk, Russia

The problem of the influence of vibrational nonequilibrium of molecules on the gas dynamic structure and the development of hydrodynamic instability in supersonic underexpanded (containing shock-wave structure) jets is currently insufficiently investigated. Earlier in [1, 2] it was shown that the vibrational nonequilibrium of gas leads to a significant changing in the gas dynamic structure of the jet flow. The hydrodynamic instability of the mixing layer of uncalculated supersonic jets was considered in [3–5] for the equilibrium case, and an inseparable connection between the development of the mixing layer instability waves and the shock-wave structure of the underexpanded jet was shown. The stability problem of underexpanded vibrational nonequilibrium flooded jets is a more complex problem because of the influence of nonequilibrium not only on the shock-wave structure, but also directly on the perturbations of different modes in the mixing layer.

In this paper we have numerically investigated the influence of vibrational excitation and relaxation of sulphur hexafluoride molecules (SF_6) on the stability and transition to the turbulent flow regime of supersonic jets flowing from axisymmetric convergent micro-nozzles (d = 5 ÷ 110 mkm) into submerged space at jet pressure ratio (JPR) n = 1.363. The choice of SF_6 as a working gas is due to the fact that SF_6 molecules have a large (up to 80%) contribution of excited vibrational degrees of freedom to the internal energy of the gas already at room temperature or slight heating.

Numerical simulation of SF_6 flow taking into account vibrational relaxation of molecules has been carried out with the help of ANSYS Fluent package on the basis of solution of unsteady three-dimensional Navier−Stokes equations using a two-temperature model of relaxation flows. The energy exchange between vibrational and translational degrees of freedom with finite relaxation time was taken into account by adding a source term calculated from the Landau−Teller equation similarly [1]. The vibrational relaxation time of SF_6 was calculated according to [6]. Both non-equilibrium and equilibrium cases were considered. The equilibrium flow field is used as the initial solution for the nonequilibrium case, in which thermal sources arise due to vibrational relaxation, which generate initial perturbations for the calculation of the unsteady nonequilibrium case. Calculations were carried out at variation of Reynolds numbers Red in the range of 350 ÷ 4000 and stagnation temperature T_0 = 300 ÷ 600 K. As a result of solving the problem, both average and pulsation characteristics of the flow were obtained.

A comparison of the characteristics of equilibrium and nonequilibrium jet flows (Fig. 1) shows that vibrational relaxation affects both the gasdynamic structure of microjets (Fig. 1*a*,*b*) and the spectral composition of perturbations (Fig. 1*c*,*d*).

Numerical investigations of the effect of the temperature of nonequilibrium jet flows on the length of their supersonic core length were also carried out while maintaining Mach number and two temperature factors (the ratio of the stagnation temperature to the ambient space temperature T_0/T_{inf}, and the ratio of the nozzle wall temperature T_w/T_{inf} to the ambient

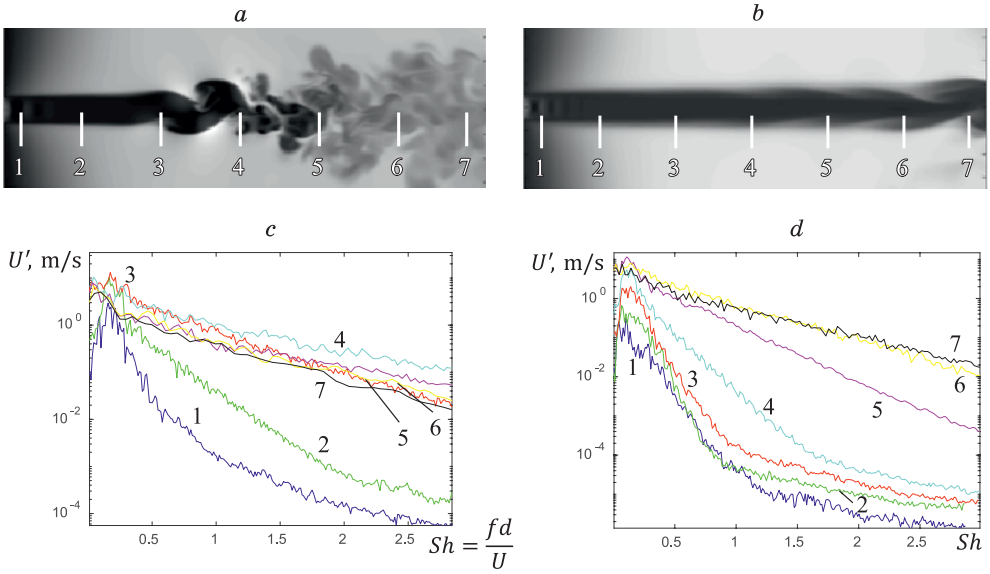

Fig. 1. Instantaneous density field (*a*, *b*); velocity pulsation spectra (*c*, *d*) при n = 1.363; T_0 = 600 K и T_{inf} = 300 K. 1–7 – points corresponding to the obtained velocity pulsation spectra. *a*, *c* – equilibrium flow; *b*, *d* – nonequilibrium flow.

space temperature). It is obtained that the supersonic core length of microjets of different temperatures in the range of numbers $600 < Re_d < 1200$ differs significantly. The maximum supersonic core length is realized for jets with $T_0 = 450$ K and $Re_d \sim 800$. The observed effect of temperature on the supersonic core length of nonequilibrium SF_6 jets indicates additional factors related to vibrational relaxation of molecules affecting stability and laminar-turbulent transition in jet flows.

The work was carried out within the framework of the state assignment of ITAM SB RAS.

REFERENCES

1. **Aniskin V., Maslov N., Mironov S., Tsybulskaya E., Tsyryulnikov I.** Specific features of the gas-dynamic structure of supersonic axisymmetric microjets of a nonequilibrium SF6 gas // Physical Review Fluids. 2020. V. 5, No. 8. 083401.
2. **Tsyryulnikov I.S., Mironov S.G., Poplavskaya T.V.** Effect of vibrational nonequilibrium of supersonic jets of CO_2 on their gas-dynamic structure // Thermophysics and Aeromechanics. 2023. V. 30, No. 4. P. 649–660.
3. **McGuirk J.J., Feng T.** The near-field aerodynamic characteristics of hot high-speed jets // J. Fluid Mech. 2021. V. 915. A120.
4. **Nogueira P.A.S., Jordan P., Jaunet V., et al.** Absolute instability in shock-containing jets // J. Fluid Mech. 2022. V. 930. A10.
5. **Edgington-Mitchell D., Xiangru Li, Nianhua Liu, et al.** A unifying theory of jet screech // J. Fluid Mech. 2022. V. 945. A8.
6. **Breshears W.D., Blair L.S.** Vibrational relaxation in polyatomic molecules: SF6 // J. Chem. Phys. 1973. V. 59, No. 11. P. 5824–5827.

DOI 10.53954/9785604990148_182

TECHNOLOGICAL POTENTIAL OF THE PULSE GAS DETONATION APPARATUS

V.Yu. Ulianitsky, I.S. Batraev, D.K. Rybin, A.A. Shtertser

Lavrentyev Institute of Hydrodynamics SB RAS, Novosibirsk, 630090, Russia

In a pulsed gas detonation apparatus (PGDA), the energy of a gas explosion is used to implement technological processes. In PGDA, detonation is generated in an extended channel – in the barrel of a detonation gun. In this case, a flow of detonation products with a temperature of up to 4500 K is formed, flying out of the barrel at a speed reaching 1500 m/sec. Detonation products contain highly active chemical reagents, such as atomic oxygen and hydrogen, the concentration of which changes significantly with variations in the fuel/oxidizer ratio, and in overriched mixtures (with excess fuel) carbon black is formed.

The industrial model of PGDA – CCDS2000 (Fig. 1), developed at the LIH SB RAS, is a computerized detonation complex [1], in which the process – shot of a detonation gun, is reproduced with a frequency of up to 10 Hz.

One of the important applications of CCDS2000 is detonation spraying, in which a portion of powder material is fed into the barrel of the detonation gun before the initiation detonation of explosive gaseous mixture. As a result of the shot, the powder particles are heated to the melting point and fly out of the barrel at a velocity of more than 500 m/sec, forming a dense coating with a bond strength comparable to the strength of the sprayed material on the surface of the substrate installed in front of the barrel. Coatings of any metals and alloys (from aluminum to tungsten), oxide and carbide ceramics and metal-ceramic composites are sprayed [2]. The microstructures of the detonation sprayed coatings are shown in Fig. 2.

Due to the high chemical activity of detonation products, it is possible to implement the controlled chemical effect on the particles of the sprayed material, forming oxide- or nitride-metal composites from metal powder, and when a spraying tungsten carbide, a metal tungsten coating can be obtained. In this case, PGDA is essentially a dynamic chemical reactor [3].

Using a specialized ejection powder feeder on the CCDS2000 facility, suspension detonation spraying is carried out, in which the coating is made from nanodispersed powder material [4]. Defect-free coatings from titania and alumina were obtained.

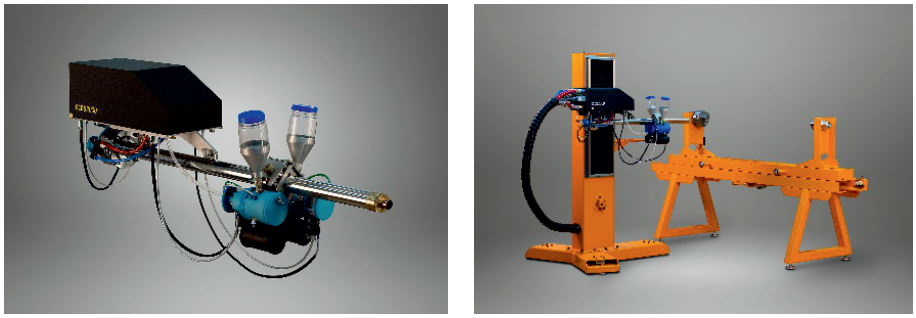

Fig. 1. CCDS2000: detonation gun (left), detonation gun with 3-axis manipulator (right).

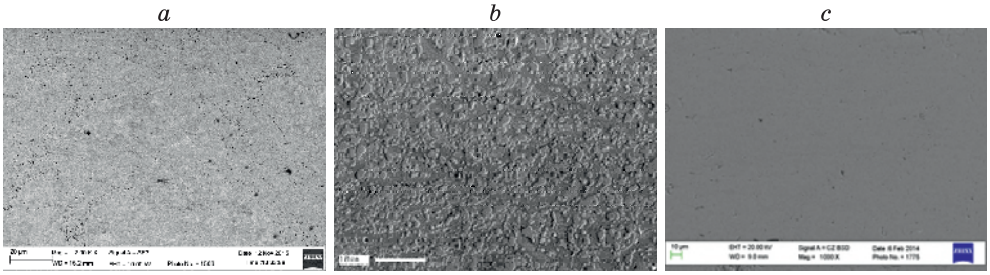

Fig. 2. The coating microstructure: a) metal, b) metal-ceramic composites, c) ceramic.

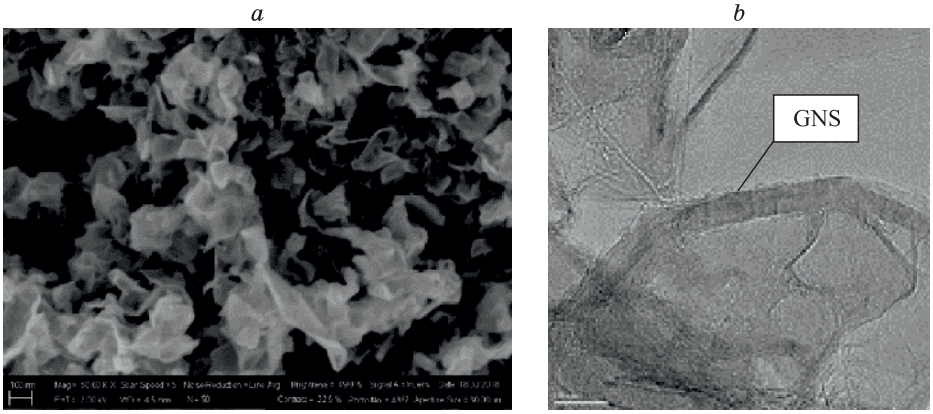

Fig. 3. Nano-sized carbon: a) magnification x50K, б) magnification x500K. GNS – graphene nanosheet.

Another application of PGDA is the detonation decomposition of hydrocarbons to produce hydrogen and nano-sized carbon condensate. In the reaction $CnHm + xO_2$, with a ratio of mixture components such that $O/C \leq 1$, in the case of detonation decomposition, the detonation products are H_2, CO and C. When $O/C = 1$, synthesis gas ($H_2 + CO$) is obtained, and at O/C ratio near zero, the detonation products are carbon black and hydrogen. When varying $O/C \leq 1$, nanoparticles of various morphologies are obtained, including graphene-like agglomerates (Fig. 3).

During the detonation decomposition of acetylene in a laboratory generator based on CCDS2000, a process was implemented with a yield of up to 10 kg of carbon and 15 m^3 of hydrogen per hour [5].

REFERENCES

1. **Ulianitsky V.Yu.** CCDS2000 – oborudovanie novogo pokoleniya dlya detonatsionnogo napyleniya. Uprochyaustchie tehnologii i poktytiya. 2013. № 10. P. 36–41. (In Russian)**.**
2. **Ulianitsky V., Shtertser A., Zlobin S., and Smurov I.** Computer-Controlled Detonation Spraying: From Process Fundamentals Toward Advanced Applications // J. Therm. Spray Technol. 2011. V. 20(4). P. 791–801.
3. **Ulianitsky V.Y., Dudina D.V., Shtertser A.A., and Smurov I.** Computer controlled detonation spraying: Flexible control of the coating chemistry and microstructure, Metals, 2019, 9, p. 1244.
4. **Shtertser A.A., Ul'yanitskii V.Y., Rybin D.K.** Suspension Detonation Spraying of Ceramic Coatings // Combustion, Explosion, and Shock Waves. – 2019. – Vol. 55. – No 4. – P. 483–490.
5. **Shtertser A.A., Ulianitsky V.Yu., Rybin D.K. et al.** Production of hydrogen and carbon black by detonation of fuel-rich acetylene-oxygen mixtures. Int. J. Hydrogen Energy. 2022. V. 47. P. 14039–14043.

DOI 10.53954/9785604990148_184

NUMERICAL MODELING OF TOLLMIEN-SCHLICHTING WAVE GENERATION BY FREE-STREAM TURBULENCE

M.V. Ustinov

Central Aerohydrodynamic Institute (TsAGI)
140180, Zhukovsky, Russia

At least three different models describing Tollmien-Schlichting (TS) waves generation by free-stream turbulence (FST) are recently known. Two of them claim that TS waves originate via interaction of free-stream vorticity with strong boundary layer non-uniformity near the leading edge [1] or with the weak non-uniformity in the vicinity of the neutral point [2]. TS wave production by means of non-linear processes in the ambient turbulent flow is considered in the third model [3]. Non-linear dependence of initial TS waves amplitude from turbulence level following from the Mack's correlation for N-factor [4] indirectly verifies the last receptivity mechanism. Till the present time it is not clear what mechanism is responsible for TS waves production by FST in wind-tunnel experiments or in flight conditions. To answer this question numerical modeling of laminar transition induced by turbulence was made in this paper. For the sake of simplicity development of periodic in space disturbances in the Stokes layer at the plate immediately set in motion was considered instead of spatial growth of perturbations in the non-uniform boundary layer. Flow field obtained from computation of decay periodic turbulence in the rectangular box was used as an initial condition. Three states of turbulence with different intensity Tu = 0.1, 0.2, 0.5% and almost equal integral scale were used in subsequent computations. Different from previous investigations of TS waves generation by periodic vertical disturbances [5,6] such approach permits us to investigate the influence of real FST spectrum and non-linear effects on the transition induced by FST.

Computations showed that two types of disturbances appear in the shear layer subjected by FST. Elongated streaks produced via lift-up effect play significant role at the initial stage of transition. Short-periodic disturbances with longitudinal wavenumber $\alpha = (0.2 \div 0.4)/\delta$ ssociated with TS waves appeared in the pulsations spectrum later. Evolution of amplitudes of these types of disturbances for different FST levels is shown in Fig. 1,a. For convenience, these amplitudes are normalized by the level of initial turbulence Tu. This figure shows, that normalized amplitudes of algebraically growing streaks for all FST levels fall into one curve at the major part of computation, except of the terminal stage of transition. It means that amplitude of these perturbations linearly depend from the turbulence level. However, it is not valid for the short-periodic disturbances associated with TS waves. Amplitudes of such perturbations grows more rapidly than turbulence level. This fact may be treated as the confirmation of non-linear mechanism of TS waves generation by FST. Nevertheless, comparison of results of solutions of full and linearized Navier-Stokes equations presented in Fig. 1,b reveal that the evolution of all types of disturbances in the shear layer is linear till the terminal stage of transition. Non-linear dependence of amplitude of short periodic disturbances from Tu is probably caused by dependence of the shape of turbulence spectrum from this parameter (or turbulent Reynolds number Rt). This spectrum exhibits more rapid attenuation with wavenumber for small Rt.

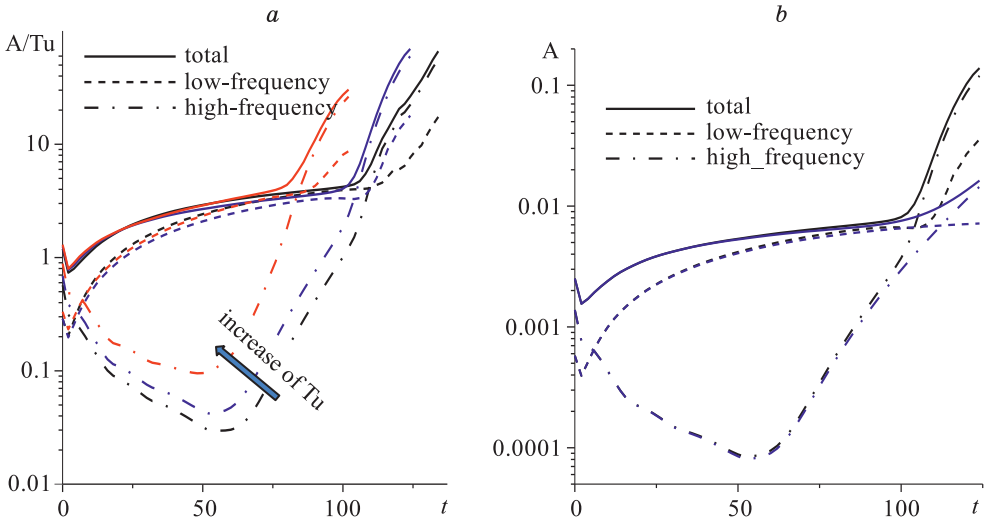

Fig. 1. Normalized amplitude of perturbations induced by FST as function of time (a), comparison of solutions of full (black lines) and linearized (blue lines) Navier-Stokes equations for Tu = 0.2% (b)

Amplitude of TS wave with given longitudinal wavenumber was found by means of projection of pulsations profile on the eigenfunction of Orr-Sommerfeld equation. Comparison of dependence of amplitude of such TS wave induced by FST on time with amplification curve found from linear stability theory makes us possible to find the location of this wave generation. Such approach reveal that TS waves are generated at the strong shear layer non-uniformity in the beginning of computation. Role of distributed generation on weak shear layer non-uniformity near the neutral point is small enough. It was also found that the amplitude of the most amplified TS wave in the neutral point A_{TS0} depends from the turbulence level in the power law $A_{TS0} \sim Tu^p$ with p = 1.6–1.8. This corresponds to linear dependence of transition N-factor from ln*(Tu)* similar to Mack's correlation [4]. However, computations give smaller coefficient of this proportionality.

REFERENCES

1. **Goldstein M.E.** The evolution of Tollmien–Schlichting waves near the leading edge//J. Fluid Mech. 1983. V. 127. P. 59–81.
2. **Zhigulev V.N., Fedorov A.V.** Study of Tollmien-Schlichting waves generation//Preprint SO AN SSSR, 1982, p. 27–33. (in Russian)
3. **Ustinov M.V.** Generation of Tollmien-Schlichting waves by free-stream turbulence// Fluid dynamics, 2014, No. 4, p. 58–72
4. **Mack L.M.** Transition prediction and linear stability theory // AGARD Conf. proc. CP-224. 1977. P. 1/1-22.
5. **Parekh D.E., Pulin P., Wlezin R.W.** Boundary layer receptivity to convected gusts and sound// Boundary Layer Stability and Transition to Turbulence FED-114/ Ed. C.L. Reda et al. N.Y.: ASME, 1991. P. 69–76.
6. **Buter T.A., Reed H.L.** Numerical investigations of receptivity to freestream vorticity // AIAA Paper.1993. No. 93-0073.

DOI 10.53954/9785604990148_186

NUMERICAL INVESTIGATION OF AN INFLUENCE OF THE ANODE SURFACE SHAPE ON NEAR-ANODE MHD FLOW FEATURES OF HIGH-PRESSURE PLASMA TORCH WITH TRANSFERRED ARGON ARC

S.P. Vashchenko[1], E.V. Kartaev[1], S.M. Aul'chenko[1, 2], V.V. Belyaev[1], O.B. Kovalev[1]

[1]Khristianovich Institute of Theoretical and Applied Mechanics, 630090, Novosibirsk, Russia

[2]Novosibirsk State Architectural-Building University, 630008, Novosibirsk, Russia

Increasing the service life of high-current, high-pressure plasma torches for nanopowder production technologies, as well as for manufacturing metals and alloys in additive technologies, depends mainly on the heat flux magnitude in the area of attachment (contact spot) of the arc on the electrodes. The anode is characterized by a direct dependence of the heat flux on the current density in the contact spot with non-equilibrium phenomena near its surface [1–5]. One of the ways to control the current density on an anode with a distributed (diffuse) mode of attachment between the arc and the electrode is to reduce the electric current density by increasing the surface area of the anode (profiling its surface) in the area of the arc spot [6, 7].

In this work the MHD flow in the channel of an atmospheric pressure argon arc melting plasma torch was simulated based on LTE approximation and plasma quasineutrality condition using the commercial software package COMSOL Multiphysics 5.6. Fig. 1 shows the temperature distribution and streamlines of argon plasma flow in the cylindrical symmetry calculation domain of interest, with arc current being equal to 1000 A. It is seen that ar-

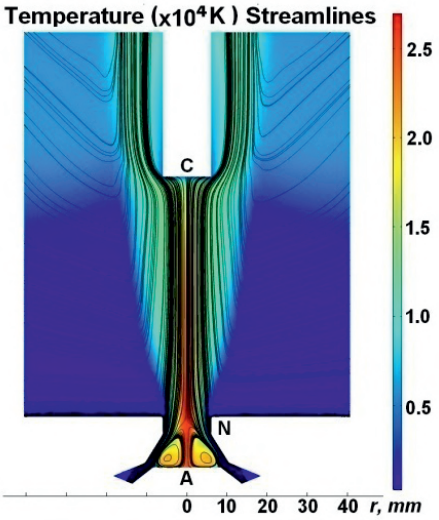

Fig. 1. The temperature distribution and streamlines of argon plasma flow in the cylindrical symmetry calculation domain of interest (electric current is equal to 1000 A, with argon flow rate of 5 g/s from anode side). A – copper anode, C – tungsten cathode, N – electrically insulated nozzle.

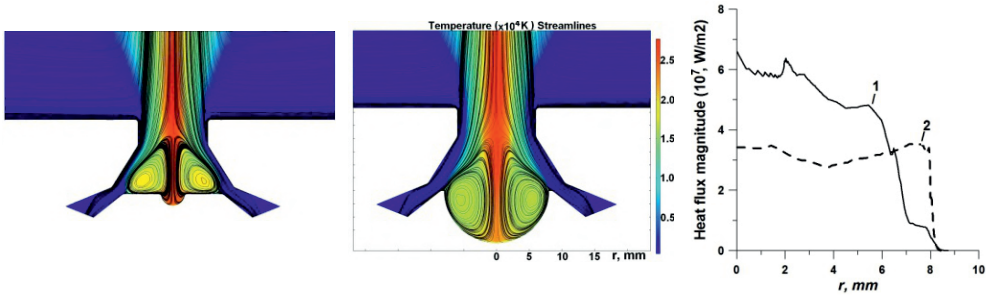

Fig. 2. Temperature distributions and streamlines in the anode unit with hemispherical blind holes with a radius of 2 mm (left), 8 mm (center). On the right – radial distributions of heat flux at the anode surface - curves 1 and 2, respectively.

gon arc confined by the nozzle N is located between the copper anode A and the tungsten cathode C, with a radial-axial supply of argon with flow rate of 5 g/s from the anode side.

To demonstrate numerically a possibility to reduce excessive thermal loads on the plane anode at high electric currents the shape of anode surface was altered. In Fig. 2 the calculation results within the anode region for hemispherical blind holes on a flat surface of a copper anode with a radius of 2 mm (left) and 8 mm (center) for arc current of 1000 A are shown.

On the right there are the radial distributions of heat flux magnitude for these anode surface profiles – curves 1 and 2, respectively.

It is seen that the heat flux magnitude decreases with increasing radius of the semispherical blind hole because of its redistribution in the radial direction due to an increased size of the recirculation zone in the hole. In addition, the radius of the diffuse attachment arc spot for a given arc current is about 3–4 mm, and in the second case, the arc spot is completely located within the semispherical blind hole, which reduces the possibility of its displacement and localization at the edge of the blind hole.

The work was supported by the Ministry of Science and Higher Education of the Russian Federation within the framework of the state assignment.

REFERENCES

1. **Zhukov M.F. et al.** Plasmatrons. Research. Problems. Novosibirsk, 1995. 202 p.
2. **Shkol'nik S.M.** Anode phenomena in arc discharges: a review // Plasma Sources Science and Technology. 2011. Vol. 20, No. 1, P. 013001. doi.org/10.1088/0963-0252/20/1/013001.
3. **Heberlein J., Mentel J., Pfender E.** The anode region of electric arcs: a survey // Journal of Physics D: Applied Physics. 2010. Vol. 43, No. 2. P. 023001. doi.org/10.1088/0022-3727/43/2/023001.
4. **Zhukov M.F., An'shakov A.S., Vashchenko S.P., Dandaron G.N.B., Zayatuyev K.** Formation of contracted anode spot in generators of low-temperature plasma // Soviet Journal of Applied Physics. 1987. Vol. 1. P. 71–76.
5. **Baksht F.G., Dyuzhev G.A., Mitrofanov N.K., Shkol'nik S.M.** Experimental investigation of the anode region of a free-burning atmospheric pressure inert gas arc: II. Intermediate current regime – multiple anode constriction // Technical Physics. 1997. Vol. 42. P. 35–38. doi.org/10.1134/1.1258649.
6. **Vashchenko S.P., Dandaron G.N.B., Zhukov M.F., Zayatuyev K.** The anode unit of electric-arc plasma torch // Patent No. 1748616, 1995.
7. **Zhaynakov A., Vashchenko S.P., Urusov R.M.** The influence of curvature of the anode unit of the plasma torch on the characteristics of the plasma flow // Proc. of 8 All-Union Conf. on Physics of Low-temperature Plasma. 1991. Vol. 1. P. 59.

DOI 10.53954/9785604990148_188

INVESTIGATION OF INTERACTION OF SHOCK WAVES WITH PERMEABLE BARRIERS IN GAS DYNAMIC INSTALLATION CST-14

S.N. Vasilieva, I.V. Guk

Joint Stock Company "Scientific and Production Association of Special Materials"
195277, Saint Petersburg, Russia

Conical shock tubes (CST) are perspective experimental gas dynamic installations. They provide an opportunity to model and study spherical shock waves that arise during detonation of explosives. Such installations can be used to study the characteristics of perspective materials, structures and means of explosion protection, to develop methods of reducing the destructive action of the explosion. In JSC NPO Specialmaterials, together with Semenov Institute of Chemical Physics RAS a gas-dynamic installation CST-14 with a solution angle of 14° was designed, developed and put into operation [1–2]. This installation allows to create controlled spherical shock waves without the use of condensed explosives in laboratory conditions. It is possible to control shock wave parameters such as duration, amplitude and impulse in the CST-14, which makes it possible to perform a wide range of experimental investigations.

In this study, we experimentally analyze the shock-wave interaction of spherical shock waves with permeable barriers with a given permeability coefficient. The aim of the work was to study the interaction of shock waves with permeable barriers in different configurations. The experiments were carried out in two stages (Fig. 1): with one barrier and with two barriers installed one after another. Parameters of shock waves were recorded by in-wall dynamic pressure gauges.

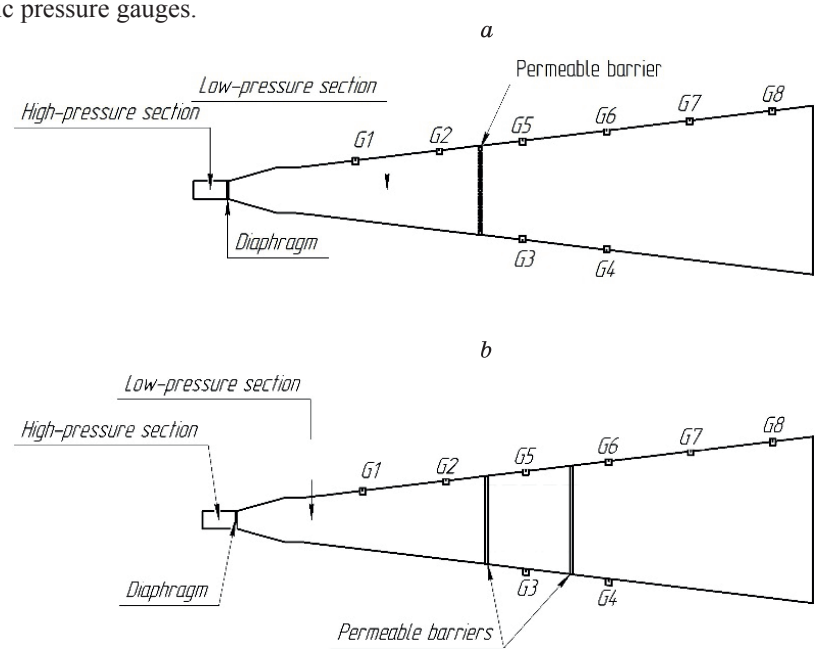

Fig. 1. Experimental study scheme: (a) first stage; (b) second stage

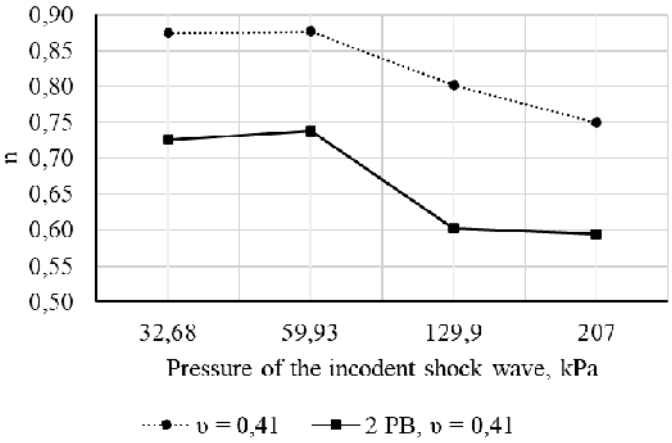

Fig. 2. Blast load amplitude dependent attenuation coefficients of incident shock wave pressure.

In the first series of experiments, the permeability coefficient of the barrier varied in the range of $0{,}21 < \upsilon < 0{,}41$.

The studies have shown that when the permeability coefficient of the barrier decreases, the amplitude of the passing shock wave decreases. It is possible to reduce the pressure in the shock front by a factor of two when using barriers with a permeability coefficient $\upsilon = 0{,}21$. It was also found that the shock wave conversion coefficient depends not only on the permeability coefficient of the barrier, but also on the amplitude of the incident shock wave.

The first stage of experiments was also modeled numerically for qualitative consideration of the gas flow pattern. The modeling showed that when passing through the permeable barrier, the shock wave front decomposes according to the location of the holes. At the moment of interaction of the shock wave with the permeable barrier, each hole begins to play the role of a separate shock wave generator, and at distances of 5–10 mm from the barrier, the shock wave front unites and further propagates a single shock wave.

The second stage of the research consisted in studying the interaction of the shock wave with successively installed barriers with the same permeability coefficient ($\upsilon = 0{,}41$) located at a distance of 250 mm from each other. The attenuation coefficients of the blast load amplitude were obtained during the study (Fig. 2):

$$n = \Delta p_{PB} / \Delta p_{without\ PB}$$

Δp_{PB} pressure in the front of a passing shock wave after passing a permeable barrier; $\Delta p_{without\ PB}$ pressure in the front of a passing shock wave in experiments without a barrier.

Conducted studies have shown that the presence of two barriers with a permeability coefficient of 0.41 can reduce the pressure in incident shock wave by 40%.

The experimental and numerical study shows that permeable barriers in various configurations can be used in the design of explosion protection equipment to reduce the parameters of the overpressure in the shock wave front.

REFERENCES

1. **Silnikov M.V., Khomik S.V., Guk I.V., Ivantsov A.N., Medvedev S.P., Anderzhanov E.K., Mikhaylin A.I., Tereza A.M.** Simulation of Interaction between a Spherical Shock Wave and a Layer of Granular Material in a Conical Shock Tube // Russian Journal of Physical Chemistry B. – 2021. – Vol. 15, No. 4. – P. 685–690. – DOI 10.1134/S1990793121040175.
2. **Silnikov M.V., Khomik S.V., Ivantsov A.N., Medvedev S.P., Anderzhanov E.K., Guk I.V., Mikhaylin A.I., Vasilyeva S.N., Teresa A.M.** Attenuation of a spherical shock wave by a perforated partition in a conical shock tube // Chemical Physics, 2022. – Vol. 41, – No. 8, – pp. 88–82.

DOI 10.53954/9785604990148_190

BACKGROUND ORIENTED SCHLIEREN WITH DIFFERENT BACKGROUND PATTERNS AND IMAGE PROCESSING TECHNIQUES

N.A. Vinnichenko, A.V. Pushtaev, Yu.K. Rudenko, Yu.Yu. Plaksina, A.V. Uvarov

Lomonosov Moscow State University, Faculty of Physics,
119991, Moscow, Russia

Background Oriented Schlieren (BOS) is quantitative refractometry technique, which becomes increasingly popular due to simplicity and low cost of the experimental setup. Instantaneous fields of the refractive index and related quantities (density, temperature, species concentration) are obtained using only a camera and a printed background pattern. The camera acquires two images of the pattern: the reference image is taken through the optically homogeneous medium and the distorted one is taken through the flow under study. The apparent displacement of the background pattern features in the distorted image with respect to the reference image is proportional to the refractive index gradient averaged over the ray path. The apparent displacement field is determined using image processing. Then, the refractive index field is obtained from the fields of its first spatial derivatives and a reference value at some location. Despite many modifications of BOS proposed in the past two decades [1], it remains unclear, which pattern and which image processing technique should be used in BOS to achieve better accuracy and spatial resolution. Another issue, especially important for BOS measurements in liquids or in gas flows containing shock waves, is robustness with respect to large displacement gradients. Displacement gradient, related to the second spatial derivative of the refractive index, leads to different displacement of the adjacent pattern elements, deformation of their images and image blur. If it is large enough, cross-correlation image processing, taken from PIV, yields erroneous displacement values. Integration of displacement (or solution of the Poisson equation) results in underestimation of the density drop across the shock wave front if the displacement value is underestimated. In [2] the performance of different image processing techniques (cross-correlation (CC), Horn-Schunck (HS) and Lucas-Kanade (LK) optical flow algorithms, Fourier Transform Profilometry (FTP) [3]) with corresponding patterns (Fig. 1) was compared using synthetic images generated with constant, sinusoidal and triangular displacement profiles. In the present study also the Phase Shifting Profilometry (PSP) [4] and M-array BOS [5] are analyzed. The conclusions are confirmed in real experimental measurements of several flows characterized by large second derivatives of the refractive index: natural convection in water near a heated vertical plate, convective plume from a heated horizontal wire, installed below the water surface, and the diffusion layers in water-glycerol and water-ethanol systems.

FTP outperforms cross-correlation and optical flow methods in spatial resolution and robustness with respect to displacement gradient. With optimal pattern period in the range 6–15 pix it yields correct results up to displacement gradient 0.8-0.9 pix/pix and can resolve perturbations with wavelength 13 pix (Fig. 2). It can substitute cross-correlation as default method for BOS. PSP is essentially multi-frame technique, i.e. several images must be taken with schlieren object assumed unchanged. However, 3-step PSP can be realized as single-frame technique with three phase-shifted images coded as RGB channels of color image. PSP is the only technique able to yield correct results for displacement gradient exceeding 1 pix/pix. Its accuracy is affected by camera noise. Optimal pattern period belongs to the

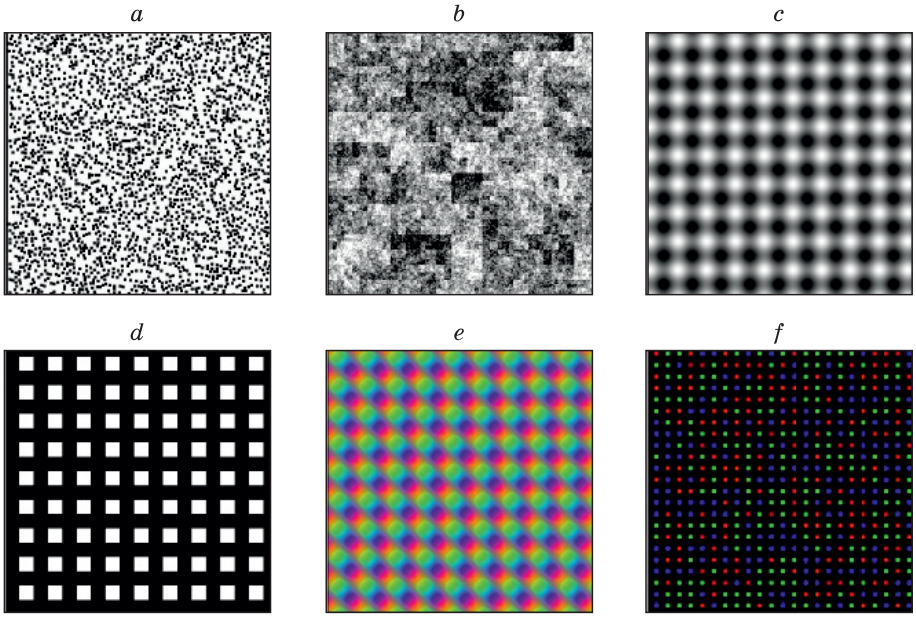

Fig. 1. Background patterns: (*a*) random dot (cross-correlation, optical flow), (*b*) wavelet-noise (optical flow), (*c*) sinusoidal fringe (FTP, PSP), (*d*) binary fringe (FTP), (*e*) color sinusoidal fringe (3-step single-frame PSP), (*f*) color-encoded regular dot (M-array BOS).

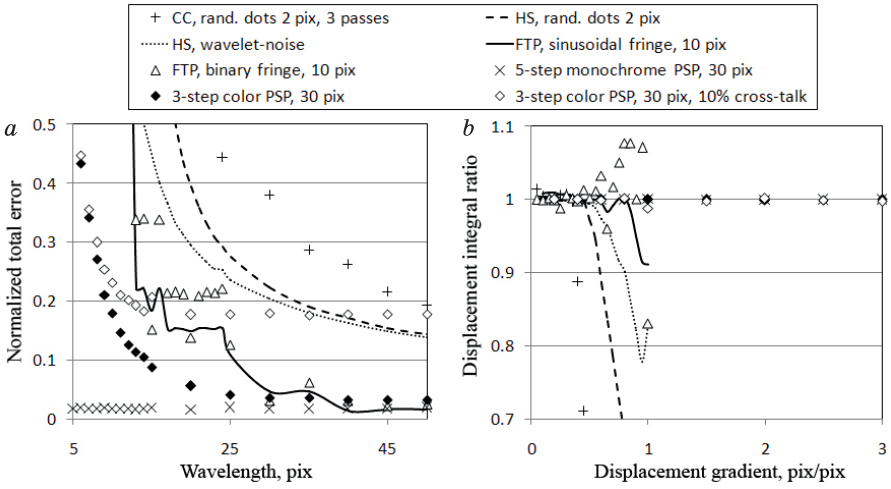

Fig. 2. Results of synthetic tests with (*a*) sinusoidal, (*b*) triangular displacement profile.

range 30–200 pix, depending on the trade-off between the noise and robustness to displacement gradient. M-array BOS enables direct observation of deformation of the dot images and formation of multiple images of the same dot. It has low spatial resolution, which can be improved using multi-frame approach [5].

This work was partially supported by Russian Science Foundation (grant 23-19-00591). Yu.K. Rudenko also acknowledges the Foundation for the Advancement of Theoretical Physics and Mathematics ”Basis” for personal financial support (grant 22-2-2-5-1).

REFERENCES

1. **Raffel M.** Background-oriented schlieren (BOS) techniques // Experiments in Fluids. 2015. Vol. 56. 60.
2. **Vinnichenko N.A., Pushtaev A.V., Plaksina Yu.Yu., Uvarov A.V.** Performance of Background Oriented Schlieren with different background patterns and image processing techniques // Experimental Thermal and Fluid Science. 2023. Vol. 147. 110934.
3. **Takeda M., Ina H., Kobayashi S.** Fourier-transform method of fringe-pattern analysis for computer-based topography and interferometry // Journal of Optical Society of America. 1982. Vol. 72 P. 156–160.
4. **Zuo C., Feng S., Huang L., Tao T., Yin W., Chen Q.** Phase shifting algorithms for fringe projection profilometry: a review // Optics and Lasers in Engineering. 2018. Vol. 109. P. 23–59.
5. **Vinnichenko N.A., Andrianova A.V., Pushtaev A.V., Rudenko Yu.K., Plaksina Yu.Yu., Uvarov A.V.** Color-encoded M-array Background Oriented Schlieren for measurements of strongly refracting objects // International Journal of Thermofluids. 2023. Vol. 18. 100364.

DOI 10.53954/9785604990148_193

A METHOD FOR STUDYING COHERENT STRUCTURES IN THE BOUNDARY LAYER AT TRANSONIC MACH NUMBERS

O.I. Vishnyakov, D.A. Bountun, P.A. Polivanov, A.A. Sidorenko

Institute of Theoretical and Applied Mechanics SB RAS
630090, Institutskaya 4/1, Novosibirsk, Russia

Unsteady processes observed in a turbulent boundary layer can be divided into coherent large-scale phenomena (structures) and small-scale chaotic flow oscillations. The size of coherent structures ranges from tenths of δ (the thickness of the boundary layer) to several tenths of δ, as some studies show. As a number of studies show, large-scale non-stationary structures are one of the factors in charge in low-frequency oscillations of separation and associated shock waves in the problem of shock wave boundary layer interaction (SWBLI) [1,2]. The latter facts, as well as the high practical significance of this problem, justify the interest of researchers in this phenomenon. The complexity of conducting research in transonic speed ranges due to a high probability of flow blocking, requires the development of new approaches to study non-stationary processes occurring in the boundary layer.

This study has two objectives. The first is to obtain information about coherent structures developing in the boundary layer for different states of the boundary layer, both in the zero pressure gradient case and for the interaction of a shock wave with the boundary layer. The second is the development of a flow diagnostic technique under the conditions of a transonic experiment, which is associated with the peculiarities of the research, namely the limited operating time and the high cost of operating such of facilities and also the high risk of blocking the flow. In this regard, it is desirable to use non-invasive optical measurement methods and surface methods using an array of sensors, which will significantly increase the volume of data obtained. In this study, measurements were performed using two methods simultaneously: hot-wire anemometry and PIV. The experiments were carried out in the T325 wind tunnel of the ITAM SB RAS at M = 1.43, stagnation temperature $T_0 \approx 289°$ K. The flow was studied on a model of a flat plate at a zero angle of attack. For hot-wire anemometer measurements, a multi component thin-film sensor was manufactured, having seven sensitive elements, operating in conjunction with an eight-channel constant temperature thermal anemometer ITAM CTA-18-8. An image of the sensor on the model is shown in the Figure. The sensor's sensitive elements (marked as a number 2 in the Figure) are located in the area sizing 2.8 by 4.5 mm, which is comparable to the local thickness of the boundary layer. PIV measurements were performed in a plane crossing one of the sensors, oriented along the flow and the normal to the surface of the model. The advantage of simultaneous use of these two measurement techniques is the ability to obtain the spectral characteristics of boundary layer pulsations due to the high temporal resolution of hot-wire anemometry and a large amount of information about the velocity distribution in space due to PIV in one experimental run of the wind tunnel. In addition, simultaneous and synchronized measurement by these two techniques allows for joint processing of the obtained data as proposed in [3]. The proposed technique is based on calculating the correlation coefficients between PIV data and the signal from the hot-wire anemometer sensor, which was previously filtered in a given frequency range, this allows one to isolate from the field of root-mean-square velocity pulsations those that are associated with pulsations of a certain frequency. In the study the

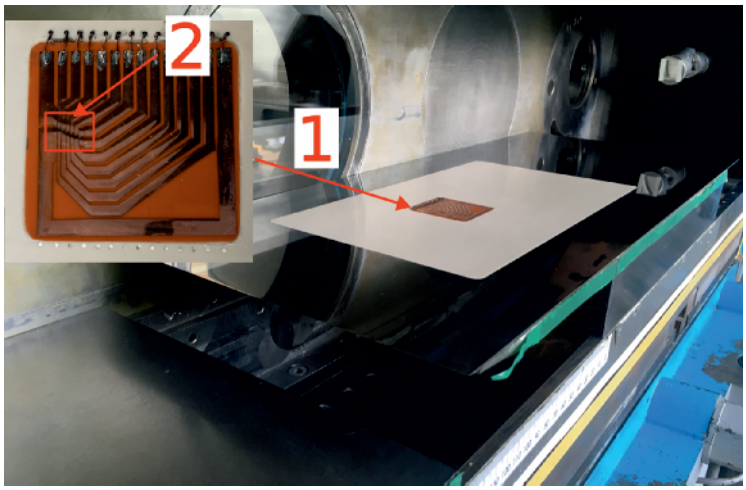

The model – a flat plate in the test section of T325 wind tunnel

1 – multicomponent sensor, *2* – array of sensing elements.

design and spatial distribution of the sensors are different in comparison of used in [3], to provide better spatial resolution of coherent structures.

The research was carried out within the state assignment of Ministry of Science and Higher Education of the Russian Federation. The study was conducted at the Equipment Sharing Center «Mechanics» of ITAM SB RAS.

REFERENCES

1. **Ganapathisubramani B., Clemens N.T., Dolling D.S.** Effects of upstream boundary layer on the unsteadiness of shock-induced separation // Journal of fluid Mechanics. – 2007. – Vol. 585. – P. 369–394.
2. **Polivanov P.A., Sidorenko A.A., Maslov A.A**. Correlation study in shock wave–turbulent boundary layer interaction // Shock Waves. – 2011. – Vol. 21. – No. 3. – P. 193–203.
3. **Vishnyakov O.I., Polivanov P.A., Sidorenko A.A.** The combined use of surface hot-wire anemometer sensors and PIV technique in the diagnosis of supersonic separated flow // XXI International Conference on the Methods of Aerophysical Research (ICMAR – 2022) (Novosibirsk, 8–14 Aug. 2022): Abstr. Pt.II. – Novosibirsk: SB RAS, 2022. – P. 171–172. DOI: 10.53954/9785604788974_171

DOI 10.53954/9785604990148_195

NUMERICAL MODELING OF MYOCARDIAL INFARCTION IN MULTIVESSEL CORONARY LESION

O.F. Voropaeva, Ch.A. Tsgoev

Federal Research Center for Information and Computational Technologies, 630090, Novosibirsk, Russia

The results of numerical modelling of the necrotic death of myocardial cells and immune response dynamics in type II ischemic infarction are presented. To describe the simulated process, a minimal reaction-diffusion mathematical model was used [1]. The model is focused on taking into account the balance of pro- and anti-inflammatory factors of aseptic inflammation and their effect on the process of cardiomyocyte death in the ischemic injury zone. The initial conditions and dynamics of the process in the infarction core are consistent with the data of known laboratory studies (see in [1, 2]). The finite-difference algorithm for the numerical solution of the initial-boundary-value problem is based on the application of the method of splitting in spatial variables [3] and the idea of the Seidel method.

The nature of the spatiotemporal distribution of substances (cell populations and inflammatory mediators) and the features of the formation of nonlinear dynamic structures of demarcation inflammation are studied (Fig. 1). The patterns of functioning of the basic mechanisms of the inflammatory response are analyzed, and the role of the main inflammatory mediators is evaluated. The study aims to address the urgent problem of analyzing general principles of governing macrophage polarization in the context of devising therapeutic strategies and refining the "therapeutic window" in complex heart attack scenarios including with multivessel coronary lesion. The research results allow us to consider the accepted reaction-diffusion model with constant diffusion coefficients as an important example of a formal mathematical description of an active environment in which two competition mechanisms operate simultaneously: local biochemical processes resist diffusion, but no less significant is the confrontation between the pro- and anti-inflammatory links of the innate immune response. One of the important driving forces in this competition is the M1/M2

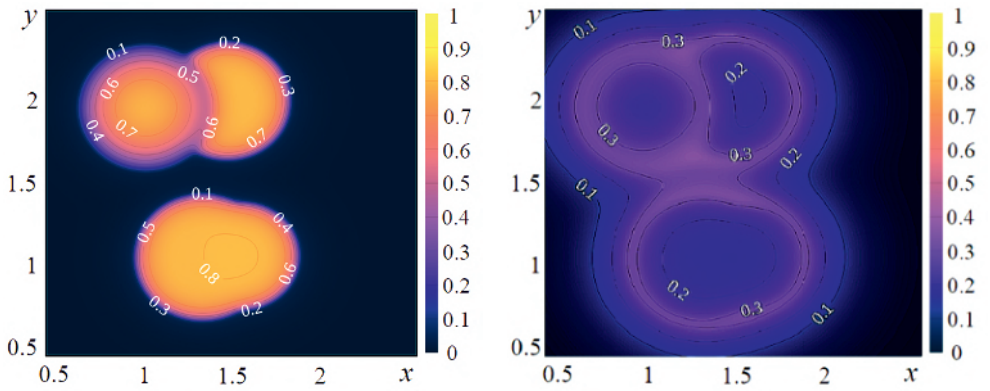

Fig. 1. Isolines of cardiomyocyte density defect (*(left)*) and anti-inflammatory interleukin IL-10 concentration (*right*) in multivessel damage to the coronary bed.

polarization of macrophages. The adequacy of the research results is confirmed by quantitative and qualitative agreement with experimental data.

REFERENCES

1. **Voropaeva O.F., Tsgoev Ch.A., Shokin Yu.I.** Numerical simulation of the inflammatory phase of myocardial infarction // Journal of Applied Mechanics and Technical Physics. 2021. Vol. 62, No. 3. P. 441–450.
2. **Voropaeva O.F., Tsgoev Ch.A.** Numerical modelling of myocardial infarction. II. Analysis of macrophage polarization mechanism as a therapeutic target // Mathematical Biology and Bioinformatics. 2023. Vol. 18, No. 2. P. 367–404.
3. **Yanenko N.N.** Fractional Step Method for Solving Multidimensional Problems of Mathematical Physics. Novosibirsk, 1967. 195 p.

DOI 10.53954/9785604990148_197

EFFECTS OF GAS CLUSTERIZATION IN THE DIRECT MONTE CARLO SIMULATION OF HIGHLY UNDEREXPANDED JETS

L.V. Yarkov, A.V. Zaitsev, Ye.A. Bondar

Khristianovich Institute of Theoretical and Applied Mechanics SB RAS
630090, Novosibirsk, Russia

Many scientific studies have been devoted to experimental or numerical modeling of the clustering process in highly underexpanded supersonic jets [1–4]. Numerical simulation of such flows is difficult because it requires taking into account the multiphase nature of the flow, the transition from the continuum to the free-molecular regime, as well as various non-equilibrium physical processes.

A kinetic model of the argon condensation process for the direct simulation Monte Carlo method (DSMC) [5] has been developed in the present work. This approach takes into account the effects of rarefaction, flow nonequilibrium and gas condensation. The model includes such processes as three-particle collision leading to the formation of dimers, attachment of monomers to clusters, evaporation of monomers from clusters, and coalescence of clusters. The model has been implemented into the SMILE++ software [7, 8], developed in the Khristianovich Institute of Theoretical and Applied Mechanics (ITAM).

The full-length report will contain the results of numerical modeling of underexpanded condensing jets under various conditions and comparison with predictions of empirical models [1, 2] and available experimental data.

The research was supported by the Russian Science Foundation (project No. 22-19-00750).

REFERENCES

1. **Hagena O.F.** Cluster ion sources // Review of scientific instruments. 1992. Vol. 63, No. 4. P. 2374–2379.
2. **Buck U., Krohne R.** Cluster size determination from diffractive He atom scattering // J. Chem. Phys. 1996. Vol. 105, No. 13. P. 5408–5415.
3. **Korobeishchikov N.G., Skovorodko P.A., Kalyada V.V., Shmakov A.A., Zarvin A.E.** Experimental and numerical study of high intensity argon cluster beams // AIP Conference Proceedings. American Institute of Physics, 2014. Vol. 1628, No. 1. P. 885–892.
4. **Yarygin V.N., Prikhodko V.G., Skovorodko P.A., Yarygin I.V.** Gas flow from a supersonic nozzle with screen into vacuum // Thermophys. Aeromech. 2016. Vol. 23, No. 6. P. 937–940
5. **Bird G.A.** Molecular gas dynamics and the direct simulation of gas flows. Oxford university press, 1994. 458 p.
6. **Kashkovsky A.V., Bondar Ye.A., Zhukova G.A., Ivanov M.S., Gimelshein S.F.** Object–Oriented Software Design of Real Gas Effects for the DSMC Method // AIP Conference Proceedings. American Institute of Physics, 2005. Vol. 762, No 1. P. 583–588.
7. **Ivanov M.S., Kashkovsky A.V., Vashchenkov P.V., Bondar Ye.A.** Parallel Object–Oriented Software System for DSMC Modeling of High–Altitude Aerothermodynamic Problems // AIP Conference Proceedings. American Institute of Physics, 2011. Vol. 1333, No. 1. P. 211–218.

DOI 10.53954/9785604990148_198

ON THE POSSIBILITY OF FAN NOISE REDUCTION BY SHIFTING SPECTRUM OF SHOCK WAVES GENERATED BY BLADES TO THE LOWER FREQUENCIES

M.A. Yudin, V.F. Kopiev, S.A. Chernyshev, G.A. Faranosov, O.P. Bychkov, M.A. Demyanov

Central Aerohydrodynamic Institute
105005, Moscow, Russia

Fan is one of the noise sources in a modern engine, which makes a significant contribution during takeoff at high angular velocities. In such operating modes, supersonic flow appears around the tips of the fan blades, which leads to the formation of a system of shock waves that propagate upstream to the exit from the engine channel. The flow is illustrated in Fig. 1.

This work is devoted to the process of shock waves propagation from the fan to the exit from the air intake.

The problem of the propagation of a system of shock waves can be reduced to the problem of the evolution of a one-dimensional periodic system, which is described by the nonlinear equation [1]:

$$\frac{\partial p}{\partial t}+\frac{\gamma+1}{2\rho_0 c}p\frac{\partial p}{\partial x}=0 \tag{1}$$

where $p=P-P_0$ – pressure disturbance, $\tilde{n}$ – speed of sound, ρ_0 – density, γ – adiabatic constant.

The solution to equation (1) in the ideal case of identical shock waves can be obtained analytically [2]:

$$\frac{\Delta P(t)}{P_0}=\frac{\Delta P(0)}{P_0}\frac{1}{\left(1+\frac{\gamma+1}{2\gamma}\cdot\frac{\Delta P(0)}{P_0}\frac{ct}{\lambda}\right)} \tag{2}$$

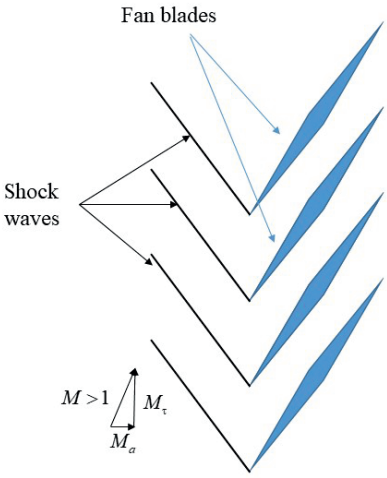

Fig. 1. Flow near the tips of the fan blades.

In fact the installation of the blades is not arbitrary, and, shock waves from the blades have different amplitudes, which are repeated with each revolution of the fan. It is impossible to develop an analytical solution for propagation of such a shock wave system. However, it is possible to construct a simple kinematic solution [3, 4] based on the analytical result. This model was compared with the two-dimensional Fluent calculation and showed good agreement.

Due to the nonlinearity of the problem of shock wave propagation, small changes in the shock wave stage in front of the fan lead to significant differences at the exit from the engine channel. The nonlinearity effect can be used to transfer energy from the main harmonic (at the blade pass frequency) to the lower ones, which can lead to a decrease in overall noise. Based on the proposed model, several calculations were performed to demonstrate the effect.

REFERENCES

1. **Goldstein M.E.** Aeroacoustics. McGraw-Hill International Book Company, 1976. 293 p.
2. **Landau L.D., Lifshitz E.M.** Course of Theoretical Physics, volume 6. Fluid Mechanics. London, Pergamon. 1987. 736 c.
3. **Fisher M.J., Tester B.J. and Schwaller P.J.G.** Supersonic fan tone noise prediction // AIAA aeroacoustics conference, Toulouse, 1998.
4. **Yudin M.A., Kopiev V.F., Chernyshev S.A., Faranosov G.A., Demyanov M.A., Bychkov O.P.** On the evolution of the shock waves systems created by the fan blades // Acoustical Physics. 2024.

DOI 10.53954/9785604990148_200

DETERMINATION OF THE MACH NUMBER FROM MEASUREMENTS OF TRANSVERSE MOLECULAR BEAM DENSITY PROFILES: OBTAINING NEW DATA IN NONEQUILIBRIUM RAREFIED FLOWS

A.E. Zarvin, E.D. Dering, V.V. Kalyada, K.A. Dubrovin

Novosibirsk State University
630090, Novosibirsk, Russia

The use of low-density supersonic jets in various studies is accompanied by considerable deviations from the calculated parameters performed under conditions of isentropic flows. Such a process of gases expansion from a source (a sonic or supersonic nozzle) is caused by a departure from the equilibrium between the vibrational, rotational and translational degrees of freedom of molecules, as well as with a certain set of initial gas dynamic parameters, the nucleation of the flow. Laboratory modeling of jet outflow from spacecraft engines, as well as studying the mechanisms of cluster formation by supersonic gas expansion into vacuum, require determining the energy of such jets. There are known developments of a number of techniques for determining energy in highly rarefied flows. In particular, electron beam spectroscopy for determining vibrational and rotational temperatures [1] should be mentioned, as well as a time-of-flight method for measuring the velocity distribution function of molecules with the determination of directional flow velocity and "parallel" translational temperature [2]. There are also known attempts to use transverse density profiles of molecular beam to determine the perpendicular temperature [3–4].

This paper describes a method for measuring the intensity across the axis of a molecular beam from supersonic nonequilibrium flows, including clustered jets, and describes the results and problems of such measurements, their errors and limitations in highly nonequilibrium jets. The method allows not only to study the features of the transverse beam profiles, to estimate the Mach number at the entrance to the skimmer, but also to consider the gas dynamics of supersonic flows before skimming. Using the presented examples of results obtained in various gases and at different gas-dynamic flow parameters, the issues of the possibility of determining the perpendicular temperature, as well as expanding the area of research by this method, including determining energy parameters in a clustered gas stream, are discussed.

The work was performed using the equipment of the NSU Applied Physics Research Center with the financial support of the Ministry of Education and Science of the Russian Federation (FSUS-2020-0039 project).

REFERENCES

1. **Muntz E.P., Abel S.J., Maguire B.L.** The electron beam fluorescence probe in experimental gas dynamics // Aerospace Technical Conference and Exhibit. Houston, Texas. Suppl. IEEE Trans. Aerospace AS-3. 1965. V. 2. P. 210.
2. **Voskoboinikov Yu.E., Zarvin A.E., Poltavets A.A., Tomsons Ya.Ya., Sharafutdinov R.G.** Determination of the velocity distribution function of molecules and its moments from time-of-flight // Journal of Applied Mechanics and Technical Physics. 1976. V. 17. No. 5. P. 625–632. https://doi.org/10.1007/BF00864148.
3. **Torello F.** Studies of translational freezing in free expanding jetsusing molecular beam techniques // AIAA J. 1971. V.9(9). 1843–1848.
4. **Bossel U.** Skimming of molecular beams from diverging non-equilibrium gas jets // Archives of Mechanics. 1974. V. 26. No. 3. P. 355–367.

DOI 10.53954/9785604990148_201

DEVELOPMENT AND TESTING OF A MATHEMATICAL MODEL TO DESCRIBE TURBULENT MULTIPHASE FLOW DURING CUTTING TRANSPORT

V.A. Zhigarev, A.V. Minakov, A.V. Shebelev, A.A. Gavrilov

Siberian Federal University
660041, Krasnoyarsk city, Russia

The development of mathematical models for the flow of a suspension of viscoplastic fluid, obeying, for example, the Herschel-Bulkley rheological law, requires additional research and taking into account several significant phenomena.

When modeling the flow of a mixture of a non-Newtonian fluid with solid particles, it is necessary to take into account the effect of localization of the shear rate between particles and the inhomogeneous distribution of local effective viscosity on scales on the order of particle sizes [1–3]. Experimental data demonstrate the dependence of the rheology of the suspension on the concentration of particles immersed in the liquid. In work [3], based on experimental data on the cylindrical Couette flow of a viscoplastic Herschel-Bulkley fluid with particles, the modulation of the rheological coefficients of the suspension is shown. The rheological properties of a suspension based on a viscoplastic fluid are explained by the nature of the flow of the medium at the particle scale level. In the presence of a macroscopic flow shear, the maximum deformation rate of the fluid flow is concentrated in the areas between the particles. As a result, the local shear rate in a liquid is a function of the particle concentration [1].

It is necessary to include in the mathematical model the dependence of the hydrodynamic resistance force on the rheology of the fluid and the local flow shear rate. The motion of a solid particle in a non-Newtonian fluid depends not only on the difference in phase velocities, but also on the local shear rate of the flow. In non-Newtonian liquids, the presence of shear caused by external factors leads to a decrease in effective viscosity and a decrease in the drag force acting on a particle immersed in the liquid. Taking into account the dependence of the hydrodynamic resistance force on the rheology of the fluid and the local shear velocity of the flow can be realized using correlations obtained on the basis of numerical calculations of the flow around a spherical particle. The rheological model of the turbulent flow of a suspension [4] includes the equations of continuity, momentum and transfer of turbulent quantities formulated for the mixture as a whole, as well as the transfer equation for the concentration of particles and the algebraic equation for the relative interfacial velocity. The approximation of the convective and diffusion terms of the momentum equation is carried out by second-order central-difference schemes. The connection between the velocity and pressure fields, which ensures the fulfillment of the continuity equation, is realized using SIMPLE, a similar splitting procedure. The values of the velocity and pressure fields are determined at the centers of the control volumes.

To eliminate oscillations of the pressure field, the Rhee-Chow approach is used, which consists of a special interpolation of the velocity vector on the faces of the control volumes. In this case, both viscous and convective terms of the equation of motion are implicitly interpreted. The convective terms of the turbulence equation are approximated by a counterflow TVD scheme. The convective terms of the concentration transfer equation are approximated

Rheological characteristics of drilling fluids and calculation parameters

Re	*U*, m/s	C_v	Rheological characteristics of drilling fluids		
			τ, Pa	*k*, Pa·s^n	*n*
6000	2.73	0.1	0.33	0.697	0.54
8500	3.11	0.1	0.23	0.479	0.58
12000	3.4	0.1	0.16	0.406	0.59
8900	2.47	0.18	0.08	0.338	0.6
11800	2.71	0.15	0.04	0.228	0.64
15000	2.96	0.15	0.01	0.124	0.7

where C_V is the virtual mass coefficient.

by a counterflow TVD scheme, the non-stationary term by a three-layer second-order scheme.

To test the model, numerical simulation of steady turbulent flows of two-phase flows in a horizontal circular pipe and an annular channel was performed.

The steady turbulent flow of a suspension in a pipe is considered [5]. The calculation area is a round pipe with a diameter of $D = 0.044$ m. To carry out the calculations, a periodic formulation of the problem was used.

The density of the drilling fluid was 1000 kg/m^3. The rheology of drilling fluids was specified from experimental data (see Table). To describe the non-Newtonian properties of the liquid, the Herschel–Bulkley rheological model was used. Spherical particles with a size of 2 mm and a density of 2600 kg/m^3 were considered as sludge particles. The gravity vector was directed perpendicular to the pipe axis.

Methodical calculations were carried out for liquids from Table for various Reynolds numbers. The rheological model gives a good agreement between the concentration profiles based on the maximum backfill value at the bottom wall, while the distribution profiles turn out to be more uniform. The rheological model provides a satisfactory agreement between the particle velocity profiles and the experiment. In this case, the fluid velocity agrees well with the experimental one at all Reynolds numbers. Based on the above, we can conclude that the developed mathematical model can be used to describe a turbulent multiphase flow during the transport of sludge particles.

The research was supported by grant No. 23-79-30022 of the Russian Science Foundation, https://rscf.ru/project/23-79-30022/.

REFERENCES

1. **Chateau X., Ovarlez G., Luu Trung K.** Homogenization approach to the behavior of suspensions of noncolloidal particles in yield stress fluids // Journal of Rheology. 2008. Vol. 52, No. 2. P. 489–506.
2. **Ovarlez G., Bertrand F., Coussot P., Chateau X.** Shear-induced sedimentation in yield stress fluids // Thermophysics and Aeromechanics. 2012. Vol. 177–178. P. 19–28.
3. **Ovarlez G., Mahaut F., Deboeuf S., Lenoir N., Hormozi S., Chateau X.** Flows of suspensions of particles in yield stress fluids// Journal of Rheology. 2015. Vol. 59, No. 6. P. 1449–1486.
4. **Gavrilov A.A., Shebelev A.V.** Single-fluid mixture model for laminar flows of highly concentrated suspensions // News of the Russian Academy of Sciences. Mechanics of fluid and gas. 2018. Vol. 2. P. 84–98
5. **Zheng E., Rudman M., Kuang S., Chryss A.** Turbulent coarse-particle non-Newtonian suspension flow in a pipe // International Journal of Multiphase Flow. 2021. Vol. 142. P. 17.

DOI 10.53954/9785604990148_203

OPTIMIZATION OF THE PROBLEM OF CALIBRATION OF AERODYNAMIC STRAIN GAUGE BALANCES USING CLUSTER ANALYSIS METHODS

S.V. Zimogorov, V.V. Lyutov, I.M. Agaletdinov, M.D. Makarkin

Central Aerohydrodynamic Institute named after prof. N.E. Zhukovsky (TsAGI), 140180, Zhukovsky, Russia

The development and creation of aircraft for various purposes is closely related to the study of their models in wind tunnels, as a result of which the main aerodynamic characteristics of the aircraft are deter-mined and the data obtained by calculation methods are refined. The main instruments in such studies are multicomponent aerodynamic strain gauge balances.

To ensure the correctness of measurements and a small error, the strain gauge balances undergo a mandatory calibration procedure before the experiment. Calibration is a time-consuming process and can take up to 15 days, taking into account the processing of an array of calibration data.

The classical approach to strain gauge balance calibration has reached its technological limit, and new methods must be used to optimize the calibration process in terms of accuracy or time.

One such solution is to use cluster analysis of the strain gauge balances under study and assign them to one of the groups according to various criteria. This approach will make it possible to use pre-prepared algorithms for calibrating strain gauge balances belonging to one cluster.

The task of calibration of strain gauge balances is reduced to determining the dependencies between the signals of the measuring strain gauge bridges on the reference loads reproduced by the machine. For multicomponent strain gauge balances, polynomials (mathematical models) of various degrees are used to describe this dependence. Classically, this dependence is described by equation (1):

$$R_i = a_i + \sum_{j=1}^{n} b_{i,j} F_j + \sum_{j=1}^{n} \sum_{k=j+1}^{n} c_{i,j,k} F_j F_k, \quad (1)$$

where:

R_i – the calculated value of the load for the i-th component;

i,j,k – component indexes;

a – offset of the function relative to zero;

n – the number of components of the strain gauge balances.

As the practice of working with strain gauge balances and the results of research by a team of authors in [1] show, this model does not always take into account the features of the design of strain gauge balances and the effect of its rigidity on the dependencies between components. In the same work, a mathematical model of a strain gauge balances (2) is considered, which contains 96 calibration coefficients for each component and more accurately describes such a phenomenon as an asymmetric response of a strain gauge balances to a sign-variable load.

$$R_i = a_i + \sum_{j=1}^{n} b1_{i,j} F_j + \sum_{j=1}^{n} b2_{i,j} \left|F_j\right| + \sum_{j=1}^{n} c1_{i,j} F_j^2 + \sum_{j=1}^{n} c2_{i,j} F_j \left|F_j\right| +$$

$$\sum_{j=1}^{n} \sum_{k=j+1}^{n} c3_{i,j,k} F_j F_k + \sum_{j=1}^{n} \sum_{k=j+1}^{n} c4_{i,j,k} \left|F_j F_k\right| + \sum_{j=1}^{n} \sum_{k=j+1}^{n} c5_{i,j,k} F_j \left|F_k\right| + \quad (2)$$

$$\sum_{j=1}^{n} \sum_{k=j+1}^{n} c6_{i,j,k} \left|F_j\right| F_k + \sum_{j=1}^{n} d1_{i,j} F_j^3 + \sum_{j=1}^{n} d2_{i,j} \left|F_j^3\right|$$

Also in the work [2], performed by the TsAGI team of authors, an analysis of various mathematical models for the calibration of strain gauge balances was carried out, which resulted in the conclusion that it is necessary to dynamically determine the dimension of the mathematical model of strain gauges, since a number of coefficients from model (2) make a negative contribution to the calibration error and are redundant in some cases.

The work is devoted to solving the problem of optimizing the process of calibrating strain gauge balances according to such criteria as time and accuracy. Cluster analysis of strain gauge balances is performed by automatically dividing a set of strain gauge balances into groups called clusters. According to the clustering results, each group should contain the most similar strain gauge balances, and objects from different groups should have pronounced differences. In general, the task of clustering strain gauge balances comes down to the following steps:

1) Compiling a sample of strain gauge balances and normalizing their characteristics;
2) Determining the properties by which the sample objects will be assessed;
3) Determination of similarities between strain gauge balances;
4) Creation of groups of similar strain gauge balances – clusters;
5) Analysis and evaluation of results.

The paper provides a mathematical justification for clustering and considers two algorithms: FOREL (formal element) and k means (k-means). Software was developed for cluster analysis, during testing of which 3 clusters were compiled from 10 different strain gauge balances.

REFERENCES

1. **American Institute of Aeronautics and Astronautics**, Calibration and Use Internal Strain Gage Balances with Application to Wind Tunnel Testing, AIAA, R-091A-2020.
2. **Petronevich V.V., Lyutov V.V., Manvelyan V.S., Zimogorov S.V.**, Research on the calibration of six-component rotating strain gauge scales for testing aircraft propellers, Vestnik MAI 2021 V. 28. No. 4 P. 48–61 (2021).

DOI 10.53954/9785604990148_204

INFLUENCE OF SORPTION MATERIALS ARRANGEMENT ON THE PROCESS OF HELIUM EXTRACTION FROM GAS MIXTURES

V.N. Zinovyev, I.V. Kazanin, K.E. Prokopyev, V.M. Fomin

Khristianovich Institute of the Theoretical and Applied Mechanics SB RAS
630090, Novosibirsk, Russia

At the Khristianovich Institute of Theoretical and Applied Mechanics SB RAS is developing a membrane sorption method of helium extraction from gas mixtures for the application in the gas production industry. A distinctive feature of the method is the use of hollow spherical microparticles as membrane elements, the wall of which has selective permeability to helium [1–4].

In addition to studying the selective properties of various hollow microspherical objects and samples of composite sorbents based on them, an important task is to find the sorption capacity of the created sorbent. Usually, as a parameter characterizing the sorption capacity of the sorbent, the ratio between the total internal volume of all hollow microparticles of the sorbent placed in the adsorber and the free volume of the adsorber V_2/V_1 is used, but in this work, instead of this ratio, the free volume ratio V_1/V_0 is introduced.

The purpose of this work is a theoretical consideration of the sorption process organization to determine the most optimal parameters of the gas separation unit, as well as conducting experiments to study the influence of the composite sorbent layout on its sorption capacity and efficiency of helium extraction from gas mixtures.

The operation of the gas separation plant is arranged as follows. A helium-containing mixture of gases is injected into the adsorber of volume V_0, filled with sorbent. Helium, from the free volume of adsorber V_1 (not filled with sorbent), penetrates through the walls of microspheres into the inner volume of particles V_2, i.e. helium sorption process takes place. In the ideal case, this process should be continued until the full equilibrium value of partial pressures of helium outside and inside the microspheres is reached. However, since in practice this can take quite a considerable amount of time, there is no need to continue the sorption process until a fully equilibrium state of the pressures. In most cases, it is sufficient to carry out sorption for some optimal time, during which the sorbent absorbs 80–90% of helium from the maximum possible value.

Let us consider the process of separation of helium-containing mixture by the membrane-sorption method from the theoretical point of view. Let the adsorber of volume V_0 is filled with the sorbent in such a way that its free volume V_1 and the free volume coefficient $k = \dfrac{V_1}{V_0}$. Thus the volume occupied by the sorbent consists of two parts: the volume occupied by the sorbent substance V_s, and the internal volume of the sorbent V_2.

Let us introduce the effective volume coefficient for convenience:

$$\gamma = \frac{V_2}{V_2 + V_s}. \tag{1}$$

A helium-containing mixture with helium volume concentration x_0 is injected into the free volume of the adsorber up to a pressure P_0, and simultaneously the sorption process is started. For helium penetrated into the sorbent the diffusion equation is valid:

$$\frac{d\nu_2}{dt} = -\frac{d\nu_1}{dt} = C_{sp} m_{sorb} \left(P_1 - P_2\right),$$

$$\nu_0 = \nu_1 + \nu_2 = \text{const}, \tag{2}$$

where: ν_0 – is the total amount of helium in adsorber, mol; ν_1, ν_2 – are the amounts of substance in free volume of adsorber and internal volume, respectively, mol; t – is the time, s; C_{sp} – is the specific helium permeability, mol/(s*g*Pa); m_{sorb} – is the mass of sorbent, g; P_1 – is the pressure in free volume of adsorber, Pa; P_2 – is the pressure in internal volume of sorbent, Pa. Considering the sorption process as isothermal and considering helium as an ideal gas for which the Mendeleev-Clapeyron equation is valid, a linear inhomogeneous equation with initial condition is solved:

$$\frac{d\nu_2}{dt} + \frac{C_{sp} RTm_{sorb}}{V_0} \frac{\gamma + k\left(1-\gamma\right)}{\gamma k\left(1-k\right)} \nu_2 = \frac{C_{sp} RTm_{sorb}}{kV_0} \nu_0,$$

$$\nu_1\left(t=0\right) = \nu_1^{(0)}, \tag{3}$$

$$\nu_2\left(t=0\right) = \nu_2^{(0)},$$

where: $R = 8{,}314$ – is the universal gas constant, J/(mol*K); T – is the temperature, K.

Based on the solution of equation (3), it was shown that the free volume coefficient k is an important factor affecting the sorption process. Based on this, a function of sorption process efficiency depending on the coefficient k – the ratio of the free volume in the adsorber to the adsorber volume – was proposed. This function can have several maxima depending on the sorption parameters. The absolute maximum of the function is reached at $k_{эф} = 0.37$.

One of the possible variants of microspheres packing in adsorber is considered – using containers from nonwoven materials. This type of packing allows to vary the coefficient k by changing the size and number of containers. The experimentally obtained value of $k = 0.7$ is lower than when using composite sorbent and can be further reduced, approaching $k_{эф}$.

REFERENCES

1. Permeability of hollow microspherical membranes with respect to helium / V.N. Zinoviev [et al.] // Engineering and Physical Journal. – 2016. – Vol. 89. – No. 1. – P. 24–36.
2. Method of separation of multi-component vapor-gas mixture / Fomin V.M., Zinoviev V.N., Kazanin I.V. and others // Russian Federation Patent No. 2508156. MKP V01D 53/02 (2006.01). Application No. 2012118350/05. Declared 03.05.2012. Published 27.02.2014. Bulletin No. 6. 2014.
3. Experimental study of helium permeability of nanostructured objects / V.N. Zinoviev [et al] // Problems of physics of ultrashort processes in strongly nonequilibrium media: Abstracts of the 9th Russian Symposium, Novy Afon, August 02–13, 2011 / Joint Institute of High Temperatures of the Russian Academy of Sciences. – Novy Afon: OIVT RAS, 2011. – P. 25.
4. Influence of composite sorbent granule packing on sorption capacity / I.V. Kazanin [et al] // XII All-Russian Congress on Fundamental Problems of Theoretical and Applied Mechanics XII All-Russian Congress on Fundamental Problems of Theoretical and Applied Mechanics: Abstracts, Ufa, August 19–24, 2019. – Ufa: Bashkir State University, 2019. – P. 171.

DOI 10.53954/9785604990148_205

TESTING OF TWO-COLOR PLIF METHOD FOR THE MIXTURE OF RHODAMINE 6G AND RHODAMINE B

A.A. Zotyeva, M.Yu. Nichik, V.M. Dulin

Institute of Thermophysics named after. S S. Kutateladze
630090, Novosibirsk, Russia

In contrast to thermal imaging and contact temperature sensors, the planar laser-induced fluorescence (PLIF) method makes it possible to record the instantaneous temperature distribution in a selected flow section. This method is based on the natural fluorescence of organic dyes, which is excited by a laser knife. Nevertheless, this method also has a number of limitations, for example, dependence on the spatial distribution of the energy of the laser knife. To correct this feature, the PLIF method is modernized by adding a second (reference) intensity peak at a different wavelength: a dye that does not depend on the measured parameter (temperature) is mixed into the liquid. The ratio of the intensity of the main dye to the intensity of the reference dye makes it possible to eliminate the influence of the spatial distribution of laser blade energy on the distribution of instantaneous temperature.

Testing of this method was carried out on a cuvette with heated stationary distilled water with the addition of two fluorescent dyes using a mixture of rhodamines B and 6G as an example. The fluid temperature varied from 38.5 to 19.5°C. The temperature of the mixture in the cuvette was measured using a thermocouple (TP.HA(K).N). Fluorescence of rhodamines was recorded using a measurement system consisting of two PCO EDGE 5.5 cameras (16 bits) and an Optronic KLM-532-2000 permanent laser with a cylindrical lens that forms a laser knife (laser energy in the recording area was 0,2 W). This equipment increases the accuracy of measurements in comparison with earlier studies [1, 2]. This advantage makes it possible to use fluorophores that are quite similar in spectrum – rhodamine 6G and B (emission peaks 580 nm and 550 nm, respectively) as dyes. The concentration of rhodamines is in the proportion 1:4, which is associated with a spectral study of the intensities of the spectra of rhodamines (see Fig. 1). To separately record the intensity of the dyes, each chamber was equipped with a light filter. The first Dantec Dynamics long-wavelength 550 nm filter transmits the total radiation of rhodamine B and 6G and cuts off the radiation

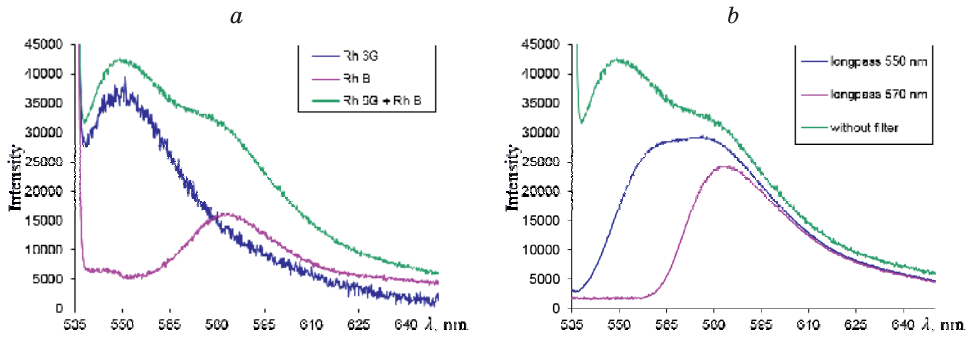

Fig. 1. Spectra of a solution of a mixture of rhodamine 6G and rhodamine B (a) without filters and (b) for various light filters.

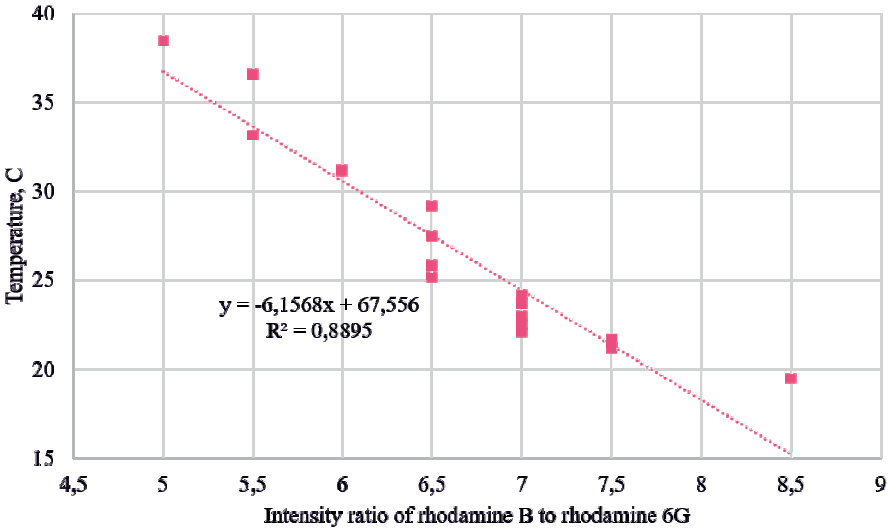

Fig. 2. Dependence of the solution temperature on the ratio of the intensities of rhodamine B and rhodamine 6G

of the laser knife, the second Dantec Dynamics long-wave 570 nm filter transmits only the radiation of rhodamine B.

Processing of the resulting photographs was carried out in several stages. The first step was to subtract background illumination from all images (a photograph of a cuvette with the laser turned off). Next, images of the cuvette from two cameras were set to the same position. This step was performed using ActualFlow software and a back projection algorithm; for this, a photograph of a cuvette with a 20×14 mm optical target placed in it was taken in advance. The next step was to calculate the emission intensity of rhodamine 6G by subtracting the two images of the cuvette to remove the emission of rhodamine B. The final step was to calculate the ratio of the intensities of the two rhodamines (B to 6G) and plot the temperature against this ratio to determine the dependence of the intensity of rhodamine B on temperature (see Fig. 2).

REFERENCES

1. **Rochlitz H., Scholz P**. Application of laser-induced fluorescence technique in a duct flow with one heated wall // Published Online 2016. URL: https://doi.org/10.1007/s00348-018-2508-1
2. **Chaze W., Caballina O., Castanet G, Lemoine F.** The saturation of the fluorescence and its consequences for laser-induced fluorescence thermometry in liquid flows // Published Online 2018. URL: https://doi.org/10.1007/s00348-016-2142-8

Content

САМОСТОЯТЕЛЬНОЕ ЭЛЕКТРОННОЕ ИЗДАНИЕ

Научное издание

Международная конференция по методам
аэрофизических исследований
1–5 июля 2024 г.,
Новосибирск, Россия
Тезисы докладов
Часть 2

На английском языке

INTERNATIONAL CONFERENCE ON THE
METHODS OF AEROPHYSICAL RESEARCH
July 1–5, 2024
Novosibirsk, Russia
Abstracts
Part II

Ответственный за выпуск А.В. Бойко
Технический редактор Н.М. Райзвих

Минимальные системные требования:
Тип компьютера, процессор, сопроцессор Pentium 4
Оперативная память (RAM) 512 Мб
Необходимо на винчестере 10 Гб
Операционные системы Widows XP
Дополнительные программные средства Adobe Acrobat 7.0

Сибирское отделение РАН
630090, просп. Акад. Лаврентьева, 17

ICMAR

ISBN 978-5-6049901-4-8